QUANTIFYING THE IMPACTS OF ANTHROPOGENIC EMISSIONS AND SPECIFIC INFRASTRUCTURES ON URBAN AIR QUALITY

A Dissertation
Presented to
The Academic Faculty

by

Abiola S Lawal

In Partial Fulfillment
of the Requirements for the Degree
Doctor of Philosophy in the
School of Civil and Environmental Engineering

Georgia Institute of Technology
December 2021

QUANTIFYING THE IMPACTS OF ANTHROPOGENIC EMISSIONS AND SPECIFIC INFRASTRUCTURES ON URBAN AIR QUALITY

Approved by:

Dr. Armistead G. Russell, Advisor
School of Civil and Environmental Engineering
Georgia Institute of Technology

Dr. Nisha Botchwey
School of City and Regional Planning
Georgia Institute of Technology

Dr. Jennifer Kaiser, Co-Adviser
School of Civil and Environmental Engineering
Georgia Institute of Technology

Dr. Kara Kockelman
Department of Civil, Architectural and Environmental Engineering
The University of Texas at Austin

Dr. James A. Mullholland
School of Civil and Environmental Engineering
Georgia Institute of Technology

Date Approved: [August 26, 2021]

To my family for their unwavering support and encouragement.

ACKNOWLEDGEMENTS

First and foremost, I give thanks to God for seeing me through this rewarding journey. I also want to thank my family. I would not be here without the support of my parents, brothers and sisters, who gave me encouragement and support every step of the way.

I would like to give thanks and acknowledge my adviser, Dr. Armistead Russell, for being nothing short of a wonderful adviser, for taking a chance on me and giving me a great opportunity. For that, I am very thankful and grateful for the mentorship, guidance, words of encouragement and support he provided me throughout my studies. I would also like to express thanks to my co-adviser, Dr, Jennifer Kaiser, for being a great mentor, supporter, and for so many useful conversations that shaped my approach to problems. Would like to also thank my committee: Dr. Nisha Botchwey for all the advice that helped develop my research, the support, and for being a wonderful collaborator, Dr. Kara Kockelman for being a great mentor, supporter, and collaborator, and to Dr. Mulholland for his kind mentorship, encouragement, and great questions.

I would like to thank collaborators I have worked with in the past, from Dr. Huizhong Shen, Dr. Yilin Chen, Dr. Joe Servadio, Tate Davis to Dr. Anu Ramaswami. To Niru and Ziqi for being the best office mates one could hope for. Thanks to lab members who helped me, Dr. Petros Vasilakos and Dr. Odman, Would like to specially mention Nash Skipper, for his invaluable assistance on so many projects and helping me trouble shoot a lot of CAMQ problems, and Dr. Hu of course for fielding my frantic emails. Thanks to other wonderful present and past lab members of Russell group. I must also express

sincere thanks to members of the Kaiser and Botchwey group as well for all their support and encouragement.

Thanks to my dear friends Dr. Smruthi Karthikekyan, Dr. Kevin Zhu and Yoyin Ibikunle for the best times during this program. To the GT housing staff and support crew, my friends and new friends I met along the way, like my daughter's pre-k teachers, Ms. Yolanda, Ms. Cynthia, Ms. Shalitha and Ms. Tena – thank you all for being there.

And last but not the least, I especially want to thank my precious little daughter, Dami, who was such an amazing trooper during this time and my inspiration to persist. It would not have been possible to get to this point without her.

TABLE OF CONTENTS

LIST OF TABLES

LIST OF FIGURES

SUMMARY

This research focuses on air quality and energy use in U.S. urban areas in relation to healthy and sustainable communities. Cities are of particular focus here, since they are responsible for 70% of all global energy use, despite currently housing 54% of the world's population and covering just 3% of global land mass area. Since urban areas' energy demand and transportation are the main drivers of air pollution, addressing the overarching impact on air quality and public health effects health requires an interdisciplinary analysis. In large part, urban-area emissions are affected by socio-economic factors, infrastructure investments (like housing and transport), regional climate, and public policies. In an effort to improve public health and city sustainability, this research explores the relationships between city infrastructure, energy, and air quality, by evaluating the impacts of environmental regulations, urban layouts, and the transportation sector on air quality and energy use.

Chapter 2's results show that, while U.S. environmental regulations have curbed pollution, as best measured through decreases in fine particulate matter ($PM_{2.5}$), the nation's $PM_{2.5}$ particles (almost exclusively aerosols) remain acidic. Aerosol acidity can increase the solubility of metal ions (e.g. Manganese (Mn), Iron (Fe), Copper (Cu)), which are highly associated oxidative stress and adverse health impacts. **Chapter 3** establishes a strong statistical relationship between residential energy use (of electricity and natural gas) and socio-economic demographic (SED) factors for Zip Code Tabulated Areas (ZCTAs) in metropolitan Atlanta, Georgia. However, vast differences in models for both energy forms exist. An R^2 of 0.95, with a low normalized error of 15% was found between natural

gas and SED factors, while the electricity model had an r^2 of 0.8 and normalized error of 33%. Additional analyses found that electricity use is affected by the urban morphology of roadways, with households in neighborhood areas of high road density using more electricity. This study also demonstrates the applicability of data transformation and machine learning methods in improving statistical regression power. Using Gram Schmidt orthogonolization improved the regression model's predictive power as evidenced by the greater ratio of significant predictors compared to other methods.

Chapter 4 assess the ozone and $PM_{2.5}$ impacts of the Atlanta Hartsfield Jackson (ATL) airport using a fine-scale chemical transport model (CMAQ). The chemical transport model (CTM) output is evaluated with three sets of observations, i) an air quality monitor for NO_x, ii) high resolution satellite-based observations from the TROPOspheric Monitoring Instrument (TROPOMI), and iii) two power plants near the Atlanta airport whose emissions are continuously measured with high accuracy. A three-dimensional airport emission inventory from full flight operations for the modeling domain is developed and compared against a base inventory with only surface airport operation emissions allocated to ATL. Results show that the magnitude and spatial extent of the airport's air quality effects will be understated if only the base inventory is used for regulatory purposes. This work underscores the benefits and capability of satellite observations and measured sources in evaluating CTM models.

Chapter 5, compares the air quality impacts of passenger vehicle fleet electrification and automation across the US to a non-automated, conventional-engine trend in Year 2050 (with future year gasoline powered passenger cars and power plants emitting much lower levels of pollution that present-day automobiles and power

generators). A mix of of Hybrid, Plug-in-Hybrid, and Battery-only electric vehicles have some air quality advantages over future-year gasoline vehicles, although the magnitude varies across species (a maximum decrease of 1 ppb was observed for 8-hour maximum daily ozone, while a net reduction of 0.1 ug/m^3 observed for $PM_{2.5}$).

Dissertation results suggest that policy, technology, demographics, and urban building decisions have a compounded effect on the efficacy of environmental regulations, air quality and energy use. Multiple factors will need to be considered to designing policies promoting equitable, sustainable cities.

CHAPTER 1. INTRODUCTION

1.1 Background

Urban areas are expected to grow rapidly in the future, along with energy use which affects emissions and thus, impacts air quality. Cities are responsible for more than 70% of anthropogenic emissions, which have been linked to climate change as well as poor air quality[1]. The emissions, emitted from these dense urban centers have far reaching and profound effects in many areas ranging from human health to global ecosystems[2]. Poor air quality, as a result of these emissions has been linked by the World Health Organization[3] to over seven million premature deaths, annually and globally. The Global Burden of Disease[4] report finds poor air quality as the number one global environmental risk. Since the main driver of urban air pollution is linked to energy consumption (both stationary and transportation related sources), addressing the overall impact on air quality and its potential effects on health and healthy cities is essential to understanding how to design sustainable cities for the future.

Sources of urban pollution causing emissions and their strengths are driven by socio-economic factors, infrastructure (i.e. transportation, housing as such), regional climate and public policy[5]. However, delineating specific aspects of these areas to specific adverse effects of urban pollution (i.e. human health and social and economic demographic disparities), is not easily done, as many of these factors are inextricably interlinked.[6, 7] This is especially the case as cities of today and the past are largely been affected by both infrastructure, economic base systems and policies. For example, the advent of certain social and economic policies, in addition to the influx of the automobile, led to urban sprawl and the allocation of industrial and manufacturing jobs in different parts of the cities. This changed the economic makeup of the city, influenced the spatial pattern of

pollution (via traffic and industry) and the exposure level for different social economic (SES) groups. This example illustrates the inextricable links between urban layout, pollution, and energy use, on the general populace and disadvantaged SES groups. It also serves to highlight the importance of future technologies, continued growth and adopted policies.

This research quantifies the impacts of specific infrastructure emissions on urban quality. Given the lagged ramifications of technological changes, this work also attempts to quantify the effects of new and existing transportation technologies on sustainable city development, by looking at the influence of city infrastructure and technology improvements.

1.2 Sustainability framework

The goal of the work described in this thesis is to add to our understanding of how to enact sustainable city design solutions. Sustainability is a broad topic with many facets that affect both macroscopic and microscopic systems. While sustainability studies explore many different topics related to urban sustainability, my research focus is on the impact of anthropogenic emissions. Two overarching issues that are addressed in differing degrees by the research conducted here are:, 1) As urban populations and the world population continue to increase[8], what impact (adverse or positive, large or small) will projected emission changes and their sources have in contributing to the sustainability of cities? And 2) What linkages are there among regulatory socio-economic factors, urban infrastructure, technological changes with air quality and the related health impacts? Both of these issues are addressed with a central focus on air quality and energy aspects.

These issues are addressed using the sustainability conceptual framework depicted in Figure 1, which illustrates four key areas (Climate, Land Use, Policy, and Regulations and Technology) to explore aspects of urban systems and their ultimate effect on air quality and health.

This framework is designed to delineate the effects of complex urban systems by evaluating specific aspects of each focus area one at a time (i.e. microscopic), allowing for the separation of dynamic, non-linear interactions between urban systems in the assessment of anthropogenic emission effects. The framework differs from previous frameworks and methods that favor a holistic systems approach of the combined effect of all four areas in an integrated study (macroscopic).[9]

Figure 1-1: Sustainability Framework

This thesis is comprised of an Introduction, plus Conclusions and Future Research chapters sandwiching four chapters detailing the main research projects with emissions and energy use being the main inputs driving analyses. Additional related work was conducted as part of this research in collaboration with students at other universities (included in Appendix A). Each chapter generally relies on different, though often overlapping, sets of analytical tools and techniques to garner insightful conclusions and analysis.

Each chapter quantifies the impacts of regulation and different infrastructure segments on air quality. By evaluating impacts of transportation technology changes, residential energy determinants, green infrastructure and anthropogenic emissions on air quality through the use of air quality models and statistical analysis. The topics of the four chapters describing the research are:

Chapter 2: Impact of air control regulations on air quality and $PM_{2.5}$ acidity.

Chapter 3: Social, economic, and urban infrastructure impact on residential energy.

Chapter 4: Quantifying effects of airport related emissions on air quality.

Chapter 5: Impact of electric self-driving vehicles on emissions and air quality.

These chapters are further detailed in the subsequent section, along with the main objectives of the research and a primary hypothesis. In many cases, additional hypotheses and objectives are explored.

1.3 Research descriptions and objectives

1.3.1 Chapter 2: *Impact of air control regulations on air quality and $PM_{2.5}$ acidity.*

The basis for this work is motivated by Servadio et al., (2019)[6], an interdisciplinary published study included in Appendix A, conducted in collaboration with students at other universalities where the relationship between health outcomes among different ethnic demographics in greater Atlanta as it relates to air quality, transportation and green infrastructure is explored. The study provided evidence that areas with poor air quality, carry a greater burden of cardiovascular and respiratory diseases and have greater percentages among African-American residents. While the etiologies of these outcomes are unclear, making targeted interventions difficult to design and implement, the study makes clear that these populations, burdened by poor

air quality, have the highest prevalence of respiratory and cardiovascular disease, which is linked with higher $PM_{2.5}$ exposure. Many studies like the "The Harvard six city"[10] link poor health outcomes and higher mortality rates to particulate matter exposure. A growing number of studies suggest that aerosol acidity plays a role in particulate composition and the solubility of metals, which in turn can impact health[11].

Since enactment of the Clean Air Act in 1970 and subsequent 1990 amendments, emission reductions have led to notable improvements in air quality over the U.S. The reduction of emissions from transportation and power sectors are noted to be substantial, including large OC, CO and NO_x reductions from automobiles along with sulfur reductions from power plants. Despite these reductions, health disparities and $PM_{2.5}$ exposure persist, with multiple studies finding differences between different socioeconomic status (SES) groups. The combined links between higher $PM_{2.5}$ exposure and adverse health outcomes, and the disproportionate exposures to lower SES groups, reinforce the call for targeted interventions and environmental regulations. While disproportionate exposure continues to be observed, finding out how particulate matter and aerosol acidity (in light of its potential role in $PM_{2.5}$ toxicity) have responded to these reductions might help explain the continued link between $PM_{2.5}$ exposure and disproportionate adverse health outcomes for disadvantaged SES groups.

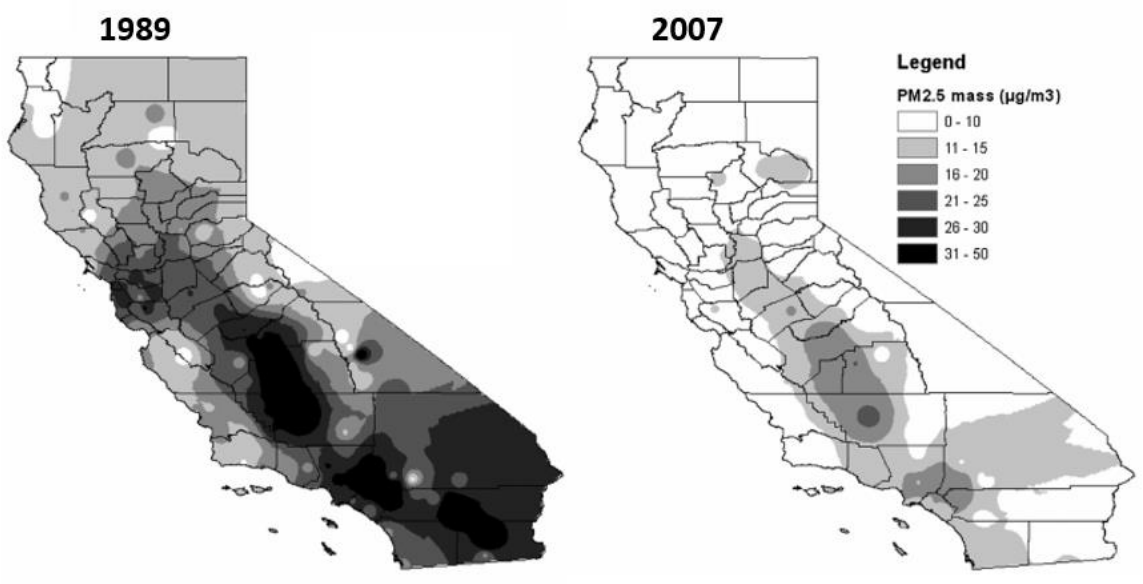

Figure 1-2: Mean annual $PM_{2.5}$ mass concentration in 1989 and 2007. Adapted from Blanchard et al., (2011)[12]

The aim of this chapter is to assess the effects of emission reductions on air quality, particularly particulate matter and aerosol (particulate matter) acidity. Here, the specific question is: How have emissions reductions impacted ambient air quality and aerosol acidity regionally over the continental U.S.? Until the Weber et al., (2016)[13] study, a general assumption in terms of fine particulate matter $PM_{2.5}$ characterization was that emission reductions of SO_2 would lead to a reduction in particulate sulfate and nitrate, and this will lead to a reduction in aerosol acidity and an increase in nitrate substitution. The potential increase in nitrate could be mitigated by concurrent reductions in NO_x emissions. With most of the acidity being associated with the sulfate in the particles, as its mass concentration in the particulate continues to decrease, an increase in nitrate substitution and a change in aerosol acidity is expected. Though Weber et al., (2016) proved that assumption to be incorrect, (i.e. acidity remained high, despite reductions in sulfate), it is uncertain if the trend will be observed in other regions since those results were observed at only one site in rural Alabama.

We proceed then under the original assumption that a reduction in aerosol acidity is linked to reductions in emissions in various regions of U.S. This study, conducted on a national scale, uses modeling and data analysis assessment of how PM levels and acidity responded to emission changes, focusing on particulate matter levels and acidity patterns. It is expected that the findings of this study will help inform policy regulations as to what and how regulation impacts future air quality and health. The driving hypothesis of this aspect of the thesis work is that emissions reductions lead to reductions in aerosol acidity, and that regions respond differently based on their location and other emissions.

1.3.2 Chapter 3: *Quantifying the impact of socio-economic and demographic variables on residential energy*

Residential energy comprises of a large amount of total energy use within the U.S. (23%)[14], yet understanding the underlying drivers of the demand poses challenges because demand varies widely across demographics, city types and regions. As cities continue to expand and change, understanding the demographic factors that influence energy use through energy modeling can support decisions in policies or changes in infrastructure that lead to more sustainable cities. Developing residential energy models poses some difficulty however, as most energy analyses are typically conducted with an engineering focus on building design parameters with just one or two social factors (i.e. income, household make up) incorporated[15, 16]. Such studies focus on deterministic factors, but rarely on the role of socio-demographic factors and their potential relationship to air quality and health. These factors can play a significant role in energy use, but their impact has not been quantified as extensively as urban layout and building design have been.

The two main objectives in Chapter 3 are 1) Evaluate which social economic factors play a significant role in energy use, and 2) Investigate the application of data transformation techniques to improve regression models. In this chapter, a statistical residential energy model using social economic demographic factors is developed to explain residential energy use in Atlanta. Energy usage to be explored includes 2010 electricity and 2009 natural gas use, with data provided by energy generating companies. Social demographic data is collected from the 2010 census. Results are analyzed at the Zip Code Tabulated Area (ZTCA) level. The predictive power of the statistical methods is investigated using data transformation techniques like orthogonolization and machine learning techniques as well. It is expected that a statistically significant relationship will be established between socio-economic variables and residential energy use and that these variables will prove to be the main determinant of energy demand.

1.3.3 Chapter 4: Quantifying effects of airport related emissions on air quality.

With the projected growth in air travel, characterization of airport impacts is essential to understanding the present and future effects travel will have on air quality, health and the environment. Airports are often located near lower SES neighborhoods and are regarded as hotspots for NO_x and particulate matter emissions. Recent work suggests they are of particular concern due to ultrafine particle (UFP) emissions from aircrafts.[17, 18] Figure 2 depicts the proximity of the five busiest airports in the U.S. to downtown areas. The top three busiest airports are under 30 km away from urban centers, and elevated concentrations of particulate matter and ozone from airport activities have been observed up to 20 km away from the airport. The implications is that the impact of current and potentially greater airport-related emissions in the future can have a notable impact on air quality and on nearby populations.

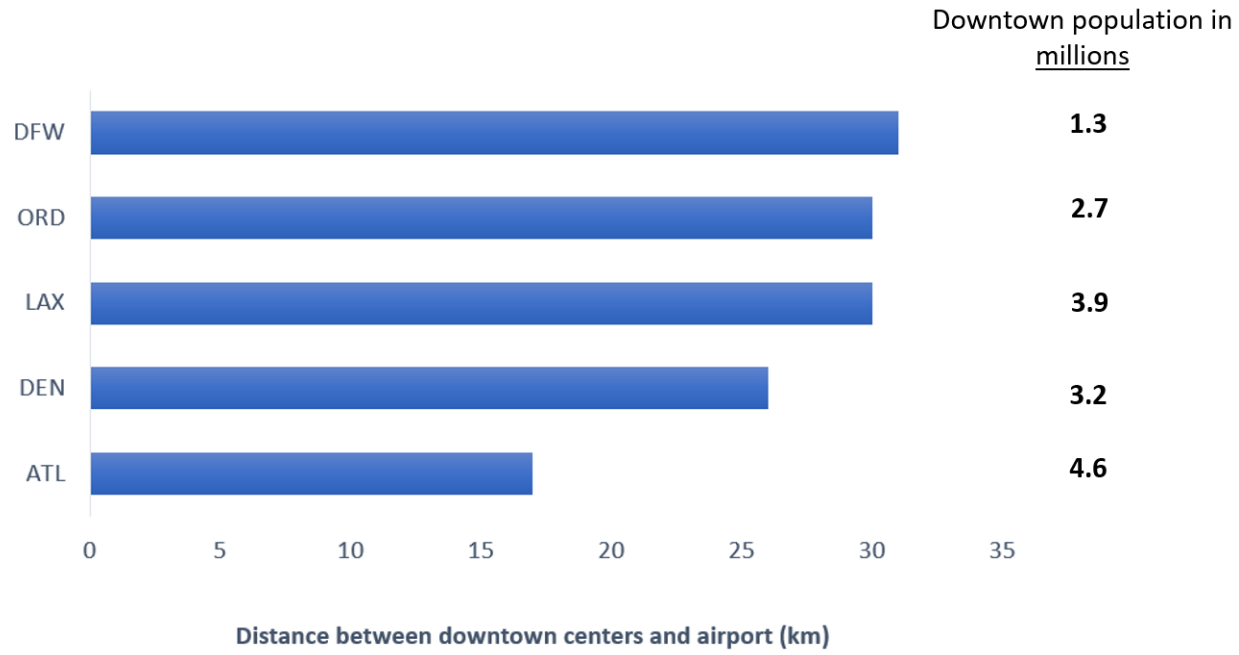

Figure 1-3: The top five busiest US airports and their respective distances to urban centers. Population of nearby downtown areas are shown as well.

Chemical Transport Models (CTMs) are often used to quantify emissions impacts of a wide range of sources, including airports. However, an accurate assessment of the impact on local air quality is difficult to ascertain with these methods. One of the reasons is that detailed 3D airport emission inventories are not widely available for regional transport models. Contributing further to the uncertainty of airport impacts is the omission of aircraft cruise emissions (full-flight emissions) as most airport inventories consist only of emissions generated from Landing and Takeoff operations (LTO) that occur at elevations below 1km[19]. Most airport emission inventories tend to allocate those emissions to the same grid and altitude height as the airport, but this practice of allocating the emissions to just the airport grid, without further spatial distribution, could potentially minimize or misrepresent the effect of airports within the general vicinity of its location[20]. Furthermore, because LTO emissions only contribute to about 10% of overall emissions from airport operations, airport inventories and its effects are probably underestimated.[21]

The effects of airport spatial allocation and air cruise emissions have been evaluated in a number of studies, but very few have been conducted at fine scales, which is noteworthy because differences in model results occur at different scales[22, 23]. So far, the findings from these studies indicate that full-flight emissions and spatial allocation have minimal effects on surface concentrations, which might explain the lack of additional studies in this regard. For instance, Vennam et al., (2017) found increases in O_3 that ranged from 0.46 -0.69 ppb, both amounting to 1.3% and 1.9% net increase overall[24]. Changes in O_3 of similar magnitude were also found by Lee et al., (2013), where a maximum increase of 1 ppb from full-flight emissions was observed[25]. The Unal et al., (2005) study of the Atlanta Hartsfield-Jackson airport (ATL), where a portion of LTO related emissions was spatially allocated a few layers above the airport, found a slight decrease in average O_3 of about 1 ppb with 3D spatially allocated emissions. Although these studies have shown minimal effects by focusing on one or more aspects (i.e. spatial allocation, inclusion of cruise emissions and fine scale modeling), results might be different if the key aspects of these studies were incorporated into a single study.

The objective of this work, is to combine satellite observations and chemical transport modeling to assess the impact of the Atlanta Hartsfield-Jackson airport (ATL) on air quality, particularly on NO_2, O_3 and particulate matter by exploring the differences between two airport inventories; a base inventory which only includes LTO emissions, allocated to the same coordinates as the airport, and a 3D airport emission inventory which includes both LTO and full flight emissions with horizontal and vertical allocation beyond the airport. A fine scale chemical transport model (CMAQ) is used, and the model outputs are evaluated with high-resolution satellite observations from TROPOMI and air quality models. It is expected that this study will

show that airport emissions are a significant contributor to local and regional air quality, and that satellite retrievals and air quality modeling can be used together to explore those impacts.

1.3.4 Chapter 5: Impact of electric self-driving vehicles on air quality

Self-driving vehicles are expected to gain a majority market share (> 60%) if not a full share by 2050[26]. For reasons that range from engineering practically and technological advancements to emissions standards and government policies such as tax incentives, these vehicles are expected to be wholly electric. The impact of this projection is not only expected to change the nature of vehicle ownership in households (which will go down), but could influence dynamic ride sharing fleets (DRS), giving vehicle access to social and economic groups that may otherwise not have access to such vehicles due to the high cost of ownership. In addition to changing the DRS market, the automation of vehicles is projected to increase the number of vehicle miles traveled as well[27]. As a result, the combination of electric cars in addition to vehicle miles traveled is likely to have a significant impact on emissions.

The impact of electric vehicles (EVs) on energy demand, emissions and air quality has been explored in a number of studies, many of which assess EV impacts in the context of various energy supply scenarios along with increased demand[28]. Many, however, do not take into account the impact of self-driving vehicles or Autonomous Vehicles (AV) in quantifying EV effects. AV utilization is expected to increase significantly in the future, along with electrification of the US fleet, which will result in increased vehicle miles traveled (VMT) from Shared Automated Vehicles (SAVs), yet its impact on air quality is seldom explored within the EV context.

In this chapter, the future effect of EV adoption is assessed under a Relaxed Energy Policy (REP) where future aggressive emissions reductions have been relaxed across multiple emission sectors. Here, the impact of vehicle electrification on light duty passenger vehicles under a less ambitious future energy policy and 2050 projected meteorology under the Representative Concentration Pathway 4.5 in the mobile sector is explored along with emission changes across other sectors. The electrified scenario is compared with a 2050 scenario where passenger cars emit no more than 10% of emissions from present day cars, – indicating that cars in the future are essentially clean. The efficacy of electric vehicle adoption along with adoption rates of autonomous vehicles in the context of the REP energy policy with future meteorology is assessed.

It is expected that the findings of this study will demonstrate that electric vehicles will yield multiple benefits in different aspects over 2050 clean gasoline cars. The benefits will have implications on energy policy, climate and air quality.

1.4 Thesis outline

This thesis is organized as follows; Chapters 2 through 5 give a detailed description of the background, methods, results, findings and conclusions reached in each study. The chapters will be followed by a summary and future work chapter. In the summary, the results findings and conclusions in all four chapters will be connected back to the main objectives of the thesis, as outlined in this chapter under sections 1.2 and 1.3. Future work is discussed as well.

1.5 Supporting Information

Appendix A. Supplementary Information

CHAPTER 2. LINKED RESPONSE OF AEROSOL ACIDITY AND AMMONIA TO SO_2 AND NO_X EMISSION REDUCTIONS IN THE UNITED STATES

Adapted from 'Abiola S. Lawal, Xinbei Guan, Cong Liu, Lucas R.F. Henneman, Petros Vasilakos, Vasudha Bhogineni, Rodney J. Weber, Athanasios Nenes, and Armistead G. Russell Linked Response of Aerosol Acidity and Ammonia to SO_2 and NO_x Emissions Reductions in the United States. Environmental Science & Technology 2018 52 (17), 9861-9873. DOI: 10.1021/acs.est.8b00711.

2.1 Abstract

Large reductions of sulfur and nitrogen oxide emissions in the United States have led to considerable improvements in air quality, though recent analyses in the Southeastern United States have shown little response of aerosol pH to these reductions. This study examines the effects of reduced emissions on the trend of aerosol acidity in fine particulate matter ($PM_{2.5}$), at a nationwide scale, using ambient concentration data from three monitoring networks – the Ammonia Monitoring Network (AMoN), the Clean Air Status and Trends network (CASTNET) and the Southeastern Aerosol Research and Characterization Network (SEARCH), in conjunction with thermodynamic (ISORROPIA-II) and chemical transport (CMAQ) model results. Sulfate and ammonium experienced similar and significant decreases with little change in pH, neutralization ratio (f=$[NH_4^+]/2[SO_4^{2-}]+[NO_3^-]$), or nitrate. Oak Grove, MS was the only SEARCH site showing statistically significant pH changes in the Southeast region where small increases in pH (0.003 to 0.09 pH units/year) were observed. Of the five regions characterized using CASTNET/AMoN

data, only California exhibited a statistically significant, albeit small pH increase of +0.04 pH units/year. Furthermore, statistically insignificant ($\alpha = 0.05$) changes in ammonia were observed in response to emission and $PM_{2.5}$ speciation changes. CMAQ simulation results had similar responses, showing steady ammonia levels and generally low pH, with little change from 2001 to 2011.

2.2 Introduction

Atmospheric aerosols, including fine particulate matter ($PM_{2.5}$), are associated with adverse effects on human health and the environment[29-35]. A key property of aerosol particles is its acidity, as it can critically affect heterogeneous chemistry (e.g., secondary aerosol formation, metal dissolution and nitrate/nitric acid partitioning), climate forcing, biogeochemical cycles, ecosystem productivity, ocean oxygen levels, and has been linked to adverse health effects[36-45].

Aerosol acidity (pH), is a function of its composition, driven largely by humidity, temperature, sulfate (SO_4^{2-}), and nitrate (NO_3^-), both of which are formed through the oxidization of sulfur and nitrogen oxides in the atmosphere[46-49]. These constituents are neutralized to some degree by reactions with ammonia gas ($NH_3(g)$) and the presence of non-volatile cations (e.g. Mg^{2+}, Ca^{2+}, K^+, Na^+) from soil dust. Chloride (Cl^-) formed from sea spray and biogenic emissions is also known to impact acidity, though these would be considered non-anthropogenic contributions to $PM_{2.5}$. In light of notable decreases in both sulfur (87% reduction from 1990-2016 of SO_2) and nitrogen oxide (56% reduction from 1990-2016 of NO_x) emissions[50], the question arises as to how aerosol pH has responded to emission changes over time and how it will evolve as emissions further change[51].

Effects of SO_2, NO_x, and precursor emissions on aerosol acidity and $PM_{2.5}$ concentrations have been studied previously[12, 49, 52-59]. Saylor et al., (2015)[53] reported a decrease in particulate ammonium $PM_{2.5}$ concentrations (NH_4^+) and an increase in NH_3(g) in response to decreased SO_2 and NO_x emissions. Weber et al., (2016)[55] conducted thermodynamic analyses of aerosol pH in the Southeast and concluded that in spite of significant sulfate decreases, particles remain highly acidic and will remain so until sulfate levels decrease to pre-industrial levels. Guo et al., (2017)[56] analyzed pH sensitivity to NH_3(g) levels in a variety of locations worldwide, and noted that about a 10-fold increase (decrease) in NH_3(g) levels is required to force a 1 unit pH increase (decrease).

In this study, trends in ammonia, speciated aerosol concentrations in $PM_{2.5}$, and aerosol acidity in the United States are examined. The presence of organic compounds have been found to have a smaller impact on aerosol pH[60, 61] and biogenic VOC emissions are not subject to emissions controls, so acidity changes are expected to arise primarily from changes in inorganic aerosol precursor emissions. While aerosol pH is not readily measured, a number of thermodynamic models such as SCAPE[62], AIM[63], and ISORROPIA-II[64] (used in this study) can be employed using concentrations of key constituents within the aerosol-gas system to estimate aerosol pH. Here, data obtained from the Ammonia Monitoring Network (AMoN), the Clean Air Status and Trends network (CASTNET), and the Southeast Aerosol Research and Characterization network (SEARCH) are used as inputs to ISORROPIA-II. The AMoN and CASTNET are nationwide networks that measure NH_3(g) and speciated $PM_{2.5}$ concentrations. SEARCH provides similar data for eight sites in the Southeastern US. In addition, a Chemical Transport Model, the Community Multiscale Air Quality (CMAQ), was used to provide information over a geographically wide domain. Data analysis with thermodynamic modeling, along with air quality modeling are used to 1) investigate spatial and temporal trends of ammonia and $PM_{2.5}$ in the United States 2) examine

how aerosol acidity has responded to reductions of sulfate and nitrate in the past 3) observe how ammonia gas levels responded, given the role ammonia plays in aerosol neutralization and nitrogen deposition and 4) better understand how pH will respond to future emissions changes.

2.3 Data and Methods

2.3.1 CASTNET and AMoN

Data from CASTNET and AMoN sites were organized into five regions of the US: Southeast (SE), Northeast (NE), Midwest (MW), Rocky Mountains (RK), and California (CA) (Figure B-1). The CASTNET database contains long-term records of air pollutant concentrations, deposition and the ecological effects of changing air pollutant emissions. At more than 90 sites across the U.S. and Canada, weekly ambient measurements were taken for gaseous species (e.g. SO_2, $HNO_3(g)$) and condensed phase species (e.g. SO_4^{2-}, NO_3^-, NH_4^+, Mg^{2+}, Ca^{2+}, K^+, Na^+, Cl^-). CASTNET also records daily average temperature and relative humidity (RH). Launched in 2007 and expanded in 2011, AMoN provides long-term records of ammonia gas concentrations across the U.S. The lack of gas phase ammonia data from AMoN prior to 2011 limits the detailed study period from March 2011 to February 2016. To provide complete ambient measurement input data for ISORROPIA-II which requires "total" concentrations (gas and condensed phase) of ammonium ($TNH_x=NH_3(g) + NH_4^+$) and nitrate ($TNO_3^- = HNO_3(g) + NO_3^-$) in the forward mode, only co-located CASTNET and AMoN sites were selected for this study. Additional details about the sites can be found in Table S1 in the Supporting Information (SI) supplement.

2.3.2 SEARCH

SEARCH was a comprehensive ambient air monitoring network designed to gather long term detailed data to characterize the chemical composition, sources of particulate matter and the spatial and temporal distributions of $PM_{2.5}$ in the Southeastern United States. SEARCH consisted of eight highly instrumented stations located in four Southeastern states AL, GA, FL and MS, consisting of three urban/rural and one urban/suburban paired sites in each state as follows: GA (Atlanta-Jefferson Street/JST, Yorkville/YRK), AL (Birmingham/BHM, Centerville/CTR), MS (Gulfport/GFP, Oak Grove/OAK), and FL (Pensacola/PNS, Outlying Landing Field/OLF). Further site location details and descriptions can be found in (Figure B-2 and Table B-2).

Data from SEARCH includes meteorology (temperature and RH), trace gas concentrations and particulate compositional data. SEARCH also measured HCl(g) in addition to particulate Cl^-. Here, we used data from 2008-2015, though not all sites were active for the entirety of the period Details of the data availability, along with the sampling frequency and site abbreviations can be found in Edgerton et al., (2012)[65] and in the SI (Tables B-2 and Table B-3).

2.3.3 Thermodynamic Modeling

2.3.3.1 ISORROPIA-II

ISORROPIA-II is a thermodynamic model that calculates the physical state, composition, phase partitioning and pH of inorganic atmospheric aerosol and is generally found to be in good agreement with other models and observations[66-68]. ISORROPIA-II has two run modes, forward and reverse. Inputs for the forward mode, which was used in this study, include known quantities such as temperature (T), relative humidity (RH), and total (gas + aerosol) concentrations. In this

case, constituents that can exist either as gases or particles—namely ammonia, hydrochloric acid, and nitric acid—are given as total ammonia (TNH_x = $NH_3(g)$ + NH_4^+), total nitrate (TNO_3^- = $HNO_3(g)$ + NO_3^-) and total chloride (TCl = HCl(g) + Cl^-), although HCl(g) was not available from CASTNET. The remaining constituents—sulfate, and base cations of magnesium, potassium, sodium, calcium — are also entered as inputs, although a fraction of some species may not be water soluble (e.g. $CaSO_4$). The reverse mode requires similar inputs, except the gas phase concentrations are determined by aerosol phase concentrations only. Measurement errors inherent in the latter mode (especially for mildly acidic aerosols) may give unrealistically large gas-phase concentrations than the forward mode which ensures more thermodynamic constraints to generate a more robust solution[68, 69]. In line with previous studies, the aerosol is assumed to be internally mixed so bulk properties are used[70, 71]. This assumption, coupled with the fact that ISORROPIA-II uses species concentrations as an input, eliminated the need to consider volumetric effects, although this study specifically explores one aerosol size: $PM_{2.5}$.

Although aerosols consist of organic and inorganic components, ISORROPIA-II only models the aerosol's inorganic constituent's effect on pH. Organic acids and organic matter do have some effect on pH, due to their contribution to water soluble ionic constituents (albeit mostly at higher pHs[71]), and associated liquid water content (LWC). Organics are also purported to affect pH by inhibiting $NH_3(g)$ uptake[61]. However, a fair amount of studies have found their contributions to LWC and pH to be ineffectual, when compared to contributions from inorganic constituents and were therefore, not considered in this study[60, 71-77]. We expand upon impacts of organic constituents, including organic acids, organonitrates and organosulfates on aerosol pH in greater detail within the SI.

In ISORROPIA-II, the user can specify the aerosol to be either in a thermodynamically stable state, where salts precipitate if saturation is exceeded, or in a metastable state, where salts do not precipitate under supersaturated conditions. ISORROPIA-II results in the metastable mode have been found to agree better with observations over a wide range of RH (20-95%) according to Guo et al., (2016)[78]. Though Guo et al., (2016) noted relatively large discrepancies at lower RH values (20-40%), Song et al., (2018)[69] in comparing ISORROPIA-II to E-AIM found relatively small differences in pH over a wide range of RH. A boxplot of RH for SEARCH and CASTNET (Figures B-3 and B-4) shows generally high values that lie within the acceptable range found in Guo et al., (2016), and above the listed mutual deliquescence relative humidity values (MDRH) in Table 6 of Nenes et al., (1998)[66] and Table 5 in Fountoukis and Nenes (2007)[64], although summer RH values for California in the CASTNET network were in the low 30s, around the crystallization RH of pure ammonium sulfate[79]. In addition to better model agreement with observations, past studies, such as those by Rood et al., (1989)[80] show that metastable aerosols, in the range of 2 μm are fairly ubiquitous at RH's between 45 and 75%. Further, recent experiments by Liu et al., (2017)[81] found that the sub micrometer aerosols were liquid down to relatively low RH, so the aerosol particles are likely to be liquid at the RH range used in this study. Thus, in this work, the metastable mode was used with the seasonal averages of total species concentrations along with temperature and RH from SEARCH and CASTNET/AMoN databases to model the seasonal average aerosol pH at each site location for each region.

2.3.3.2 ISORROPIA-II Model Evaluation

As pH is difficult to measure, model evaluation of predicted pH is assessed by comparing predicted LWC and partitioning ratios among semi-volatile constituents (i.e. NH_4^+, $NH^3(g)$) between the gas and particle phase against observations. In comparison with other models,

ISORROPIA-II performs well, and its performance has been well documented and evaluated in several studies[64, 71]. Here, we use ISORROPIA II 2.3, which addresses the issue identified Song et al. (2018), and includes other algorithmic improvements. The differences between the updated version and version 2.1 are small: the average pH for the SEARCH sites changed less than 0.01 units, and about 0.1 for the CASTNET sites (Table B-4 and B-5). Additional discussion on model evaluation can be found in the SI as well.

2.3.4 Neutralization ratio f

While thermodynamic models can estimate pH, other parameters have been employed to serve as proxies for *in-situ* pH to indicate the degree of acid neutralization with ammonia in lieu of pH, though the utility of such measures is in question[68]. One commonly used proxy is an ion ratio, otherwise referred to as the "neutralization ratio" of the condensed species of particulate ammonium (NH_4^+) to sulfate (SO_4^{2-}) and particulate nitrate (NO_3^-), although in many cases, the latter is omitted[71, 82, 83].

Such proxies are not necessarily a good indicator of pH, as discussed by Hennigan et al., (2015)[68] and Guo et al., (2016)[78]. One weakness of this measure is that it does not include the presence or role of non-volatile cations, (which are not always available), nor the effects of aerosol water variations (from RH changes) on pH. However, despite these aforementioned short-comings, these proxies are still used in studies[70, 84] to understand aerosol dynamics and acidity changes in response to emissions precursors, so we include it here for completion and discuss it further in the SI. Of note, the neutralization ratio, *f* in this study is calculated using observed seasonal molar averages of NO_3^-, SO_4^{2-}, and NH_4^+ as follows:

$$f = \frac{[NH_4^+]}{2[SO_4^{2-}] + [NO_3^-]} \quad (1)$$

2.3.5 Chemical Transport Modeling

The Community Multiscale Air Quality (CMAQ) Model simulates the formation and fate of air pollutants by solving the general atmospheric dynamic equations which takes into account atmospheric reactive chemistry in addition to other physical processes (i.e. coagulation, deposition)[85]. ISORROPIA-II was used to calculate pH and inorganic species partitioning in CMAQ. Simulations were conducted using CMAQ version 5.0.2[85] for the Eastern continental US for the years 2001 and 2011, with a 12km horizontal grid resolution (Figure B-5). This region experienced large reductions in SO_2 emissions over this time, which is why the domain was chosen for more in depth study[59]. Emissions were developed using SMOKE, version 6, along with the National Emissions Inventory (NEI)[86, 87]. The Weather Research Forecast (WRF) version 3.6.1[88] was employed to generate meteorological fields. Using CMAQ results, seasonal maps in 2001 and 2011 of pH and gas-phase ammonia were created for the Eastern US.

A detailed evaluation of the model and how well it captured trends in PM and gaseous species is found elsewhere, along with further discussion in the SI[89, 90]. In general, the model achieved the performance goals set by Emery et al., (2017)[91] and captured observed sulfate and ammonium trends .

2.3.6 Ambient Data analysis

Species concentrations (TNH_x, TNO_3^-, TCl, SO_4^{2-}, Mg^{2+}, Ca^{2+}, K^+, Na^+), average temperatures and relative humidity from all three networks were averaged by season to compensate for limited years of available data and seasonal effects for the trend analyses conducted here[47]. These seasonal averages for winter (December to February), spring (March to May), summer (June-August), and fall (September to November) were used as inputs to ISORROPIA-II to model seasonal average aerosol pH at each site and region. The modeled pHs from ISORROPIA-II, along with the observation data were compared as seasonal time series trends, (Figures 2-1 to 2-3, Tables 2-1, 2-2), reflecting spatial and temporal effects. Linear regressions for selected speciated $PM_{2.5}$ components, pH, ammonia-gas partitioning ratio R_N ($R_N = [NH_3(g)]/ [TNH_X]$) and *f* as functions of time were performed and the slopes were evaluated for statistical significance. Yearly percent changes were estimated from the slopes and intercepts. Throughout this paper, statistical significance for these trends is assessed at $\alpha = 0.05$ (Tables B-6 and B-7). To assess the impact of finer temporal scales, monthly averaged species concentrations of the SEARCH sites were calculated and used to generate modeled pH with ISORROPIA-II. The results were evaluated similarly as the seasonal averages above with trends assessed for statistical significance (Table B-8).

For sake of brevity, only a few data tables and plots are shown here while additional figures and data tables can be found in the SI. The choice of variables to include in the main text are based on the sulfate/nitrate/ammonium aerosol model as these components largely influence $PM_{2.5}$ pH and constitute the bulk of its inorganic mass[71, 79, 92].

2.4 Results and discussion

2.4.1 CMAQ and ISORROPIA Modeling Results pH

ISORROPIA-II calculated aerosol pH was low at the beginning of the observational periods (SEARCH: 0.8-2.0. CASTNET/AMoN: 2.3-2.7), with small increases in pH (i.e. < 1 pH unit) over time (Table 2-1, Table 2-2, Figures 2-2a and 2-3a). While almost all SEARCH sites (except CTR) and CASTNET/AMoN regions (except RK, which has only one collocated network site, Figure B-1) exhibited positive trends for pH, only CA and OAK saw statistically significant changes and those increases were less than one pH unit over the period of study.

Similar pH values were found using CMAQ (Figure 2-1) in comparable regions. CMAQ-derived pHs in the upper Midwest region were typically between 3.5 and 4 in most seasons except spring for both years, which matched the MW pH of 3.7 from CASTNET/AMoN. pH for the Southeast region from CMAQ were about 1.5-2.0, which agreed well with the overall SEARCH site average of 1.8 and is also consistent with observations from Guo et al., (2015)'s study within the same region[71]. The CMAQ simulated pH over the years 2001 and 2011 with CMAQ also showed a small, typically positive trend. We discuss reasons for these differences in regional pH values in subsequent sections as we look at the impact of different species concentrations on pH.

Table 2-1: Results from the linear regression analysis for: pH, sulfate (SO42-), particulate nitrate (NO3-), particulate ammonium (NH4+), gaseous ammonia (NH3(g)), total ammonia (TNHx), and ammonia gas molar partitioning ratio, (RN=[NH3(g)]/[TNHx]) in all five regions in the CASTNET/AMoN network. Bolded results were found to be statistically significant at α=0.05. (Note: Yearly percent changes are estimated from the slope and intercept and tabulated)

Parameter	Metric	Units	NE	SE	MW	RK	CA
pH	Slope	pH/year	2.2E-2	1.9E-2	2.5E-2	-2.3E-4	**3.8E-2**
	Intercept	pH	2.3	2.5	3.6	2.7	**2.9**
	% Change	%/year	3.9%	3.0%	2.8%	-0.03%	**5.2%**
SO_4^{2-}	Slope	ug m^{-3} /Year	**-5.3E-2**	**-6.0E-2**	**-4.2E-2**	**-1.2E-2**	-1.7E-2
	Intercept	ug m^{-3}	**2.4**	**2.6**	**2.2**	**0.58**	1.1
	% Change	%/year	**-8.7%**	**-9.1%**	**-7.5%**	**-8.3%**	-6.3%
NO_3^-	Slope	ug/m^3/Year	1.1E-2	-2.7E-3	5.5E-3	-2.0E-3	-4.7E-3
	Intercept	ug m^{-3}	0.76	0.71	1.5	0.2	0.87
	% Change	%/year	5.6%	-1.5%	1.5%	-4.0%	-2.2%
NH_4^+	Slope	ug m^{-3}/Year	**-1.7E-2**	**-1.7E-2**	-1.1E-2	-4.2E-3	**-7.6E-3**
	Intercept	ug m^{-3}	**0.95**	**0.81**	1.0	0.23	**0.49**
	% Change	%/year	**-7.3%**	**-8.4%**	-4.4%	-7.2%	**-6.2%**
NH_3(g)	Slope	ug m^{-3}/Year	-2.1E-3	2.5E-2	-1.5E-2	-3.6E-3	2.6E-2
	Intercept	ug m^{-3}	0.79	0.94	2.1	0.51	2.0
	% Change	%/year	-1.1%	11%	-2.9%	-2.8%	5.4%
TNH_X	Slope	ug m^{-3}/Year	**-1.9E-2**	7.9E-3	-2.6E-2	-7.8E-3	1.9E-2
	Intercept	ug m^{-3}	**1.7**	1.8	3.1	0.74	2.4
	% Change	%/year	**-4.5%**	1.8%	-3.4%	-4.2%	3.1%
R_N	Slope	1/Year	3.8E-3	**9.8E-3**	6.9E-4	3.8E-3	4.0E-3
	Intercept	NA	0.47	**0.54**	0.68	0.66	0.79
	% Change	%/year	3.3%	7.2%	0.4%	2.3%	2.0%

2.4.2 Sulfate (SO_4^{2-})

Analysis of the sulfate concentration data showed statistically significant yearly reductions in sulfate (SO_4^{2-}) across most CASTNET regions (except CA, Figure 2-2b, Table 2-1 and Table B-7), highlighting the effects of reduced SO_2 emissions[59]. SO_4^{2-} across the CASTNET network varied regionally with the lowest concentrations (based on trend intercept) seen in RK (0.6 ug/m^3) and the highest observed in the SE (2.6 ug/m^3).

Comparable SO_4^{2-} results (Figure 2-3b) were observed at all SEARCH sites (except PNS) which all saw major reductions. PNS data did not extend past 2009 (Table B-2) and limited data

at this site did not allow for capture of sulfate reductions that were observed elsewhere. Significant downward trends were noted at CTR, JST, OLF, YRK and BHM with yearly reductions of -7% to -12% (Table 2-2). SO_4^{2-} concentrations (from trend intercepts) at SEARCH sites ranged from 1.6 ug/m^3 at PNS to 4.5 ug/m^3 at YRK, with an overall average of 3.2 ug/m^3, much higher than the SE region concentration from CASTNET trend of 2.6 ug/m^3. While these differences may be attributed to spatial variation and characteristics of the sites in both networks (i.e. climate, source apportionment), the median SO_4^{2-} values in both cases had fewer discrepancies (Figure B-6).

Organosulfates may be present, and there is a possibility that they could lead to artifact sulfate in the measurement process, though this is expected to be minimum, particularly in areas like CA, as the presence of these compounds are likely to be associated with isoprene oxidation[93]. Further, OS reactions within the aerosol tend to yield other OS compounds which do not contribute to inorganic SO_4[2,94].

Table 2-2: Results from the linear regression analysis for: pH, sulfate(SO42-), particulate nitrate (NO3-), particulate ammonium (NH4+), gaseous ammonia (NH3(g)), Total ammonia (TNHx), and ammonia gas molar partitioning ratio (RN= [NH3(g)]/[TNHx]) at all SEARCH sites. Bolded results were found to be statistically significant at α=0.05. (Note: Yearly percent changes are estimated from the slope and intercept and tabulated)

	Metric	Units	CTR	GFP	JST	OAK	OLF	YRK	BHM	PNS
pH	Slope	pH/yr	-2.6E-3	1.7E-2	9.9E-3	**9.1E-2**	2.7E-3	4.2E-3	2.2E-3	9.1E-3
	Intercept	pH	1.5	1.7	1.8	**0.76**	1.6	2.0	1.9	1.8
	% Change	%/year	-0.70%	3.9%	2.3%	**48%**	0.69%	0.86%	0.44%	2.0%
SO_4^{2-}	Slope	ug m^{-3}/Yr	**-6.2E-2**	-9.0E-2	**-8.7E-2**	-7.7E-2	**-5.5E-2**	**-1.3E-1**	**-7.3E-2**	8.9E-2
	Intercept	ug m^{-3}	**3.0**	3.1	**3.7**	2.9	**3.0**	**4.5**	**3.6**	1.6
	% Change	%/year	**-8.4%**	-12%	**-9.3%**	-11%	**-7.2%**	**-11%**	**-8.1%**	22%
NO_3^-	Slope	ug/m^3/Year	4.9E-4	4.4E-5	2.6E-3	1.1E-2	6.5E-4	1.0E-3	4.8E-3	6.9E-3
	Intercept	ug m^{-3}	0.10	0.14	0.21	0.047	0.11	0.20	0.13	0.15
	% Change	%/year	1.9%	0.13%	4.8%	92%	2.4%	2.0%	15%	18%
NH_4^+	Slope	ug m^{-3}/Year	**-2.0E-2**	-1.3E-2	**-2.7E-2**	-9.7E-3	**-1.2E-2**	**-4.4E-2**	**-1.9E-2**	5.7E-2
	Intercept	ug m^{-3}	**0.96**	0.85	**1.3**	0.81	**0.89**	**1.6**	**1.2**	0.40
	% Change	%/year	**-8.2%**	-6.0%	**-8.3%**	-4.8%	**-5.3%**	**-11%**	**-6.4%**	56%
NH_3(g)	Slope	ug m^{-3}/Year	1.4E-3	3.1E-3	4.5E-3	1.5E-2	2.1E-3	-1.2E-2	**-3.3E-2**	-2.5E-2
	Intercept	ug m^{-3}	0.19	0.55	1.1	0.12	0.28	1.5	**1.9**	0.65
	% Change	%/year	2.9%	2.3%	1.7%	49%	3.0%	-3.1%	**-7.0%**	-15%
TNH_X	Slope	ug m^{-3}/Yr	**-1.8E-2**	-9.5E-3	**-2.3E-2**	5.0E-3	**-9.7E-3**	**-5.6E-2**	**-5.2E-2**	3.4E-2
	Intercept	ug m^{-3}	**1.1**	1.4	**2.4**	0.93	**1.2**	**3.2**	**3.1**	1.1
	% Change	%/yr	**-6.4%**	-2.7%	**-3.8%**	2.1%	**-3.3%**	**-7.1%**	**-6.8%**	12%
R_N	Slope	1/Yr	**5.5E-3**	5.5E-3	**8.1E-3**	**1.4E-2**	**5.1E-3**	**6.1E-3**	-7.4E-4	-4.1E-2
	Intercept	NA	**0.17**	0.40	**0.45**	**0.14**	**0.25**	**0.52**	0.62	0.67
	% Change	%/yr	**13%**	5.4%	**7.1%**	**40%**	**8.2%**	**4.7%**	-0.48%	-25%
pH	Slope	pH/yr	-2.6E-3	1.7E-2	9.9E-3	**9.1E-2**	2.7E-3	4.2E-3	2.2E-3	9.1E-3
	Intercept	pH	1.5	1.7	1.8	**0.76**	1.6	2.0	1.9	1.8
	% Change	%/year	-0.70%	3.9%	2.3%	**48%**	0.69%	0.86%	0.44%	2.0%
SO_4^{2-}	Slope	ug m^{-3}/Year	**-6.2E-2**	-9.0E-2	**-8.7E-2**	-7.7E-2	**-5.5E-2**	**-1.3E-1**	**-7.3E-2**	8.9E-2
	Intercept	ug m^{-3}	**3.0**	3.1	**3.7**	2.9	**3.0**	**4.5**	**3.6**	1.6
	% Change	%/year	**-8.4%**	-12%	**-9.3%**	-11%	**-7.2%**	**-11%**	**-8.1%**	22%

2.4.3 Particulate Ammonium (NH_4^+)

Reductions in observed SO_4^{2-} were matched by similar reductions in particulate ammonium (NH_4^+) in both networks. SEARCH sites with significant decreases in SO_4^{2-} had significant decreases in NH_4^+ that ranged from -0.012 ug/m^3 NH_4^+/year at OLF to -0.044 ug/m^3 NH_4^+/year at YRK. This trend was consistent with findings in the study by Saylor et al., (2015)[53] and Shi et al., (2017)[95].

CASTNET SO_4^{2-} and NH_4^+ results showed comparable trends to SEARCH, albeit some minor differences. The highest decrease of NH_4^+ (Table 2-1) was in the NE and SE (-0.02 ug/m^3 NH_4^+/year) and the lowest decrease was in CA with (-0.008 ug/m^3 NH_4^+/year). While the RK and MW regions saw reductions in SO_4^{2-}, only in the NE, SE and CA regions were reductions in NH_4^+ statistically significant.

2.4.4 Particulate nitrate (NO_3^-), Total nitrate (TNO_3^-), and Nitric acid gas (HNO_3)

Our analysis showed no statistically significant changes in $PM_{2.5}$ NO_3^- concentrations as SO_4^{2-} levels fell at CASTNET and SEARCH sites (the observations did not include coarse particle nitrate concentrations, which could be substantial in regions with sea salt or high dust loadings). In agreement with past studies, the NO_3^- concentrations were considerably lower than SO_4^{2-} concentrations (Table 2-1, Table 2-2), and remained so throughout the course of the study[48, 57, 96]. These low levels of NO_3^-, led to minimal effects on NH_4^+ levels in response to observed NO_x reductions. A general decrease in fine particulate TNO_3^- and HNO_3(g) was observed (except at PNS where monitoring ceased after 2009; See SI Figures B-7, B-8, B-13 and B-14), but only the HNO_3(g) trends in the NE and SE regions from CASTNET were significant.

These observations, when viewed with additional factors (i.e. temperatures) explain, in part, why the MW and RK did not have significant reductions in NH_4^+ despite high reductions in SO_4^{2-}. For instance, besides having the lowest SO_4^{2-} levels in the network, RK winter time temperatures were consistently lower than other regions (Figure B-12), providing favorable NH_4NO_3 formation conditions[46]. In the MW, the combination of low winter time temperatures and high NH_3(g) concentrations promotes NH_4NO_3 formation[97]. Further, pHs in the MW were generally higher than in other regions (consistently above three), another favorable condition for NH_4NO_3 formation[55].

To further investigate pH and NO_3^- results in the MW, we examined regional cation trends (Figure B-9 and Figure B-10) at all CASTNET sites. The MW had higher nonvolatile cation concentrations compared to other regions, an observation which can be attributed to contributions from dust, as shown in Ivey et al., (2015)[98]. Elevated nonvolatile cation concentrations led to higher pHs and increased portioning to aerosol nitrate. Similar observations have been reported in a number of studies which also show that high pH and more nitrate partitioning can be attributed to such aerosol components from dust when conducting a bulk analyses, assuming an internal mixture[74, 95, 99-101]. And this conclusion still holds, even if the aerosol is to a degree externally mixed.

While the study by Allen et al., (2015)[101] suggests that aerosol NO_3^- formation in submicron particles could occur as $NaNO_3$ and $Ca(NO_3)_2$ as opposed to ammonium nitrate, the high NH_4^+ concentrations in the MW support NH_4NO_3 formation, as the available cation data find too little of these components to explain much of the nitrate. We conclude this based on the low fall-spring temperatures in the MW, the seasons during which high nitrate is found, which would likely promote NH_4NO_3 formation. Further, when compared to CA trends with similar NH_3(g)

and cation levels, the lack of cold temperatures did not promote extra NO_3^- formation in CA as it did in the MW (Figure B-19). Also, the concentrations of NH_4^+ and NO_3^- in the MW (where NO_3^- levels were comparable to SO_4^{2-}) tended to be the highest in the entire network.

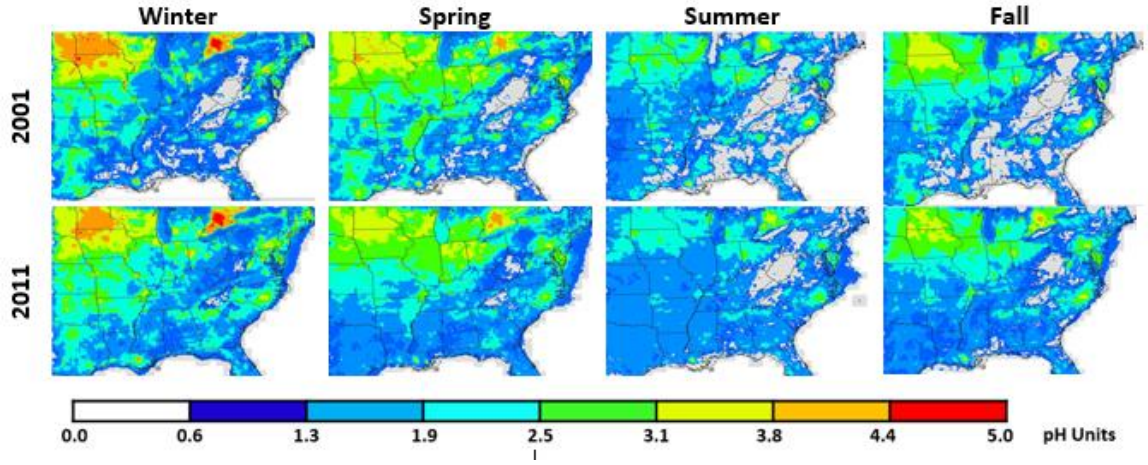

Figure 2-1: CMAQ-derived pH fields for 2001 and 2011 found using seasonal average compositions

2.4.5 Total Ammonium (TNH_x), Ammonia gas ($NH_3(g)$), and R_N

As with pH, annually-average NH_3(g) concentrations changed very little across the study period. CASTNET/AMoN, NH_3(g) remained stable, showing statistically insignificant changes at the 95% confidence interval in all regions from 2011 to 2015. Results for TNH_x were varied, with RK, MW and the NE showing yearly decreases of about -4% for all 3 regions, while the SE and CA regions exhibited yearly increases in TNH_x (+0.008 ug/m^3 and 0.02 ug/m^3 respectively). However, the slope from the linear trends in all regions (except the NE) were insignificant at α = 0.05. TNH_x peaks for MW (Figure 2-2), showed slightly different patterns than other sites (i.e. spring vs. summer peaks) which we attribute to contribution of NH_4^+ from NH_4NO_3 formation at

lower temperatures, fertilizer use and increasing volatilization from animal waste in warmer months.

Only CTR, JST, OLF, YRK, BHM SEARCH sites showed statistically significant decreases in TNH_x ranging from -3%/year to -7%/year, but no statistically significant change in NH_3(g) concentration was observed except at BHM (-7%/year). This negative downward trend result for TNH_x was also observed by Saylor et al., (2015), which is in contrast to expected increases in emissions[102]. However, this trend is explained by both the rapid deposition of NH_3(g), leading to a pseudo-state state balance between emissions and gas-phase deposition, leading to small changes in NH_3(g), accompanied by a reduction in aerosol ammonium tied to sulfate and nitrate.

Simulated seasonal and annual CMAQ concentrations of NH_3(g) showed relatively steady concentrations over the ten-year period (Figure 2-4 and Figure B-20), though wintertime NH_3(g) concentrations decreased in the upper northern states with smaller changes elsewhere.

A noticeable and consistent increase in the molar concentration ratio of NH_3(g) to TNH_x (R_N=[NH_3(g)]/[TNH_x]) was observed at all CASTNET/AMoN (Figure 2-2g) and SEARCH (except PNS and BHM Figure 2-3g) sites, another trend also noted by Saylor et al., (2015). This seasonal trend of increased R_N was significant at over 60% of SEARCH sites, CTR, JST, OAK, OLF, and YRK and in the SE region from the CASTNET/AMoN network. The slope for R_N at OAK is substantially higher than at other sites, though the observational period was short.

2.4.6 Neutralization Ratio f

The observed changes in species concentrations had a minor impact on the neutralization ratio *f* (Table B-9) at the CASTNET/AMoN or SEARCH network sites (apart from OLF; Table B-10). While values obtained for *f* were similar with other studies, as earlier stated, *f* is an inadequate proxy for acid neutralization or acidity[68, 95]. Results from the MW, where the presence of other cations besides NH_4^+, lead to an elevated pH, illustrate this point. Additional limitations of *f* are discussed further in the SI.

2.4.7 Fine Temporal Analysis

A comparison of modeled pH using a finer temporal scale was conducted at SEARCH sites. Instead of seasonal averages, monthly averages were used as inputs into ISORROPIA-II. Results of monthly modeled pH were statistically the same at all sites except at OAK. However, the p-values between both temporal scales results were similar, differing only by 0.005 points (Tables B-6 and B-8). This difference, which could be attributed to measurement errors does not obscure or contradict the overall results from the seasonal average analysis which points to minimal pH changes, despite significant reductions of sulfate at all sites. In fact, the statistical analysis results for other speciated $PM_{2.5}$ at this finer resolution mostly matched previous results at all the sites, with one or two sites changing (i.e. NO_3^-, SO_4^{2-} had same site statistical results, while TNH_x results changed, with OLF no longer showing statistical significance).

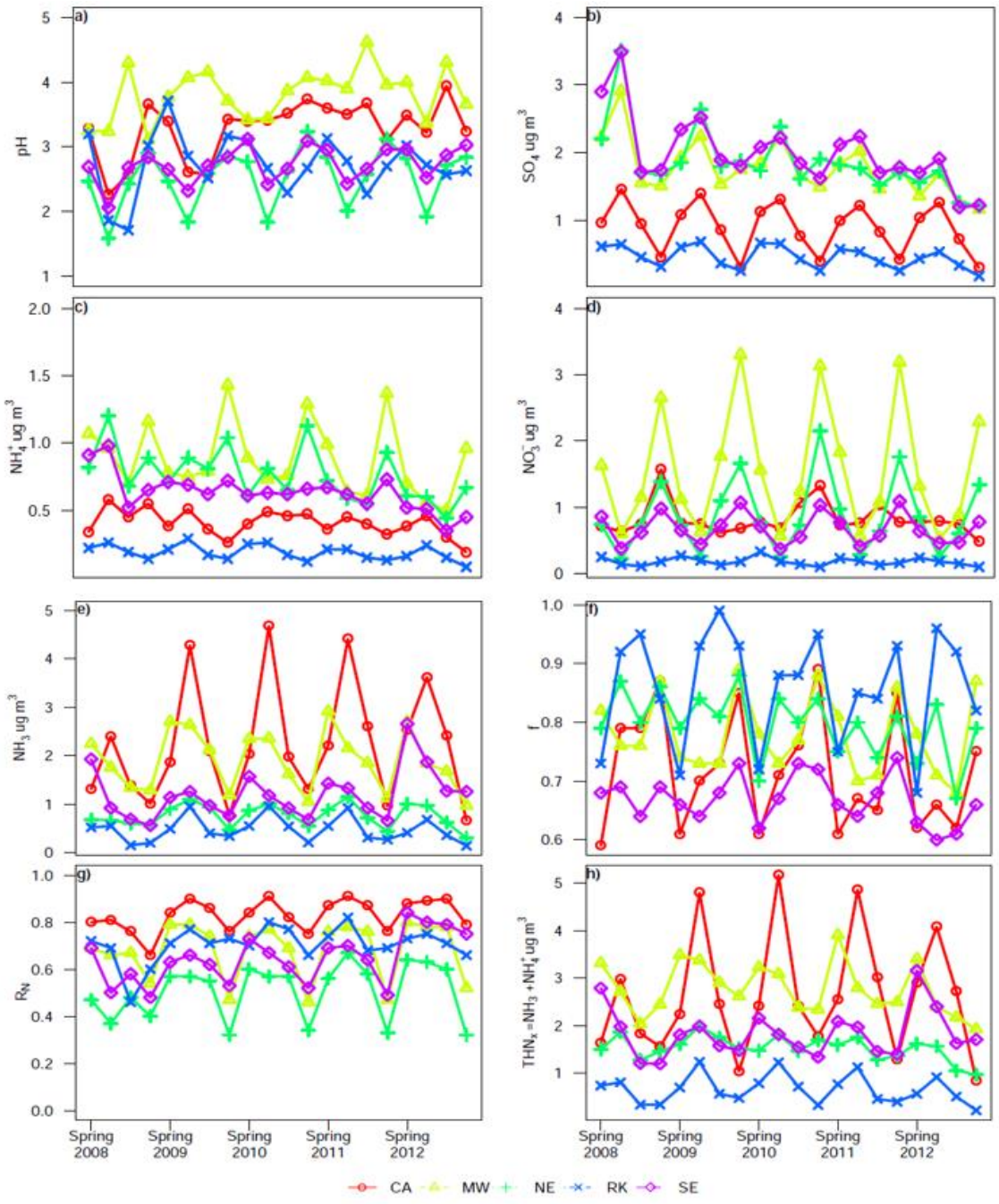

Figure 2-2: Linear regression time series trends for CASTNET/AMoN co-located sites labeled as follows, (2a): pH (2b): Sulfate (SO42-), (2c): Particulate ammonium (NH4+), (2d): Particulate nitrate (NO3-), (2e): Gaseous ammonia (NH3(g)), (2f): Neutralization Ratio (f), (2g): Gaseous ammonia partitioning molar ratio to total ammonia (RN), (2h): Total ammonia (TNHx). (CA: California; NW: Midwest; NE: Northeast; RK; Rocky Mountains; SE: Southeast).

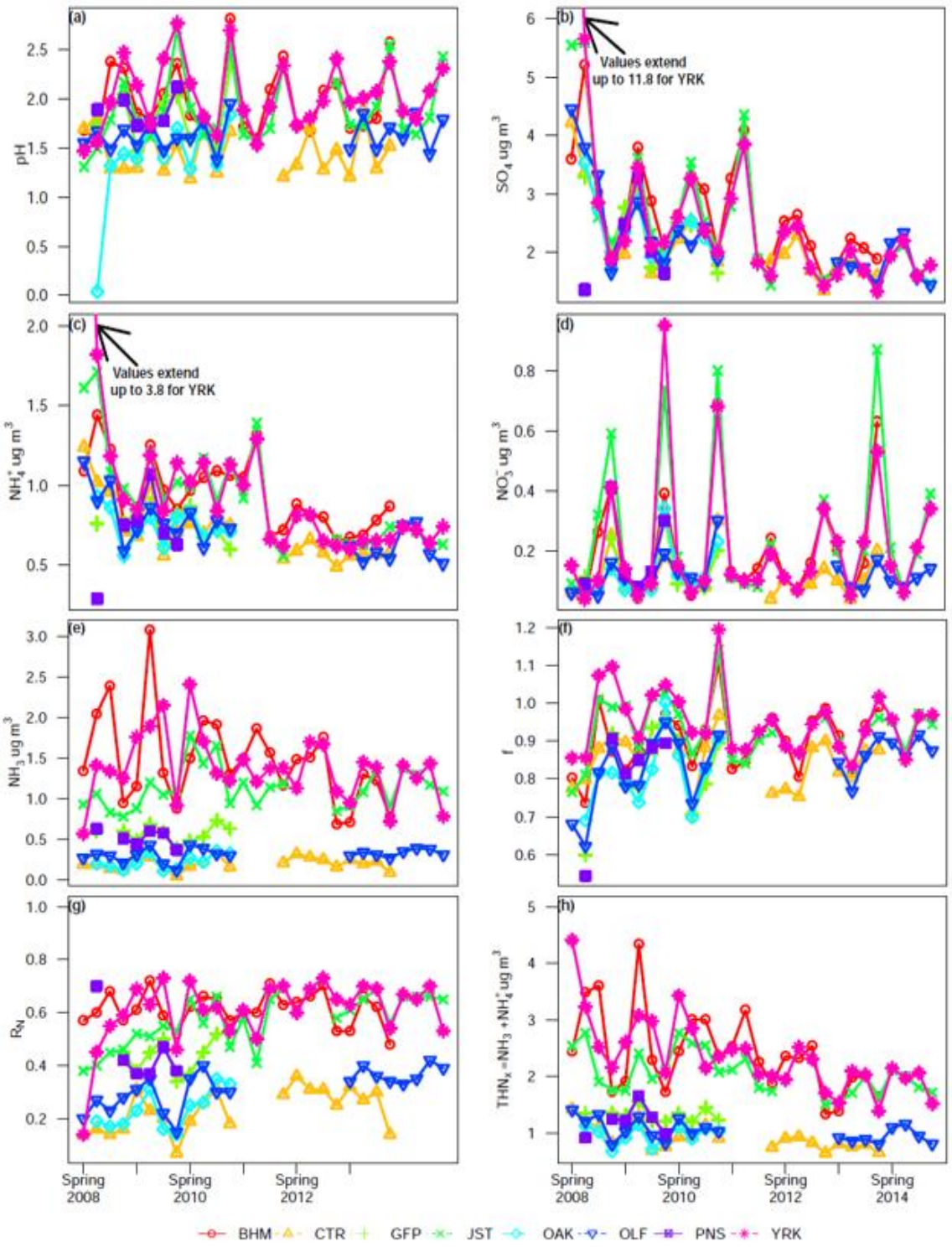

Figure 2-3: Linear regression time series trends for SEARCH sites labeled as follows, (3a): pH (3b): Sulfate (SO42-), (3c): Particulate ammonium (NH4+), (3d): Particulate nitrate (NO3-), (3e): Gaseous ammonia (NH3(g)), (3f): Neutralization Ratio (f), (3g): Gaseous ammonia partitioning molar ratio to total ammonia (RN), (3h): Total ammonia (TNHx). (Note: Results of PNS trends for sulfate, ammonium, and ammonia molar fraction are affected by limited data). (Note: Abbreviation for sites mentioned in Data and Methods section).

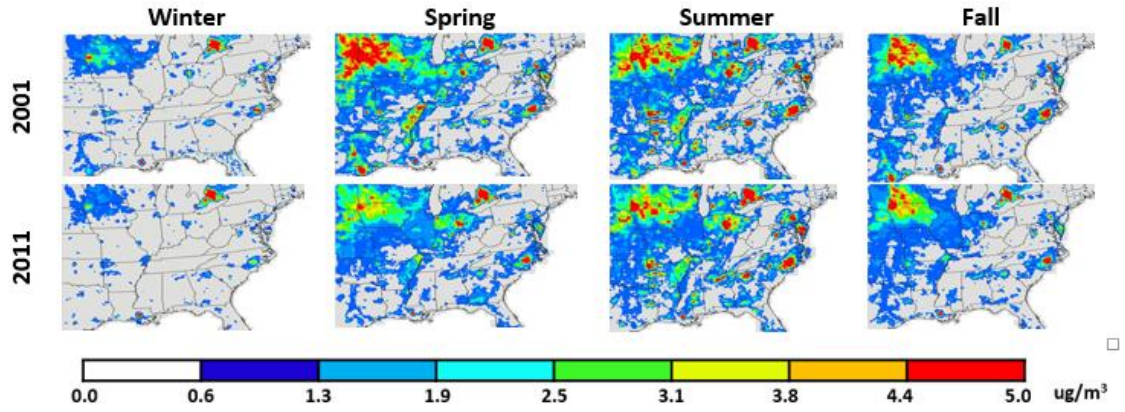

Figure 2-4: Seasonal average ammonia concentrations simulated by CMAQ for 2001 and 2011. The respective seasons, Winter, Spring, Summer, Fall consider temporal effects

2.5 Implications

Similar to prior empirical analysis in the Southeast, the results show that neither sulfur nor nitrogen oxide emission reductions are substantially impacting aerosol acidity at a national level for $PM_{2.5}$ particles. The two locations with statistically significant—but small—pH trends (< 1pH unit yr^{-1}), a near-coast SEARCH site in Mississippi (OAK) and another in California, did not have statistically significant SO_4^{2-} reductions (though annual average sulfate levels did decrease), or high SO_4^{2-} levels at the beginning of our analysis period as compared to other sites. Due to large contributions of $PM_{2.5}$ from vehicle motors[103], California had the second lowest SO_4^{2-} levels overall (Figure 2-2b), and also saw higher levels of NH_3(g) than most CASTNET/AMoN regions (Figure 2-2e). Similarly, OAK had the lowest SO_4^{2-} concentration (except PNS), although not considerably lower than CTR, and a high increase rate of NH_3(g) and NH_3(g) partitioning than other SEARCH sites. Thus, the common factor between OAK and California appears to be a combination of much lower SO_4^{2-} levels, higher NH_3(g) molar fraction increases and the presence of other cations. This means that if the contribution of nonvolatile cations doesn't change

significantly over time (as found in this analysis, Figures B-21 to B-23 & Tables B-6 to B-7), much lower levels of SO_4^{2-}, in addition to higher NH_3(g) concentrations are needed before significant changes in pH, or larger degrees of neutralization will be observed. This was also noted in Weber et al., (2016).

For example, the potential coupled effect of low SO_4^{2-} concentrations and high NH_3(g) on pH is further illustrated by comparing observations from JST, YRK and BHM SEARCH sites, all of which had high initial SO_4^{2-} levels and higher NH_3(g) concentrations than OAK and showed no statistically significant changes in pH. This demonstrates that even if NH_3(g) emissions were to remain stable or increase slightly as projected by Behera et al., (2013)[104] and Paulot et al., (2016)[102], it would not have a significant influence on acidity as aerosol sulfate levels decrease in response to reductions.

Observed reductions in SO_4^{2-} did not necessarily lead to NO_3^- substitution, as hypothesized, or as seen in other studies[57, 105]. This is because neutralization of SO_4^{2-} solely by NH_3(g) at current levels did not lead to substantially higher pHs or increases in gaseous ammonia which would promote NO_3^- formation. This effect of NH_3(g) levels on NO_3^- formation was also discussed in Blanchard et al., (2003) and Weber et al., (2016).

The NH_3(g) partitioning ratio (R_N) increased across all regions and most sites (except PNS and BHM) due to reduced SO_2 and NO_x emissions, as evidenced by reductions in $PM_{2.5}$ sulfate concentrations while NH_3(g) remained steady for reasons discussed earlier. Similar results observed by Saylor et al., (2015) and Shi et al., (2017)[95] indicate that this is not unexpected. Even in areas like the MW, where high levels of ammonium nitrate did not lead to significant reductions in NH_4^+, there was still a slight positive increase in NH_3(g) partitioning. However, the increased

partitioning contributions, along with projected emission increases of NH_3(g) did not appear to have any statistically significant impact on NH_3(g), which is impacted by the rapid cycle that exists between emissions and deposition rates[79, 102, 106]. This, along with observations noted in Guo et al., (2017) show that existing or higher levels of NH_3(g) are not likely to impact aerosol pH much. Results also show that R_N is also not likely to be impacted by NH_3(g) projected emissions as a result, but more by SO_2 and NO_x emissions.

TNO_3^- trends were also small, despite NO_x reductions[57, 79, 107, 108]. This is partly impacted by the fast deposition of HNO_3(g), along with a steady ammonia concentration. These findings in this study, would apply specifically to fine particulate nitrate, not coarse mode nitrate.

The statistically insignificant changes in pH corroborate and extend the findings by Weber et al., (2016) and further support that aerosol pH has been impacted little by reductions in sulfur dioxide and nitrogen oxide emissions across the US. Despite differences in slope direction of both trends due to differences in data (i.e. seasonal trend vs summer), both studies show insignificant changes in pH. The study also shows that reduced NO_x emissions had little impact on acidity (high or low) and that NH_3(g) levels remained stable. Lower sulfate levels with an abundance of ammonia, coupled with the presence of nonvolatile cations will be needed to see significant pH increases and acidity levels decrease. A thermodynamic analysis on the effects of different levels of ammonia on aerosol pH substantiate these findings[109]. Further, it is clear that earlier assumptions that NH_4NO_3 would increase due to sulfate reductions did not consider that the continued low pH, which is unfavorable to NH_4NO_3 formation in most regions and would prevent substantial increases in particulate NH_4NO_3. What remains unclear, however, is how long it will take to see significant changes in aerosol acidity as SO_2 and NO_x emissions continue to decline, but based on the results of the study and others, it is likely to be substantial. While reductions in aerosol acidity

may not change much in response to SO_2 and NO_x emission decreases, this does not mean that air quality improvements, in general will not be realized as particulate matter levels will continue to decrease in response[57, 110, 111].

Lastly, despite the limited amount of data (i.e. both CASTNET and SEARCH data only ranged between four to seven years), the conclusions and observations found are in line with other studies focusing on spatially limited data over larger time periods (Saylor et al., 2015; Weber et al., 2016). Further, air quality modeling results found in Vasilakos et al., (2017), along with the CMAQ results in this study, all of which have longer time and can link the results directly to emissions changes, found similar spatial and temporal patterns as the observations.

2.6 Acknowledgments

This publication was made possible by funding from the US EPA under grants R834799, R835882, and 83588001, the US NSF under award 1444745 and the Health Effects Institute. Its contents are solely the responsibility of the grantee and do not necessarily represent the official views of the supporting agencies. Further, the US government does not endorse the purchase of any commercial products or services mentioned in the publication

2.7 Supporting Information

Appendix B. Supplementary Information

CHAPTER 3. ORTHOGONALIZATION AND MACHINE LEARNING METHODS FOR RESIDENTIAL ENERGY ESTIMATION WITH SOCIAL AND ECONOMIC INDICATORS

Adapted from 'Abiola S. Lawal, Joseph L. Servadio, Tate Davis, Anu Ramaswami, Nisha Botchwey, Armistead G. Russell. Orthogonalization and machine learning methods for residential energy estimation with social and economic indicators. Applied Energy, https://doi.org/10.1016/j.apenergy.2020.116114

3.1 Abstract

The objective of this study is to identify the key factors that influence residential energy use in energy modeling. In doing so, we explore the impact of data transformations and analysis methods in developing residential energy models using social, economic, and demographic indicators at the zip code level in Atlanta, GA and for the entire state of Georgia. Orthogonalization algorithms, machine learning and variable selection techniques and ordinary least squares (OLS) are used to generate models for annual energy use for each zip code. Using log transformed yearly electricity estimation with orthogonalization yielded better estimates than other transformations [R^2=0.80, normalized root mean squared error (NRMSE) =0.33, parameters=15] and results for natural gas estimate were better (R^2=0.95, NRMSE=0.15, parameters=9). As expected, both models showed that socio-demographic factors are significant predictors. For natural gas, income and household make-up are the most important factors while electricity has a broader variety of indicator types. For electricity, despite the model accounting for 80% of electricity variation, the NRMSE was still moderately high (0.33). When electricity

use was separated into two clusters (high and low usage), the high use clusters appeared to match the interstate infrastructure morphology. These results show that electricity use, unlike natural gas use, is influenced by the morphology of the interstate roadway infrastructure and other social demographic factors.

Keywords: Residential energy estimation, machine learning, predictive models

3.2 Introduction

Energy use within the United States is primarily distributed among four main sectors: commercial, transportation, industrial and residential [112], [113], [114]. While industrial and commercial uses account for over 50% of total US energy consumption, residential consumption alone consists of about 23%, a fraction that will likely increase with future projected population increases[115]. Not only is the residential energy sector one of the major sources contributing to greenhouse gases (GHGs), it is also affected by climate change. For instance, Wang et al., (2017)[116] found that residential cooling loads were highly sensitive to climate change and would increase energy demand up to 30% in 2050, and the Annual Energy Outlook 2020 report[117] from the Energy Information Administration (EIA) projects a noticeable increase in cooling demand due to an increase in the number of cooling degree days. Results from these studies and others, show that the impact of climate on residential energy consumption could be quite substantial in future years to come.

The direct links between energy utilization, economic growth, and population to GHG emissions[118] and energy forecast trends show that CO_2 will only continue to increase considerably without effective mitigation measures [119], [120]. As urban cities tend to have highly integrated infrastructure systems[121] and high projections of population growth, they do and will continue to

account for a significant portion of energy demand and hence CO_2 emissions [120], [122]. Understanding the factors that drive energy demand is key to determining how to implement strategies for CO_2 mitigation, particularly in cities. Given the significance of the residential sector on climate (i.e. GHG emissions[123]) and energy consumption, it is very important to understand the critical factors that drive residential demand in order for policy makers to develop effective mitigation strategies. However, understanding residential energy use and the influencing factors usually starts with knowing and benchmarking actual energy consumption at fine spatial resolutions. Unfortunately, privacy concerns among others [15], [124], makes it difficult to obtain high resolution residential energy use from energy suppliers, leading many energy estimators and modelers to employ a variety of approaches and techniques to develop energy models[125]. These models generally fall under two types, deterministic (engineering) and statistical models[124]. Although we discuss both model types in further detail, this study will primarily employ statistical models.

Energy studies that utilize deterministic models typically employ engineering design parameters such as floor space, temperature, building size and occasionally, an estimate of occupancy activity as a variable [16], [126]. Although these models generally yield good correlations and estimates of energy use, they tend to fall short in accurately predicting post-design energy consumption as they do not capture actual occupancy characteristics such as behaviors, preferences, family size and economic makeup. Thus, these deterministic models tend to be more useful in guiding final building design parameters[124], and in exploring and evaluating different technologies and engineering parameters regarding building efficiency design than to estimate actual energy use. Further, another pitfall in using deterministic models is that they typically require experts to weigh in on what variables to use[127].

The latter factor points to one of the key advantages of statistical models. While deterministic models require detailed user knowledge, particularly of engineering principles, in determining the variables to incorporate, statistical models seek to estimate mathematical relationships between selected predictor variables to a response variable under the assumption that there is an association that is expressed in the empirical data[15]. Therefore less expert knowledge is needed, and the development and solution of complex engineering approaches are avoided. For this reason, statistical models are frequently used, though in many cases they are often combined with deterministic models and parameters to form hybrid models [16], [126].

In the case of deterministic, hybrid and statistical methods, some variables typically considered include household size, median income, household income, and gender demographics, though the number of these variables types in deterministic models might be limited. Such predictor variables relating to occupancy characteristics have been explored in few energy residential and commercial building modeling studies [128], [129], [130], [131], [132] and were found to be critical to energy use. For statistical and hybrid models, incorporating such variables is a complex process as a large amount of predictor variables can be selected. The sheer number of variables that can interact as result of many predictors, results in a high data dimensionality problem which is typically prone to errors from over fitting or multicollinearity [114], [15], [124], [133], [134], [15, 114, 124, 133-135]. The challenges of such problems are in selecting the critical variables from the large number of predictors that go into the final model. However, whittling down a large number of variables poses difficulties and the literature on variable selection techniques for high dimensional feature reduction in energy estimation is covered in only a few studies. Methods used in these studies include principal component analysis (PCA) or stepwise regression [135], [135, 136]. Forward and backward selection algorithms are other methods[135], though the latter is not possible when the

number of predictor variables **(p)** is greater than the number of observations **(n)**. Other studies utilize machine learning methods such as decision tress, artificial neural networks[137], [138], [138, 139], but these are even fewer in number than the aforementioned methods within this area of study.

In the development of a residential statistical energy model in this study, we aim to address the issue of high dimensional data and variable selection techniques with machine learning methodologies and data transformation techniques. We propose an orthogonalization method which has been used in some studies [140], [141] with varying degrees of success, but never in an energy estimation study. We demonstrate how orthogonalization facilitates variable reduction in high dimensional analysis and improves statistical model performance versus other data transformation methods. Our overall goal here is to show how these methods can improve statistical estimations of energy use and highlight the influencing factors that impact residential energy use.

3.3 Materials and Methods

3.3.1 Materials: Data Set

The area of our analysis includes the Zip Code Tabulated Areas (ZCTA) around and within the counties of the Atlanta-Sandy Springs-Roswell GA Metropolitan Statistical Area[142], and then the remaining ZCTAs in the greater state of Georgia in the United States. The first set of ZCTAs mentioned fall within 36 Georgia counties (SI Fig 1), which we refer to as metro Atlanta going forward in this study. We rely mainly on the American Community Survey (ACS)[143] which is run by the Census Bureau for our predictor variable data. Though other studies have utilized other databases such as the Public Use Microdata (PUMS) [144], [145], the Residential Energy Consumption Survey (RECS)[146] and the Residential Building and Energy Simulation (RBES)[147], those databases focus more on national and regional trends as opposed to the local and state analysis. Of note, the

ACS, which is managed by the United States Census Bureau, is the leading provider of quality data regarding the United States population characteristics, and provides the statistical quality standards for error estimates which are generally tabulated with each ACS data set. More information can be found at www.census.gov [148], [149].

Information for Georgia is collected for all 737 ZCTAs from the 2010 Decennial ACS and 2010 5-year estimates[143]. The ACS 2010 estimates were used in cases where Decennial 2010 data was not available for certain variables. 350 derived and primary variables (referred to as predictor variables) were gathered for both zip code and census tract spatial domains. Primary variables refer to predictor variables that are used directly from the ACS tables without any modification, while derived variables refer to those that are derived by combining two or more primary variables. A detailed list of all the variables can be found in SI Table C-1 (Appendix C). Overall, there were a total of 99 primary variables and 251 derived variables. 151 variables came from the 2010 Decennial dataset, 197 came from 5 Year estimate Tables and 2 were derived with ACS data and 2010 land use data from TigerLine Shapefiles, tabulated by the Census Bureau[150].

We developed models for two residential energy sources: electricity and natural gas. The electricity dataset consists of 2010 annual electricity data obtained from Georgia Power, while yearly natural gas use was obtained for 2008 from Atlanta Gas Light (SI Tables C-2 and C-3).

3.3.1.1 Predictor Variables

The predictors reflect a diverse range of information from social, economic to demographic in each ZCTA. For example, a social indicator might refer to the number of households, an economic indicator would refer to the median value of houses or household earned income, while demographic indicators could refer to the number of females, males, or African American and

Hispanic population in a particular zip code. Except for one discrete variable which was created to discretize the decadal age of housing units, all variables are continuous. Generally, the predictor variables fall under 7 broad categories (Table 3-1).

3.3.1.2 Response Variable (Energy Data for Electricity and Gas)

The electricity data from Georgia Power is for postal zip codes, largely situated in metropolitan Atlanta and captures 2010 annual residential electricity use. A total of 220 observations were collected for this study, although after data cleaning the number dropped to 196 due to the lack of data for some variables. Data for natural gas, included with the 2008 annual gas use was supplied for only 40 postal zip codes. These known energy ZCTAs served as the model training set, and the postal zip code for both energy forms were matched with the ACS ZCTAs that shared the same zip code identifier. The use of energy provided directly from the providers, rather than energy estimates that would have been required, further reduces sources of uncertainty and errors.

3.3.1.3 Spatial Domain.

With the exception of the energy data, all the predictor data sets cover two different regional sizes (i.e. census tracts vs ZCTA). The energy data were only available at the zip code spatial resolution for limited number of ZCTAs. Scaling methods (discussed in subsequent sections) were used to obtain energy estimates at a wider spatial domain (i.e. metropolitan Atlanta ZCTAs vs all Georgia ZCTAs).

Table 3-1: Predictor Variables

Main Category	Predictor Type Examples	
Economics	Poverty Inequality	Monthly Costs
	Income	Income Inequality
	Work Force Population	Wealth Resource
Population Demographics	Gender	Age
	Total Population	Ethnicity
Housing Occupancy and Tenancy	Owned vs Rented	
	Number occupied units	
Education	Education Level	
Housing Units and Amenities	Year built	Housing structure (i.e. detached)
	Housing Amenities: No of Vehicles	Household Amenities: No of Room
	Housing Amenities: Plumbing	
Land Use (Urban Morphology)	Population density	No of Occupied Housing Units
	Housing density	Vacant Housing Units
Household characteristics	Household Makeup	Household Size
	Household type	

3.3.2 Methods

The methods, some of which include machine learning, regression and data transformation methods are described as follows and were evaluated using a wide range of techniques.

3.3.2.1 Machine Learning Methods

One set of methods we utilized to develop predictive energy models were based on machine learning. The entire data set (i.e. all 737 ZCTAs) were sorted into different data subsets (predictive and model)[151]. The model data set typically consists of known response variables: residential

energy use in this case (gas and electric) along with a full set of predictors and is used to find the appropriate variables and regression coefficients. The predictive data set also consists of predictor variables, but with unknown response values which will be estimated from the results generated from the model data set. The model data set is typically further divided into additional subsets, such as training, test, validation and withheld subsets. As in other studies, we use cross validation statistical metrics from the withheld and/or test data set to select the best model and the validation data set (also taken from model training set) to evaluate final model performance. For our data set, the zip codes with given energy use from Georgia Power and Atlanta Gas Light serve as the model data set. The remaining ZCTAs were the predictive data sets.

3.3.2.2 Data transformation

Developing statistical models usually involves data transformation as a way to improve model performance by minimizing the impact of outliers, skewed distributions and differences in scaling among predictors [134], [135]. This can be the most critical step in development of statistical models[152] and can drastically affect the results of analyses. Interestingly, few energy modeling studies have explicitly investigated the impact of transformations.

Common data transformation methods include conversion of variables into discrete values [134], [145], lognormal transformations [139], [139, 153] or z-scores which normalizes according to mean and standard deviation [135], [154]. The transformation of predictors variables via z-scores and log transformations not only mitigates the impact of outliers, but allows for performance and statistical diagnostics of the model, such as residual plots and regression coefficient confidence intervals to be assessed using normal distribution table properties. Other methods such as principal component analysis (PCA), which not only reduces dimensionality within a data set, also eliminates

multicollinearity by transforming the predictors into a new set of variables that are orthogonal to each other [155], [156], [157], [155-158]. However, the new PCA variables (i.e. eigenvectors) do not allow for direct relation or association of any observation with each predictor. Therefore, making direct inferences of the exact impact a predictor might have in a statistical model that uses PCA is not easily done.

In this study, to address the issue of normality, scaling and multicollinearity, we utilize a less commonly used data transformation method known as Gram-Schmidt orthogonalization. Gram-Schmidt is an orthogonalization method for converting a set of vectors into an orthonormal basis. This method has been used in some large data studies [140], [141], [159] though to a much lesser extent in energy modeling studies. In general, an advantage of this type of orthogonalization versus other methods like PCA is that unlike the orthogonalized predictor components obtained in PCA (i.e. X^{nxp} vs V^{pxp} where X is original matrix with n observations and p predictors, and V is the transformed matrix with p predictor dimensions), it retains the same vector space dimensions, as the original predictor matrix (i.e. X^{nxp} vs. V^{nxp}). Thus, each new predictor column is easily discerned and can be compared directly to the original observations. Like z-scores, the predictor values in this case are unitless and standardized, therefore, the model coefficients in the regression are also standardized. Similar to z-scores [160] which can increase the regression predictive analytic power by removing the variability in raw values and improving the signal to noise ratio via standardization, orthogonalization in this regard does the same thing with an extra advantage of having essentially all the variables be orthogonal to each other and uniformly distributed.

Though other orthogonalization methods (e.g. Householder and Givens transformations) exist [161], [162], Gram-Schmidt orthogonalization is more commonly used. Both a Classical (CGS)

and Modified Gram-Schmidt (MGS) exist and we assess the performance of both methods. A more thorough description can be found in the supplement (Appendix C).

3.3.2.3 Regression and Improvement techniques

Statistical regression methods assess the relationship between variables to a response variable [135], [147]. The most commonly known method for regression is Ordinary Least Squares (OLS). The OLS model, as represented by equation 1 shows the expression for a multivariable linear regression model (MVR). Here, y is the response variable, X is a predictor variable, theta Θ represents the parameters and ∈ is the error term. The subscript *i* refers to each observation.

$$y_i = \theta_0 + \theta_1 X_{i1} + \theta_2 X_{i2} + \cdots \theta_p X_{ip} + \in_i \qquad (2)$$

Model performance and general diagnostics generated from OLS are analyzed using normal probability distributions to test for statistical significance and require certain assumptions such as that the error variances are assumed to be equal and are independent for statistical significance to be assessed appropriately. Additional assumptions assume that the errors are normally distributed with a constant variance ~ $N(0, \sigma^2)$ [135].

Besides data transformations, there are other ways to improve results of regression models. Common techniques utilized in some studies involve clustering methods, to group observations into similar classes before regression. For instance, Gao et al. (2014)[163] clustered buildings by certain features and Hsu (2015)[164] separated homes from cold and hot regions to improve regression results. However, such methods were impractical for our study as we did not yet have a specific set of predictors to cluster with and we could not assume energy use clustering would

be effective. So we employed a less commonly used method known as ensemble averaging. A description of this method is discussed further in the supplement.

3.3.2.4 Variable reduction and selection techniques

As noted in Hsu [15], not many papers discuss in detail, variable selection techniques or the complications arising from high dimensional (or big data sets) including the interaction of many variables and combinations. As previously mentioned, the danger with multicollinearity that can arise from many variables is to cause errors in parameter estimates. Thus, concerted efforts are necessary to reduce the dimensionality of variables needed in the final model.

Variable selection techniques fall under supervised and unsupervised techniques. Supervised selection methods typically involve an initial elimination of redundant variables by the researcher, using some cut off criterion to perform the variable selection (i.e. Pearson's correlation coefficient or the t-test) [147], [147, 165].

An unsupervised learning technique on the other hand, can perform variable selection by finding patterns not necessarily known or obvious to the researcher. Such methods include the use of PCA and variations of it such as Partial Least Square Regression (PLSR)[136] among others for dimensionality reduction [155], [156], [157], [158] [155-158, 166]. The advent of machine learning has introduced many methods in unsupervised variable selection techniques as well. We investigated such methods that included techniques like random forest, regression trees, elastic net and lasso, and neural networks, but similar to other cases, the results were varied and were inconclusive [167], [167, 168].

In this study, we used the stepwise fit algorithm for variable reduction. Stepwise fit is an interactive algorithm[169] which considers all possible combinations for all the variables and selects which parameters will remain in the model based on the chosen criteria, in this case a significance level. A widely used technique in many studies [151], [163], its implementation and theory has been covered extensively in many statistical textbooks [170].

3.3.2.5 Model Evaluation and Diagnostics

Many energy use studies, though based on different methods, are similar in their approach in assessing the model with statistical metrics [167], [167, 171]. Hsu (2015)[164] analyzed the stability of clusters by evaluating coefficient stability against the number of clusters for each method. Lyu et al. (2017)[141] conducted a similar analysis to assess the effect of the number of features on classification accuracy. Hsu[15], in his 2015 energy study used the mean-square error (MSE) of cross validation sets to determine the best parameter for different statistical regression techniques and parameters.

In similar fashion here, we use averaged values of tabulated statistics (Table 3-2) from cross validation sets to evaluate model performance. In addition, model diagnostics were conducted with the residual plots to check normality assumptions and independent distributions on error. The t statistic was evaluated to determine the significance of each parameter and the Variance Inflation factor (VIF), which tests for multicollinearity was also evaluated. Other model diagnostics recommended in other studies include other results such as the prediction intervals[172].

Table 3-2 Statistical variables for model validation

Metric	*Metric Formula*	*Metric Formula*
SSE_U	$\hat{\sigma}^2 = \frac{\sum_{i=1}^{n} {e_i}^2}{n-p} = \frac{SS_E}{n-p} = \frac{\sum_{i=1}^{n}(y_i - \hat{y}_i)^2}{n-p}$	Unbiased Sum of residuals
SSE	$\hat{\sigma}^2 = \sum_{i=1}^{n} {e_i}^2 = SS_E = \sum_{i=1}^{n}(y_i - \hat{y}_i)^2$	The biased estimated residual sum for a model with *n* observations
MSE	$MSE = \frac{SS_E}{N} = \frac{1}{N}\sum_{i=1}^{N}(y_i - \hat{y}_i)^2$	Mean Square Error
RMSE	$RMSE = \sqrt{MSE} = \sqrt{\frac{SS_E}{N}} = \sqrt{\frac{1}{N}\sum_{i=1}^{N}(y_i - \hat{y}_i)^2}$	Root Mean Square Error
NRMSE	$Mag = \frac{\sqrt{\hat{\sigma}^2}}{\bar{y}_i} = \frac{\sqrt{\frac{1}{n-p}\sum_{i=1}^{N}(y_i - \hat{y}_i)^2}}{\frac{1}{N}\sum y_i}$	Normalized Root Mean Error.
SSR	$SS_R = \sum_{i=1}^{N}(\hat{y}_i - \bar{y}_i)^2$	Variation of the Regression
SST	$SS_T = SS_E + SS_R$	Total Sum of the variance SS_T
R^2	$R^2 = \frac{SS_R}{SS_T} = 1 - \frac{SS_E}{SS_T}$	Coefficient of Determination (Variance percentage from the regression)
R^2 adjusted	$R^2 = \frac{SS_R}{SS_T} = 1 - \frac{SS_E}{SS_T}$	Unbiased coefficient of determination
NMB	$NMB = \frac{1}{N}\sum_{i=1}^{n}\frac{(y_i - \hat{y}_i)}{y_i}$	Normalized Mean Bias

3.3.2.6 Model Set Up

One of the main objectives of this study was to explore the impact of different data transformation techniques to address multicollinearity in generating statistical models for energy use. We focus mainly on orthogonal data transformation techniques and not only incorporate variations of Gram-Schmidt orthogonalization methods, but also principal component analysis methods for comparison. In addition, as it is widely used, we explore the impact of z-scores as well. In total, 5 different transformation techniques are explored (z-score, CGS, MGS, PCA, and PLSR) in this study.

For all five transformation methods, we evaluated at two spatial extents; metropolitan Atlanta ZCTAs and all Georgia ZCTAs. In the case of orthogonalization methods (CGS and MGS), as the order of orthogonalization affects the output (see supplement), orthogonalization of the matrix occurred after the predictor vectors were arranged in descending order with the Euclidean norm, denoted as $\|\mathbf{v}\|$.

Annual electricity use ranged from 1.4×10^4 to 2.8×10^8 Kwh/year. To reduce the range, as in other studies[137], we transform the electricity response into a log normal variable using Box-Cox log transformation. Here, for the Box-Cox transformation, we use a lambda value of 0.5 on the y response as it gave the best results (SI Figure C-14). For natural gas, no transformation was necessary and the range here was no more than 2 orders of magnitude. We find this was similar to the studies by Chen et al. (2016)[153] and Salari et al. (2017)[171].

In total, 196 and 32 observations were used for electricity and natural gas respectively as the full model training set for metro Atlanta. The predictive data set for greater Georgia ZCTAs were 410 for electricity and 575 for gas use. Using a seeded random generator, an initial validation

data set (6% (n = 6) electricity and 5% (n=3) gas) was taken from the full model training data set and additional sub sample set was taken for the withheld. A 10 fold and 5 fold cross validation (CV) sample set was used for electricity and natural gas respectively, with the CV representing a withheld dataset. We describe in further detail within the supplement, the model evaluation process.

3.4 Results

3.4.1 Data Transformation Method Analysis

In comparing all methods, we find that the modified orthogonal algorithm (MGS) best preserves orthogonality among all the predictors. Unlike MGS, the round-off errors with CGS[173] causes the predictors to lose orthogonality properties as the sequence proceeds. Another benefit of MGS is that the matrix rank matches the number of predictor column vectors. All other transformation methods, beside MGS yield a matrix with a lower rank (i.e. rank is less than number of predictor columns), which is an indication of a low orthogonality among predictors with those methods. Figure 3-1 shows how well the MGS method compares with data transformation methods using CGS, z-scores and none at all.

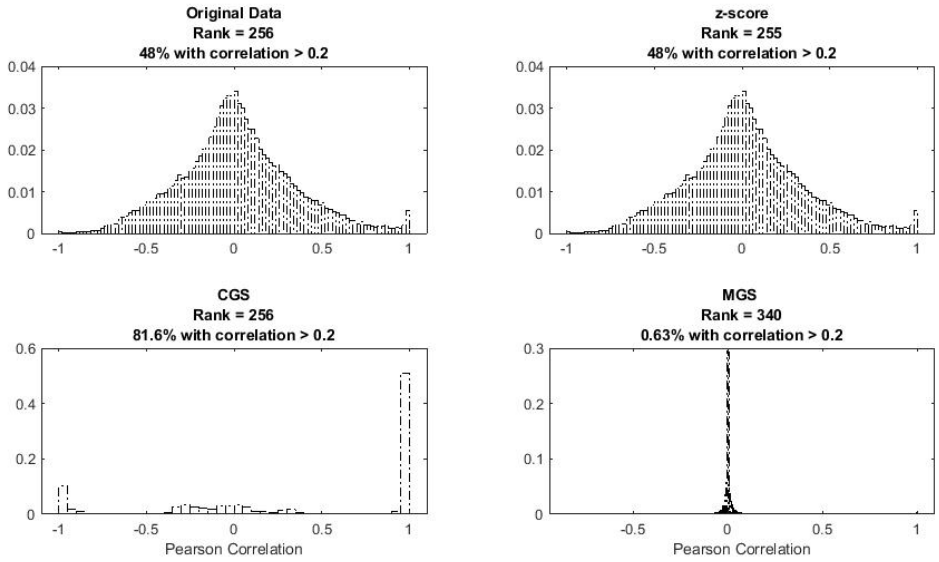

Figure 3-1: Probability distribution of predictor's correlation coefficients.

3.4.2 Regression model results

The results are presented for all the data transformations in Tables 3-3 to 3-6, with details of model predictors in Table 3-7 to 3-10. The best performing model or statistically significantly predictors are highlighted in emboldened font. The results of all transformation methods for all 196 metropolitan ZCTAs listed in Table 3 indicate that MGS had the best results overall. The original data set and z-score transformation showed evidence of multi-collinearity and similar estimation bias (NMB). The CGS method appeared to have comparable results with MGS training set R^2 values, even with a smaller number of predictors, but it had the highest NMB and NRMSE for all 3 data sets (i.e. full, withheld, validation) as compared to other methods. The principal component methods (PLSR and PCA) did not appear to offer any significant advantages over the MGS, even with more predictors. However, four of the MGS predictors were found to be insignificant (Table 3-7). Although the maximum VIF was above the recommend value of 10 for

some of the predictors from the MGS method, it was only for two variables and it was not substantially higher than the recommended cutoff. As presented in SI Fig C-6, only two predictor categories (v5-Number; SEX AND AGE - Male population & v10-Estimate; VALUE - Median (dollars)) exhibited high Pearson correlation coefficients with each other and coincidentally, they were the same predictors with slightly high variance inflation values above the recommended cutoff value of ten[171].

Table 3-3: Differences in model performance among the data transformation techniques for Metropolitan Atlanta ZCTAs for electricity use (n = 196), are presented here.

			Full				Ensemble		
No	Data Method	Model size	Train R^2	Train NRMSE	Train NMB	Train Max VIF	Average Withheld R^2	Avg Withheld NRMSE	Avg Validation NRMSE
1	None	12	0.77	0.35	-0.68	961	0.69	0.40	0.22
2	Z scores	12	0.77	0.35	-0.68	961	0.69	0.40	0.22
3	CGS	6	0.75	0.37	-0.79	1.41	0.68	0.40	0.24
4	**MGS**	**15**	**0.79**	**0.33**	**-0.61**	**13**	**0.75**	**0.35**	**0.17**
5	PCA	20	0.77	0.37	-0.70	N/A	0.70	0.39	0.23
6	PLSR	20	0.78	0.35	-0.65	N/A	0.73	0.36	0.23

Evaluation of the performance of different transformation techniques on the full data set (n=606) was performed (Table C-4). In all cases, the data set was transformed before separating the known observations (n = 196 training data set) from the unknowns (n = 410). Selection of the final model was based on the measure of the metrics for R^2, NRMSE, VIF, and NMB for the training, as well as the R^2 for the withheld. Similar to previous results, MGS had the best statistical performance.

Table 3-4: Differences among the data transformation techniques with the training data set in modeling electricity use for all Georgia ZCTAs (n = 606) are shown.

			Full				Ensemble		
No	Data Method	Model size	Train R^2	Train NRMSE	Train NMB	Train Max VIF	Average Withheld R^2	Avg Withheld NRMSE	Avg Validation NRMSE
1	None	3	0.71	0.40	-0.92	1.3	0.65	0.35	0.30
2	Z scores	3	0.71	0.40	-0.92	1.3	0.65	0.35	0.30
3	CGS	6	0.75	0.37	-0.79	1.12	0.75	0.29	0.21
4	**MGS**	**15**	**0.79**	**0.34**	**-0.55**	**1.6**	**0.82**	**0.25**	**0.24**
5	PCA	20	0.77	0.37	-0.69	N/A	0.74	0.29	0.24
6	PLSR	20	0.78	0.35	-0.64	N/A	0.76	0.28	0.23

Natural gas (Table 3-5) use in metropolitan ZCTAs in Atlanta was assessed with the same setup as electricity, although PCA and PLSR analysis was not conducted here due to the small training data set size of only 32 observations. Further, unlike electricity estimates and similar to the study by Chen et al. (2016)[153], log transformation of natural gas use was not necessary, as seen in the Box-Cox plot (SI Fig C-15) [174]. Although the MGS model had the best results in terms of eliminating multicollinearity, a look at the *p*-values in the regression models (SI Tables C-9 and C-10), as well as the correlation color maps (SI Fig C-22) suggest that the CGS had the most statistically significant variables in its model. MGS performance here can be explained, partially, by the small size of the training set. It should also be noted here that with MGS, the small training set size required a small addition of 1E-7 to the predictors in the training set. This value was also added to the other transformation methods to ensure consistency.

Table 3-5: Differences in model performance among the data transformation techniques for Metropolitan Atlanta ZCTAs for gas use (n=32) are presented here.

			Full				Ensemble		
No	Data Method	Model size	Train R^2	Train NRMSE	Train NMB	Train Max VIF	Average Withheld R^2	Avg Withheld NRMSE	Avg Validation NRMSE
1	None	9	0.98	0.08	0.00	11	0.99	0.05	0.17
2	Z scores	10	0.98	0.09	-0.02	19	1.00	0.04	0.20
3	**CGS**	**9**	**0.95**	**0.15**	**-0.02**	**13**	**0.95**	**0.11**	**0.21**
4	MGS	11	0.94	0.17	-0.05	5	0.94	0.13	0.28

Utilizing the full data set (n=606) for gas estimation, the data set was transformed before separating the known observations (n = 32 training data set) from the unknowns (n = 574). The MGS model had the best performance in eliminating multicollinearity among the predictors, which were largely significant (Table 3-6; SI table C-17)

Table 3-6: Differences among the data transformation techniques with the training data set in modeling gas use for all GA ZCTAs are shown (n=606).

			Full				Ensemble		
No	Data Method	Model size	Train R^2	Train NRMSE	Train NMB	Train Max VIF	Average Withheld R^2	Avg Withheld NRMSE	Avg Validation NRMSE
1	None	10	0.98	0.09	0.00	23	0.99	0.06	0.19
2	Z scores	10	0.98	0.09	0.00	23	0.99	0.06	0.19
3	CGS	9	0.96	0.13	-0.02	14	0.97	0.11	0.18
4	**MGS**	**10**	**0.95**	**0.15**	**-0.02**	**2**	**0.93**	**0.13**	**0.09**

3.4.3 Model assessment

Overall, the MGS method had the best results for electrical energy usage predictions (Tables 3-3 & 3-4) and ensemble averaging improved results, generally for all methods (SI Figs C-12 and C-13). While the scatter, residual and quartile plots (SI Figs C-2 TO C-4, C-25 TO C-27) for all methods look fairly similar, the correlation color maps (SI Figs C-5 & C-6) show that orthogonalization is effective in reducing multicolinearity. Most of the predictors in the CGS and

MGS models were significant at an alpha level of 0.05 and lower, and correlation between most variables was noticeably reduced, when compared to z-scores and untransformed model results. For the electricity models, as the diagnostic plots between CGS and MGS were similar, the MGS model was selected as the better model as it led to other statistical metrics being improved. The proposed order of orthogonality also shows good success as well and the orthogonal models had better performance than PCA and PLSR models. Exploring the interaction effects [175], [175, 176] plots between the predictors and electricity use of the MGS model (Table C-3) further shows the impact of transformation in regression models. Most of the untransformed predictors had little to no interaction effect with the dependent variable (SI Fig C-10) than the transformed variables (SI Fig C-11) for which most had a strong interaction effect with the dependent variable.

For metropolitan ZCTAs, results for gas estimation show that the CGS model was the best. While diagnostics plots were similar in performance across the board (SI Figs C-18 TO C-20), correlation among variables in CGS was better than MGS and the other transformations (SI Fig C-22). Although the models with no transformation and z-scores did perform better than the orthogonalized models based on most of the metrics (Table 3-5), most of the variables were not statistically significant at alpha of 0.05.

A couple reasons explain the poorer performance of MGS over CGS with the metropolitan ZCTAs in gas usage estimation. The small size of the training set affected MGS orthogonalization, as successful orthogonalization with MGS was not possible without adding a small numerical value 1E-7 to the data set when only the 32 metropolitan ZCTAs were used. This value was added for all transformations to ensure consistency. Further, in the final step of the variable selection, the small training set made it difficult to select the optimum variables, and so it is possible that with a larger training set, MGS performance would have improved in comparison to CGS. This

assumption is reflected when using all GA ZCTAs (n=606) to orthogonalize and in the correlation plots (Table 3-6, SI Figs C-22 and C-32). With a larger data set, the MGS model performed as well as the other transformations, but had more significant predictors and lower correlation (SI Tables 14 to 17) and so was chosen as the best model.

Based on the performance of the models, we discuss results of the electricity models using MGS results and results for natural gas using the CGS for the metropolitan ZCTAs and MGS for all GA ZCTAs in the discussion section.

3.5 Discussion

3.5.1 Interpretation of regression results

Assessing the impact of the predictor coefficients in the MGS and CGS regression models will be similar to methods used in z-score interpretation and analysis [177]. In z-score models, the relative magnitudes of these parameter coefficients, in addition to the *p*-values emphasizes the importance of that predictor on the dependent variable. While the interpretation of orthogonalized predicted coefficients is similar, unlike z-scores where the influence of an observation predictor value represents the magnitude of deviation away from the mean, the orthogonal predictors do not hold the same meaning, although they do reflect an orthogonal reference to other predictors in the data set.

Thus, to assess the regression results and their implication on the social indicators, we employ two techniques here. First, we look at the magnitude of the regression coefficients as the relative contribution and importance of each predictor together with the significance value on the dependent value. As we were able to show higher correlation with ZCTA annual energy use with

transformed variables than the data in its original format, this assessment is still insightful. Second, as in the case of the electricity model, we conduct principal component analysis to assess the variation in variables with energy use. We discuss the results of metropolitan electricity and gas use in further detail and include results of the model when all GA ZCTAs are used.

3.5.1.1 Metropolitan Atlanta ZCTA electricity use

The results of the MGS orthogonalized model (Table 3-3) were analyzed by assessing the impact of each predictor (Table 3-7). Note, all variable numbers in this section are from Table 3-7 and are denoted with a "v" prefix based on the magnitude of regression coefficient and statistical significance. We also map the predicted electricity use by ZCTA alongside actual electricity use (SI Fig C-33) with the MGS model, which show similar patterns of spatial distribution. Of note, all variables, with exception of median dollar value of the house and male population (the only largely two positive transformed variables: SI Fig C-16) were normally distributed with a mean of zero.

The indicators in the model fall into gender, ethnic, education, tenancy and economic categories (Table 3-1). Two variables in particular, male population, and median house value had high VIFs and represent a significant impact on electricity use as indicated by their regression coefficients and *p*-values. Both also have the largest regression coefficients relative to the others.

The median house value (v10) with the largest regression coefficient and the most significant predictor stands out and highlights the importance of economic resources with energy use. The male population (v5) as well as the female population over 18 (v2) were other significant variables, though with opposite regression coefficient signs. Although v5 did not specify an age, it likely refers to the older male population members, based on the presence of significant variables

such as variable 8 which refers to the Percent Tot Male Pop Bachelor and Higher degree/>25yr Tot Male Pop.

Total population (v15) within each ZCTA was significant, unlike the total population per number of housing units (v4), indicating that total population as opposed to population density is more critical in metropolitan ZCTAs energy models, a finding seen in other studies[153]. The tenancy ratio between renters and owners (v9) showed up as statistically significant along with family households (v11) and both essentially had the same regression coefficients and direction, indicating that the ratio of renters and owners and family households are similarly connected with electricity use.

The presence of household types (i.e. families and non-families), education, median house value and income variables in the statistical model, indicate that household types, education, tenancy types and economic resources are significant drivers of electricity use. Of interest, population density was not a factor in the final model, meaning that electricity use is not necessarily driven by certain demographic land use patterns.

Lastly, within the population demographics category, ethnicity, specifically the demographic of white which includes Hispanic populations (v1) was significant. As all the metropolitan Atlanta ZCTAs consists largely of this demographic, any variation of this predictor would have a significant influence on estimated energy use.

Table 3-7: Linear Regression fit of final model. ZCTA electricity use is the dependent variable.

Variable No	Variable Name	Model Coefficient	p-values
1	**White with Hispanic population**	**-4.1E+04**	**0.00**
2	**Number; SEX AND AGE - Female population - 18 years and over**	**1.9E+04**	**0.00**
3	Female/Male ratio pop 25 and older	9.3E+03	0.06
4	Total Population / Number of housing units	-8.1E+03	0.11
5	**Number; SEX AND AGE - Male population**	**-9.6E+04**	**0.00**
6	Number; RACE - Total population - One Race - Some Other Race	-8.8E+03	0.07
7	**100*Owner Occupied by Age < 24/Total Owner-Occupied Households**	**1.1E+04**	**0.04**
8	**Percent Tot Male Pop Bachelor and Higher degree/>25yr Tot Male Pop**	**1.1E+04**	**0.02**
9	**Ratio Renter-occupied housing units to Owner-occupied housing units - Some college or associate degree**	**-1.3E+04**	**0.03**
10	**Estimate; VALUE - Median (dollars) of house**	**2.8E+05**	**0.00**
11	**Number; HOUSEHOLDS BY TYPE - Total households - Family households (families) [7]**	**-1.3E+04**	**0.01**
12	**100*No of occupied Housing Units with Wood/Total Occupied Housing Units**	**-1.2E+04**	**0.01**
13	**Estimate; INCOME AND BENEFITS (IN 2011 INFLATION-ADJUSTED DOLLARS) - Median nonfamily income (dollars)**	**3.3E+04**	**0.00**
14	Percent; EMPLOYMENT STATUS - In labor force pop over 16	-7.2E+03	0.10
15	**Number; SEX AND AGE - Total population**	**6.5E+04**	**0.00**

To better interpret the model results and the direction of predictor influence on electricity use (i.e. high or low), we applied PCA. Utilizing the k-means algorithm in MATLAB, we saw evidence of two prominent clusters for known electricity use (Fig 3-2). A boxplot of both energy clusters showed that the areas in the red were categorized as high energy use ZCTAs, while those in color blue were considered low energy ZCTAs (see also SI Fig. C-9). For the log transformed electricity clusters, a total of 92 ZCTAs fell in the high use with about 104 in the other.

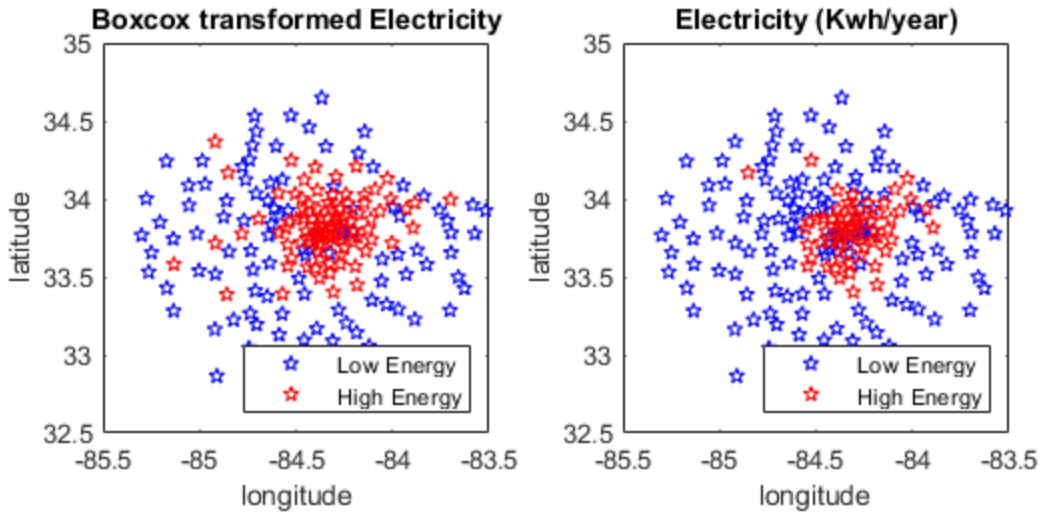

Figure 3-2: The spatial distribution of high and low ZCTA electricity use clusters. (Boxcox transformed and un-transformed clusters.)

Using the k-mean clusters for grouping between high and low energy use, a principal component analysis plot was constructed with the transformed predictors together with log transformed electricity use in R using the gg-biplot package[178] in Fig 3-3. A summary of the PCA components is found in the SI table C-18.

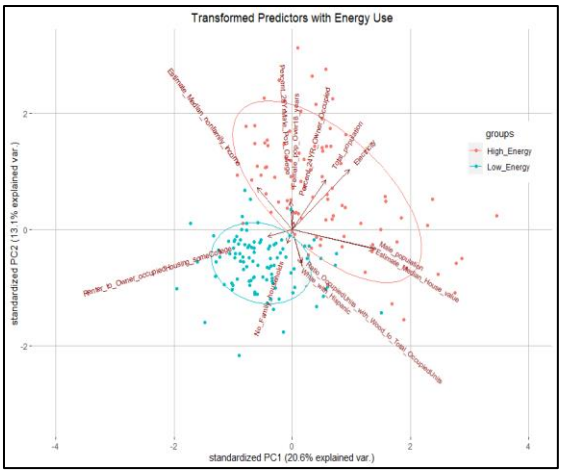

Figure 3-3: Model variables distribution of ZCTA electricity use and statistically significant variables along the first two principal components

The plot shows the distribution of the observations into respective energy clusters obtained from the k-means algorithm and indicates which significant predictors from the regression influences the distribution of the clusters. In the high energy cluster, we find that variables such as owner tenancy (v7), female population over 18 (v2), male population (v5), total population (v15), income for non-families (v13), male with bachelor degrees (v8), median housing value (v10), are associated with high energy use, while variables such as white with Hispanic (v1), rent tenancy (v9), family households (v11) are associated with low energy use.

The results create an interesting profile of electricity distribution with the ZCTA demographic makeup reflecting that educated, home owners, non-families, populations with economic resources are key drivers of energy use and that ZCTAs with demographics of higher proportion of white populations and family households tend to have a lower energy use. Conversely, the presence of family households, especially those with children has been shown to be associated with higher electricity costs, contradicting some of the associations here[179].

3.5.1.2 GA ZCTA electricity use

The predictive model was used to generate electricity estimates for all 606 ZCTAs and we find housing median value and median income to be influential predictors in addition to the predictors labeled as white with Hispanic population, total population, female population median house value, median nonfamily income (SI Table C-12). The percentage of housing units built later than 1950 was also significant.

While both electricity spatial ZCTAs have predictors that fall into similar categories (Table 3-8), there are some differences among some of the variables. For instance, regarding educational attainment, within the metropolitan ZATCs, higher education (i.e. college) are key characteristics whereas for the larger ZCTA dataset, education slightly beyond high school was a predictor. Household characteristics in rented units for GA ZCTAs came up as significant whereas family households for metropolitan ZCTAs were highlighted instead, although in both cases, family households were the main drivers.

Although there were some common significant variables (a total of 4 listed in Table 3-8), the vast differences in some of the metrics highlight the difficulty in comparing different regional social economic characteristics as they pertain to electricity use.

Table 3-8: Electricity model significant predictor variable category. Predictor numbers match those in SI Table C-1

Category	Metropolitan ZCTAs	Georgia ZCTAs
Economics	161,185	161, 185
Population Demographics	1,9,18	1, 18, 22, 27
Housing Occupancy and Tenancy	4,7,9,82,336	67, 103, 201, 319
Education	296, 336	319
Housing Units And Amenities	236	152, 201, 209
Land Use (Urban Morphology)	1	1, 209, 67
Household characteristics	49	103

3.5.1.3 Metropolitan Atlanta Gas Use

Here we assess the results of the 32 ZCTAs for gas results (Table 3-9). Although all the transformation methods, in addition to MGS and CGS compare fairly well, in terms of performance diagnostics, the CGS model performed better with the most significant predictors in the model. A side by side map of predicted natural gas use from the CGS model (SI Fig C-34) next to that of actual natural gas use shows nearly identical results.

The results show that income and household demographics reflect gas estimation use. Two of the significant economic predictors, household income and per capita income (v7, v8) were as important as median house value (v5), the latter which also showed up in electricity models as a significant variable, a finding similar to that of Gassar et al., (2019)[180]. Total population (v3) as well as household population (v6) had significant *p*-values. Along ethnic demographic variables, the African American population was the only significant predictor demographic here.

Table 3-9: Linear Regression fit of final model. ZCTA natural gas use is the dependent variable.

Variable No	Variable Name	Model Coefficient	*p*-values
1	**Number; RACE - Total population - One Race - Black or African American**	**-1.60E+04**	**0.03**
2	Estimate; INCOME AND BENEFITS (IN 2011 INFLATION-ADJUSTED DOLLARS) - Median family income (dollars)	1.82E+06	0.17
3	**Number; SEX AND AGE - Total population**	**1.11E+07**	**0.00**
4	**Number; SEX AND AGE - Male population**	**-3.20E+06**	**0.00**
5	**Estimate; VALUE - Median (dollars)**	**2.01E+05**	**0.00**
6	**Number; RELATIONSHIP - Total population - In households**	**2.30E+06**	**0.01**
7	**Estimate; INCOME AND BENEFITS (IN 2011 INFLATION-ADJUSTED DOLLARS) - Per capita income (dollars)**	**-2.63E06**	**0.00**
8	**Estimate; INCOME AND BENEFITS (IN 2011 INFLATION-ADJUSTED DOLLARS) - Median household income (dollars)**	**6.77E+06**	**0.01**
9	Estimate; INCOME AND BENEFITS (IN 2011 INFLATION-ADJUSTED DOLLARS) - Median nonfamily income (dollars)	-1.61E+06	0.15

3.5.1.4 GA ZCTAs gas use

Out of all the models, the MGS model (Table 3-6) was certainly the best and in fact, energy estimates using some of the other models (i.e. no transformation and z-score) gave largely erroneous natural gas estimates for over half of the 574 ZCTAs, whereas the CGS model had 6 and the MGS model had 2 (excluded from SI Fig C-35), and in the case of MGS, is likely to improve if the training set had been larger. Similar to the metropolitan tracts for gas use, total population was a significant predictor but there was slightly more variation with the predictors in terms of the categories. We found population demographics such as female population were significant, in addition to homes rented by populations over the age of 55 for occupied households. The two significant economic metrics which were related to monthly housing costs were also

significant. We categorize the predictors according to social economic and demographic category (Table 3-10).

Table 3-10: Natural Gas significant predictor variable category. Predictor numbers match those in SI Table C-1

Category	Metropolitan ZCTAs	Georgia ZCTAs
Economics	161,178,184	266, 270
Population Demographics	1,9,23	1,15
Housing Occupancy and Tenancy		87
Education		
Housing Units And Amenities		224
Land Use (Urban Morphology)	1	349
Household characteristics	37	

Overall, the variables for both models (gas and electricity) are similar to the variables selected by Salari et al. (2017)[171] in terms of critical social economic factors. However, unlike the impact of electricity, the variables that impact gas use appeared to be more influenced by household makeup and household economics, whereas with electricity, a much wider range of variables influence demand.

3.5.2 Impact of clustering and spatial analysis on electricity use in the metropolitan ZCTAs.

In this section, we focus on analyzing metropolitan electricity use in further detail. The results of the MGS model show a strong statistical relationship between the transformed selected predictors and electricity use. However, while electricity use showed evidence of prominent clustering (Fig 3-2), not a single transformed predictor (SI Fig C-8) showed evidence of a clustering pattern identical to that of electricity clustering. Even predictors such as the median value of homes which had a high regression coefficient in the statistical model, did not exhibit any

strong sign of similar spatial clustering with electricity. Although one untransformed predictor (v4, SI Fig C-7) did appear to match electricity clustering (Table 3-7), Total Population/Number of Housing units (referred to as TPH herein), it was a non-significant variable in the statistical model. When we did analyze TPH spatial patterns of electricity use per capita for each ZCTA together with population further (SI Fig C-36), we found that while population clustering did not have a similar pattern with electricity use as mentioned previously, TPH had an inverse associative pattern with electricity, with low occupancy units spatially clustered with high electricity use ZCTA and vice versa. The inverse relationship seen here between electricity per capita and occupancy was also noted in a study by Dar-Mousa et al. (2019)[181]. Fig 5 of their study showed that electricity per capita is higher in lower population density areas, a similar finding here, as measured with TPH. These results suggest that total population and density are not the sole drivers of high electricity use. As the electricity per capita clusters show, both clusters have essentially similar population size (SI Fig C-36g), yet one cluster uses more electricity than the other, showing that there are other factors that need to be considered.

The spatial clustering results showed that none of the significant variables were similar in clustering pattern to electricity. In addition, most of the variables themselves, did not present any form of clustering in any case, transformed or otherwise (SI Figs C-7 and C-8). In fact, only with a few transformed variables, did we see any evidence of clustering, two variables, male population and median house value and for both variables, it was only 41 and 33 out of 196 metropolitan ZCTAs zip codes for which this was the case respectively. While with untransformed variables, two variables, namely median house value and percent of 25-year-old males with bachelor or higher with degrees had some clustering with 55 and 30 observations out of 196 respectively. Further clustering analysis was conducted to see if all the combined predictors (transformed or

original) followed the similar energy spatial clustering pattern shown in Fig 3-4. But none of the combined predictors showed similar clustering patterns with electricity, despite evidence of clustering of the predictors in PCA (Fig 3-3).

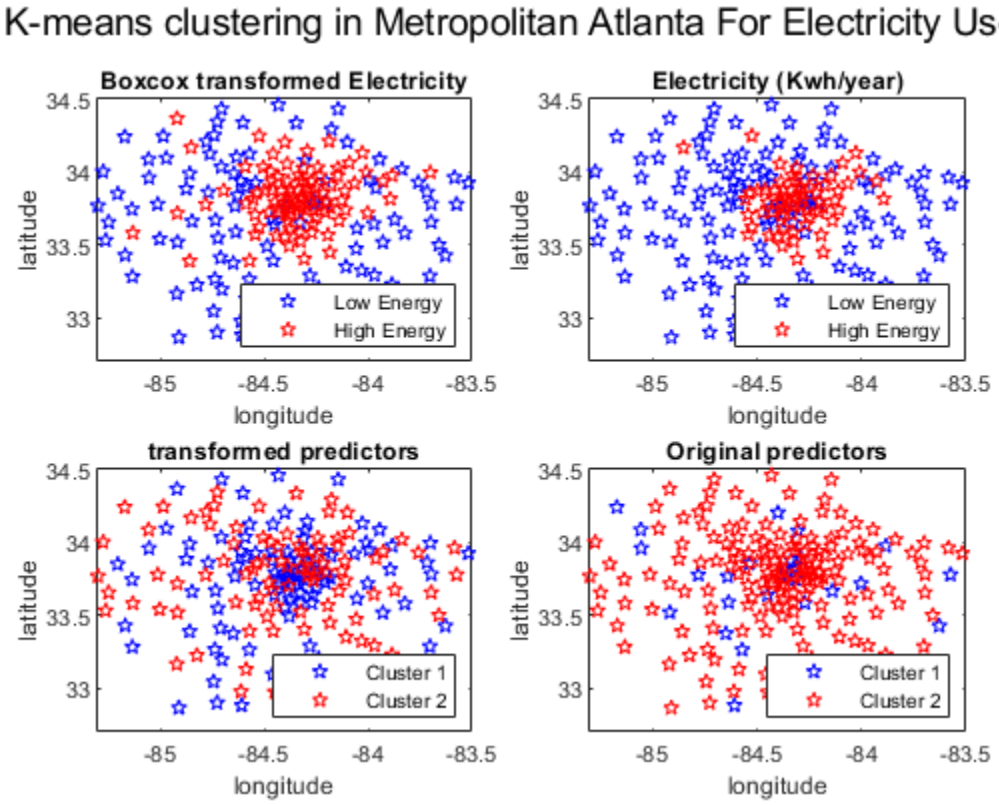

Figure 3-4: Clustering by k-means, plotted spatially with geographical coordinates

To further assess the impact of clustering, we performed PCA with both transformed variables and untransformed significant variables, without electricity as a variable. Results showed that while the variability of energy use varies spatially (Figs 3-3 & 3-4), the same cannot be said for the demographic variables (Figs 3-4 & 3-5), despite the strong statistical relationships of the predictors with electricity use. It was therefore clear that the social demographics could not adequately explain the entire variation in residential electricity use.

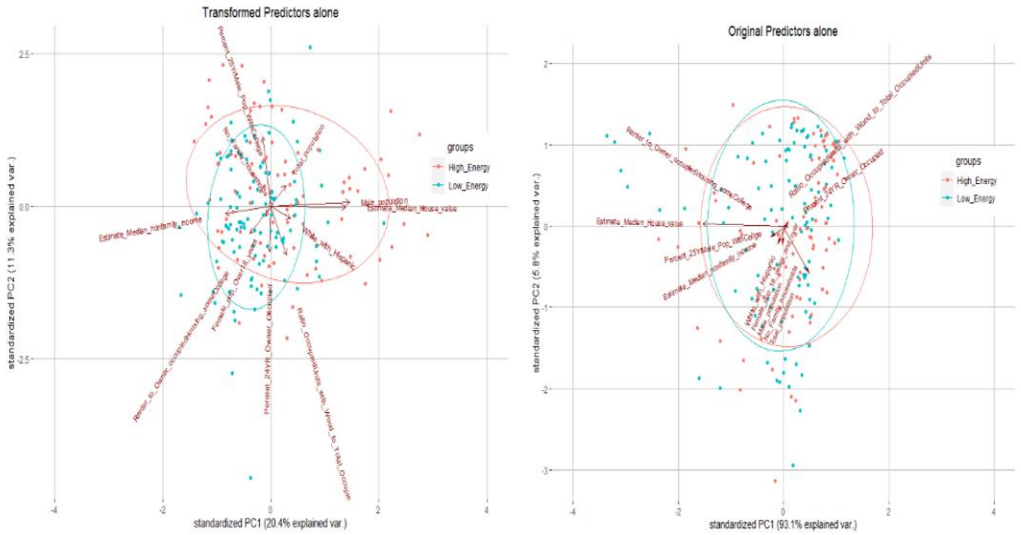

Figure 3-5: bi-plot of components for transformed and untransformed predictors

With no apparent clustering or spatial pattern found with ZCTA electricity use and the variables, we overlaid all the electricity use clusters over a geographical feature map of the metropolitan area (SI Fig C-23).

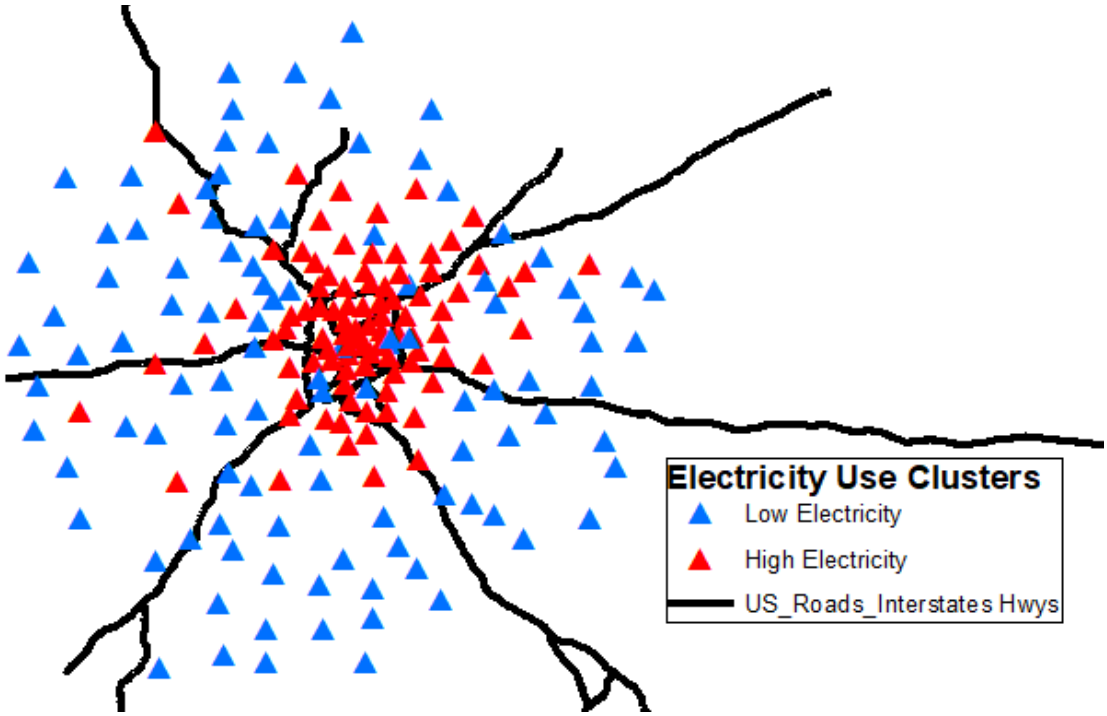

Figure 3-6: Electricity high and low clusters mapped along major interstate roadways[182]. (Map source: Map created using ARCGIS® software by ESRI (ESRI 2015[183]). Note: electricity here is log transformed.

The results (Fig 3-6, SI Fig C-24) indicate that annual high electricity use ZCTAs are largely clustered within the perimeter of the I-285 interstate, while the annual low use ZCTAs are outside its perimeter. As the social economic predictors in the final model could not explain this spatial clustering, the conclusion here is that the morphology of the city plays a significant role in determining electricity use. The impact of city morphology on electricity use has been related to the urban heat island (UHI) effect [184], [184, 185], however, not many have been able to quantify the actual impact on electricity demand, due to the reasons mentioned earlier. Even if data are available, few studies explore the link between the transportation sector and residential electricity use. Dar-Mousa et al. (2019)[181] attribute the differences in electricity spatial pattern to building design and socioeconomic factors, even though the higher electricity per capita areas are closely situated near high density roadways.

Within the metropolitan ZCTAs, the urban heat island effect could be brought about by a number of variables such as impervious, light absorbing, surfaces such as buildings and roadways [186], [186, 187]. There are also parts of urban morphology which tend to mitigate the impact of UHI such as green spaces like parks and tree canopy[188, 189]. Although not the main focus on this study, we conduct some preliminary analysis to try to delineate the impact of some of these variables on electricity distribution. We explore this by using data which serve as representative proxies for the following urban forms: roadway infrastructure, impervious surfaces, pervious surfaces and water bodies. To analyze the impact of roadways, we obtained a proxy, by using fine scaled modeled air quality data within the metropolitan Atlanta zip codes, as documented in Bates et al. (2018)[190]. The data for impervious surfaces was gathered from the Atlanta Regional Commission (ARC) LandPro data set (2012)[191] and consists of impervious surfaces like roadways, buildings and other categories of the built environment. The last two data sets were for pervious surfaces which comprises largely of green spaces and then water bodies and were also gathered from ARC. The four data sets were collected for 159 metropolitan ZCTAs within a similar time frame like the electricity data. The air quality data was obtained as modeled nitrogen oxide (NOx) concentrations[190]. LandPro data from ARC was utilized by aggregating land cover data by zip code for pervious, impervious surfaces, and water bodies. Impervious surface data was calculated by aggregating roadways, buildings, and other built infrastructure. Pervious surfaces were calculated by aggregating parks, forests, wetland, and other pervious greenspace land cover. Finally, water bodies were calculated using the area in each ZCTA covered by lakes, rivers, ponds, and other water bodies. The pervious, impervious and water body data were obtained as percentage areas within the ZCTAs.

Generalized linear regression models using electricity use clusters as factor predictors of each urban form were constructed and we explored the sensitivity of the regression by using more than two clusters in all models. All regression models were constructed as follows;

$$\eta(UrbanForm) = \beta_0 + \sum_{i=1}^{n} \beta_i \, ElecClust_i \qquad (3)$$

Here, urban form refers to each of the four urban form variables (pervious surface, impervious surface, water bodies and NO_x), *n* refers to the number of clusters in the model and *i* refers to the cluster number. The function $\eta()$ refers to the appropriate link function for each variable's model. NO_x concentration was modeled with a natural log link for a lognormal regression, and impervious surface, pervious surface and water bodies were modeled with a logit link for beta regression. Cluster numbers are designated such that the lower cluster numbers have higher mean values of each urban form variable, representing ranks. The results of the models are tabulated in Table 3-11.

Table 3-11: Results of regression models exploring the relationships between urban forms and electricity clusters. Tabulated here are regression coefficients of the independent variables (i.e. cluster numbers) in the model and standard errors. Cluster 1, representing the cluster with the highest electricity use, was the referent cluster

No of clusters used in model	Ranked cluster number	NOx concentration	Impervious surface percent	Pervious surface percent	Water bodies percent
Model using two clusters	Cluster 2	-0.51 (0.08)	-0.47 (0.16)	1.11 (0.18)	-0.60 (0.15)
Model using three clusters	Cluster 2	-0.47 (0.09)	-0.48 (0.20)	0.88 (0.22)	-0.35 (0.19)
	Cluster 3	-0.57 (0.09)	-0.55 (0.19)	1.30 (0.22)	-0.55 (0.18)
Model using four clusters	Cluster 2	-0.17 (0.13)	0.055 (0.27)	0.56 (0.29)	-0.27 (0.25)
	Cluster 3	-0.61 (0.13)	-0.35 (0.27)	1.22 (0.30)	-0.72 (0.26)
	Cluster 4	-0.69 (0.12)	-0.49 (0.27)	1.62 (0.29)	-0.76 (0.25)

These results indicate that roadway infrastructure has a statistically significant association with electricity use, potentially from heat absorption by roadway surface albedo[192]. Tail pipe emissions, which include CO_2 (i.e. NOx is a proxy for all mobile emissions)[193] could also be a contributing factor in increased residential energy electricity demand in a number of ways. For instance, higher CO_2 levels have also been found to reduce evapotranspiration [194], [195], [196]. Contrary to expectations, water surfaces also had a positive association with electricity use. Water bodies, though typically not as effective as green spaces space [197], [198], [199], are known to have a cooling effect in an urban setting, though factors such as geometry, wind speed and surface area play a role[200]. However, some findings have shown that the high heat capacity of water kept the air temperature above it high and increased urban heat island intensity respectively[201]. This would be particularly true at night as the skin temperature of hard surfaces drops more quickly. Wong et al. (2012)[202] found that high humidity areas and low wind would limit abilities of water surfaces to provide adequate cooling and Sun et al. (2012)[200] observed that water body geometry could lead to a negative impact on urban cooling intensity. Urban dwellings might be a factor here as well. Amani-Beni et al. (2018)[203] found that a building hampered wind speed and reduced the cooling effect of some water bodies. It is clear though that a more thorough evaluation of water body cooling in urban settings is required. Pervious surfaces such as tree canopy had the opposite effect to roadways as expected [204], [205], [206], [204-207]. All impervious surfaces together, while significant, was slightly less so than roadway. This was not too surprising as the impervious surface metric consisted of roadways and buildings. The magnitude of the effect of buildings here is not so clear, even though building albedo does impact on UHI [208]. Although we did include some building variables in the original set of predictors, these did not appear in any of the resulting statistical models, suggesting the importance of roads.

3.5.3 Comparison of study methods to other case studies

A side by side comparison of model results with other studies is not easily done, mainly due to the diversity of models, scenarios, objectives, scope and variables involved in residential energy modeling, all of which makes transferability of the results to other scenarios impractical[209]. Further in most cases, as mentioned in the introduction, residential energy studies tend to use models that are largely deterministic, relying on physical inputs and engineering principles to guide energy design and are primarily intended to be more helpful in construction and design phase than post design energy use, which was the main subject of this investigation. To that effect, the focus of this section will be on the advantages and disadvantages of the general approaches and techniques used here.

One main notable advantage in the design and set up of this study, was the acquisition of actual energy data to validate the accuracy of our model results for both electricity and natural gas, unlike the bulk of most studies that generally rely on data from statistical based estimates or bench marks[15] to validate their results, which can lead to some measure of error in building the model. Secondly, the regression techniques (OLS) and variable selection method (stepwise) that were chosen are generally accessible, relatively easy to implement by researchers in various disciplines and also allows for easier interpretation of model results than other utilized methods such as Artificial Neutral Networks[210]. Thirdly, another advantage of our study approach was to focus largely on post energy models which included a large number of social economic and ethnic demographics, than pre-design energy use models which are largely based on building stock and features. This difference is significant as actual energy consumption is known to deviate substantially from energy estimates derived with the latter method[15]. Thus the models built in this study are able to capture the extent of the true variability in energy use.

Our approach also allowed us to consider a large amount of predictor variables in combination with the variable selection algorithm and cross validation metrics to obtain the best model predictors, unlike others studies where the variables would have already been selected beforehand[211] and could fall short of capturing a significant portion of electricity use variability. For instance, Karatasou S. and Santamouris M. (2019), presented an energy model with some pre-selected social economic variables, but the model only accounted for 42% of energy variation, whereas in our case, we were able to account for 80% of electricity use variation and 95% in gas use[212]. However, this was also one of the major drawbacks of the study, in that gathering and sorting through a large data set of variables proved to be quite time intensive.

Of note, a disadvantage of the orthogonal transformation technique used here, was that it did require the use of additional tools (i.e. PCA and clustering) for interpretation of model results. However, it was those additional methods that were key in elucidating the impact of UHI in residential electricity energy use. As a result, we would conclude that the techniques and approaches used in this study provided several advantages that far outweighed the few drawbacks of our approach.

Lastly, it is worth noting that utilization of machine learning algorithms in estimating post residential energy use have increased substantially in recent publications. While they do have advantages over OLS methods, as many such studies report low errors in their estimates[213], there are still some limitations. For instance, if there are other underlining causes explained by variables not considered in the model development, one may not understand the true reasons behind energy use variation and the model might still perform poorly as a result. Further, because we used a statistical model, unlike a machine learning algorithm, we were able to directly evaluate the influential effect of model variables in our models. Studies that employ machine learning

algorithms generally have to utilize additional tools, such as a Generalized Linearized Model (GLM), or multivariate regression to further evaluate the variables. Essentially a statistical model is still needed[213],[214] to understand model variables and such models(used in this way) might still be subject to multicollinearity without some transformation as was done here. Future machine learning algorithm based studies, may however benefit from incorporating methods as was done here such as PCA and k-means to understand variation in their models if possible.

3.6 Conclusions

In general, orthogonalization methods have advantages over other data transformation methods, one of which is to eliminate multicollinearity and improve statistical model performance for energy estimation. Although there are possibly some limitations of these methods if the data set is too small, and model interpretation requires several additional tools, as was the case here, the advantages it offers in regard to statistical model stability is noteworthy. In addition to method application, we also demonstrate here, the effect of ensemble averaging which reduces the signal to noise ratio in regression estimates and proved to have a noticeable advantage over non-ensemble techniques.

The goal of this study was to develop a predictive energy model by determining the social indicators that affect residential energy use for natural gas and electricity. The methods and techniques utilized here demonstrate the predictive capability of orthogonalization in obtaining good energy estimates, particularly in the case of natural gas. Even with a small training data set for natural gas, generated estimates for Georgia zip code tabulated areas were statistically better. While further evaluation of these and other methods used to estimate gas usage would be useful,

the methods outlined here show potential to be utilized in generating even finer spatial scale estimates over broader spatial extents, providing all variable data is available.

Despite the fact that results show that sociodemographic factors play a substantial role in energy usage estimation, noticeable differences in model predictors exist between electricity and natural gas use. Electricity use is affected by a variety of key demographic variables, including income, education and population playing major roles. Income and household make up are key determinants of gas usage. Further, while socioeconomic variables comprise of the bulk of the determinants in natural gas use, electricity use is highly influenced by more than just these. It was observed that the high electricity use clusters did cluster more with urban morphology, in particular roadways than with sociodemographic factors. These results suggest urban form and function have a notable impact on electricity use.

Past energy studies have typically focused on improving and assessing building efficiency to evaluate electricity use. As it is quite possible that the urban heat island effect can attenuate the benefits of building designs on energy demand, it is critical to consider the impact of urban heat island in generating accurate energy estimates. Assessing the impact of urban heat island effect in cities requires looking at the albedo effect of city infrastructure with a focus on road infrastructure. As illustrated in this study, the urban heat island effect from roadway infrastructure morphology and its use may impact the distribution of electricity use and demand. This observation might explain in part, why some models might fail in post design energy estimation as they do not typically capture this phenomenon.

It is important to note that while this trend was observed for metropolitan zip codes in Atlanta Georgia, trends in different climates and city settings may differ. Future studies should

consider the impact of urban heat island by incorporating city spatial pattern analysis of energy use to determine if this affects electrical energy use.

3.7 Acknowledgements

The authors are grateful for the funding support of the National Science Foundation under grant 1444745–SRN: Integrated urban infrastructure solutions for environmentally sustainable, healthy, and livable cities. All co-authors are also part of the Sustainable Healthy Cities Network which is funded under the same grant. The authors would especially like to thank Professor Valarie Thomas, from the Department of Industrial and Systems Engineering at the Georgia Institute of Technology for insightful feedback and providing key energy data that made this project viable.

3.8 Supplementary Information

Appendix C. Supplementary Information

CHAPTER 4. ASSESSMENT OF AIRPORT-RELATED EMISSIONS AND THEIR IMPACT ON AIR QUALITY IN ATLANTA, GA USING CMAQ AND TROPOMI

Adapted from 'Abiola S. Lawal, Armistead G. Russell and Jennifer Kaiser. Assessment of Airport-Related Emissions and their Impact on Air Quality in Atlanta, GA using CMAQ and TROPOMI. Currently under review in Environmental Science & Technology'.

4.1 Abstract

Impacts of emissions from the Atlanta Hartsfield-Jackson airport (ATL) on ozone (O_3), ultrafine particulates (UFPs), and fine particulate matter ($PM_{2.5}$) are evaluated using the Community Multiscale Air Quality (CMAQ) model and high-resolution satellite observations of NO_2 vertical column densities (VCDs) from TROPOMI. Two airport inventories are compared, an inventory using the emissions where landing and take-off (LTO) processes are allocated to the surface (default), and a modified (3D) inventory that has LTO and cruise emissions vertically and horizontally distributed, accounting for aircraft climb and descend rates. The 3D scenario showed reduced bias and error between CMAQ and TROPOMI VCDs compared to the default scenario [i.e. Normalized Mean Bias: -43%/-46%. Root Mean Square Error: 1.12/1.21 (10^{15} molecules/cm^2)]. Close agreement of TROPOMI-derived observations to modeled NO_2 VCDs from two power plants with continuous emissions monitors was found. The net effect of aviation related emissions was an increase in UFP, $PM_{2.5}$ and O_3 concentrations by up to 6.5×10^2 particles/cm^3 (~38%), 0.7 µg/m^3 (~8%) and 2.7 ppb (~4%) respectively. Overall, the results show 1) spatial allocation of airport emissions has notable effects on air quality modeling results and

will be of further importance as airports become a larger part of the total urban emissions, and 2) the applicability of high-resolution satellite retrievals to better understand emissions from facilities such as airports.

4.2 Introduction

Airports are often located near urban centers and contribute substantially to severe pollution and poor air quality[20, 215-217]. Airport operations, including landing and take-offs (LTO) lead to emissions of particulate matter and ozone (O_3) precursors such as nitrogen oxides (NO_x), which are not confined to the airport. For instance, Hudda et al., (2020)[17] found increased UFP particle number concentrations (PNC) in residential areas up to 4km downwind of the Logan International Airport in Boston, Massachusetts. In an earlier study, Hudda et al., (2014)[18] observed enhanced particulate matter and NO_2 concentrations at distances up to 10km away from the Los Angeles International Airport (LAX) in California. The health impacts of ozone and particulate matter associated with airport emissions have adverse respiratory and cardiovascular health effects[218-220]. Airports are high emitters of ultrafine and fine particulate matter (UFP and $PM_{2.5}$), which have been shown by a number of studies to have strong associations with adverse health outcomes[10, 221-223]. While emissions of NO_x ($NO_x = NO + NO_2$) and PM from on-road vehicles and electricity generating units (EGUs) have significantly decreased across the United States[224, 225], air travel and the resultant emissions are growing[226], such that airports may have an increased relative role in near-future air quality. The adverse effects of these pollutants, in addition to other aviation related concerns (i.e. climate, noise) are one of the many reasons why airports are increasingly becoming an area of growing concern.

Chemical transport models (CTMs), are often used to quantify airport impacts on urban air quality. CTMs rely on an accurate representation of emissions, however most inventories for regional CTMs tend to represent aircraft emissions as a surface-level source, neglecting the three-dimensional aspect of air traffic. In a study centered on the Atlanta Hartsfield-Jackson International Airport (ATL), Unal et al., (2005)[20] demonstrate that allocating landing and takeoff (LTO) emissions in three dimensions can decrease average modeled O_3 by ~1 ppb compared to the two-dimensional default emissions scenario. Woody et al., (2016)[227] using a plume treatment for the same emissions, showed an increase in particulate matter over traditional methods without the plume treatment. Additionally, emission inventories typically include only landing and takeoff emissions, omitting emissions at cruising altitude which have some impact[20, 21, 228]. For example, Vennam et al., (2017)[24] found increases in daily maximum 8 hour O_3 that ranged from 0.46-0.69 ppb over the Northern Hemisphere. Similarly, Lee et al., (2013)[25] found a maximum increase of 1 ppb for average O_3 when including full flight emissions, compared to the default scenario from their global model. Finally, choice of model resolution can affect the modeled impact of aviation-related emissions on ozone and PM concentrations.[22, 23] Model evaluation using near-airport observations is also limited.

Although these studies, among others have shown limited effects of using 3-D emissions, on air quality by focusing on one or more factors (i.e. spatial allocation of LTO emissions, inclusion of cruise emissions, and high- resolution modeling), studies are limited in comparing the compounded effect of these factors to default aviation inventories (i.e. that contain only LTO emissions, with no spatial allocation beyond the airport) that are used in high-resolution regional CTMs for regulatory purposes. Yim et al., (2015)[229] focused on quantifying how aviation related air quality and health related impacts compare with aviation attributable costs such as climate,

while Quadros et al., (2020)[230] explored air quality sensitivities to inventory perturbations from emission increases or intercontinental transport from other regions.

Here, we use the Community Multiscale Air Quality model (CMAQ) to evaluate the impact of the emissions from the ATL airport on ozone, $PM_{2.5}$ mass and UFP number concentrations in Atlanta during August of 2019. We develop a 3D emission inventory using EPA's 2016v1 Emissions Modeling Platform LTO emissions, and cruise emissions from the Aviation Emissions Inventory Code (AEICv2.1) emissions repository. We evaluate model results using ground-based air quality monitors and high resolution NO_2 retrievals from the satellite-based TROPOspheric Monitoring Instrument (TROPOMI), and demonstrate the ability of TROPOMI to provide constraints on emissions in our modeling domain using two power plants located near Atlanta. We assess model assumptions and sensitivities by evaluating the differences in ozone and particulate matter using both inventories. Finally, we quantify the impact an increase in ATL emissions would have on urban air quality.

4.3 Methods

4.3.1 Model Configuration (WRF-SMOKE-CMAQ)

WRF-SMOKE-CMAQ[231-233] was used to simulate air quality in the Atlanta metropolitan area during August of 2019. The 244 km × 244 km model domain was centered on ATL, with a horizontal resolution of 4 km and 32 vertical layers extending to ~16 km (100 hPa). Boundary and initial conditions were taken from a hemispheric CMAQ model, and a 10-day period was used for model spin-up[234-236]. We used CMAQv5.3.2 with the aerosol module AERO7 and the gas-phase Carbon Bond 6 (CB6) mechanism[235, 237]. Data fields from the National Center for Atmospheric Research (NCAR)[238-240] were used as inputs for the Weather Research and Forecasting (WRF)

model version 4.1, with the results processed using the meteorological chemistry interface process (MCIP v 5.1)[241] to generate meteorological input fields for SMOKE and CMAQ.

Anthropogenic emissions were calculated using the 2016v1 Emissions Modeling Platform[77] together with 2019 meteorology. The 2016v1 platform is a comprehensive and detailed inventory estimate of annual US emissions from all sources complied by the Environmental Protection Agency (EPA) as part of the National Emissions Inventory Collaborative (NEIC)[242]. Data is provided by State, Local, and Tribal air agencies for sources in their jurisdiction and is supplemented by data provided by the EPA[183]. Emission sources include onroad (e.g. cars, trucks), point (e.g. power plants, commercial facilities), non-road (e.g. construction, lawn equipment, locomotives, aircrafts), nonpoint (e.g. residential heating, asphalt paving), and event sources related to wild fires and prescribed burns. Emissions from the power plants were updated using Continuous Emissions Monitoring System (CEMS) data from 2019[19]. Lightning NO_X emissions were calculated using the statistical parameterization method described in Kang et al. (2019)[243]. Emissions from biomass burning were not incorporated and are anticipated to have little impact on the analysis here, as the prescribed burning season is not in effect during this time period[244]. We refer to the 2016v1 platform as 2016 National Emission Inventory (2016 NEI) herein.

4.3.2 Airport Emissions (NEI and AEIC)

While our model domain includes small regional airports, we focus our analysis on ATL which dominates aviation-related emission in the region. We use the NEI as our default inventory for airport-related emissions. The inventory includes contributions from Ground Support Equipment (GSE) and aircraft LTO cycles. GSE emissions comprise 11.5% of total NEI ATL NOx emissions. NEI LTO emissions include all phases of surface aircraft activity (i.e. landing,

take off, taxiing, and idling). The 2016 NEI airport inventory assigns both GSE and LTO emissions to two airport grids at ground altitude.

A modified airport emissions inventory (herein called "3D") was created using NEI GSE+LTO emissions and full-flight emissions from the Aviation Emissions Inventory Code (AEICv2.1) emissions repository. AEIC emissions are available at a resolution of $1^{o} \times 1^{o}$ for the year 2005[245, 246]. We determined 2019 cruise emissions by multiplying the ratio of AEIC cruise to AEIC LTO emissions (both in years 2005) by 2016 NEI GSE+LTO emissions. Besides the inclusion of cruise emissions, no modifications were made to the NEI aircraft emission rates which were incorporated into the 3D inventory. A tabulated inventory of the major species can be found in Table S1 in the supplement.

All airport-related emissions were given the same temporal profile as NEI LTO emissions. As detailed in the NEI Technical Support Document (TSD)[247], all phases of surface aircraft activity (i.e. landing, take off, taxiing and idling) are combined in LTO cycles, with no delineation between the different phases in each cycle. Diel activity patterns are derived from the Aviation System Performance Metrics data[248]. Monthly and day-of-week activity profiles are calculated using FAA Operations Network Air Traffic Activity data[182].

Total GSE, LTO, and cruise emissions were then allocated vertically and horizontally within the modeling domain. First, the fraction of total emissions at each altitude in the AEIC NO_2 emissions profile were used to vertically distribute emissions in the CMAQ vertical grid. The vertical profile distribution of ATL NO_x emissions is shown in Figure D-1, and is similar to the AEDT derived profiles in Vennam et al., (2017). Emissions were then horizontally distributed using plane take off and climb rates to calculate emission locations within the first 8 vertical layers

(below ~1000 m.) using an FAA recommended standard Rate of climb (ROC) rate of 200 feet per nautical mile[249, 250]. In the remaining upper layers (layers 9 to 32, > ~1000 m), the emissions were allocated corresponding to the vertical profile in the AEIC (Figure D-2).

The airport inventories (default and 3D) are combined with the remaining sectors (e.g. onroad, point, dust, nonpoint, biogenic etc.) to produce the inventories used in the subsequent air quality modeling. Additional details about the inventory development and spatial allocation can be found in the supplement.

4.3.3 Observations

4.3.3.1 TROPOMI NO_2 retrievals

TROPOMI follows a sun-synchronous orbit with an overpass time near 1:30 pm local solar time. We use the offline Level 2 v1.3 TROPOMI NO_2 product developed by KNMI[163, 251] accessed at NASA's Goddard Earth Sciences Data and Information Services Center (GES DISC, https://tropomi.gesdisc.eosdis.nasa.gov/). The data is filtered to exclude pixels with solar zenith angles greater than 60°, quality flag (qa_value) less than 0.5, and cloud cover fraction (CLCF) criterion of less than 0.3. A total of 24 days were available for data downloading, of which seven days had to be discarded, due to missing data from pixels needed for analysis, resulting in a total of 17 days available for comparison of TROPOMI and CMAQ NO_2 VCDs. The level 2 (L2) product provides tropospheric vertical column densities (VCDs) and the associated air mass factors (AMFs), which are calculated using vertical distributions from the TM5-MP model at $1^o \times 1^o$. In line with Cooper et al., (2020)[252], we use the provided averaging kernels and model vertical profiles from our higher resolution model to produce alternative AMFs, which are then used to recalculate TROPOMI VCDs.

For all CMAQ-TROPOMI comparisons, TROPOMI L2 data were remapped to the CMAQ grid using the oversampling technique developed by Zhu et al., (2017)[253] and described in further detail by Sun et al., (2017)[254]. With the oversampling technique, all pixels that intersect a given CMAQ grid cell are averaged together, with each observation's contribution weighted by the amount of overlap and observation uncertainty. Uncertainty is calculated as the absolute error of the standard deviation of the observation. CMAQ NO_2 VCDs are sampled at the times of TROPOMI data availability and averaged (i.e., 17 days, 13:00-14:00 LT).

4.3.3.2 Surface NO_x observations

Hourly surface NO_x observations from an EPA urban background monitoring site (Figure 1) were used to assess model performance[255]. The site uses a Thermo Environmental Chemiluminescence NO-NO_2-NO_X Analyzer (model 42i)[256, 257]. Observations are expected to be biased high due to interferences of NO_z species (i.e. NO_z = HNO_3, HNO_2, PAN)[258, 259].

4.4 Results

4.4.1 Evaluation of CMAQ and emission inventories with in-situ observations

Before using CMAQ to estimate impacts of airport-related emissions, we first evaluate model performance using ground-based NO_x observations and TROPOMI NO_2 retrievals.

4.4.1.1 CMAQ-AQS performance assessment

Figure 4-1 shows measured and modeled NO_x diel cycles. Default and 3D airport emission scenarios yield near-identical modeled NO_x concentrations at this site. Hourly modeled and observed NO_x concentrations were well correlated (r = 0.93). Especially in the morning and late evening, the model is biased low compared to observations, as has been observed in previous

studies[260]. At the time of TROPOMI overpass, modeled urban NO_x concentrations compare well with in-situ observations, with a root mean square error (RMSE) of 1.5 ppb.

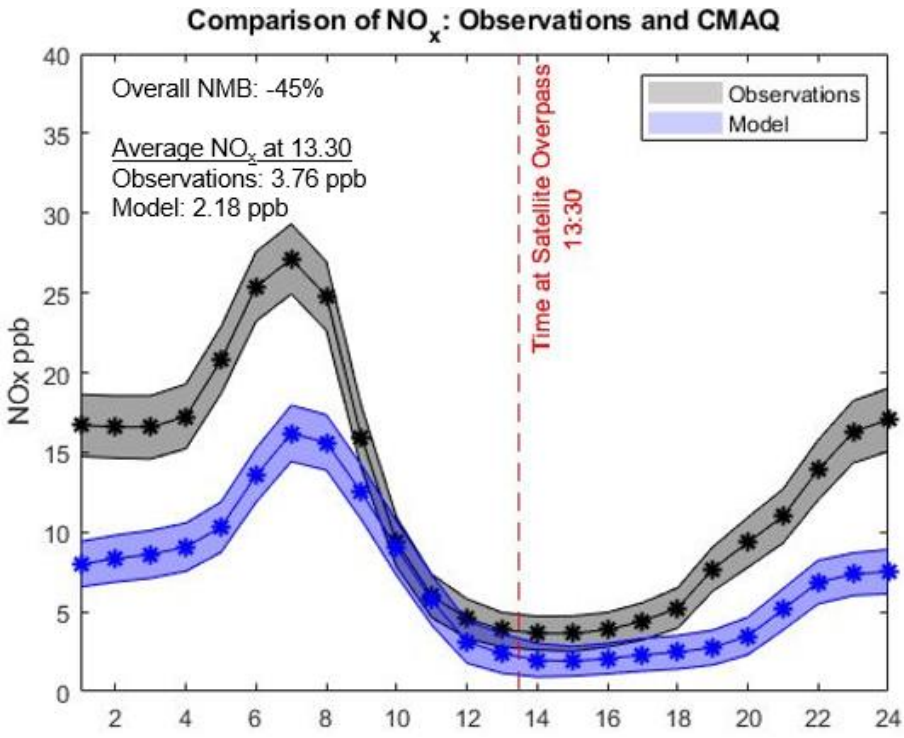

Figure 4-1: Observed and modeled surface NOx at the South DeKalb monitoring site in August 2019. Shaded regions indicate the standard deviation across the study period. The difference between model and observation at time of TROPOMI overpass is small

4.4.1.2 CMAQ-TROPOMI agreement assessment

As documented in previous studies, we find AMFs derived from a high spatial resolution CTMs improve TROPOMI-model agreement. TROPOMI VCDs calculated with CMAQ-adjusted AMFs ($TROPOMI_{CMAQ}$) showed notably improved agreement over the default TROPOMI NO_2 retrievals, with about 60% increase in VCDs near the airport (Figure D-3). $TROPOMI_{CMAQ}$ captures enhancements seen in CMAQ, including the hotspots over ATL, and two EGUs, Plant Bowen and Plant Scherer (Figure 4-2). Compared to CMAQ, $TROPOMI_{CMAQ}$ is biased high in

rural areas and low in highly polluted areas. Other studies have similarly reported a low TROPOMI bias to modeled and observed NO_2 VCDs in densely populated urban areas[261, 262]. The normalized mean bias (NMB) of CMAQ to $TROPOMI_{CMAQ}$ over the entire domain is not significantly impacted by choice of aviation emission inventory (3% difference in NMB).

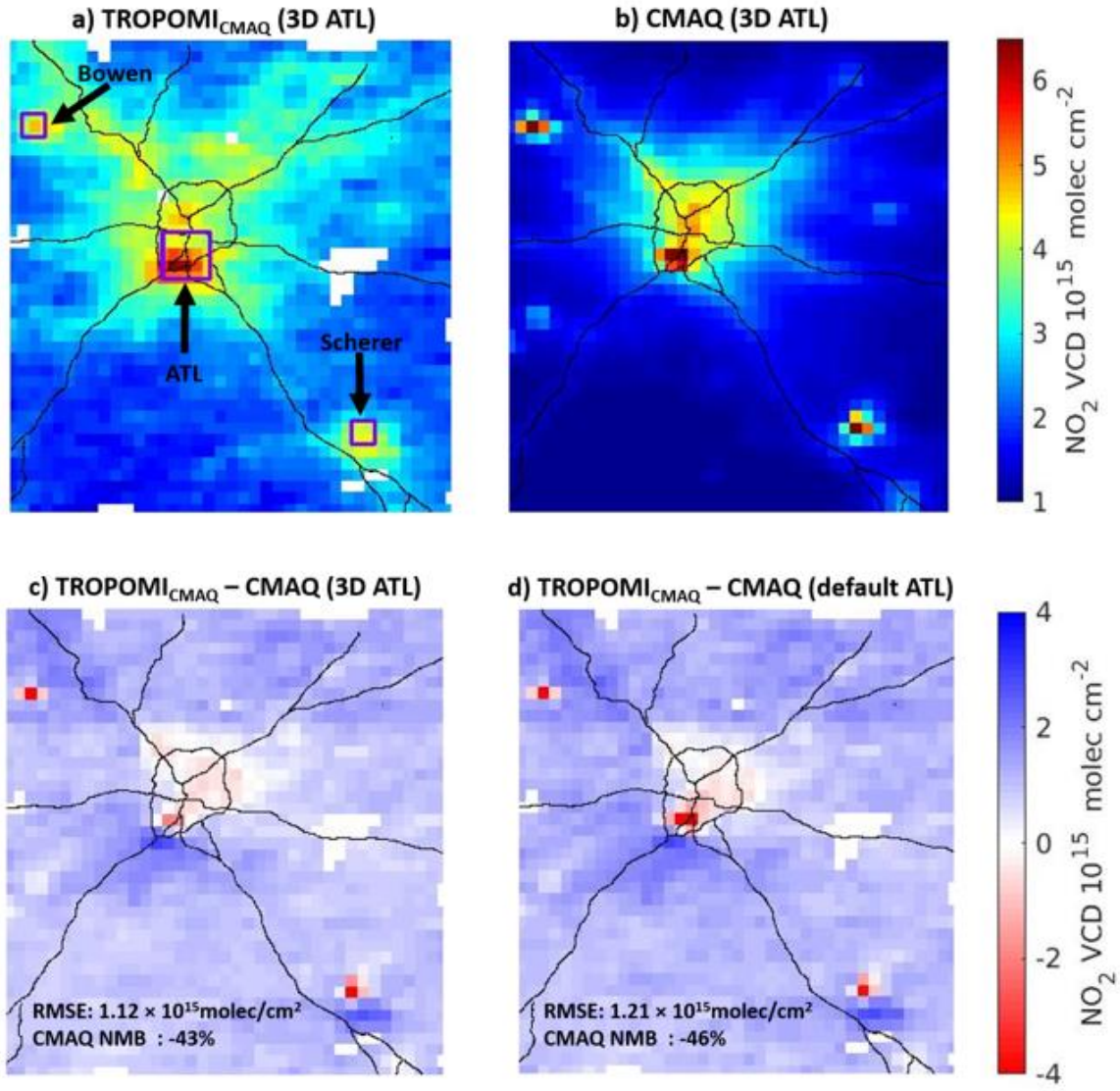

Figure 4-2: Results represent a 17-day average between 1300-1400 (~ 1330) for CMAQ and TROPOMI retrievals. a) TROPOMICMAQ NO2 VCD b) CMAQ NO2 VCD (3D inventory) c) TROPOMICMAQ – CMAQ with 3D ATL inventory d) TROPOMICMAQ – CMAQ with default ATL inventory. Purple boxes in panel 2a show the areas used to compare TROPOMI VCDs with CMAQ VCDs at the labeled sites.

4.4.1.3 TROPOMI observations near the power plants

Similar to Goldberg et al., (2019)[263], two EGUs (Bowen and Scherer) were used to evaluate $TROPOMI_{CMAQ}$ accuracy near major NO_x emission sources in our domain. Both power plants are isolated from other sources, and their NO_x emissions are continuously measured and constrained

in CMAQ. Good agreement between $TROPOMI_{CMAQ}$ and CMAQ in the vicinity of the power plants provides confidence in our use of TROPOMI retrievals to assess airport-related emissions, which have a higher degree of uncertainty.

In the 9 grid cells surrounding and including each facility (boxes in Figure 4-2a), biases in TROPOMI are much smaller than the bias over the whole domain (Bowen: 6.0 to 9.8%, Scherer: 0.5 to 4.5%, SI: Table D-2). To assess how sensitive VCDs are to modeled emissions, emission inputs for both EGUs were multiplied by scale factors of 0, 0.5, 1, 1.5, and 2. $TROPOMI_{CMAQ}$ was then compared with modelled concentrations for all five EGU scale factor scenarios. $TROPOMI_{CMAQ}$ agreed closely with the 9 grid cell average around Scherer and Bowen with the EGU base case (Figure 4-3). This also shows that $TROPOMI_{CMAQ}$ VCDs and associated AMFs are not significantly affected by sector emission adjustments (except when the source emissions are removed), meaning that adjustments of airport emissions will not drastically affect the $TROPOMI_{CMAQ}$ VCDs. This is shown in Figure 4-4, as choice in inventory has negligible impact on near-airport $TROPOMI_{CMAQ}$.

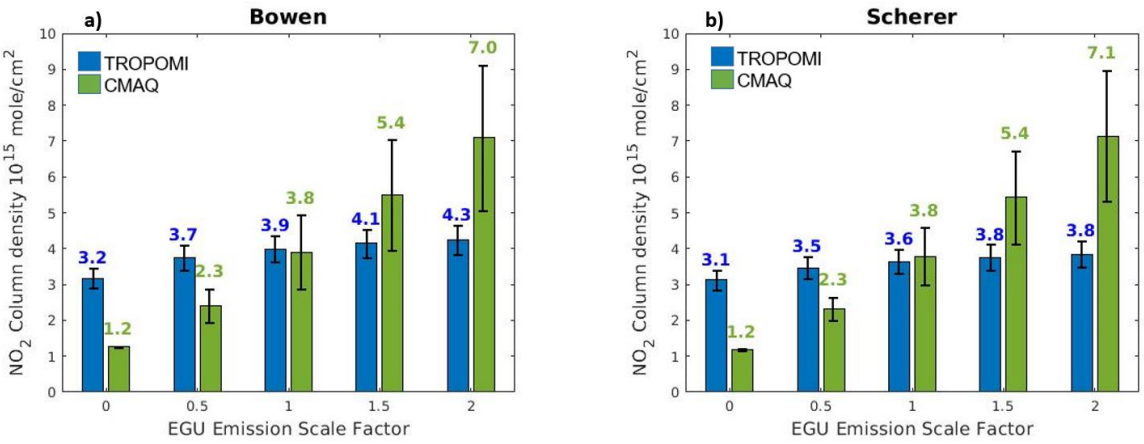

Figure 4-3: TROPOMICMAQ and CMAQ NO2 VCDs at different emission scale factors for Bowen and Scherer. Results represent a 17-day average at ~1330.

4.4.2 TROPOMI and CMAQ NO_2 VCD sensitivities to airport inventories

The 3D inventory results in closer CMAQ/TROPOMI$_{CMAQ}$ agreement for near-airport NO_2 VCDs compared to the default emissions scenario. Using a cutoff value of 4.5×10^{15} molecules/cm^2 to distinguish between highly polluted and less polluted areas, as was similarly done in Ialong et al., (2020), the greatest absolute difference for high NO_2 VCDs with the 3D airport inventory is 0.93×10^{15} molecules/cm^2, compared to 1.4×10^{15} molecules/cm^2 in the default scenario (Table D-2). The improvement can be attributed in part to the dilution of emissions in the 3D inventory, which results in less steep gradients in modeled NO_2 VCDs near the airport (Figure 4-4), but also to NO_X titration and less nitric acid production as modeled by CMAQ[264]. Only a few metrics for the airport grid points such as the spatial Pearson correlation coefficient were better with the default inventory than the 3D (SI: Table D-3).

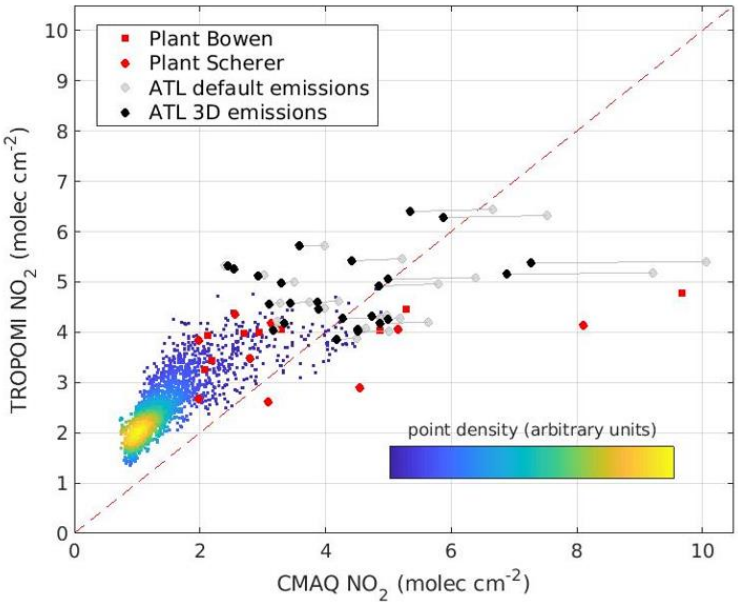

Figure 4-4: TROPOMICMAQ vs CMAQ NO_2 VCDs including highlighted results for EGUs and ATL from associated grids (see Fig 4-2a).

4.4.3 Airport inventory effects on ozone and particulate (UFP and $PM_{2.5}$)

In Figure 4-5 (a-c), we show monthly averages of modeled maximum daily average 8hr ozone (MDA8 O_3), ultrafine particulate (UFP) particle number concentration, and $PM_{2.5}$ mass concentration using the 3D inventory. We also show monthly averaged differences between a) the 3D and default emission inventory (d-f), and b) the 3D and simulations without all aircraft emissions (g-i). The differences capture the spatial impacts of the airport emissions and effect of using the enhanced (3D) inventory.

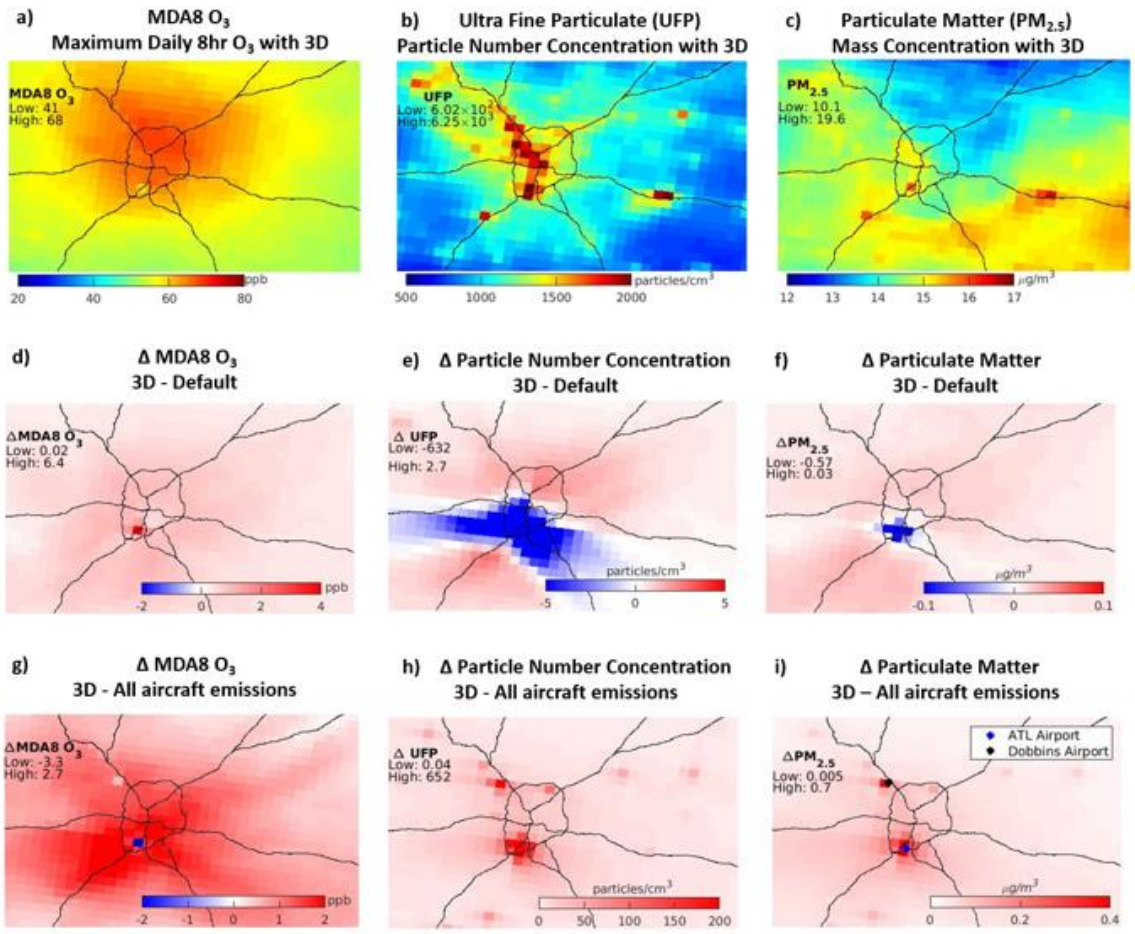

Figure 4-5: Averages for the month of August for Maximum Daily 8hr O3, UFP number concentration and PM2.5 mass concentration. First row (a to c) shows concentrations using the 3D inventory. The second row (d to f) is the difference between the modified and default inventory. The third row (g to i) shows the impact of all aircraft emissions

4.4.3.1 MDA8 O_3

Reallocated emissions with the 3D inventory led to MDA8 O_3 increases throughout the domain (Fig.4-5d). The regional ozone increases are likely attributed to an increase in ozone production efficiency (OPE) as more NO_x was distributed more broadly to NO_x-limited areas, accompanied with a reduction in NO_2 deposition[265]. The reduced ground level NO_x emissions led

to increases up to 6 ppb near the airport because of spatial re-allocation and decreased near-field scavenging.

Setting all airport emissions to zero (using the 3D inventory) led to higher MDA8 O_3 at the airport, but lower in the surrounding areas (Figure 4-5g) for the $3D_{Aircraft=0}$ scenario. The higher MDA8 O_3 at the airport for $3D_{Aircraft=0}$ is due to reduced scavenging. Downwind of the airport, increases as high as 2.7 ppb are found from airport-related emissions for 3D. This increase is similar to the difference when using the 3D versus the default inventory and highlights the impact using of spatially allocated emissions.

4.4.3.2 UFP number and $PM_{2.5}$ mass concentration

For the particulate matter analysis, we focus on particle number concentration (PNC) for UFP and particle mass concentration (PMC) for $PM_{2.5}$. We use the CMAQ simulated mode particle distribution for both species in this study, referring to CMAQ simulated i-mode (Aitken) particles as UFPs and i+j-mode particles (accumulation) as $PM_{2.5}$[266-268]. For both inventories, the modeled maximum concentrations for both PNC and PMC at ATL were higher than those of nearby sources (i.e. mobile and area) (Fig 4-5, b and c). This agrees with previous studies that indicate high particulate emissions from aircraft and airport-related activities[21, 22, 215], with some reporting up to 10-fold increases of particulate emissions from landing and take-off cycles (LTO) alone[23].

However, the effect of horizontal and vertical spatial reallocation with the modified inventory dilutes the emissions at the airport, resulting in maximum decreases of 0.6 $\mu g/m^3$ (3.4%) in $PM_{2.5}$, and 6.3×10^2 particles/cm^3 (20%) in UFPs (Figure 4-5 e and f). Conversely in the surrounding areas, the 3D inventory led to increases of UFP PNC at distances ~16 km away from the airport and beyond in some directions. Although the magnitude of these differences decrease

at distances further away from the airport, the increases are seen over most of the metropolitan area. $PM_{2.5}$ PMC exhibits the same spatial pattern.

Removing all aviation related emissions from the 3D demonstrates the net effect of the airport. Here we see substantial impacts in PMC and PNC over the entire modeling domain from airport operations (Figure 4-5 h and i). The range of decrease in PNC was 0.04 to 6.52×10^2 particles/cm^3 (0.002% to 38.6%), while the decreases in PMC ranged from 0.005 μg/m^3 to 0.7 μg/m^3 (0.02% to 8.4%). The greater percent change in PNC is an indication that near airport activity has a larger effect on number concentration than mass concentration[217, 269]. Hudda et al., (2014)[18] measured enhanced PMC at distances 10-16 km away from the Los Angeles International Airport, although in this case, airport impacts extend well beyond the ranges reported in their study. These results provide further evidence that airports enhance background particulate matter concentrations over large distances in appreciable amounts.

4.4.3.3 Impact of increased emissions on ozone, $PM_{2.5}$ and UFP

A sensitivity assessment conducted using the Integrated Source Apportionment Method (ISAM) in CMAQ[270, 271] indicate that both airports and mobile sources are significant contributors to ozone, $PM_{2.5}$ and UFP. Both contribute up to about 5 ppb for August average O_3 and ~15 ppb for MDA8 O_3 (Fig D-4), though airport impacts are more locally constrained to its immediate vicinity, while on-road effects are spatially distributed. Many of the approaches to lowering ozone have focused on mobile sources more so than airports. As emissions from cars decrease, an increase in aviation could impede efforts to meet the ozone National Ambient Air Quality Standard (NAAQS). Air quality monitors in DeKalb and Fulton Counties (Fig D-5) are actively used to monitor ozone for compliance as the metropolitan area is in nonattainment[272].

To evaluate the effect of potential increasing airport operations, airport emissions were increased for both default and 3D inventories by a factor of 1.5 to approximate a projected 20-year growth, while keeping other sectors at current emission levels[226]. Source apportionment sensitivities showed increases in ozone of almost 3 ppb in areas close in proximity to the air quality monitors for both inventories (Fig. 4-6). However, the 3D net increases were greater in magnitude and spatial extent than those of the default for both MDA8 O_3 (max ΔMDA8 O_3: 2.5 vs 1.9 ppb) and Daily Maximum O_3 (max ΔDMAX O_3: 2.8 vs 2.0 ppb). With particulate matter, the spatial extent and pattern were similar for both inventories, however the default showed higher net increases than the 3D, as result of the dilution effect of spatial allocation. Monthly averaged maximum net increases of 2.6 $\mu g/m^3$ for $PM_{2.5}$ and 2.1×10^{-3} particles/cm^3 for UFP were observed with the 3D, while those of the default were double that of the 3D. Although actual air travel growth and demand may not yield such emission increases, these results show that any incremental increase is likely to raise ozone and PM levels, off-setting decreases from mobile source reductions.

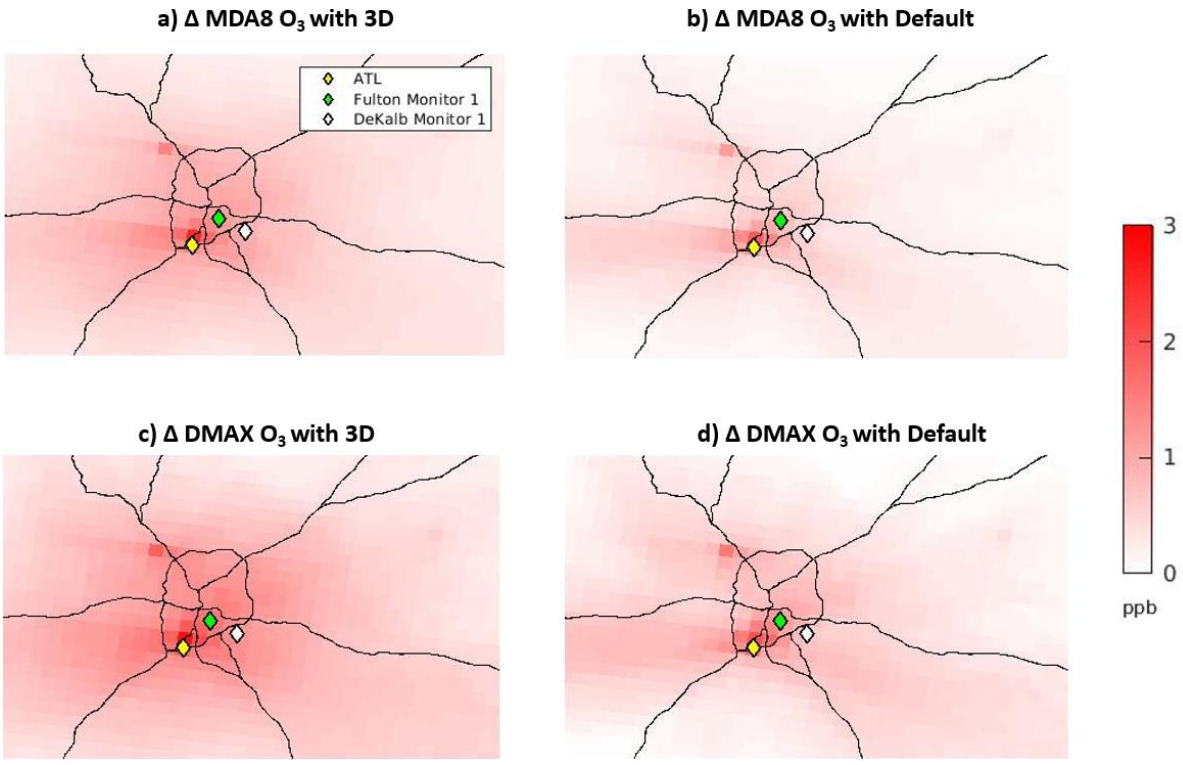

Figure 4-6: Monthly averages for Maximum 8hr O_3 and daily maximum O_3. Each figure represents the difference between a 20-year projected increase in emissions to current levels for each inventory and ozone metric.

4.5 Discussion

This study is unique in its combined use of a three-dimensional aircraft inventory, high resolution satellite retrievals and a fine scale air quality model to gain new insights about airport effects on air quality. Satellite-based observations have some measurement error and uncertainty[273, 274] and generally tend to be biased low in high NO_x regions, the base case results with both EGUs show that TROPOMI and CMAQ observations compared well, supporting the use of such observations to evaluate high NO_x emitting categories such as airports and aircraft[261, 262] and demonstrating TROPOMI's reliability in high NO_x regions. We minimize some of the uncertainty in using satellite retrievals to evaluate model assumptions by using high resolution

model-generated vertical profiles to reduce uncertainty in the AMFs. Besides the uncertainties in satellite retrievals due to AMFs, an additional source of error in NO_2 measurement retrieval can be attributed to the uncertainty in precision, which is around 10%[151, 273, 275]. However, this was much lower than the spatial heterogeneity bias (Figure 4-2, Tables D-2 & D-3) observed throughout the modeling domain, and had limited impact on our analysis.

We evaluate the sensitivities of the AMFs and satellite observations to inventory perturbations by comparing the satellite retrievals of NO_2 vertical column densities with emissions from two EGUs that are continuously monitored. The results show that TROPOMI retrievals are not affected much by inventory perturbations, lending confidence that changes in the inventory will not affect satellite fields much. This analysis illustrates the benefits of including sources with measured emissions in model-satellite comparisons, as well as using high resolution models to calculate AMFs. It also indicates that TROPOMI can be used in air quality management studies to assess the impact of airport emissions. TROPOMI retrievals also did not appear to be impacted by choice of airport inventory.

One of the novelties in our work, is the use of high-resolution satellite observations and evaluation with power plants to minimize and quantify the main uncertainties induced by the assumptions in this study, which include the estimation of full-flight emissions from AEIC and the spatial re-allocation of said emissions. Although power plants have previously been used to validate TROPOMI retrievals, as in Goldberg et al., (2019)[263], the methods in our study are different. For instance, we use a chemical transport model and emissions inputs in our study to compare with TROPOMI, while Goldberg et al., (2019) use TROPOMI top-down inventory estimates derived via a line integral function to compare directly with EGU inventories. We also adjust EGU emissions to demonstrate that the assumptions made in the estimation of the 3D

emission inventory do not significantly impact the satellite retrieval analysis, highlighting the capability of TROPOMI to constrain emissions.

The TROPOMI-CMAQ comparison results showed that the 3D inventory had lower biases for ATL with NO_2 VCDs, so we use the improved inventory (3D) to evaluate airport effects on air quality. We also evaluate the sensitivities in our assumptions and model by quantifying the differences in ozone and particulate matter responses between the 3D and 2D inventory and further test these assumptions by simulating cases where all airport emissions are removed. Of note, the differences assessment also minimizes model uncertainty in aerosol formation from semi-volatile particulate precursors that would otherwise, affect the conclusions drawn in this study regarding $PM_{2.5}$ and UFP impacts[235, 276-280].

For ozone, the net effect of removing all airport emissions showed that airport operations lead to enhanced ozone levels over the entire domain (except at the airport). Our analysis also showed that using the standard NEI 2016 would underestimate ATL impacts on ozone. This has implications for demonstrating ozone attainment in Atlanta and recommended measures needed to meet regulatory standards, as additional emissions increases at ATL are likely to make future attainment more difficult. For $PM_{2.5}$ and UFP, the enhanced (3D) inventory led to simulated reductions near the airport, but higher levels elsewhere in the domain. Like ozone, the net effect of airport operations resulted in elevated concentrations over the entire domain for both $PM_{2.5}$ PMC and UFP PNC. This suggests that the urban population in Atlanta is exposed to higher levels of particulate matter due to airport operations, and that projected emission increases from future airport travel will continue to elevate such concentrations over the city and general area. These findings provide further evidence that as aviation emissions continue to increase, spatial reallocation of airport emissions will be necessary to assess the extent of airport effects. Further,

given that the results here indicate that estimates of airport effects using default inventories would be an underestimate in both magnitude and spatial extent, it will be important to consider using a 3D inventory in future assessment simulations.

The use of a 3D allocation of emissions had differing impacts than past studies with 3D allocated emissions showed. For instance, in Vennam et al., (2017), modest increases up to 1 ppb in annual averaged MDA 8 O_3 were noted, while this study found average August MDA 8 O_3 increases as high as 6 ppb near the airport, and up to 2 ppb in the surrounding area of the airport (~20 km). Also, in contrast to Unal et al.'s (2005) study of aviation impacts, which was conducted for the same airport, at the same spatial resolution and during the same month, our study showed an increase in maximum and average ozone instead of a decrease. Differences between our ozone results and that of Unal et al.'s, (2005) study could be attributed to differences in inventory development and the spatial allocation methods used. For example, they utilized the Emissions and Dispersion Modeling System (2001 EDMS version 4.01) which has since been replaced with the Aviation Environment Design Tool (2015 AEDT)[281], to develop the inventory for gaseous pollutants (i.e. SO_x, CO, NO_x and VOCs). They also had to rely on literature emission factor estimates to develop the particulate matter inventory and to assign appropriate spatial and temporal inventory profiles to their simulations. Lastly, although the study was conducted using data from 2000-2001, nearly twenty years ago with a very different emissions mix, the fact that full flight emissions were not included in their study cannot be overlooked. Overall, irrespective of the different methods, both studies conclude that an accurate airport emission inventory and spatial allocation is valuable for air quality modeling.

4.6 Implications

We find airport impacts modeled using a more spatially representative emission inventory with full flight emissions are greater than the default NEI inventory indicates. This underscores the need to include accurate airport emissions inventories with full flight emissions and spatially allocated emissions. The study also demonstrates the ability of TROPOMI observations in combination with regional modeling to assess emissions over concentrated sources and provides insight into the sensitivity of modeled AMFs to emissions. Modeled ozone, UFP, and $PM_{2.5}$ concentrations using the 3D inventory show that aviation impacts extend beyond the airport. The effect on ozone is particularly important, not only because the results indicate more exposure to larger populations, but also because it could play a role in ozone attainment demonstration, since increased demand in air travel will result in more ozone. In a city like Atlanta which is currently under a marginal attainment classification, meeting the NAAQS requirements in the future could prove difficult if airport emissions continue to increase.

4.7 Acknowledgements

The authors are grateful for the funding support of the National Science Foundation under grant 1444745–SRN: Integrated urban infrastructure solutions for environmentally sustainable, healthy, and livable cities, as well as from NASA's Health and Air Quality Applied Sciences Team (HAQAST) program (Grant #80NSSC21K0506). We also acknowledge past and current members of the NSF SRN's and NASA's HAQAST teams for their support on this project. We also want to express thanks to Dr. Jim Boylan at the Georgia Department of Natural Resources for useful discussions, as well as to Dr. Petros Vasilakos and Nash Skipper for their invaluable assistance on this project. The contents of this paper are solely the responsibility of the grantee and do not

necessarily represent the official views of the supporting agencies. Further, the US government does not endorse the purchase of any commercial products or services mentioned in the publication.

4.8 Supporting Information

Appendix D. Supplementary Information

CHAPTER 5. THE IMPACT OF VEHICLE ELECTRIFICATION AND AUTONOMOUS VEHICLES ON 2050 AIR QUALITY IN THE UNITED STATES

Adapted from ‘Abiola S Lawal, Jooyong Lee, T. Nash Skipper, Huizhong Shen, Ph.D, Yilin Chen, PhD, Anu Ramaswami, Ph.D., Kara M. Kockelman, Ph.D., P.E., Armistead G. Russell, Ph.D. The Impact of Vehicle Electrification and Autonomous Vehicles on 2050 Air Quality in the United States. (Draft)

5.1 Abstract

The impact of electric vehicles (EVs) on energy demand, emissions and air quality has been explored in a number of studies, many of which assess EV impacts in the context of various energy supply scenarios along with increased travel demand. Most, however, do not take into account the impact of self-driving vehicles, otherwise referred to as Autonomous Vehicles (AV) or Shared Autonomous Vehicles (SAVs) in quantifying EV effects. In this study, we assess the future impact of AVs, SAVs and EVs under an energy policy (EP) where relaxed controls are enacted across multiple emission sectors. A moderate climate projection under the Representative Concentration Pathways (RCPs) 4.5 is used. The 2050 EV scenario is compared with an alternative 2050 scenario where passenger cars are gasoline powered. In all cases, the on-road fleet of internal combustion vehicles (ICVs) are expected to be more efficient and less polluting than they are at present, such that non-tailpipe emissions are a major fraction of the particulate matter emissions, limiting the positive impacts of EVs on air quality. Both 2050 future scenarios are also compared with the 2011 emission inventory, where passenger cars emitted more pollutants, to assess the

impacts of regulations over time. The results for both 2050 RCP 4.5 scenarios presented in this chapter for future climate projection scenarios, found significant reductions from 2011 in primary and secondary pollutants. Despite the added increase in VMT due to AV and SAV utilization with electric vehicles in the 2050 scenario with electrification, the difference between the two 2050 scenarios (with/without electrification) showed reductions due to fleet electrification in NO_x (max ~0.5ppb), O_3 (max~2ppb), and daily maximum 8HR O_3 (max~2ppb).

Keywords: Air quality, Emissions, Fleet electrification, Autonomous Vehicles.

5.2 Introduction

The transportation sector has a significant influence on the environment, as it consumes about 30%[282] of all energy use within the U.S., and is largely responsible for the bulk of emissions within cities[283, 284]. Mobile source emissions from the transportation sector, including particulate matter ($PM_{2.5}$), nitrogen oxides (NO_x) and volatile organic compounds (VOCs), are known to have adverse environmental impacts and health effects[6, 285, 286]. The latter two listed pollutants are key in the formation of tropospheric ozone (O_3), which also has adverse impacts on human health and the environment[287]. Cleaner standards imposed by the federal government on internal combustion vehicles (ICVs) have been effective at reducing emissions of these pollutants[288, 289]. A study by Song et al. (2008)[290] found that mobile source emission reductions due to federal regulations reduced daily maximum hourly ozone by about 10ppb in a number of case runs. While there is an ongoing trajectory in regulations for cleaner vehicles, a number of scenarios affect future reductions of both primary and secondary pollutants. Firstly, there is the risk that energy policies that pushed for reduced emissions could be rolled back, stalled or dismantled in the future by policy makers for various reasons[291]. But more to the point, even in scenarios where stringent

policies remain, obtaining a neutral carbon footprint for climate mitigation solutions or obtaining zero emissions will be nearly impossible with a fleet of predominantly ICVs. This problem is further exacerbated with an expected rise in vehicle miles traveled (VMT) and population increases[8].

Many states such as New York[292] plan to achieve a zero carbon footprint by 2050, and a significant change in auto fleets will be crucial to achieving this goal. A zero-carbon emissions footprint in cities can be assisted by using Electric Vehicles (EVs), which consist of Hybrid Electric Vehicles (HEVs), Plug-in-Hybrid Electric Vehicles (PHEVs) and Battery Electric Vehicles (BEVs). So far, EVs have shown potential for reducing primary pollutant emissions and secondary pollutants in a number of studies, although their full effect in the context of tighter vehicle emission regulations are somewhat modest. For instance, Nopmoncol et al. (2017)[293] conducted a study where 2030 electrification of the on-road and off-road mobile sector were evaluated with noticeable improvements in ozone of 1ppb and $PM_{2.5}$. However, they found the changes were largely attributed to reduced emissions from on-road ICVs, despite using a mix of cleaner energy sources for the marginal increase on electricity grid demand (~5%) from EVs. The study concluded that most of the improvements with electrification were seen from the off-road sector vehicles like lawn mowers and marine vehicles, which had not been subject to the same levels of emission reductions, and not from on-road electrical vehicles.

While there is consensus that primary pollutants are reduced with fleet electrification, its effects on ozone and $PM_{2.5}$, in conjunction with ongoing emission controls make the potential benefits less obvious. As noted in Schnell et al. (2019)[28], observing appreciable improvements in secondary pollutant concentrations like ozone from electrification is further complicated because it varies by season, region etc. Therefore, the impact of EV power trains (i.e. HEV, PHEV and

BEV) on the aforementioned pollutants might appear to be modest in conjunction with current federal policies unless energy generation shifts to renewable or cleaner sources[293-295]. However, even without non-renewable energy sources, under different Representative Concentration Pathways (RCPs) and warmer climate scenarios, the impact of EVs might be more noticeable than ICVs, particularly in regard to ozone formation[255].

The future effects of EVs will not only be influenced by the energy mix, climate and power train, but also by the adoption of AVs, which could lead to an increase in VMT. Although automation is not strictly confined to electric cars, electrification does allow for easier automation[296], and with automation will come the ability for many people to utilize more traveling options through the self-driving feature of AVs and Shared Autonomous Vehicles (SAVs)[297]. SAV in particular, can affect car ownership and price, especially if utilized by ride sharing companies like Uber and Lyft who can employ a fleet of SAVs, resulting in an increase of vehicles use by the consumer, an increase in vehicle utilization, and therefore lower prices and even more VMTs[298]. Thus, for this reason and others previously mentioned, self-driving vehicles are expected to have larger market share (~ 36%)[299] of electric vehicles by 2050[26, 300]. The associated impact is not only expected to change vehicle ownership by households, but could increase the use of SAVs, and in doing so, provide vehicle access to socio-economic groups that may otherwise not have access to such vehicles for multiple factors[301]. As SAV utilization via automation and electrification is expected to account for a significant and growing portion of annual VMTs[299], the combination of electric cars and increased vehicle miles traveled will impact emissions, in part, because non-tailpipe emissions are a growing fraction of the PM emissions from vehicles. As a result of increased VMT, a noticeable increase in the use of electricity and emissions from power plants is a secondary effect of electrification and automation. An increased VMT contribution from SAVs

could significantly increase energy demands, whereas increased EV demand on electricity production has been previously considered marginal[295].

Air quality impacts from increased VMTs by SAVs have not been explored extensively. Further, while some look at the impact of electrification with increased VMTs in future years, not many address it with the full impact of other sectors (point, area etc.), changes under relaxed energy policies, as well as the effect of climate change and projected meteorology. Here, we do a full assessment and incorporate a mix of electric vehicle types, unlike other studies that limit their focus to one or two types of electric vehicles. We focus on electrification of the light duty vehicle (LDV) fleet in the year 2050 with a mix of power train technologies (i.e. HEV, PHEV and BEV). We make use of Chemical Transport Models (CTMs) and an EPA mobile emission simulator in this study to simulate air quality under two temporal base line scenarios (2011 and 2050 without electrification) to compare with 2050 electrification scenarios. We limit the input factors of this study to EV adoption and increased travel demand in 2050 under a moderate RCP climate scenario. We do not focus on the potential impact of increased electricity demand from EV and AV adoption. Our objectives in this study are to answer the following:

1) How will increased vehicle miles from automation impact air quality in the future?
2) What will be the impact of electrification and power train of the vehicle fleet on air quality?
3) What is the impact of improved ICV efficiency on electrification impacts?

5.3 Methods

Chemical transport modeling was conducted using CMAQ[231], driven by emissions developed and processed by SMOKE with meteorological inputs developed from the Weather Research and Forecasting (WRF) model[231, 302].

5.3.1 Emissions.

The 2011 National Emission inventory (NEI)[303] was used for the base case of 2011, while 2050 projected emissions were scaled up using statistical projections of future energy demand and emissions factors. With the exception of the mobile transportation sector, most of the details for these emissions scales are found in Shen et al. (2019)[304], and briefly described in subsequent paragraphs.

5.3.1.1 VMT and VPOP projections for 2050 electrification

2050 projections were developed using the 2011 NEI emission inventory, a national household survey and EPA emission factors from MOVES. The survey data is a projection analysis of U.S. household adoption rates of electric and autonomous vehicles between 2017 and 2050 as well as use of shared autonomous vehicles[299, 305]. A statistically representative sample of 1414 U.S. households was used in the survey, and the description of survey data for each household covered the annual number of miles traveled if using an autonomous vehicle (AV) or a human operated vehicle (HV). Also taken into account was the cost of keeping and not keeping HV capabilities in the vehicle. A total of 12 scenarios were performed for 5%, 7.5% and 10% AV pricing reduction rates with HV option (i.e. AV with/without HV, AV/HV and 3 price ranges). For purposes of our research, the 5% price adjustment with HV capability retention scenario was used. In addition to vehicle automation and its impact on adoption rate purchase, the power train makeup for the vehicles in the survey, as shown in Figure 5-1, consisted of the following: a) Gasoline, b) Diesel, c) Plug in Electric Hybrid (PHEV), d) Hybrid Electric Vehicles (HEV) and e) Battery operated vehicles (BEV).

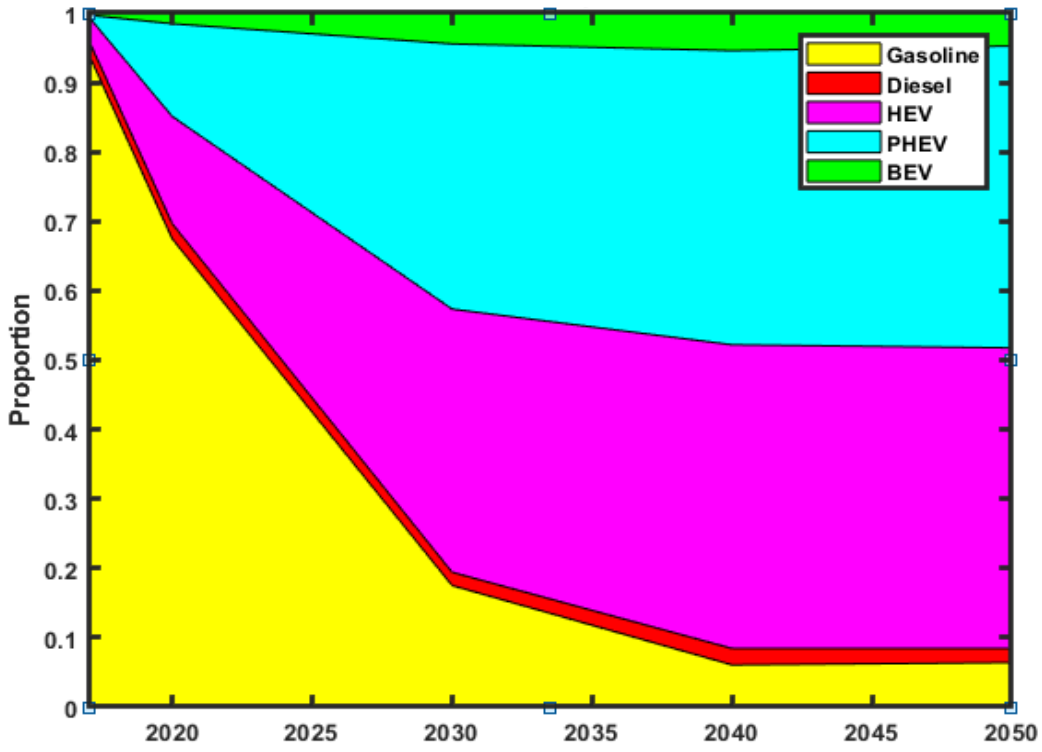

Figure 5-1: Power train make-up of electric fleet

The survey results were projected from 2017 to 2050 and included fleet turnover data and the number of miles driven with SAVs. The survey showed a general decrease in household VMT (personal miles) driven and an increase in miles driven with SAVs. A breakdown of the survey data after scaling up to national estimates is shown in Figure 5-2 and additional details can be found in Quarles et al. (2018, 2020)[299, 300] and Lee and Kockelman (2019)[305].

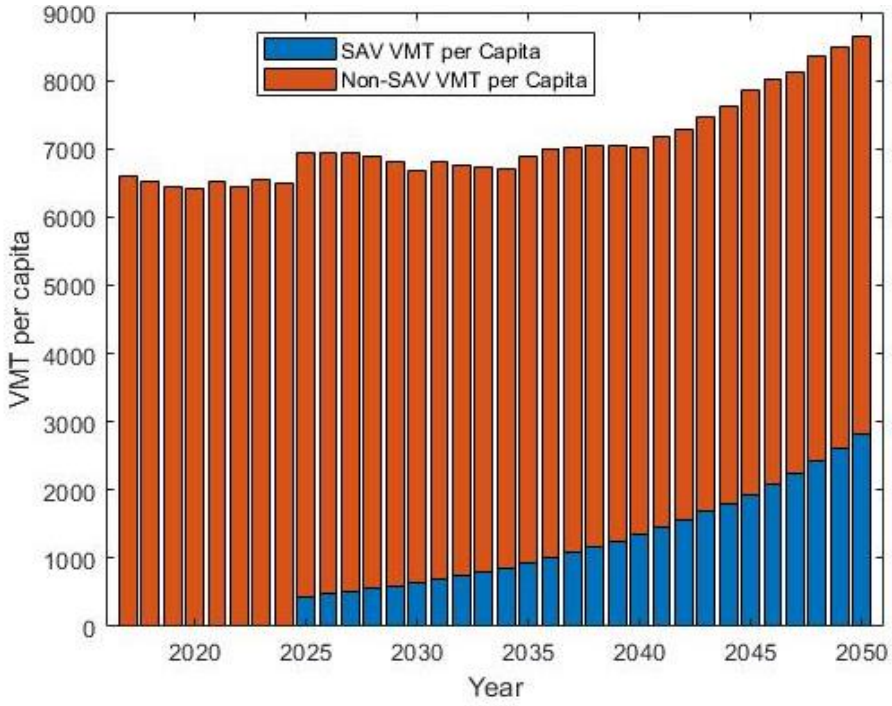

Figure 5-2: Break down of VMT per Capita Miles

Statistical projections of household and national population were used to scale up the survey data to obtain a national estimate of vehicle miles traveled (VMT) for the 2050 electrification scenario. Projected household and population data tables from Statista[306, 307], together with 2011 NEI data, state motor vehicle registrations from the Federal Highway database[308] and projections from the Energy Information Administration[14] provided VMT and Vehicle Population (VPOP) data. The month of July was chosen to evaluate the impact of ozone in the summer months, and 2050 was chosen to allow time for sufficient market share of EVs. The scaled up VPOP and VMT data were then used as inputs into a mobile emission estimator to generate emissions for different pollutants

5.3.1.2 Emission estimates and scale up factors

The EPA's Motor Vehicle Emissions Simulator (MOVES2014b)[309] was used to develop scale up factors for mobile emissions in the 2050 electrification scenario. The MOVES program

has been used in similar studies such as those by Pan et al. (2019)[272] and Gunseler et al. (2017)[310]. As described on the EPA website[281], MOVES is a "state-of-the-science emission simulator" that captures emissions from mobile sources using different emission factors (EFs) for different vehicle types (i.e. motorcycles, LDVs) in a variety of automotive processes such as running exhaust or evaporative processes. Emission factors are estimated or cataloged by the EPA in MOVES as far back to 1960 (although MOVES yearly input starts at 1990) for all vehicle types and power trains. The EFs also vary for each vehicle under different driving conditions (i.e. speed and road type) and meteorology (i.e. temperature and humidity). Due to emission controls and technological improvements, emission factors for all fuel types are expected to improve in future years, and MOVES will capture these changes. More information about MOVES can be found on the EPA website[281].

Although MOVES is used widely for mobile estimations, one of its short comings, in studies such as this as noted by Guensler et al. (2017)[310], is that MOVES does not have a source category for HEV or PHEV vehicles. Studies utilizing MOVES, follow Guensler et al. (2017)[310] by treating HEVs as gasoline vehicles and, in many cases, treat PHEVs as BEVs. However, while HEVs at higher speeds and PHEVs (when not in electric mode) tend to run similarly to gasoline vehicles, there is no mechanism in MOVES to account for low speeds when HEVs engage in regenerative breaking to run on electric mode or when PHEVs deplete their battery power source and switch to gasoline. Another short coming of using MOVES in this study is the lack of fuel economy when calculating fuel differences. As noted by Guensler et al., (2017)[310], the fuel economy for fully electric vehicles and gasoline vehicles are listed as the same in MOVES.

As MOVES does not have emissions factors for hybrid or plug in hybrid electric cars, but it does for BEVs, we develop our own method of categorizing. For HEV vehicles, we split the

VMT proportions by speed and road type. We assume that HEVs will run primarily on their electric motor below a certain speed threshold and thus simulate the proportion of miles as BEVs for that speed range and above that as gasoline cars. With PHEV cars, we use a baseline that a PHEV battery can drive up to a certain mile range before the gasoline engine is utilized, and split the VMTs based on the number of VMTs driven in households with one or two cars. For one-car households, we subtract the yearly average of miles driven for households and place the number of miles above battery range as gasoline and assign the VMTs driven for the second car in the household as BEV miles traveled.

We used a slightly different method to approach the final scale up from 2011 to 2050 than outlined in Pan et al., (2019)[272]. Where they modified EFs generated by MOVES to get spatially gridded emission input files, we used the calculated VMT and VPOP obtained in the preceding steps as direct inputs into MOVES to get 2050 emissions estimates. The MOVES output of emissions was then scaled with 2011 NEI summed emissions to obtain emission scale up factors used to multiply the Sparse Matrix Operator Kerner Emissions (SMOKE)[244] generated 2011 gridded emission files to get the 2050 gridded input field for the Chemical Transport Model (CTM).

5.3.1.3 Energy and emission projections from other sectors

The energy projection from other sectors, such as residential, commercial, industrial, and power were estimated using the Georgia Institute of Technology's National Energy Modeling System (GT-NEMS) [311-313]. GT-NEMS is a computational general equilibrium model based on the 2018 distribution of the U.S. Energy Information Administration's (EIA) National Energy Modeling System. The estimates were conducted using less stringent Relaxed Energy Policies

(REP). Biogenic emissions were estimated with an updated version of the Biogenic Emission Inventory System (BEIS)[314]. To get the future biogenic emissions, BEIS was driven by the 2050 meteorology. The simulation showed a 13% increase in biogenic emissions compared to current levels. Additional details can be found in Shen et al.(in submission)[312].

5.3.2 Meteorology projections

As outlined in Shen et al. (2019)[304], climate and meteorology predictions were made using bias-corrected output data from the National Center for Atmospheric Research's Community Earth System Model version 1 (CESM1)[315]. The data which were spatially downscaled to 36-km resolution using the Weather Research and Forecasting Model version 3.8.1[302]. The climate scenario we chose was the Representative Concentration Pathway (RCP) 4.5, being representative of a climate scenario with moderate increase in temperature. During the WRF downscaling, spectral nudging was applied to temperature, horizontal winds, and geopotential heights, with a wave number of 3 in both zonal and meridional directions and a nudging coefficient of 3×10^{-4} s^{-1} for all the variables.

5.3.3 Air quality modeling with Chemical Transport Models (CTM)

Similar to the study by Pan et al. (2017)[272], we used the SMOKE-WRF-CMAQ[231, 244, 290] set up to model atmospheric concentrations. SMOKE was used together with 2011 NEI emissions to generate gridded emissions together with meteorology projections from the Weather Research Forecasting Model (WRF)[247]. Then scale up factors (as outlined in previous sections) were applied to the gridded SMOKE emissions to scale up to emissions in 2050 for all the emission sector sources like area and point. Scale up factors computed by Shen et al. (2019)[304] were used to scale up emissions from other sectors in the 2050 REP base case. For the 2050 electrification scenario,

the mobile sector was scaled up using computed emission factor results from MOVES. Of note, the 2050 REP base case mobile sector does not consider electric vehicles.

The Community Multiscale Air Quality (CMAQ) modeling system v5.0.2 with Chemical Bond (CB) mechanism 5 simulated the impact of atmospheric processes (transport, deposition, reactions etc.) and emission changes on air quality. Details for the model are documented in Byun et al., (2006)[231]. The simulation runs were conducted for the month of July at a 36km x 36km grid resolution over the entire U.S., using 2050 projected meteorology and 2050 projected BEIS for all cases.

5.3.4 Scenario simulations

We consider three scenarios (Table 1).

- Emissions Temporal: 2011 and 2050 (July)
- Meteorology: 2050 Projected meteorology
- 2050 Energy Policy: 2050 Relaxed Energy Policy (REP)
- Resolution: 36 km X 36km grid size.

3 Simulation Cases for emissions

1. 2011 Emission base case with 2050 projected meteorology and 2050 BEIS.
2. 2050 Projected Emissions under REP with 2050 projected meteorology, 2050 BEIS, and 2050 emissions with no fleet power train changes.
3. 2050 Projected Emissions under REP with 2050 projected meteorology, 2050 BEIS, and 2050 emissions with increased VMT and fleet power train changes.

5.3.5 Data analysis

The changes in NO_x, SO_x, $PM_{2.5}$ O_3-8HRMax, and monthly averaged ozone are assessed in this study under the three scenarios. All scenarios are conducted using the same meteorology so that the impact of emissions changes can be clearly assessed in the same climate scenario to help quantify the effect of potential emission reductions due to electrification. We not only explore the

spatial profile of each pollutant, but we also assess the spatial and nominal concentration differences among all three scenarios.

Table 5-1: Scenarios

Case	1	2	3
Emissions Scenario Year	2010	2050	2050
Ref_Base Case	1	1	1/2
Future Energy policy (REP/Aggressive)	N/A	REP	REP
Marginal Energy Adjusted for EV Charging on the grid	NA	N/A	No
Meteorology	2050	2050	2050
Climate: Representative Concentration Pathway	4.5	4.5	4.5
Biogenic emission file	BEIS 2050	BEIS 2050	BEIS 2050
Electrification Scenario	None	None	5%_with HV

5.4 Results

Future emissions decrease substantially in 2050, despite increasing travel demand (Figure 5-3). This decrease reflects the impact of increased efficiency controls and emission regulations in all sector sources like point sources (i.e. Electrical Generating Units [EGUs]), to the mobile sector and area sector (i.e. residential homes) and replacement of higher emitting vehicles in the fleet. The impact of these changes on both mobile and EGUs is particularly noticeable when looking at the spatial distribution of NO_x emissions (Figures 5-3 a-c).

The impact of tighter regulations and controls on $PM_{2.5}$ and SO_2 on the EGUs yielded improvements in the 2050 scenarios when compared to the 2011 base case (Figures 5-3 d-f, Figures 5-3 m-o). Most of these changes were observed in the southeastern region of the country (e.g.,

Hennerman et al. (2016)[90]). The regulations also had an impact on ozone, which has been observed in studies by Henneman et al.(2017, 2017)[90, 265] as well as others[316].

The concentration and spatial distribution of monthly averaged ozone over the region and daily averaged 8 hour maximum ozone (O_3-8HRMax) show noticeable improvements in 2050 when compared to the 2011 base case. For the monthly averaged ozone concentration and averaged O_3-8HRMax, the impact of electrification between the two future scenarios is evident (Figures 5-4 g-l). Overall, there is a about a 0-1 ppb decrease in daily 8 hour maximum ozone and a decrease of about 1-2 ppb in monthly averaged ozone. The direct impact of electrification on ozone here is clear, similar to other studies[28].

For NOx, the 2050 REP base case (Figure 5-3) is spatially similar to the 2050 electrification scenario but the NOx spatial distribution (Fig 5-4c) captures the impact of an electrified fleet in the future year scenario along major interstate roadways. Between the two future year scenarios, there are modest reductions of NO_x emissions with the electrified fleet scenario cut by as much as 0.5pbb. NO_x reductions between 2011 and 2050 range from 0 to 1ppb across the country, with the highest reductions seen mainly in the Southeast, which reflects the regulation impact on EGUs and on transport (Fig.5-4).

Pollutant	2011 Base Case	2050 REP Base Case	2050 Electrification
NOx	a 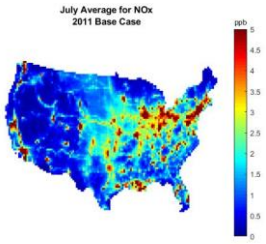	b 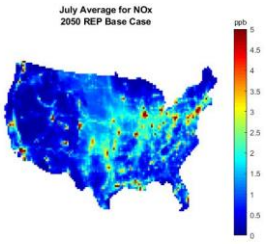	c 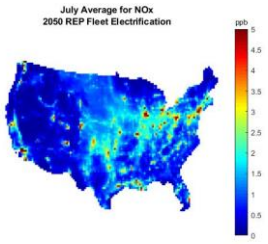
$PM_{2.5}$	d 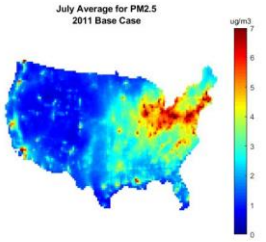	e 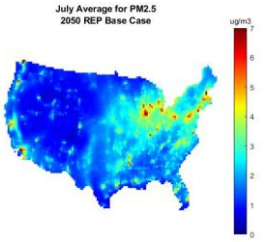	f 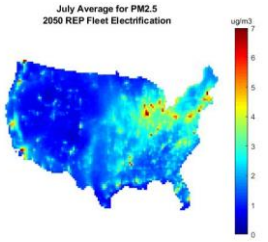
O_3	g 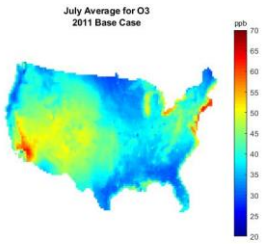	h 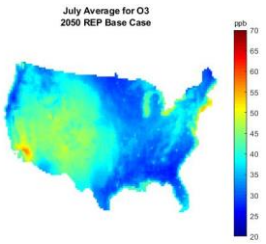	i 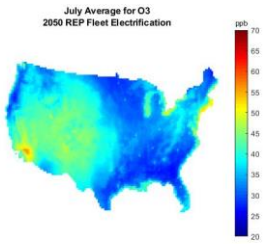
O_3 8hr max	j 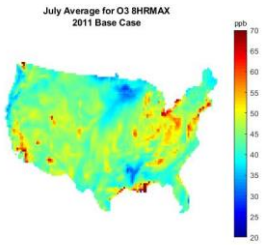	k 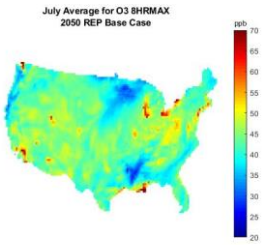	l 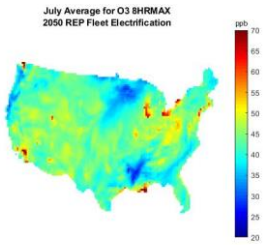

SO_2	m 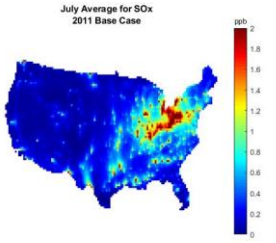	n 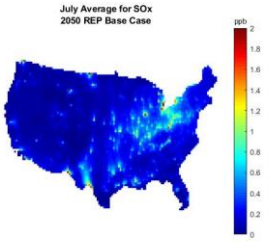	o 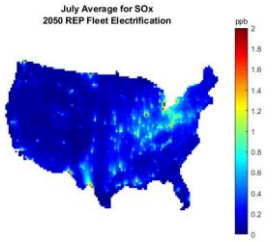

Figure 5-3: Plots show the simulated, monthly averaged spatial concentrations of NOx, O3, PM2.5, Maximum 8hr O3 and SO2 for the month of July using 2050 meteorology and 2011 and 2050 emissions.

Primary differences of particulate matter emissions show a spatial pattern different than NOx between future years and the 2011 base year (Figure 5-4). In the Southeast, we see an obvious reduction in $PM_{2.5}$ in orders of 2 ug/m^3 for $PM_{2.5}$ and a negligible change overall in other areas of the country between the 2011 and 2050 scenarios. Between the 2050 scenarios, electrification shows a decrease in primary pollutants, which was expected. However the change was miniscule, reflecting the efficiency in motor vehicle emission regulations. The reduction in $PM_{2.5}$ from electrification covered a broader spatial extent and was not restricted to roadways, which highlights a positive impact in secondary particulate matter.

Changes in sulfur dioxide spatial concentrations between the 2010 base year and future years are observed. Notable reductions in SO_2 levels are found in the Southeast from regulations on power plants emissions. Between the two 2050 future scenarios, there is a slight increase in SO_2 concentrations in the electrification scenario. SO_2 was the only pollutant to show an increase in concentration with the electrification scenario over the 2050 REP base case however, this change is negligible (~ 0.005 ppb).

Pollutant	2050 REP – 2011 Base	2050 Electric –2011 Base	2050 REP – 2050 Electric
NOx	a 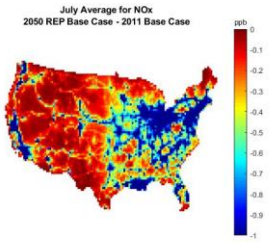	b 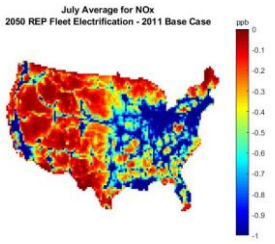	c 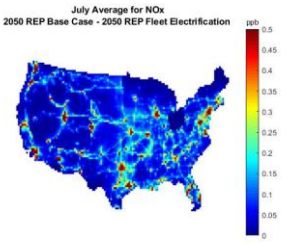
$PM_{2.5}$	d 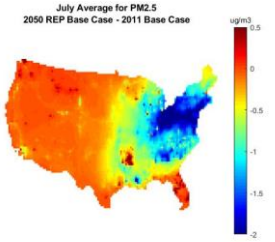	e 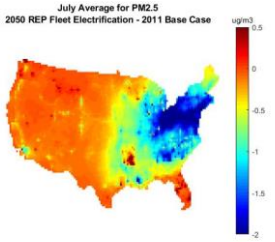	f 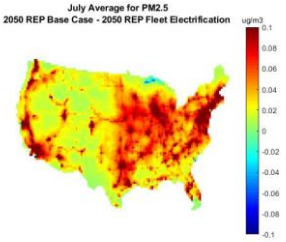
O_3	g 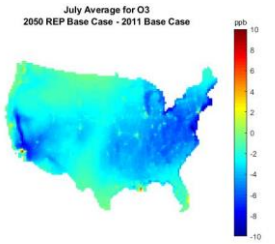	h 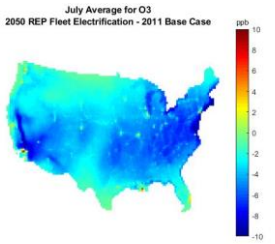	i 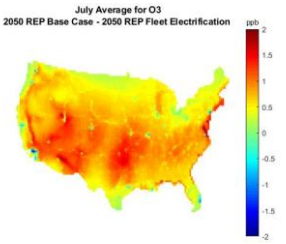
O_3 8hr max	j 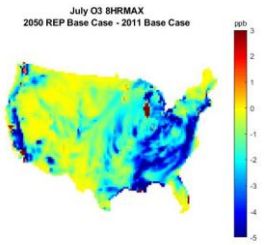	k 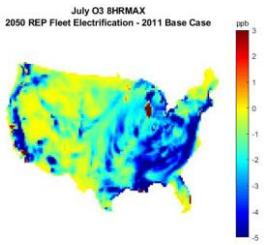	l 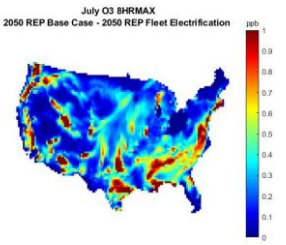

SO_2	m 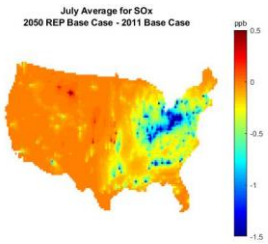	n 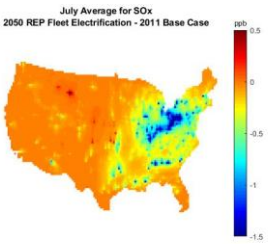	o 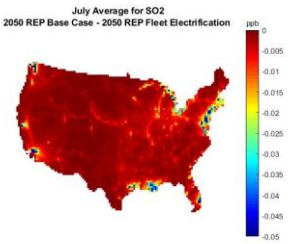

Figure 5-4: Plots show the differences in simulated, monthly averaged spatial concentrations of NOx, O3, PM2.5, Maximum 8hr O3 and SO2 for the month of July using 2050 meteorology and 2011 and 2050 emissions

5.5 Discussion

Similar to previous studies, modest decreases in pollutant species were observed with electrification except for SO_2, although this increase was small. We did not consider the incremental demand on electricity consumption from PHEVs and BEVs here, although with a less-clean energy mix, the increased electricity demand of the electrified fleet could increase SO_2 emissions and possibly NO_x and $PM_{2.5}$[317]. While studies by Pan et al., (2019)[272] and Nichols et al.,(2015)[295], showed increases in energy demand from EVs are expected to be miniscule, a study by Li et al., (2016)[318] which incorporated incremental energy demand showed an increase in primary pollutants of SO_2 and NO_x from power plants with a less clean energy mix. Future work would incorporate the added demand load from EVs, and SAVs on electricity charging to evaluate the impact of different energy mixes.

The 2011 and 2050 reductions for NO_x, SO_2 and $PM_{2.5}$ are largely noted in the Southeast, as a result of tighter regulations on the energy centers located in the region. The effect of fleet electrification in 2050 can be seen with NO_x along the interstate roadways and urban centers. Substantive ozone improvements between 2011 and 2050 appear to happen both in the Southeast and West Coast and there is a noticeable decrease in daily maximum 8Hr O_3 throughout the country. The electrification effect on ozone is evident (Figure 5-4). While ozone is lower in both

future scenarios over 2011, electrification yielded further reductions of about 1 ppb to 2 ppb. Reductions in daily average maximum ozone are noted with an improvement of about 1ppb in most areas in the electrification scenario. Schnell et al. (2019)[28] also found modest reductions with ozone in conjunction with electrification. $PM_{2.5}$ reductions from fleet electrification are generally more spatially spread out in the Southeast, highlighting the impact of dispersion and particulate formation in the atmosphere. The magnitude of the reduction is limited (~ 0.1 ug/m^3), because tail pipe emissions from ICVs are also expected to be quite low in the future.

The projections of the future years, show that EVs will have a noticeable, albeit minimal impact with respect to current emission regulations in all sectors and with highly efficient ICVs on primary pollutants. Similar results were also observed by Brady et al., (2011)[319], who concluded that overall changes were minimal. However, given the current energy mix or less renewable mix if marginal electricity increments were taken into account, the results could be that EV adoption might further increase the amount of emissions, as has been noted in a few studies, although this is also highly dependent upon the EV power train as well[294]. This becomes important if all the cars eventually become fully electric and will be powered by the electric grid. Under a relaxed energy policy scenario, this might result in more pollution, although it is likely to be concentrated near the power energy sources.

Under different energy scenarios (i.e. renewable/non-renewable), warmer meteorological and climate projections with different RCP pathways could show an advantage of EVs over ICV vehicles, especially in regard to secondary pollutants like ozone and particulate matter. The spatial distribution of ozone and $PM_{2.5}$ (Figures 5-4 f and 5-4 i) under the electrified scenario highlight this potential effect. In a warmer climate and with cleaner fuel sources, there is a bigger potential for EV cars to reduce the number of peak ozone days under NO_x limited scenarios[320]. Therefore,

the impact of EV adoption on air quality under more carbon intensive RCPs is likely to be significant given that studies by Shen et al. (2019)[304] and Zhang et al. (2017)[255] show that greater ozone level exceedances is expected under warmer climates. The spatial distribution of positive ozone abatement (Figure 5-4 i) in the electrified scenario highlights the benefits of minimizing NO_x on roadways. Therefore, EVs can be effective in mitigating ozone exceedances in a more adverse climate.

Lastly, while the study finds that the 2050 fleet scenario presented here, comprising of a mix of electric car types (HEVs, PHEVs, and BEVs) have some advantages over future gasoline vehicles in terms of improving air quality, the results suggest that moving to a fleet of Battery Electric Vehicles (BEVs) is where larger impacts might be realized.

The results here demonstrate EVs potential in improving air quality through reduction of primary and secondary pollutants. However when evaluated in the context of a life cycle assessment study, the mitigation effect from the use phase of EVs is not enough to offset the greenhouse gas (GHG) emissions from the production phase if less renewable sources are used[321]. It is for this reason that studies like Dillman et al., (2020)[322], urge that de-carbonization measures should be prioritized over electrification.

While GHG mitigation is a priority in the life cycle assessment studies of EVs, the full measure EV efficacy also needs to consider the impact of materials and natural resource depletion, as well as the recycle and end of life phase. There also needs to further analysis that includes impact of primary and secondary pollutants during the entire life cycle (“cradle-to-grave”) that goes beyond quantification of net increases, but includes air quality modeling as was done in this study to quantify the effects during the use phase of the vehicle. Only by including the full impact

of embodied emissions associated with EVs, can their efficiency over fuel powered vehicles be effectively assessed.

5.6 Conclusions

When compared with the 2050 REP base year, electrification found reductions in all primary pollutants except SO_2. However, due to continuing emissions reductions in EGUs and ICVs with current standards, the benefits are modest. EV impacts are likely to be more noticeable for secondary pollutants like ozone and particulate matter, particularly under warmer climate conditions. It is also worth noting that EVs, unlike aging ICVs that can become high emitters due to emissions-equipment failures, are still much cleaner. Further, EVs become cleaner as the nation's power plant investments evolve away from coal, and even away from natural gas, toward a much greater share of nearly-zero-emission renewable feed stocks. Thus EVs stand poised to make significant improvements to 2050 air quality in the U.S. than currently projected, however, a full life cycle analysis that incorporates embodied emissions associated with EVs should also be considered.

5.7 Acknowledgements

The authors are grateful for the funding support of the National Science Foundation under grant 1444745–SRN: Integrated urban infrastructure solutions for environmentally sustainable, healthy, and livable cities.

CHAPTER 6. SUMMARY, CONCLUSIONS AND FUTURE RESEARCH

6.1 Overview

Impacts of various city infrastructure elements, such as transportation and residential buildings that support human activities and society can be both beneficial and adverse. Given the limited resources available, the current focus is on identifying how to make our societies more sustainable (i.e., support current and future well-being, including human and environmental health). In this thesis, we focus on the linkages between specific energy consuming infrastructure components and air quality, recognizing that exposure to air pollution (particularly particulate matter and ozone) is the largest risk factor associated with disability-adjusted life years lost (DALYs: a metric used to quantify adverse impacts of disease factors). The work described in this thesis quantified linkages between various infrastructure components and air quality. This work has led to both general and specific conclusions and, as most research does, areas ripe for future study. Here, general insights from the research are identified, and proposals for future work are suggested. Most of the work here has been published, in review or in preparation for submission. We discuss the conclusions here in the context of societal and environmental policy, implications using the sustainability framework introduced in Chapter 1.

6.2 Conclusions

The research described in this thesis investigated how infrastructures and the policies that regulate the emissions from those infrastructures affect air quality. Each study used different sets

of tools to investigate various linkages, resulting in individual sets of conclusions as detailed in subsequent sections.

6.2.1 Chapter 2: Decades of progressive environmental policies are needed to reverse the impact of anthropogenic emissions on air quality.

In **Chapter 2**, ambient data was compiled from three national monitoring networks, (AMoN, CASTNET & SEARCH) to assess the effect of emissions controls and related policies on aerosol acidity. Gaseous and particulate matter composition served as inputs for ISORROPIA, a thermodynamic equilibrium model that calculates particle thermodynamics, including composition and acidity (pH) from species concentrations in both phases (gas and solid/aqueous particulate). Data were available over a span of 5 to 8 years, depending on the network. Spatial mapping (2001 and 2011) of CMAQ-modeled acidity outputs were found to be largely consistent with observations. Aerosol acidity is due to acidic components present in the aerosol, which in this case is mainly sulfate and nitrate. The presence of sulfate drives aerosol acidity low (pH < 2). Its effect is buffered by the presence of cations, such as ammonium and non-volatile cations (e.g., sodium and calcium) and low temperatures, which allows for increased ammonium and nitrate aerosol partitioning to the condensed phases at slightly elevated pH values (i.e. > 3).

The same trends observed in Weber et al., (2016) were found to be true nationwide, as estimated aerosol acidity failed to change despite significant reductions in emissions and sulfate. Further, because the aerosol particles are highly acidic, nitrate substitution was limited. The results show that particles will remain acidic, both in rural and in urban sites, for decades to come. This trend as seen across the U.S., has the following implications: 1) aerosol acidity remains high and will likely continue to affect $PM_{2.5}$ toxicity, 2) despite large reductions in $PM_{2.5}$ mass

concentrations, disadvantaged socio-economic groups (SES), typically comprised of low-income and minority populations, will continue to be exposed to poor air quality and particulate matter with high acidity, possibly linking the disproportionate health outcomes observed with $PM_{2.5}$ more than any other pollutant, and 3) while air regulations have had a significant impact on air quality, it will take a substantially long time to see the restoration of atmospheric particle acidity to pre-industrial levels.

6.2.2 Chapter 3: The link between urban morphology and energy use is quantified

In **Chapter 3**, the relationships between socio-economic and demographic (SED) variables and energy are found between two types of residential energy use, electricity, and natural gas. A statistical residential energy model that uses socio-economic demographic factors to explain energy use is developed for Zip Code Tabulated Areas (ZCTAs) in metropolitan Atlanta for both residential natural gas consumption and electricity consumption. Residential energy use for electricity (2010) and natural gas consumption (2009) from energy providers to those ZCTAs was provided. Most of the SED data was obtained from the 2010 American Survey. With the sheer volume of variables considered (> 330), a number of techniques were employed to facilitate variable selection and address multicollinearity. Data transformation and machine learning methods to improve statistical regression power were explored. For data transformation methods, Z-scores, principal component analysis and two orthogonalization methods were investigated. Of those choices, the Modified Gram Schmidt orthogonalization method proved to be effective at improving the predictive power of the models and minimizing multicollinearity among variables. A number of machine learning regression tools (i.e. random forest, regression trees) and regression models (i.e. logistic regression) performed poorly and were set aside in favor of training and cross-

validation sets with linear regression. A stepwise algorithm facilitated variable selection and pared down the number of variables to be more manageable.

For both models, we expected to see a strong link between the SED variables and certain elements of building type (i.e., house with amenities, apartment vs single-family home). The prevailing presumptions at the start, were that post-design energy use is mostly driven by SED factors, and a statistical model accounting for a large range of variables would be able to establish that link sufficiently. While natural gas use was predicted very well with socio-demographics, electricity use proved to be more complex. An r^2 of 0.95, with a low normalized error of 15% was found for the model relating natural gas use and SED factors, and the electricity model had an r^2 of 0.8, but a higher normalized error (33%). Both models were able to account for high variability in energy use, but the electricity model had a high bias in prediction while natural gas did not. Further analysis using principal component, geospatial mapping and additional regression modeling showed that urban morphology, particularly near roadways, plays a significant role in electricity use, with ZCTAs in high road density areas using more electricity.

The differences between the natural gas and electricity use models highlight that city infrastructure is as critical as socio-economic factors in affecting energy use. This study illustrates that policies regarding city layout and infrastructure choice can inadvertently create more issues and that efficient building designs might not be enough to address increasing energy use and demand. Lastly, although the urban heat island (UHI) effect on energy use has been studied extensively, this is one of the few studies that quantifies the impact of that effect by using energy use data directly from energy providers, as opposed to using an estimated energy value. This reduced the uncertainty in our model and can benefit studies of the impact of infrastructure on UHI and UHI on electricity consumption.

6.2.3 Chapter 4: Airport emission related impacts on air quality are underestimated with regulatory emission inventories.

In **Chapter 4,** the effects of airport emissions (in this case the Atlanta Hartsfield-Jackson airport [ATL]) on air quality are explored. This airport has consistently been the busiest in the world (though COVID changed that this past year). Here, a fine scale chemical transport model (CTM), in this case the Community Model of Air Quality (CMAQ), along with satellite and ground-based observations are employed to link airport related activities to air quality. CMAQ is used by regulatory agencies, such as the Georgia Department of Natural Resources (GaNDR) and the U.S. EPA, to develop emission control strategies, and the enabling of regulatory policies, to achieve their air quality goals. The research here quantified the differences between the use of two different inventories, a 3D inventory with both surface and cruise emissions spatially allocated (horizontally and vertically), and the base inventories with only surface airport operation emissions allocated at the same altitude and location as their associated airports. The base inventory has the landing and takeoff (LTO) emissions allocated only to the surface and was obtained from the EPA's 2016v1 Emissions Modeling Platform[77] (2016 NEI). The 3D emissions is developed by combining the LTO emissions from the 2016NEI with estimated cruise emissions from the Aviation Emissions Inventory Code (AEICv2.1) emissions repository. Both inventories are combined with emissions from other sectors (e.g. onroad, point, non-road) in the 2016 NEI to serve as inputs for the CMAQ model.

The CMAQ results are evaluated using ground-based and high-resolution satellite-based observations from the TROPOspheric Monitoring Instrument (TROPOMI). Model evaluation with observations is generally limited, as near-airport monitors are sparse. Although temporally limited, the satellite data provides a significant advantage with a more complete spatial coverage of

observations, albeit only at the overpass time. We minimize some of the uncertainty introduced by our assumptions regarding spatially allocated airport emissions by evaluating the differences between the 3D and base inventory in ozone and particulate matter concentrations, and by comparing model outputs with TROPOMI observations. We also minimize the uncertainty of how satellite-based observations are transformed to estimated NO_2 vertical column densities (VCDs) derived using air mass factors, replacing default AMFs with those derived from CMAQ, and assessing TROPOMI's ability to provide consistent VCDs with CMAQ modeled results around two power plants whose emissions are continuously measured.

The results show that if base inventories are used in regulatory assessments, airport effects would be underestimated both in spatial extent and magnitude, with a low bias for ozone and a potentially locally high bias for PM (but low bias regionally). For instance, a 6 ppb net increase in maximum daily ozone is seen when looking at the 3D-base inventory differences. Additional increases in ATL emissions also led to more ozone. Simulated $PM_{2.5}$ and UFP were locally lower using the original inventory that concentrates emissions at the airport, but higher levels elsewhere in the domain with the 3D inventory. We also observed that the net effect of airport operations resulted in elevated concentrations of ozone and particulate matter over the modeling domain.

The findings show that urban populations are exposed to elevated concentrations of ozone and particulate matter due to airport operations and that additional increases in airport emissions, will result in more ozone. Also, an increase in airport emissions could present difficulties in the future for metropolitan Atlanta to demonstrate ozone attainment, even with cleaner automobiles in the mix. The overall conclusion of this study is that accurate airport emission inventories with spatially allocated emissions are valuable for air quality modeling.

6.2.4 Chapter 5: Electric cars have advantages over gasoline vehicles in mitigating pollution.

One aspect of the work detailed in this thesis assessed the potential efficacy of an electric automated fleet of passenger cars on 2050 air quality in the US. The study in **Chapter 5** examined a future where gasoline powered passenger cars emit much lower levels of pollution than present day automobiles, and considered the likely air quality impacts of going from a largely gasoline-fueled automobile fleet to one with increasing levels of automated, electric vehicles and VMTs. The chemical transport model CMAQv5.0.2 ran at 36km over the U.S. for the month of July. The EPA's 2011 National Emission Inventory (2011 NEI) served as the base data for all emission sectors, catalogued in the NEI for the CMAQ simulations. Two future (2050) emission inventories were developed by scaling the 2011 NEI while 2050 projected emissions scale factors, developed using statistical projections of future energy demand and emissions factors from Georgia Institute of Technology's National Energy Modeling System (GT-NEMS)[311-313]. A base 2050 emission inventory with mostly internal combustion vehicles (ICEVs) was developed by multiplying the 2011 NEI by the projected 2050 GT-NEM scale factors for 2050. This case represents the scenario with cleaner gasoline powered vehicles. In the alternate 2050 emission inventory, most of the passenger cars were replaced with electric vehicles. Both future scenarios consider the same relaxed energy policy and climate (i.e. RCP45).

The 2050 electrified scenario found reductions in ozone and particulate matter, compared to the case with a pure gasoline fleet, though the benefits are modest due to continuing emission reductions in ICVs. ICVs in 2050 are expected to have low primary emissions of $PM_{2.5}$ and NO_x, such that the benefits for those species were small. However, EV impacts were more noticeable for secondary pollutants like ozone. Even with the increased VMTs, Dynamic Ride Sharing (DRS),

between the two 2050 scenarios (with/without electrification), the electrified fleet scenario led to appreciable reductions in O_3.

Benefits of EV use increase if the nation's mode of generating electricity evolves away from coal to natural gas and, to a greater share of nearly early-zero-emission renewable feed stocks. This becomes increasingly important as the fraction of VMT becomes fully electric and all transport is powered by the electric grid. Thus EVs stand poised to make significant improvements to 2050 air quality in the U.S., and their use in autonomous vehicles that have higher annual VMT may be particularly attractive.

6.3 Synergistic effect of urban infrastructure, technology and policy

The studies show how policy, urban infrastructure, transportation and city layout impact energy and air quality. We see the effectiveness of environmental regulations in curbing emissions, but disadvantaged communities are still disproportionately exposed to high levels of pollution, a result of urban infrastructure, transportation, city layout and regulatory policies. Efforts to curb energy use have led to the development of energy efficient buildings and appliances. However, poor urban infrastructure and layout could offset some of the gains made with these improvements. Regulations have led to dramatic reductions in emissions in Atlanta, but emissions associated with the airport and residential energy use will contribute to total ozone and PM levels in the future. Further, while emissions from cars on a-per-mile basis may be dropping, VMT is increasing and mobile sources will continue to be a major contributor to air pollution. The move to electric vehicles will bring substantial benefits on pollution, but these benefits may be smaller than expected as the result of regulations that will see increasingly cleaner cars in the future.

While gains have been made through the enactment of environmental regulations and innovation, a strategy that considers infrastructure, technology and policy together might be more effective, than implementing plans that focus on one aspect of infrastructure at a time. Such a solution for example would combine battery powered electric vehicle adoption with a 100% renewable energy source for power generation. A multilayered method might therefore be worth considering, in planning for the evolution of cities to be more efficient, sustainable and equitable.

6.4 Contributions to science: expands our knowledge of how the built environment impacts air quality

This thesis quantifies how aspects of urban infrastructures impact air quality. While this work has focused on just a few components of the multiple infrastructures that help our cities function, it shows that multiple factors must be taken into account to address urban sustainability and human well-being. It further demonstrates that the compounded effects of urban infrastructures, play a significant role in the effectiveness of mitigation measures. For example, the potential role of the proximity and layout that multiple elements of city infrastructure have on air quality is not often directly considered, thus leading to areas of relatively high pollutant levels and areas that will not respond as planned to controls. The compounded effect can actually lead to worsening air quality, or in regulations having muted impacts. This is a potentially significant underlying factor and future polices and targeted intervention will benefit if these factors are considered.

Overall, the findings from this study indicate that the integrated application of a wide range of techniques and topics (i.e. air quality modeling, energy analysis, statistics, machine learning,

satellites, data visualizing) was effective at elucidating and delineating the complex, non-linear synergistic interactive effects of urban infrastructure.

6.5 Sustainably focus and policy suggestions

6.5.1 Chapter 2: Progressive policies, targeted intervention and city planning are needed

Aerosol acidity remains high, except in areas where crustal elements and colder temperatures will lead to significantly lower aerosol acidity in response to controls. This means targeted interventions may be required to mitigate the effects on disadvantaged communities that are exposed to elevated levels of $PM_{2.5}$. Because aerosols are likely to remain acidic for decades, long term planning should consider more measures to reduce $PM_{2.5}$ and aerosol acidity. A move toward zero emission cities that includes electric cars and renewable feed stock for electric generating units will go a long way to reducing the burden experienced by disadvantaged SES groups. Urban infrastructure layout and access to green spaces can also help mitigate the adverse effects in areas with higher air pollution exposure.

6.5.2 Chapter 3: A closer look at urban infrastructure is needed to mitigate energy use.

Per capita energy use has historically been higher in urban areas, and that is expected to be the case in the future as well. This contributes to higher pollution levels. As cities continue to expand and change, understanding the key demographic factors and the role of city infrastructure could help guide policy decisions to develop healthier and sustainable solutions.

6.5.3 Chapter 4: Airport locations and different modes of transportation need to be considered

Airports are generally located near urban areas and are hotspots of NO_x and particulate matter emissions. Tank farms and vehicles going to and from airports can also be significant

contributors to VOC emissions as well. The impact of the future growth of airports can have a notable impact on air quality and on urban populations, particularly those living in the immediate vicinity, though the impacts can be widespread. Not all airport-related emissions are as readily controlled as automobiles, which now have effective on board controls, and further reductions are being found from the increasing use of EVs. Solutions here should consider converting onroad modes of transportation to mass transit near airports or fleet electrification.

6.5.4 Chapter 5: EVs could lead to zero-emission cities more quickly than other sectors.

Currently, the traffic sector is responsible for a large fraction of the air pollutant emissions within cities and 29% of all energy use within the U.S. (Energy Information Administration)[27]. As cities continue to expand, along with projected population increases and vehicle miles traveled increases, motor emissions will continue to have a large impact on city air quality. A significant change in auto fleet make up could have a considerable impact on this component. However, EV adoption alone is not enough, because sources of electric also need to be considered. Moving to low or zero-emitting renewable sources would support an electrified transportation infrastructure and healthier cities. This will go a long way toward reducing the burden of disease experienced by disadvantaged communities, particularly those that live near major roadways.

6.6 Future work

From the results in **Chapter 2,** further investigation is needed to develop causal relationships between geography and infrastructure to racial disparities in health and pollution exposure. Quantifying the spatio-temporal dependencies of city-health linkages requires a lot of ambient air data, but unfortunately the scarcity of air quality monitors poses barriers to conducting such studies. In lieu of that, a few studies are beginning to incorporate readily accessible, fine-

scale, satellite-based observations from instruments like TROPOMI as was done in Chapter 4 of this thesis. The wide spatial coverage TROPOMI offers can be used in a proposed study to link spatial and racial disparities with pollution exposure and infrastructure.

Another suggested study would be to expand upon the "Harvard six city" study, which linked $PM_{2.5}$ exposure to mortality by using metrics such as particulate composition and acidity. Data fusion techniques that interpolate both air quality monitor data with modeled fields from chemical transport models as in Senthilkumar et al., (2019)[323] provide reasonably accurate particulate speciated data over large domains, though that data is not always readily accessible, and takes an inordinate amount of resources to develop. This proposed study would focus on disadvantaged social economic groups (SES), typically comprised of low-income and minority populations that tend to be disproportionately exposed to poor air quality and more adverse health outcomes. The objective would be to compare the particulate composition and pH in different urban areas with mortality rates from select geographic regions. Questions that could be asked and answered here include: 1) Is there a change in the leading causes of mortality linked to air quality as the composition of aerosols changed? 2) Is there a causal link between pH and particulate composition to the health and exposure disparities across cities? The study would utilize health prevalence data at the census tract level as the response variable to link city infrastructure and health with ethnic social demographics. Mortality and morbidity data could be obtained from the National Center for Health Statistics, a database maintained by the Center for Disease Control (CDC).[324] Exposure to air pollution and prevalence rates would be quantified across social demographics to understand the impact of speciation of particulate matter and acidity.

The research described in C**hapter 3**, which was conducted at the ZCTA level, could be expanded by conducting energy estimations at finer spatial scales, like the census tract level for

instance. Given the impact of infrastructure, another modeled approach could consider including more of those features (i.e. green space) into the mix as well. The statistical model could be combined with computational models like the Urban Canopy Model[325], which uses an integrated, multiscale urban modeling system to simulate effects such as urban heat islands that create unique urban micro-climates. Another suggestion would be to expand the work of Chapter 3 by including multiple cities and examining the patterns of energy use, urban layout and climate across these municipalities. The study could also incorporate seasonal effects that were not considered in Chapter 3.

For the study in **Chapter 4**, where airport related emission impacts were assessed, a future study could consider incorporating other sectors, such as the onroad sector to explore interaction effects with airport emissions. A closer look at the 2020 Covid period, combined with observations from air quality monitors and satellites, would be a good starting point to explore these interactive effects and could supplement the findings in Chapter 4. Another idea would be to include airports other than Atlanta. The techniques for vertical and horizontal allocation used in the 3D inventory can also be improved by including flight path and activity data.

In Chapter 4, satellite observations were used to evaluate our assumptions about the spatially allocated inventory. However, care must be taken to minimize the amount of uncertainty associated with these measurements. In the chapter, we discussed how we minimized the uncertainty in TROPOMI observations, by substituting default vertical profiles with those derived from the fine scale air quality model (CMAQ). A study could explore the sensitivities of model-derived AMFs to the planetary boundary layer height in the model. Future work could also focus on ways to validate, or quantify the uncertainty in satellite-derived VCDs by getting measurements of NO_2 vertical profiles to compare with TROPOMI, as is being done in the Kaiser and Russell

group here at Georgia Tech. Expanding the validation technique used in this thesis between TROPOMI and power plants' NO_2 VCDs to other U.S. sites could also prove useful in further demonstrating TROPOMI's capabilities and quantifying the uncertainties.

Lastly, the deployment of TEMPO, the first space-based instrument to monitor air pollutants hourly across the U.S.[326], offers an opportunity to incorporate finer scale satellite observations (i.e. ~1 km TEMPO vs ~ 4km TROPOMI) with similarly scaled chemical transport modeled simulations in air quality studies. TEMPO provides an opportunity to continue the overarching work in this study to delineate the interactive effects of urban infrastructure with air quality, but at much finer scales. Combined with the increased temporal resolution (i.e. 12hrs TEMPOS vs ~ 1hr TROPOMI), this will increase our understanding of how the built environment affects air quality and the efficacy of regulations.

The study in **Chapter 5** could be developed further by considering additional scenarios than what has been done so far in this thesis. In the chapter, the efficacy of EVs over gasoline passenger cars, under a relaxed energy policy in a moderate climate, was explored. A future study could consider a different energy fuel mix for the charging sources of these EVs, and it could also assess the electrification of the entire onroad fleet, including buses and trucks. This could be done under different climate scenarios as well (i.e. RCP 8.5 and RCP 4.5). A modest EV automation adoption scenario was considered here, as evidenced with the net increase in VMTs over the base case, but different adoption rates of automation should be considered in a future study because automation will be a substantial share of VMTs in the future.

The current study limits its assessment to air quality metrics, but does not consider health benefits or the reverse. A mortality assessment should be included when considering the efficacy of EV adoption.

Chapter 5 looks at two 2050 scenarios, however, some form of electrification could be considered in the present day fleet. It provides an opportunity to look at the synergistic effect of multiple modes of transportation in an urban area. For instance, electrification of half of the passenger car fleet today could change some of the results arrived at in Chapter 4. EVs also provide an opportunity to assess the effects of urban infrastructure with policies (i.e. a policy stating only renewable fuels for EGUs can have different effects if EVs are considered). EVs clearly provide an opportunity to assess what kind of policies should be enacted.

Lastly, although EVs are likely to improve urban air quality, the "cradle-to-grave" aspect of the batteries needs to be considered as well. From the resources used for manufacturing, to the environmental cost, to their final deposition, their lifecycle needs to be explored. This analysis is necessary for us to understand the ways EVs can affect our lives, and whether or not they offer a sustainable or viable option for the next 50 to 100 years.

APPENDIX A. SUPPLEMENTAL MATERIAL FOR CHAPTER 1

Adapated from Joseph L. Servadio, ScM[b], Abiola S. Lawal, MS[c], Tate Davis[a] , Josephine Bates, MS[c], Armistead G. Russell, PhD[c], Anu Ramaswami, PhD[d], Matteo Convertino, PhD[b, e], Nisha Botchwey, PhD, MPH. Demographic Inequities in Health Outcomes and Air Pollution Exposure in the Atlanta Area and its Relationship to Urban Infrastructure. Journal of Urban Health.

https://link.springer.com/article/10.1007%2Fs11524-018-0318-7

https://doi.org/10.1007/s11524-018-0318-7

Additional Content can be found at:

https://pubmed.ncbi.nlm.nih.gov/30478764/

Demographic Inequities in Health Outcomes and Air Pollution Exposure in the Atlanta Area and its Relationship to Urban Infrastructure | SpringerLink

Acknowledgement: The authors acknowledge funding from NSF Award #1444745 “SRN: Integrated Urban Infrastructure Solutions for Environmentally Sustainable, Healthy, and Livable Cities.”

APPENDIX B. SUPPLEMENTAL MATERIAL FOR CHAPTER 2

B.1 Impact of organonitrates and organosulfates

The observations used in this analysis are from both filter-based and on-line measurements, neither of which have been thoroughly evaluated as to how organonitrates and organosulfates may interfere with what is reported as "nitrate" and "sulfate" aerosol. On the other hand, the filter-based and on-line measurements compare quite well (Edgerton et al., (2012)[65], and have been evaluated for precision.

Despite the lack of quantification of organonitrates, its impact on pH is at best uncertain as their mechanisms, rates and fates in particulate matter are still indeterminate[327]. Further, as Lee et al., (2016)[328] point out, their contribution to organic mass (OM) fraction is very small (less than 8%). In addition, as found in this study (Table 1, Table 2), overall contribution of nitrate to $PM_{2.5}$ is very low, particularly in the Southeastern region. Thus based on its minimal contribution it is unlikely that these constituents will have a substantial impact on pH, as corroborated by Vasilakos et al., (2018)[329].

Of note, contributions of organosulfates to inorganic sulfate are expected to be minimum, especially in areas with minimal biogenic volatile organic compounds (BVOCs), like California, as the presence of organosulfates compounds are likely to be associated with isoprene oxidation[93]. Further, as observed with organonitrates, organosulfates are likely to contribute more towards organic matter, not inorganic sulfate[94].

However, as studies by Song et al., (2018)[69], Vasilakos et al., (2018)[329], Pye et al., (2018)[60] and Nah et al., (2018)[330] show, any contributions to aerosol organic mass by

organosulfates and organonitrates are not expected to have a significant on aerosol pH as organic matter is not found to have a big impact.

B.2 Impact of organics on pH

A fair number of studies, such as those by Wang et al (2018, 2016)[97, 331] and Silvern et al., (2017)[61] have discussed the impact of organic and organic acids on aerosol acidity as significant. However, studies by Pye et al., (2018)[60] and Vasilakos et al., (2018)[329], paint a different picture. Pye et al., (2018) show that when organic and inorganic phases are mixed or exist in the same phase, there is only a 0.1-unit increase in median aerosol pH. Such a mixture between organic and inorganic compounds, they note, would likely happen in the presence of inorganic compounds such as bisulfate, which would be indicative of a low pH mixture. They observe that the only time pH with organic components were noticeably higher than ISORROPIA results, was when the organic phase was deemed immiscible. Even in that scenario, the predicted pH increase was only a fraction of one pH unit.

These results are similar to what Vasilakos et al., (2018)[329], and Song et al., (2018)[69] both found; an increase in organic acids to the base case scenario with no organic acids in E-AIM showed minimal impact on aerosol pH. Both studies assume that the components are miscible and consist only of one phase as the aerosol is assumed to be metastable phase with no liquid phase separation. This theory is supported by observations noted in Marcolli et al., (2004)[332] and Liu et al., (2017)[81] which shows that fine particulate aerosols are likely to be liquid and miscible. Further, in the study conducted by Losey et al., (2018)[84], it was found that both WSOM and inorganic constituents are likely to exist in the same liquid phase at very low relative humidity (RH) values when the ammonium to sulfate ratio is low, which would also be indicative of high acidity, as was found in our study.

Therefore, under these assumptions, the impact of organic acids on aerosol pH is likely to be low.

Wang et al., (2018)[331] bring up the point that water contributions from water soluble organic matter (WSOM) plays a significant role in estimating pH, however, Guo et al., (2015)[71] and Song et al., (2018)[69] show that the aerosol water associated which organic species had little to no impact on predicted pH value for fine particulate matter. Furthermore, Song et al., (2018) also explored the impact of their contribution to aerosol water content (AWC), and found it to be insignificant in their study.

Similar findings in terms of contributions to aerosol water content (AWC) by organics were noted in by Dick et al., (2000)[76]. In their study, they found that the water content associated with organics is considerably smaller than that associated with sulfate. Other experimental measurements conducted by Nah et al., (2018)[330] found that water soluble organic acids such as oxalic, formic and acetic acid only comprised on average, 6% of total organic matter and even less (4%) of the water soluble organic matter. This observation by Nah et al., (2018) is a clear contrast to what Wang et al., (2018) observed in their study, where a large part of AWC and WSOM mass was attributed to oxalic acid. This discrepancy only serves to highlight the difficulties in drawing direct comparisons between different regions and pollutant sources.

Nah et al., (2018) and Dick et al., (2000) discuss the minimal contribution of organics to AWC, but don't explore the impact of increased organics like Song et al., (2018) and Vasilakos et al., (2018)[329]. Their results however show that their impact on pH, even when increased to large proportions of aerosol mass is still negligible.

It is important to note however, that Wang et al., (2016, 2018)[97, 331] and Silvern et al., (2017)[61] studies were run under a set of different conditions than those of Nah et al., (2018), Song et al., (2018) and Vasilakos et al., (2018) and focused on different objectives. For instance,

Silvern et al., (2017) focused mainly on the inhibiting properties of organic matter coating to ammonia uptake in the aerosol, while Wang et al., (2016, 2018) explored the impact of pH on reaction mechanics. However, the conditions that form the crux of the crucial arguments in Wang et al., (2016, 2018) studies are vastly different than those in this study and others earlier mentioned. For instance, both studies of Wang et al., (2016, 2018) essentially explore and draw crucial conclusions about the possible mechanisms of NO_2 mediated Secondary Organic Aerosol (SOA) formation and hygroscopic particle growth results at higher pHs. At those higher pH values, it is likely that sulfate is almost fully neutralized. As such, drawing direct inferences about impacts of organics on pH from those higher pH studies to others conducted at lower pH would result in large discrepancies.

B.3 Neutralization Ratio

Though *f* represents the degree of neutralization for SO_4^{2-} and NO_3^- with NH_3(g), the ability of NH_3(g) to neutralize both constituents can be complicated by other processes. In addition to those mentioned in Hennigan, et al. (2015)[68], a study by Silvern et al., (2017)[61,] suggested that organic matter could inhibit neutralization by reducing NH_3(g) uptake into aerosols,[333, 334]. However, this was cast to doubt by the role of nonvolatile cations in Guo et al., (2017)[100] and in the conclusion summary by Pye et al., (2018)[60]. Other studies such as those by Sakalys et al., (2016)[83] where reported decreases in NH_3(g) uptake with particle size was observed are also worth considering. Results from other studies that revealed formation of amines and organic matter with NH_3(g) via competing reactions might also be considered as factors here for inadequate neutralization[97, 335, 336], though thermodynamic studies show that incomplete neutralization can be expected at the NH_3(g) levels typically found[109].

Additional theories that explain neutralization complexities can be found in the study by Huang, et al. (2011)[49]. In the study, Huang, et al. observed that at molar ratios of NH_4^+/SO_4^{2-} greater than 1.5, kinetic rates of SO_4^{2-} neutralization slowed down significantly while rates for NH_4NO_3 formation increased rapidly, meaning SO_4^{2-} neutralization above 1.5 was largely suppressed by NH_4NO_3 formation. It is fair to note however, that the study took place in China, where the concentration profile in the ambient air could have different effects on the results and whether nitrate is higher in those cases is unclear. While similar observations have been observed by Kumar et al. (2016)[337], it is important to note that aerosol pH, in some parts of China are substantially higher than in most US regions as shown in Guo et al., (2017)[109], and might have considerable bearing on such observations. In this study however, there is no evidence from our trends that excess production of NH_4NO_3 took place as the results show that the concentration of NH_4^+ was affected by the presence of SO_4^{2-} not NO_3^- (except in MW). Furthermore, as pointed out by Weber et al. (2016)[55], NH_4NO_3 formation is largely unaffected at pH below three, and since the intercept for the mean pH trends show all sites with substantially low pH (except MW), no NH_4NO_3 formation is likely to be taking place, so there is no reason to suppose that the exact same phenomenon is happening here.

B.4 Further California pH analysis

While no significant decrease in SO_4^{2-} or NO_3^- were observed in California, the significant increase in pH coupled with the significant decrease in NH_4^+ could indicate the reduction of other components besides sulfate or nitrate. The study by Shi et al. (2017), showed that high pH can be attributed to other aerosol components such as dust[95], which could also explain the California results. Figure S51 shows high mass proportions of dust components in that region.

B.5 ISORROPIA-II evaluation to other inorganic thermodynamic models

Many studies have evaluated the differences between inorganic thermodynamic models. Zhang et al., (2000)[338] conducted an evaluation of five different thermodynamic inorganic models and found that all the models tend to agree remarkably well when one is very careful to show that different conditions might favor a particular inorganic thermodynamic model over another. Ansari and Pandis (1999)[67] evaluated 4 models and recommended ISORROPIA as the model of choice based on its computational efficiency and general agreement with other benchmark models.

Both studies highlighted various reasons for differences in model performance. In some scenarios, differences in predicted pH tended to occur under special cases such as low RH[64] or in estimations of activity coefficients, which can have significant effects as noted in Kim et al., (1993)[339]. Errors in input variables, including the list of electrolytes taken into consideration in each model, computational methods or differences in predicted aerosol water content were discussed as other factors that could impact predicted aerosol pH between models.

Most model evaluations are typically conducted by comparing how well the model's predicted gas-aerosol partioning fractions of inorganic constituent's measures against observations[64, 67, 68]. Such comparisons are typically used as a gauge to determine how well the model predicts pH[64, 71]. In this regard, ISORROPIA-II has been found to have fairly good agreement with observation measurements and with other models.

Guo et al., (2015)[71] found ISORROPIA-II's predicted aerosol liquid water content correlated fairly well with observations with an R^2 of 0.74 In that same study, comparisons of observations with predicted NH_3(g) gas partition fraction from ISORROPIA-II resulted in ratios

near 1. Nowak et al., (2006)[340] also got good agreement with observed NH_3(g) results from ISORROPIA-II.

As stated earlier, ISORROPIA-II was found to have fairly good agreement with other models. In Hennigan et al., (2015)[68], E-AIM and ISORROPIA-II showed fairly good pH agreement when the forward mode (as used in this study) was employed. Results of studies conducted by Vasilakos et al., (2018)[329] and Song et al., (2018)[69], showed that any differences between these different inorganic thermodynamic models, under the conditions of this study would not be significant; differences were relatively small (a fraction of a pH unit).

In terms of uncertainty, under certain scenarios, uncertainty in modeled pH can increase or decreases. For instance, Guo et al., (2015) found that higher relative humidity (RH) values and temperatures in the summer resulted in higher uncertainty estimates. In Fountoukis and Nenes (2007)[64], differences between ISORROPIA-II and SCAPE results occurred at low RH values.

However, under the conditions of this study, ISORROPIA-II in the forward, metastable mode was found to provide the best results and agreement with observations, provided RH values were not in the extreme ranges[69, 78].

B.6 CMAQ Model Evaluation

The performance of photochemical grid models like the Community Multiscale Air Quality model (CMAQ) is typically assessed within a 4-tier frame work. The first component of this frame work, as outlined in Dennis et al., (2010)[341] is an operational evaluation assessment. In this aspect, the model is evaluated to see how well it performs in comparison to ambient air observations and lab measurements. A number of statistical metrics such as Pearson's correlation coefficient (R^2), Normalized Mean Bias (NMB), and Normalized Mean Error (NME) is used in this evaluation. The dynamical evaluation component of the 4-tier frame work evaluates how

well the model captures changes in concentrations in response to emissions and meteorology, while the diagnostic evaluation explores model performance in capturing atmospheric dynamic reactions, dealing more with the processes within the model, variability and sensitives to model inputs. Lastly, the probabilistic evaluation component utilizes a combination of statistical methodologies and metrics (i.e. confidence interval analysis, ensemble averaging) to assess model uncertainty in matching observations.

Many studies have used part or all aspects of these frame works to assess CMAQ performance, but as results can vary regionally and across varying spatial scales and other domains, it is critical to use consistent criteria and benchmarks to assess performance. The criteria and bench mark goals for key gaseous and aerosol species (e.g. NH_4^+, SO_4^{2-}, $PM_{2.5}$) as outlined in Emery et al., (2017)[91] provides a consistent, reproducible and useful assessment in this regard.

An application of these bench marks was used by Henneman et al., (2017)[90] to capture the operational, dynamic and diagnostic evaluation of CMAQ in response to emission and meteorological changes in the Eastern part of the United States. Within the operational evaluation component of the study, Henneman et al., (2017) found that most of the $PM_{2.5}$ species met the metrics goals set by Emery et al., (2017). The diagnostic component of the study captured CMAQ sensitivity changes in emissions and meteorology. The results of the diagnostic evaluation showed that CMAQ results were influenced more by changing emissions than metrology over the decade of interest. In addition, Henneman et al., (2017) also compared the performance of CMAQ with statistical modeling to evaluate the result of the diagnostic evaluation and found consistent results between both methodologies.

The use of CMAQ in this study focused primarily on capturing spatial and temporal dynamic trends of pH and ammonia gas in response to gaseous precursor emission changes.

Dynamic evaluation can provide impact of emission changes over a longer time period which was the focus here. Within the dynamic evaluation component in Henneman et al., (2017) CMAQ model results met the criteria bench mark goals for all $PM_{2.5}$ species except Organic Carbon (OC).

CMAQs efficacy has been evaluated in many studies with results showing similar performance in capturing CMAQ's performance in regard to operational and dynamic components. Cohan et al., (2014)[342] captured the ability of CMAQ and other photo grid models to assess modeled attainment tests and found an 94.8% success rate for predictions with 110 monitors in meeting NAAQS design values for attainment. Dennis et al., (2010)[341] found CMAQ was able to capture trends of NO_x and CO (albeit some difference in magnitude) in response to emissions fairly well in both operational and probabilistic evaluations. Godowitch et al., (2010)[343] was able to demonstrate the ability of CMAQ to capture NO_x change with observed NO_x concentration and Marmur et al., (2009)[344] captured CMAQs ability to match profiles of primary species in particulate matter at SEARCH sites.

The results of these studies, highlights CMAQ's ability to capture responses to emissions changes fairly well, and the use of such models continues to be critical in light of future emissions controls.

Table B-1: Co-located CASTNET and AMoN sites by regions. CASTNET site measurements follow the start date of co-located AMoN site. The Longitude and Latitude refers to the location of the CASTNET sites. Data collected at these sites during the time period: March 2011 to February 2016

Amon	CASTNET	Region	State	CASTNET Site	Longitude	Latitude
CA67	JOT403	California	CA	Joshua Tree NP	34.069569	-116.38893
CA83	SEK430	California	CA	Sequoia NP - Ash Mountain	36.489469	-118.82915
CA44	YOS404	California	CA	Yosemite NP - Turtleback Dome	37.713251	-119.7062
IL46	ALH157	Midwest	IL	Alhambra	38.869001	-89.622815
IL11	BVL130	Midwest	IL	Bondville	40.051981	-88.372495
IL37	STK138	Midwest	IL	Stockton	42.287216	-89.99995
OH54	DCP114	Midwest	OH	Deer Creek	39.635888	-83.260563
KS31	KNZ184	Midwest	KS	Konza Prairie	39.10216	-96.609583
WI35	PRK134	Midwest	WI	Perkinstown	45.206525	-90.597209
NE98	SAN189	Midwest	NE	Santee Sioux	42.829154	-97.854128
CT15	ABT147	Northeast	CT	Abington	41.84046	-72.010368
PA00	ARE128	Northeast	PA	Arendtsville	39.923241	-77.307863
NY67	CTH110	Northeast	NY	Connecticut Hill	42.400875	-76.653516
PA29	KEF112	Northeast	PA	Kane Exp. Forest	41.598119	-78.767866
NJ98	WSP144	Northeast	NJ	Wash. Crossing	40.312303	-74.872663
MD99	BEL116	Northeast	MD	Beltsville	39.028177	-76.817127
CO88	ROM206	Rocky Mountains	CO	Rocky Mtn NP Collocated	40.278129	-105.54564
NC06	BFT142	Southeast	NC	Beaufort	34.884668	-76.620666
AR03	CAD150	Southeast	AR	Caddo Valley	34.179278	-93.098755
KY98	CDZ171	Southeast	KY	Cadiz	36.784053	-87.85015
NC26	CND125	Southeast	NC	Candor	35.26333	-79.83754
NC25	COW137	Southeast	NC	Coweeta	35.060527	-83.43034
FL11	EVE419	Southeast	FL	Everglades NP	25.391223	-80.680819
GA41	GAS153	Southeast	GA	Georgia Station	33.181173	-84.410054
FL19	IRL141	Southeast	FL	Indian River Lagoon	27.849215	-80.455595
KY03	MCK131	Southeast	KY	Mackville	37.704678	-85.048706
WV18	PAR107	Southeast	WV	Parsons	39.090434	-79.661742
VA24	PED108	Southeast	VA	Prince Edward	37.165222	-78.307067
AL99	SND152	Southeast	AL	Sand Mountain	34.289001	-85.970065
TN01	GRS420	Southeast	TN	Great Smoky NP - Look Rock	35.633482	-83.941606

Table B-2: List of SEARCH sites, location, name and type (i.e. urban, residential). The "Data Collection Start/End Date" reflects the seasons during which SEARCH data for base cations (Mg^{2+}, Na^{+}, Ca^{2+} and K^{+}) are available. Certain ion data are unavailable during seasons shown in "Seasons with insufficient data"

State/ Site Name	City Location	Type	Site Operating Timeline Start-End Date	Data collection Start /End Date	Seasons with insufficient data	No. of Seasons with data
GA/JST	Atlanta Jefferson St	Urban	8/01/98-NA	Spring '08/Winter '15	Spring '12, Summer '12, Fall '12	25
GA/YRK	Yorkville	Rural	5/6/98-NA	Spring '08/Winter '15	N/A	28
AL/BHM	N. Birmingham	Urban	10/23/98-NA	Spring '08/Winter '14	N/A	24
AL/CTR	Centreville	Rural	5/11/98-NA	Spring '08/Winter '14	Spring '11 Summer '11 Fall '11	21
MS/GFP	Gulfport	Urban	4/13/99-NA	Summer '08/Winter '11	Fall '08	10
MS/OAK	Oak Grove	Rural	5/16/98-12/13/10	Summer '08/Winter '11	N/A	11
FL/PNS	Pensacola	Urban	2/01/99-12-13-09	Summer '08/Winter '10	Spring '08	6
FL/OLF	Outlying Landing Field #8	Suburb	1/4/99-NA	Spring '08/Winter '15	Spring '11 Summer '11 Fall '11 All 2012 Winter '13	20

Table B-3: Details of the data available along with the sampling frequency at SEARCH

Class	Analyte	Sample Device	Substrate	Measurement Frequency
$PM_{2.5}$	Mass	FRM	Teflon, 47mm	Daily
	Anions	PCM	Teflon, 47mm	3-day
	Cations	PCM	Teflon, 47mm	3-day
	Vol-nitrate	PCM	Nylon, 47mm	3-day
Trace Gases	NH_3	denuder	Citric acid coated	3-day
	NH_3			Hourly
	HNO_3			Hourly

Table B-4: Tabulated results of the linear regression analysis for pH, calculated for all eight sites in the SEARCH network with original ISORROPIA-II code, and modified ISORROPIA-II code. Bolded results were found to be statistically significant at α=0.05

Metric	Site	Old Code	Code with Corrections
pH site Averages	CTR	1.5	1.5
	GFP	1.8	1.8
	JST	1.9	1.9
	OAK	1.4	1.4
	OLF	1.6	1.6
	YRK	2.0	2.0
	BHM	2.0	2.0
	PNS	1.9	1.9
p Values	CTR	0.715	0.753
	GFP	0.592	0.582
	JST	0.260	0.250
	OAK	**0.047**	**0.047**
	OLF	0.484	0.458
	YRK	0.604	0.574
	BHM	0.839	0.864
	PNS	0.817	0.794
Slope	CTR	-2.6E-03	-2.3E-03
	GFP	1.7E-02	1.7E-02
	JST	9.9E-03	1.0E-02
	OAK	9.1E-02	9.1E-02
	OLF	2.7E-03	2.9E-03
	YRK	4.2E-03	4.6E-03
	BHM	2.2E-03	1.8E-03
	PNS	9.1E-03	1.0E-02
Intercept	CTR	1.5	1.5
	GFP	1.7	1.7
	JST	1.8	1.8
	OAK	0.8	0.8
	OLF	1.6	1.6
	YRK	2.0	2.0
	BHM	1.9	2.0
	PNS	1.8	1.8

Table B-5: Tabulated results of the linear regression analysis for pH, calculated for all eight sites in the CASTNET network with original ISORROPIA-II code, and modified ISORROPIA-II code. Bolded results were found to be statistically significant at α=0.05

Metric	Site	Old Code	Code with Corrections
pH site Averages	RK	2.7	2.7
	CA	3.3	3.0
	MW	3.8	3.6
	NE	2.5	2.6
	SE	2.9	2.8
p Values	RK	0.990	0.989
	CA	**0.025**	0.147
	MW	0.122	0.802
	NE	0.219	0.215
	SE	0.081	0.051
Slope	RK	-2.3E-04	-2.5E-04
	CA	3.8E-02	2.7E-02
	MW	2.5E-02	-8.8E-03
	NE	2.2E-02	2.3E-02
	SE	1.9E-02	3.1E-02
Intercept	RK	2.7	2.7
	CA	2.9	2.8
	MW	3.6	3.7
	NE	2.3	2.3
	SE	2.5	2.6

Table B-6: Tabulated statistical results of the p-values from the linear regression analysis for all SEARCH sites using seasonal mean concentrations. Bolded results were found to be statistically significant at α=0.05

Critical Variables	*CTR*	*GFP*	*JST*	*OAK*	*OLF*	*YRK*	*BHM*	*PNS*
pH	0.715	0.592	0.260	**0.047**	0.484	0.604	0.839	0.817
Na^+	0.649	0.342	**0.032**	0.530	0.050	0.809	0.155	0.351
SO_4^{2-}	**0.001**	0.106	**0.001**	0.137	**0.001**	**0.004**	**0.003**	0.595
TNH_x	**0.001**	0.479	**0.008**	0.760	**0.027**	**0.000**	**0.013**	0.621
TNO_3^-	0.770	0.742	0.745	0.230	0.470	0.736	0.993	0.522
Cl^-	0.811	0.944	0.285	0.570	0.103	**0.002**	0.836	0.483
Ca^{2+}	**0.003**	0.099	0.117	0.327	0.179	0.065	**0.003**	0.479
K^+	0.805	0.699	0.509	0.622	0.066	0.301	**0.011**	0.440
Mg^{2+}	0.335	0.929	0.754	0.715	0.145	0.739	**0.000**	0.361
Relative Humidity	0.935	0.311	0.520	0.411	0.643	0.970	0.205	0.098
Temperature	0.440	0.434	0.523	0.377	0.526	0.431	0.372	0.293
NH_4^+	**0.000**	0.237	**0.000**	0.376	**0.001**	**0.001**	**0.002**	0.330
$NH_3(g)$	0.552	0.787	0.465	0.093	0.256	0.212	**0.040**	0.284
NO_3^-	0.816	0.996	0.666	0.223	0.650	0.846	0.370	0.833
$HNO_3(g)$	0.517	0.636	0.910	0.247	0.104	0.298	0.131	0.272
f	0.675	0.352	0.976	0.235	**0.043**	0.274	0.174	0.078
R_N	**0.014**	0.437	**0.000**	**0.037**	**0.001**	**0.030**	0.697	0.120
Total Cations	0.849	0.644	0.063	0.615	0.098	0.079	**0.001**	0.837
Total Cations-Na^+	0.21	0.50	0.78	0.92	0.700	**0.027**	**0.001**	0.473

.

Table B-7: Tabulated statistical results of the p-values from the linear regression analysis for all CASTNET/AMoN regions, using seasonal mean concentrations. Bolded results were found to be statistically significant at α=0.05

Critical Variables	*RK*	*CA*	*MW*	*NE*	*SE*
pH	0.990	**0.025**	0.122	0.219	0.081
NO_3^-	0.401	0.643	0.883	0.632	0.772
$NH_3(g)$	0.721	0.588	0.550	0.821	0.225
NH_4^+	0.054	**0.041**	0.301	**0.022**	**0.000**
f	0.997	0.474	0.757	0.057	0.270
SO_4^{2-}	**0.050**	0.252	**0.006**	0.004	**0.001**
TNHx	0.517	0.712	0.231	**0.048**	0.701
TNO_3^-	0.351	0.480	0.568	0.721	0.195
$HNO_3(g)$	0.454	0.628	0.112	**0.007**	**0.001**
Na^+	0.332	0.817	0.938	0.210	0.102
Cl^-	0.741	0.602	0.518	0.083	0.797
Ca^{2+}	0.192	0.817	0.325	0.900	0.272
K^+	0.279	0.812	0.206	0.346	**0.022**
Mg^{2+}	0.178	0.585	0.216	0.893	**0.032**
Relative Humidity	0.851	0.945	0.521	0.961	0.481
Temperature	0.723	0.943	0.539	0.506	0.497
Total Cations	0.193	0.786	0.253	0.342	**0.042**
Total Cations-Na^+	0.191	0.775	0.298	0.801	0.070
R_N	0.211	0.127	0.888	0.410	**0.014**

Table B-8: Tabulated statistical results of the p-values from the linear regression analysis for all SEARCH sites using monthly average concentrations. Bolded results were found to be statistically significant at α=0.05

Critical Variables	*CTR*	*GFP*	*JST*	*OAK*	*OLF*	*YRK*	*BHM*	*PNS*
pH	0.186	0.628	0.183	0.052	0.077	0.717	0.723	0.851
Na^+	0.418	0.763	**0.025**	0.446	0.147	0.838	**0.019**	0.207
SO_4^{2-}	**0.000**	0.334	**0.000**	0.410	**0.001**	**0.000**	**0.000**	0.480
TNH_x	**0.000**	0.882	**0.006**	0.422	0.076	**0.000**	**0.000**	0.418
TNO_3^-	0.218	0.739	0.680	0.193	0.126	0.456	0.402	0.872
Cl^-	0.818	0.409	0.139	0.598	0.400	**0.001**	0.987	0.194
Ca^{2+}	**0.000**	**0.049**	0.206	0.193	**0.042**	**0.009**	**0.000**	0.248
K^+	0.268	0.682	0.158	0.346	**0.043**	0.927	**0.000**	0.741
Mg^{2+}	0.051	0.926	0.409	0.730	0.203	0.757	**0.000**	0.281
Relative Humidity	0.752	0.787	0.922	0.748	0.713	0.793	0.072	0.092
Temperature	0.768	0.970	0.495	0.513	0.829	0.500	0.448	0.503
NH_4^+	**0.000**	0.513	**0.000**	0.934	**0.004**	**0.000**	**0.000**	0.334
$NH_3(g)$	0.322	0.641	0.212	0.066	0.388	0.091	**0.007**	0.742
NO_3^-	0.384	0.506	0.384	0.164	0.766	0.986	0.516	0.673
$HNO_3(g)$	0.133	0.895	0.688	0.269	**0.004**	0.092	**0.006**	0.420
f	0.528	0.607	0.503	0.338	0.101	**0.020**	0.104	0.087
R_N	**0.000**	0.474	**0.000**	0.066	**0.008**	**0.002**	0.709	0.201
Total Cations	**0.000**	**0.000**	**0.044**	**0.000**	0.050	0.129	**0.000**	**0.007**
Total Cations-Na^+	**0.000**	**0.000**	0.344	**0.000**	0.156	**0.040**	**0.000**	**0.000**

Table B-9: Tabulated results of the linear regression analysis for the neutralization ratio, calculated for all five regions from the CASTNET/AMoN network using seasonal mean measured concentrations. Bolded results were found to be statistically significant at α=0.05. The 't' represents time as seasons.

	Neutralization Ratio
Northeast	Northeast *f* = -4.1E-03*t + 0.84
Southeast	Southeast *f* = -1.8E-03*t + 0.69
Midwest	Midwest *f* = -8.2E-04*t + 0.79
Rocky Mountains	Rocky Mountains *f* = 1.5E-05*t + 0.86
California	California *f* = -2.8E-03*t + 0.75

Table B-10: Tabulated results of the linear regression analysis for the neutralization ratio, calculated for all eight sites in the SEARCH network using seasonal mean measured concentrations. Bolded results were found to be statistically significant at α=0.05. The 't' represents time as seasons.

	Neutralization Ratio
CTR AL	f = -8.8E-04*t + 0.86
GFP MS	f = 1.2E-02*t + 0.74
JST/GA	f = 6.1E-05*t + 0.93
OAK/MS	f = 1.1E-02*t + 0.74
OLF/FL	**f = 4.1E-03*t + 0.78**
YRK/GA	f = -2.2E-03*t + 0.98
BHM/AL	f = 3.4E-03*t + 0.86
PNS/FL	f = 4.8E-02*t + 0.56

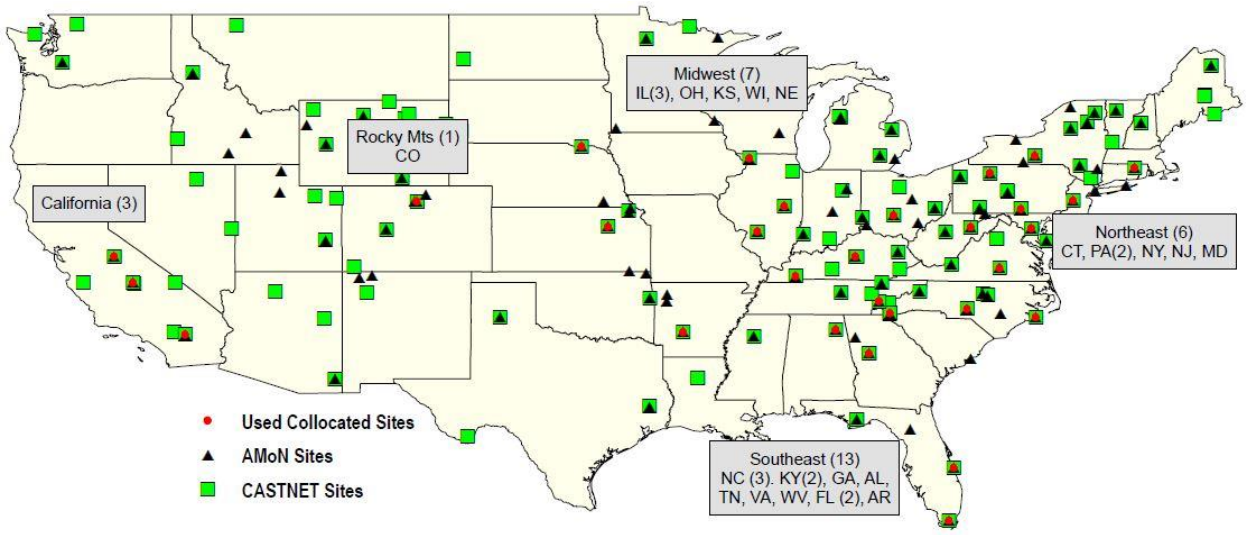

Figure B-1: Spatial map of the CASTNET and AMoN sites, including the co-located CASTNET and AMoN sites used in this study. Specific site locations are provided in Table S1. SEARCH sites were located in the Southeast. (Map source: Map created using ARCGIS® software by ESRI, in conjunction with US EPA data) (ESRI 2015[183] and US EPA 2017[345]).

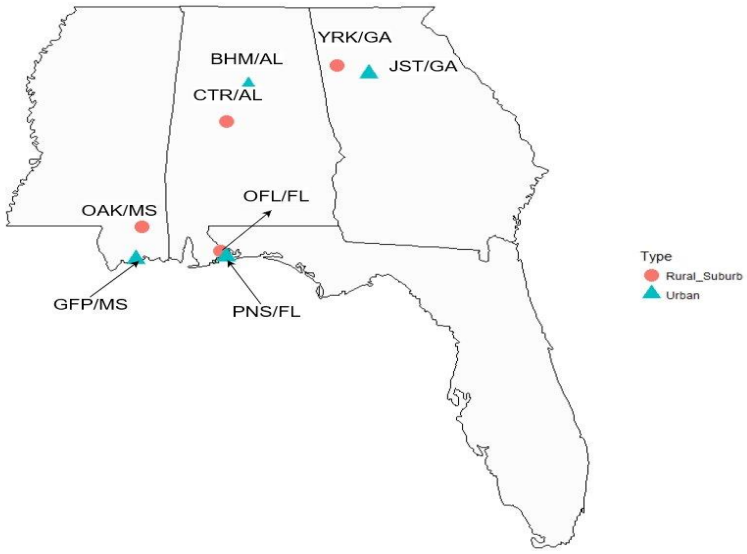

Figure B-2: SEARCH sites SEARCH sites were located in the Southeast. (Map source: Created using R's map source library[346, 347] in conjunction with data from https://my.usgs.gov/gcmp/site/list/943855[348])

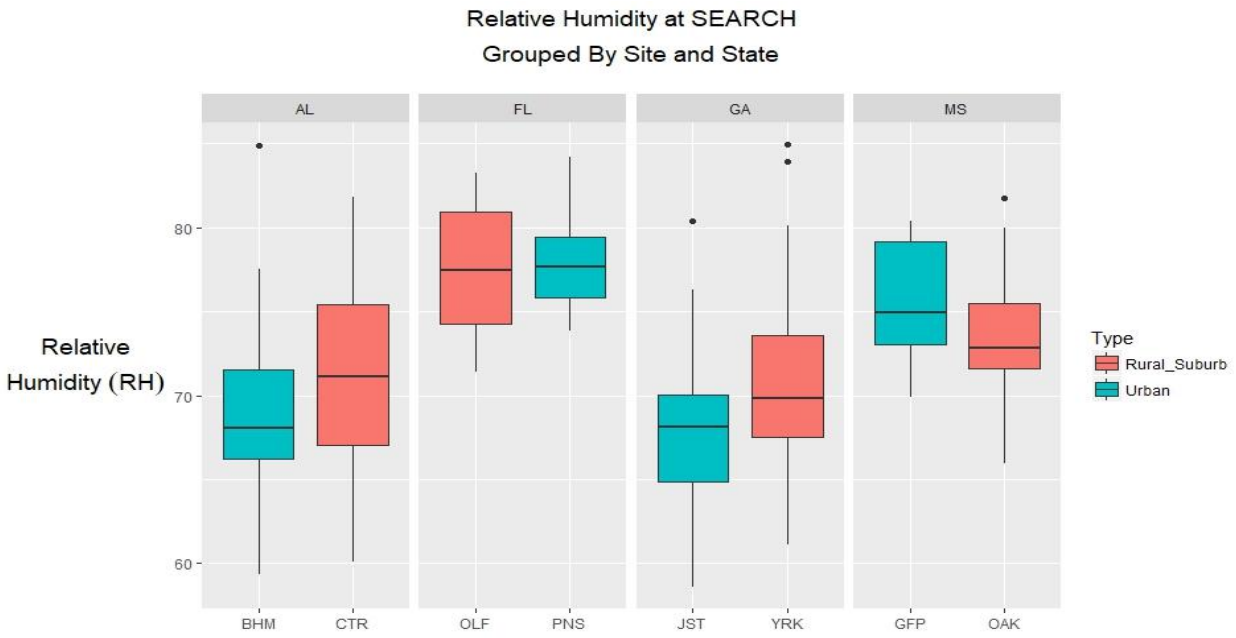

Figure B-3: SEARCH plot for Relative Humidity

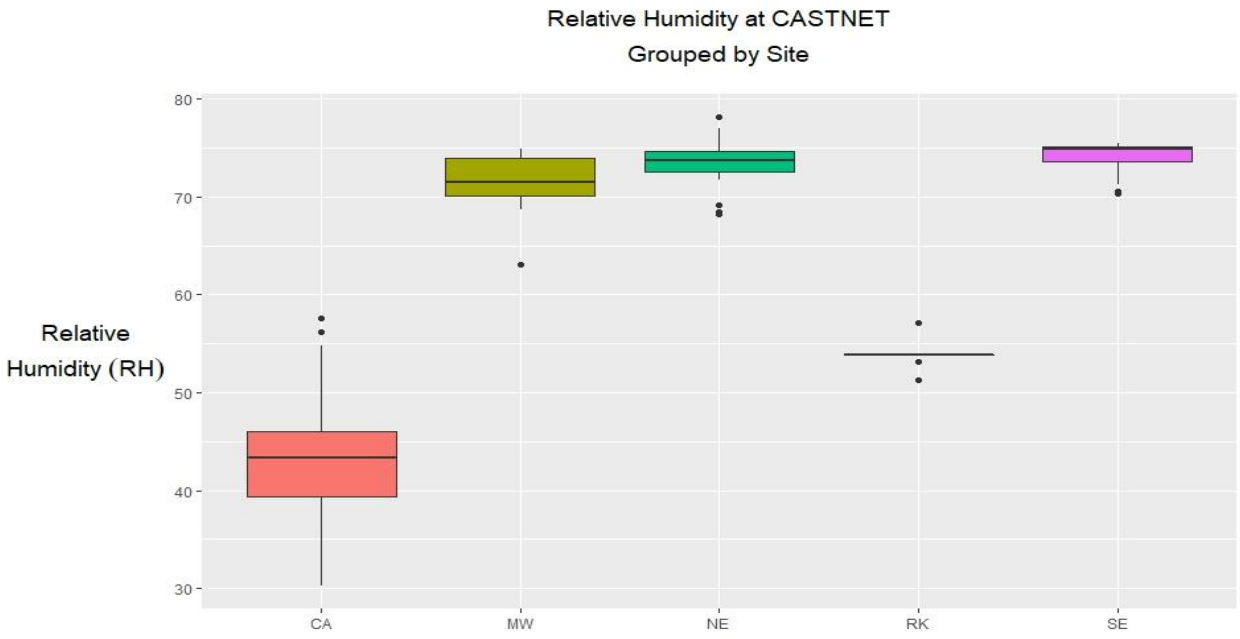

Figure B-4: CASTNET plot for Relative Humidity

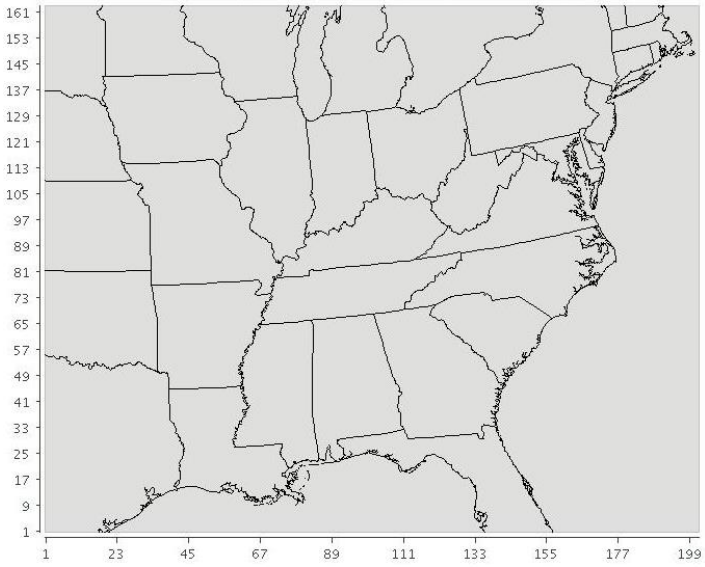

Figure B-5: CMAQ simulation domain with spatial resolution of 12km

FIGURE S6

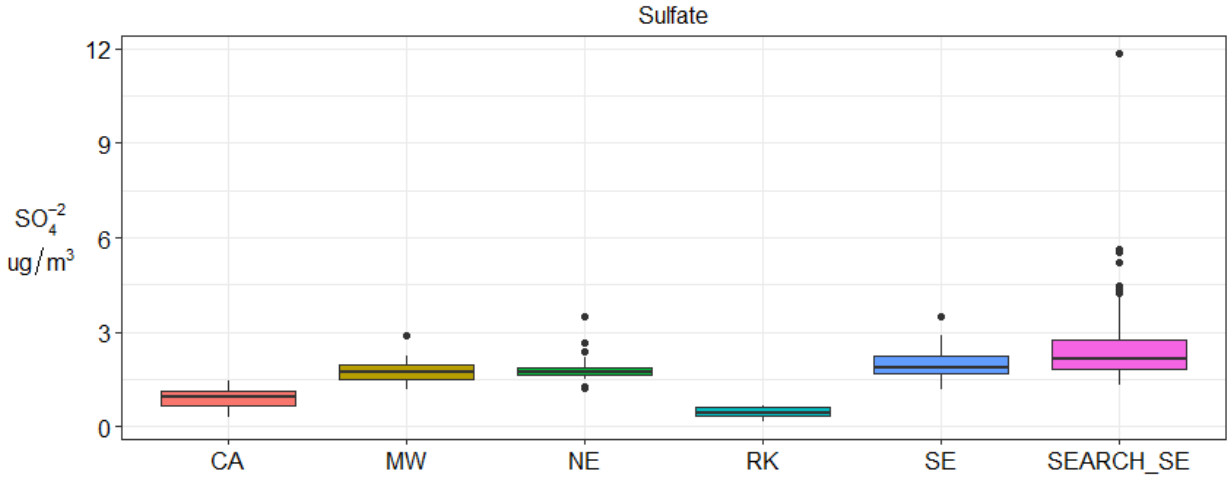

Figure B-6: CASTNET/AMoN and SEARCH plots for SO_4^{-2}. BOXPLOT FOR SEARCH and CASTNET/AMoN MONITORS

TREND FIGURES FOR CASTNET REGIONS

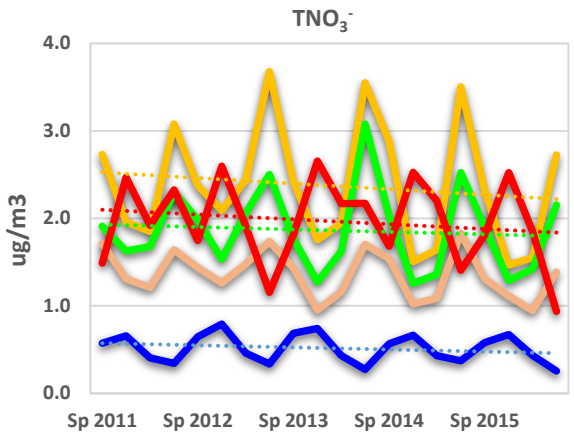

Figure B-7: TNO3-=HNO3(g)+NO3

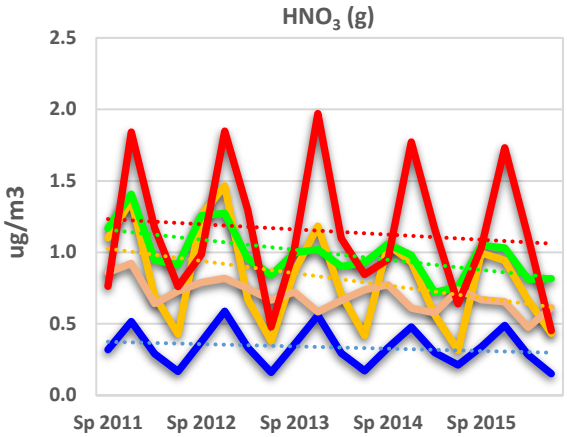

Figure B-8: HNO3(g)

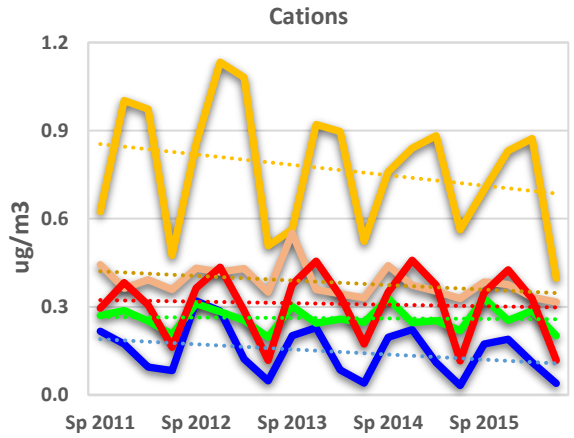

Figure B-9: Trends for total cations without Na^+
Cations = $K^+ + Mg^{2+} + Ca^{2+}$

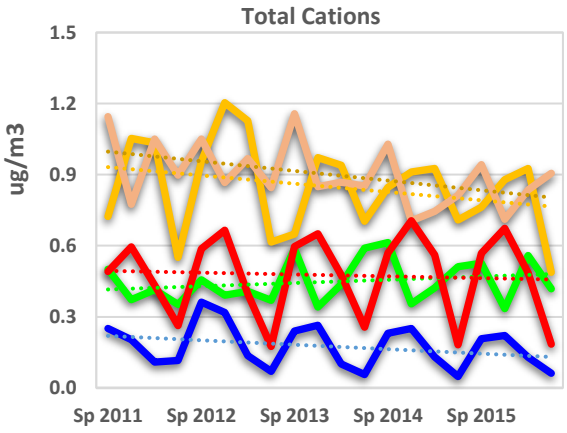

Figure B-10: CASTNET trends for total cations
Total Cations = $K^+ + Mg^{2+} + Ca^{2+} + Na^+$

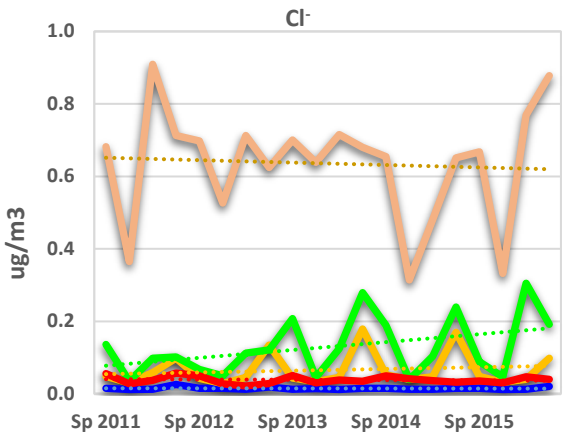

Figure B-11: CASTNET trends for Cl

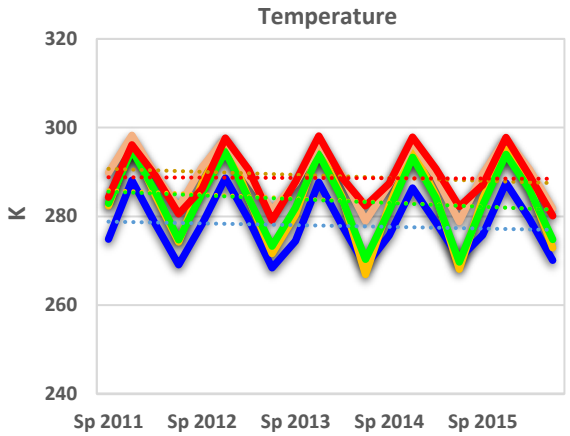

Figure B-12: CASTNET trends for Temperatur

TREND FIGURES FOR SEARCH SITES

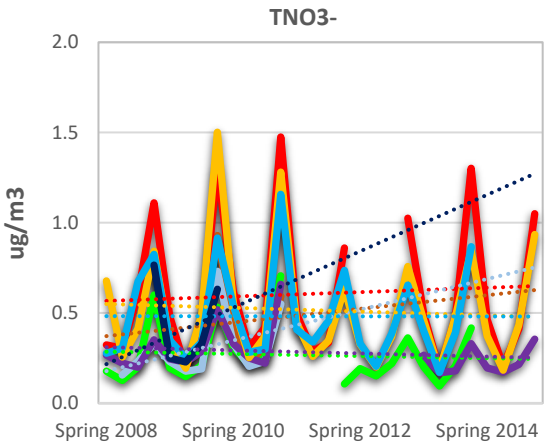

Figure B-13: SEARCH trends for TNO_3^-=HNO_3(g)+NO_3^-

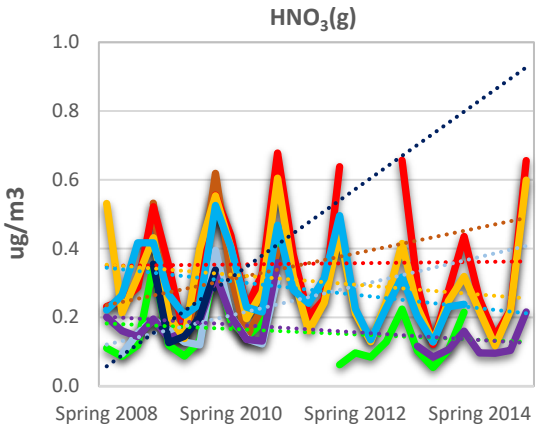

Figure B-14: SEARCH trends for HNO_3(g)

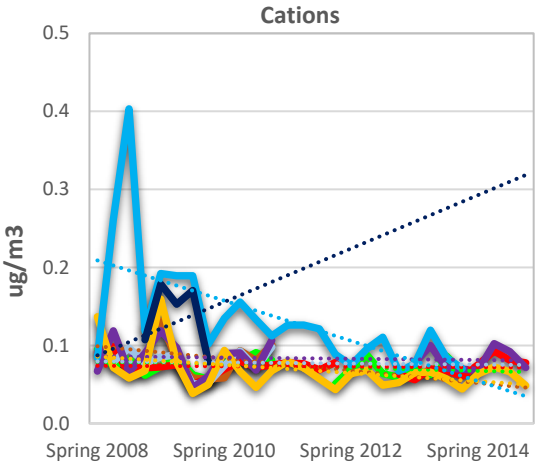

Figure B-15: SEARCH trends for total cations without Na^+
Cations = $K^+ + Mg^{2+} + Ca^{2+}$

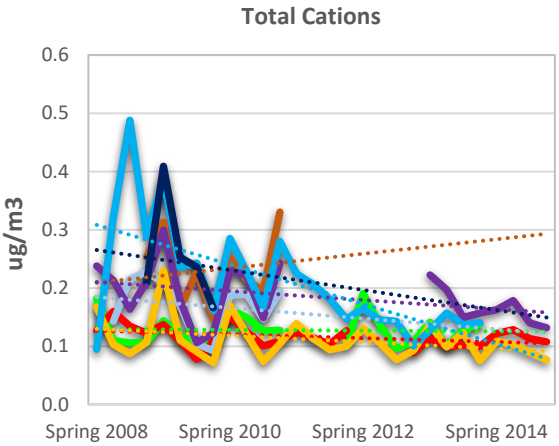

Figure B-16: SEARCH trends for total cations
Total Cations = $K^+ + Mg^{2+} + Ca^{2+} + Na^+$

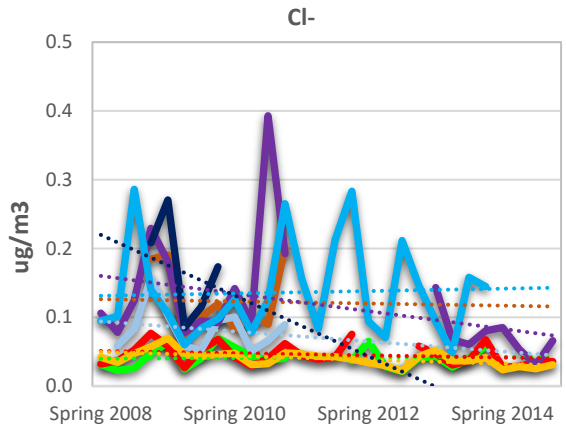

Figure B-17: SEARCH trends for Cl^-

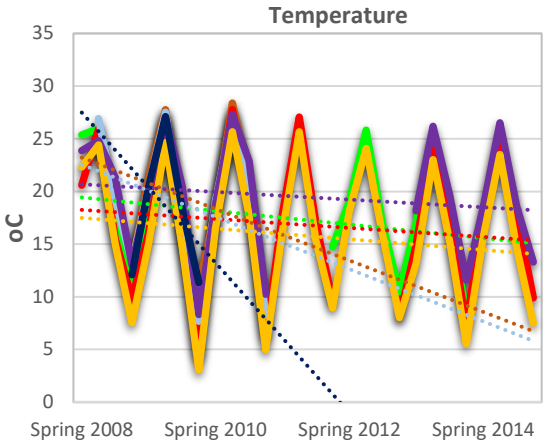

Figure B-18: SEARCH trends for Temperature

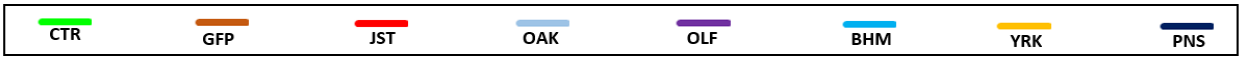

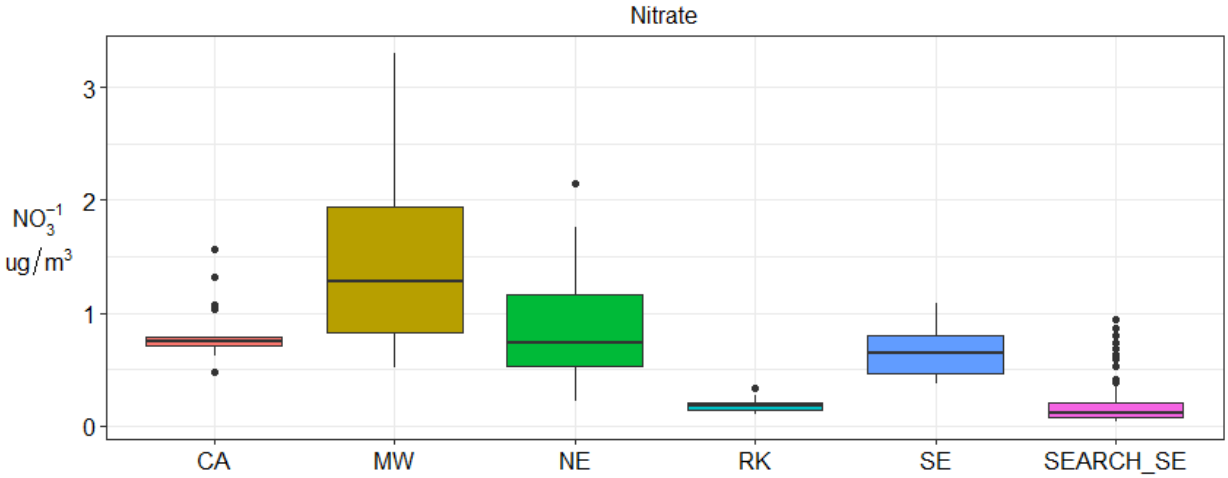

Figure B-19: CASTNET/AMoN and SEARCH plots for NO_3^-

BOXPLOT FOR SEARCH and CASTNET/AMoN MONITORS

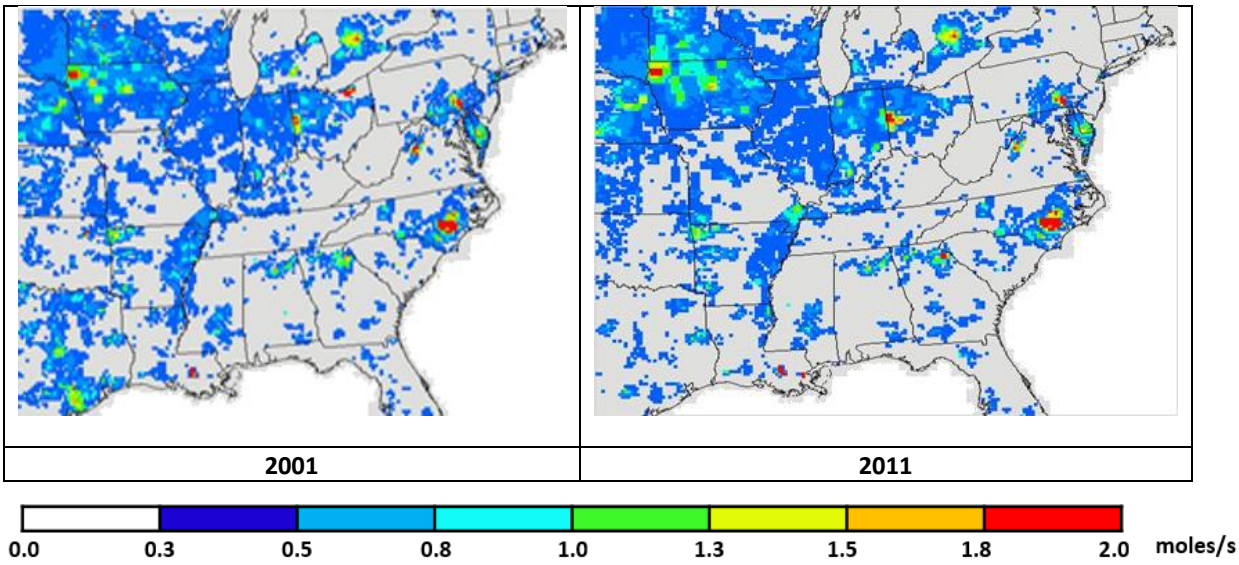

Figure B-20. Annual averaged ammonia emission (moles/s) simulated by SMOKE at 2001 and 2011.Emission trend of NH3_CMAQ 2001 and 2011.

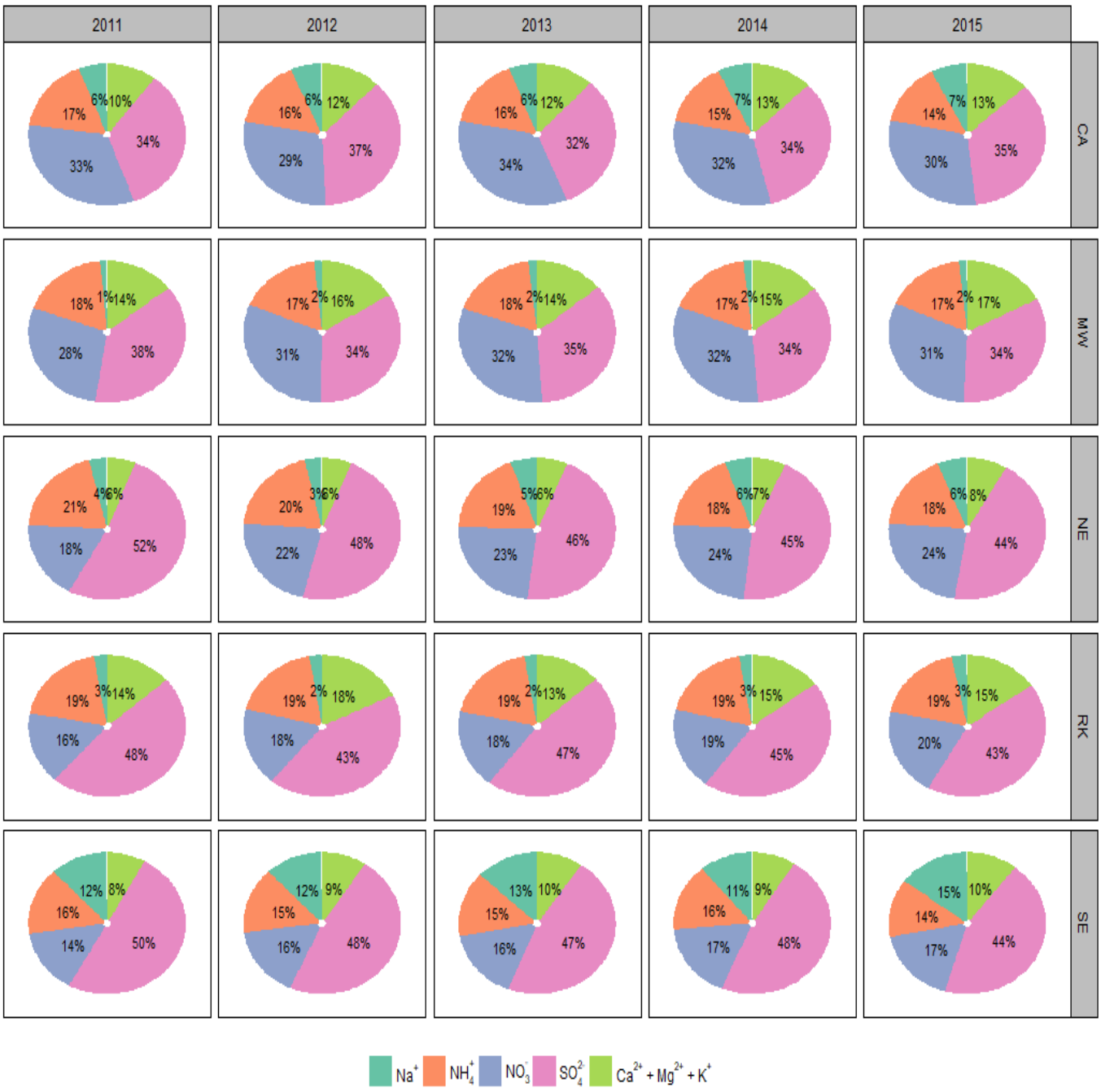

Figure B-21: CASTNET/AMoN pie charts
Depicting annual mass concentration for inorganic constituents

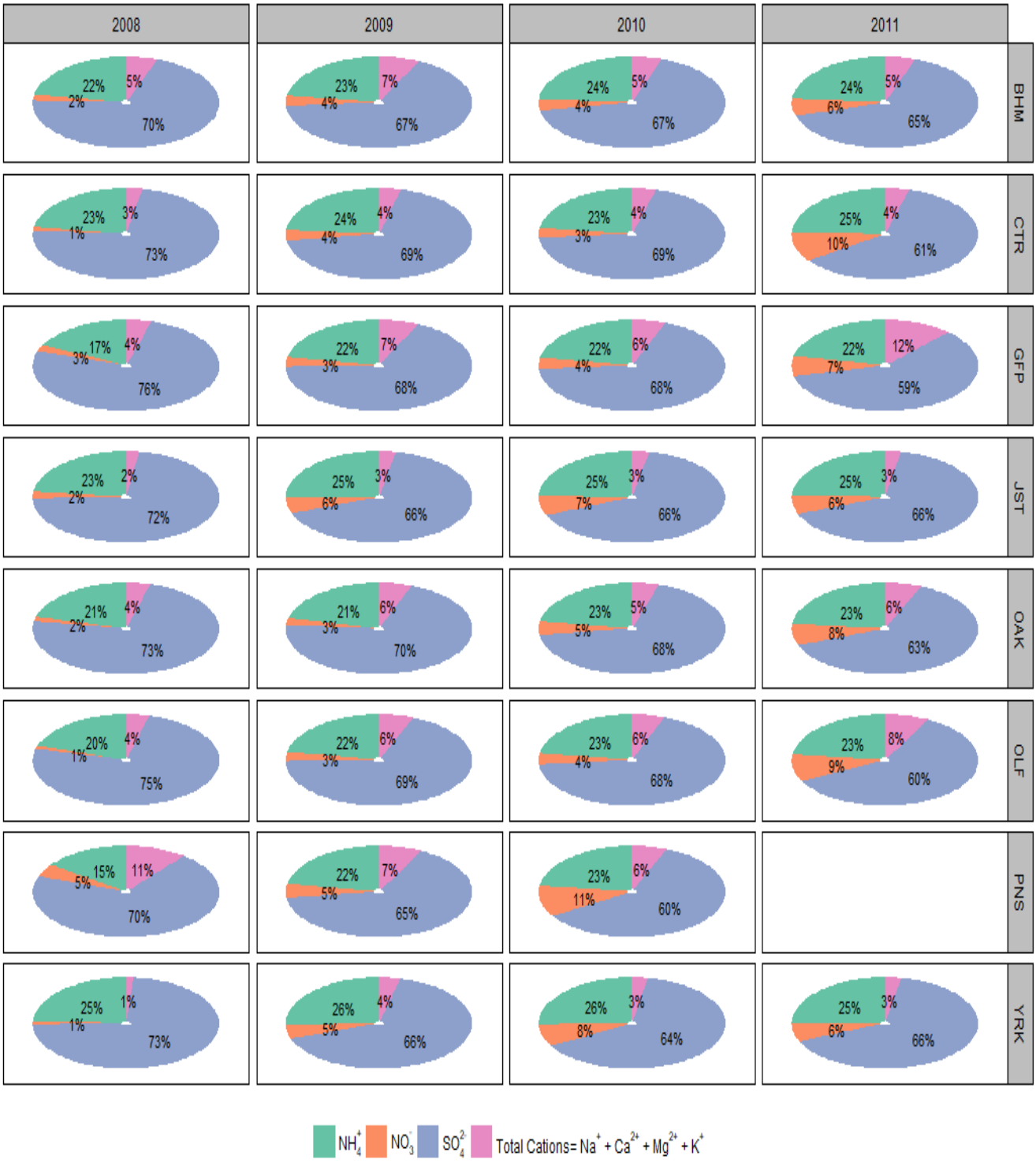

Figure B-22: SEARCH site pie charts.
Depicting annual mass concentration for inorganic constituents

Figure B-23: SEARCH site pie charts
Depicting annual mass concentration for inorganic constituents

APPENDIX C. SUPPLEMENTAL MATERIAL FOR CHAPTER 3

Adapted from ‘Abiola S. Lawal, Joseph L. Servadio, Tate Davis, Anu Ramaswami, Nisha Botchwey, Armistead G. Russell. Orthogonalization and machine learning methods for residential energy estimation with social and economic indicators. Applied Energy, https://doi.org/10.1016/j.apenergy.2020.116114

Table C-1 can be found in supplement (link below), labeled as Table S1

https://ars.els-cdn.com/content/image/1-s2.0-S0306261920315336-mmc4.docx

Orthogonalization and machine learning methods for residential energy estimation with social and economic indicators - ScienceDirect

Geographical Description of Area for Energy Estimation

Training Data from Atlanta Metropolitan Statistical Area in red

Geographic distribution (36 counties out of 159 counties in GA)

Number of GA 2010 ZCTAS: 735

Number of GA Postal Zip codes: 951

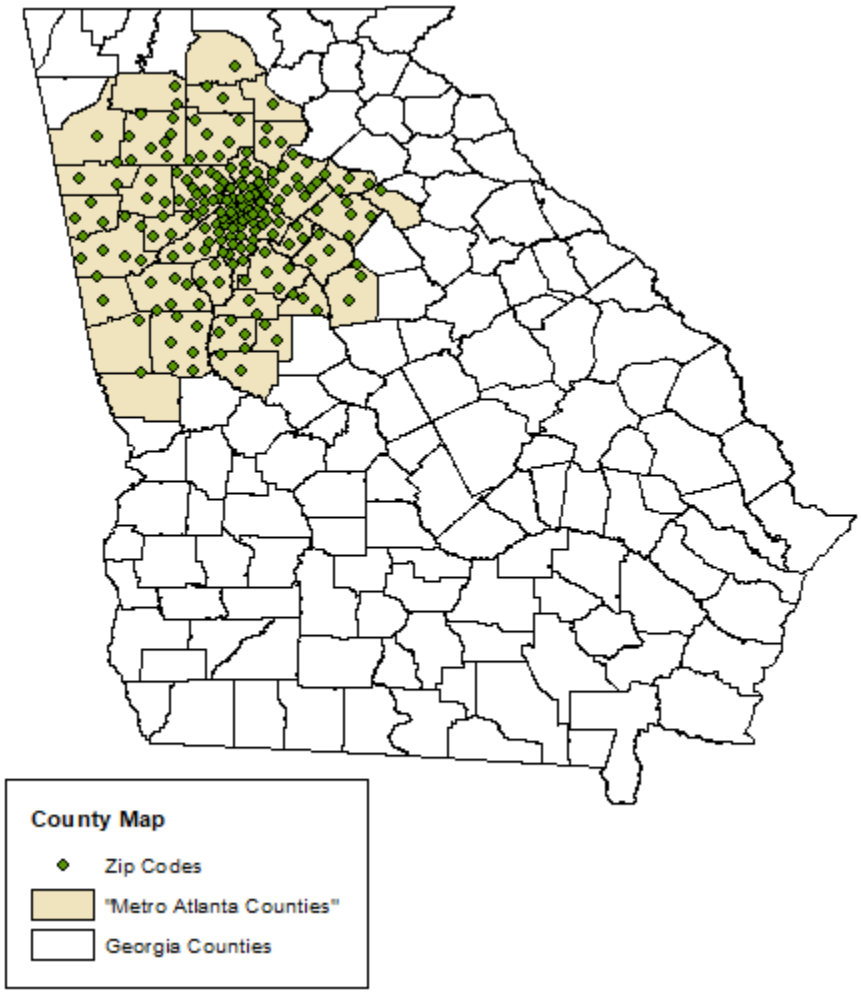

Fig C-1: Map of counties in GA. Metropolitan counties are in light brown.

(Map source: Map created using ARCGIS® software by ESRI (ESRI 2015[183])[248].

Table C-2: Descriptive Statistics for Electricity Use from Georgia Power.
196 Training Data Set observations

Metrics	Electricity Log Transformation	Electricity Kwh/year
Min	233	1.4E4
1st Quartile	6376	1.0E7
Median	13189	4.3E7
Mean	14548	7.3E7
3rd Quartile	21903	1.2E8
Max	33280	2.8E8

Table C-3: Descriptive Statistics for Natural Gas Use from Atlanta Gas Light
32 Training Data Set observations

Metrics	Natural Gas Log Transformation	Natural Gas KJ/year
Min	4.5E5	5.2E10
1st Quartile	1.1E6	2.9E11
Median	1.4E6	4.9E11
Mean	1.4E6	5.2E11
3rd Quartile	1.7E6	7.1E11
Max	2.1E6	10.8E11

Results of Metropolitan ZCTA electricity estimations

Table C-4: Results from training data set for metropolitan ZCTAs electricity use for all transformation techniques. Results reflect the best performing model from each technique.

METRICS	NO TRANSFORMATION	Z-SCORES	CGS	MGS
FULL TRAIN R^2	0.77	0.77	0.75	0.79
FULL NRMSE	0.35	0.35	0.37	0.33
FULL NMB	-0.68	-0.68	-0.79	-0.61
FULL MAX VIF	961	961	1.40	13
WITHHELD R^2	0.69	0.69	0.68	0.75
WITHHELD NRMSE	0.40	0.40	0.40	0.35
VALIDATION NRMSE	0.22	0.22	0.24	0.17
MODEL SIZE	12	12	6	15

Table C-5: Results from training data set for metropolitan ZCTAs electricity use in Atlanta with Principle Component Analysis (PCA). Results reflect the number of components included

Metrics	PCA				
Full Train R^2	0.62	0.73	0.74	0.76	**0.77**
Full NRMSE	0.49	0.39	0.38	0.37	**0.37**
Full NMB	-0.96	-0.81	-0.77	-0.74	**-0.70**
Withheld R^2	0.41	0.62	0.63	0.66	**0.70**
Withheld NRMSE	0.55	0.44	0.43	0.41	**0.39**
Validation NRMSE	0.43	0.17	0.20	0.21	**0.23**
Model size	2	5	10	15	**20**

.

Table C-6: Results from training data set for metropolitan ZCTAs electricity use in Atlanta with Partial Least Squares (PLSR). Results reflect the number of components included.

Metrics	PLSR				
Full Train R^2	0.66	0.74	0.76	0.77	**0.78**
Full NRMSE	0.46	0.37	0.36	0.36	**0.35**
Full NMB	-0.91	-0.82	-0.74	-0.68	**-0.65**
Withheld R^2	0.49	0.64	0.68	0.72	**0.73**
Withheld NRMSE	0.51	0.43	0.40	0.38	**0.37**
Validation NRMSE	0.34	0.20	0.21	0.23	**0.23**
Model size	2	5	10	15	**20**

Table C-7: Model variable predictors results as seen in SI Table 4 for model built with MGS transformation. Tabulated here are predictor descriptions, regression coefficients and VIF values. The variable numbers here can be matched with the variables in SI Table C-1.

Variable No	Variable Name	Regression Coefficient	p_values	VIF
22	White with Hispanic	-40968	9E-14	1
18	Number; SEX AND AGE - Female population - 18 years and over	19483	8E-05	1
305	Male/female ratio pop 25 and older of Total Housing	9342	6E-02	1
59	Total Population / Number of housing units	-8123	1E-01	1
9	Number; SEX AND AGE - Male population	-95907	3E-03	13
31	Number; RACE - Total population - One Race - Some Other Race	-8767	7E-02	1
82	100*Owner Occupied by Age < 24/Total Owner-Occupied Households	10866	4E-02	1
296	Percent Tot Male Pop Bachelor and Higher degree/>25yr Tot Male Pop	10685	2E-02	1
336	Ratio Renter-occupied housing units to Owner-occupied housing units - Some college or associate's degree	-12924	3E-02	1
161	Estimate; VALUE - Median (dollars)	279945	5E-12	11
49	Number; HOUSEHOLDS BY TYPE - Total households - Family households (families) [7]	-12829	1E-02	1
236	100*No of occupied Housing Units with Wood/Total Occupied Housing Units	-12449	9E-03	1
185	Estimate; INCOME AND BENEFITS (IN 2011 INFLATION-ADJUSTED DOLLARS) - Median nonfamily income (dollars)	32968	2E-07	2
167	Percent; EMPLOYMENT STATUS - In labor force pop over 16	-7206	1E-01	1
1	Number; SEX AND AGE - Total population	65325	6E-25	1

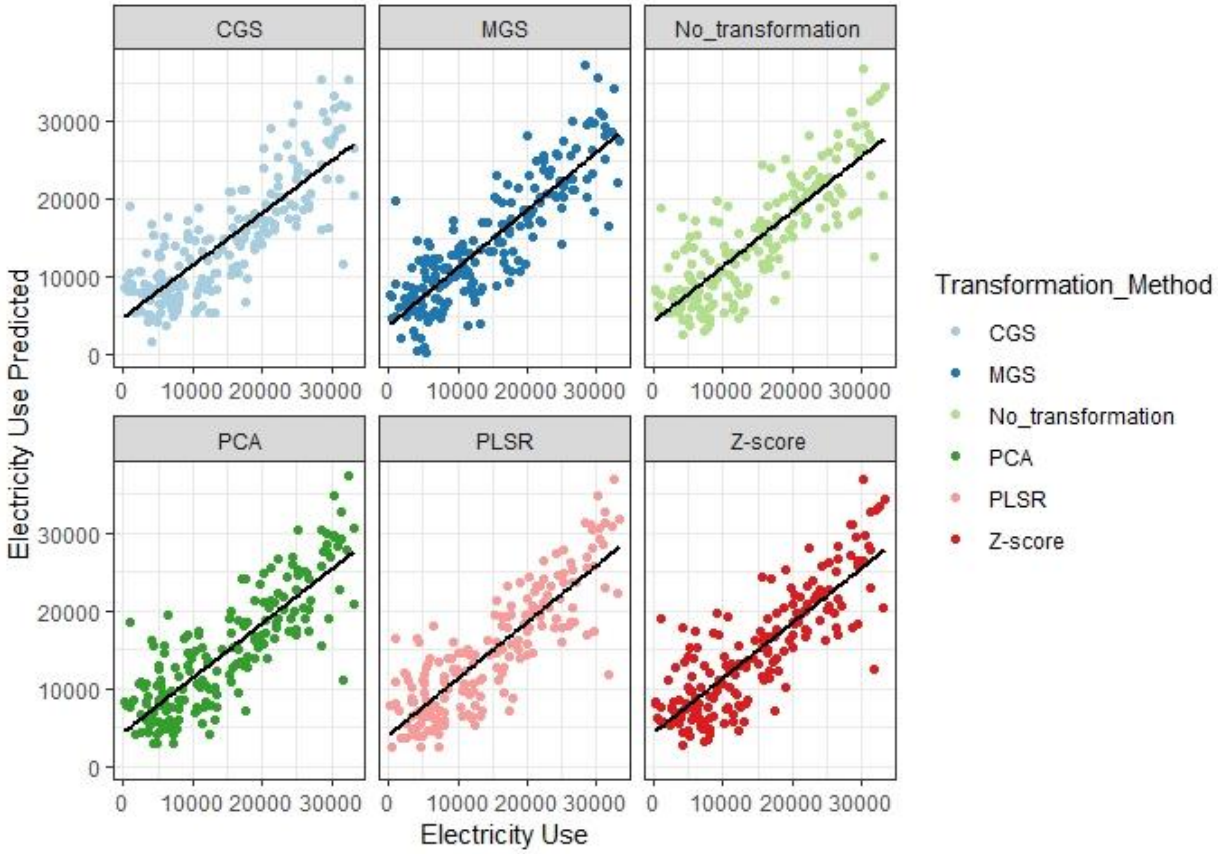

Fig C-2: Results of predicted electricity use plotted against known electricity use in the metropolitan ZCTAs for the full model training set (n = 196). These are the results from the selected model as tabulated in Table C-4 of the SI. Note: Electricity use here (originally in Kwh/yr) is log transformed.

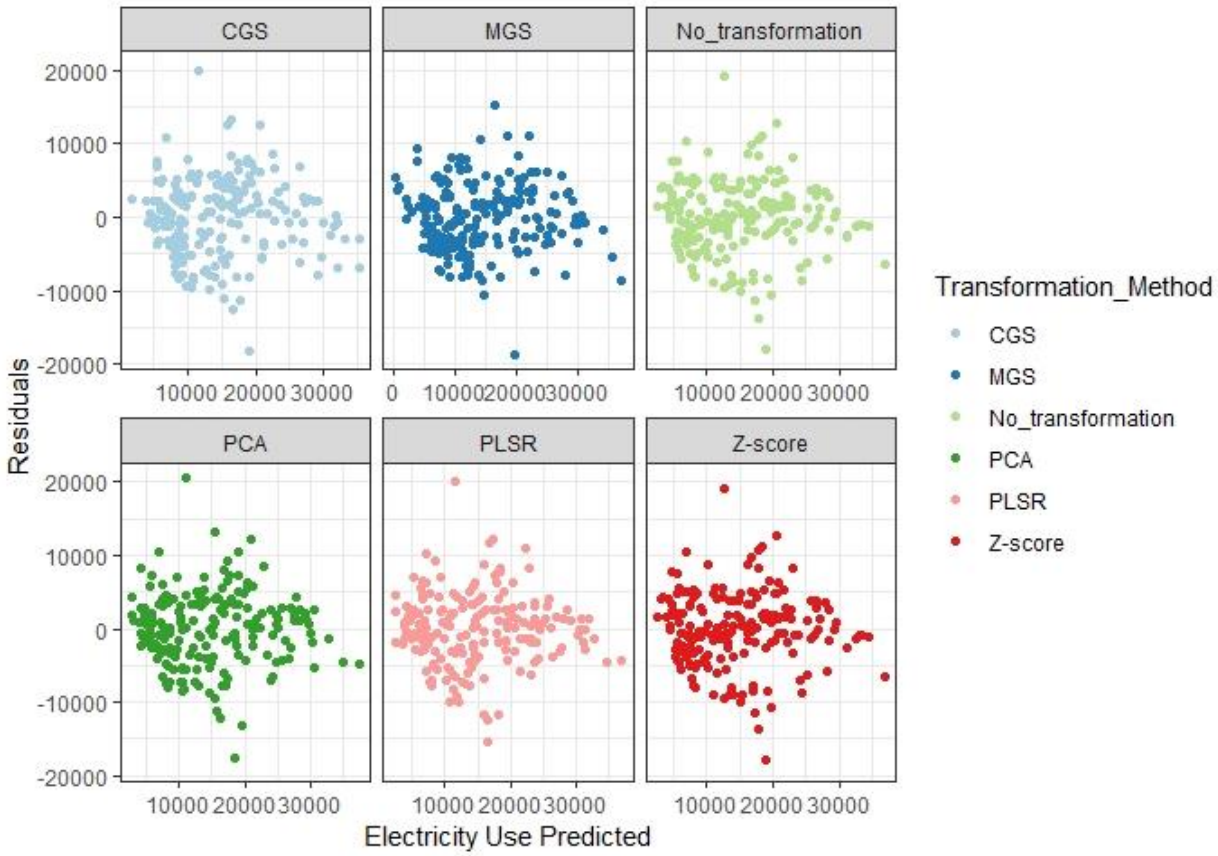

Fig C-3: Model residuals for all transformation method in metropolitan ZCTAs for the full model training set (n = 196) for electricity estimation. These are the results from the selected model as tabulated in Table C-4 of the SI. Note: Electricity use here (originally in Kwh/yr) is log transformed.

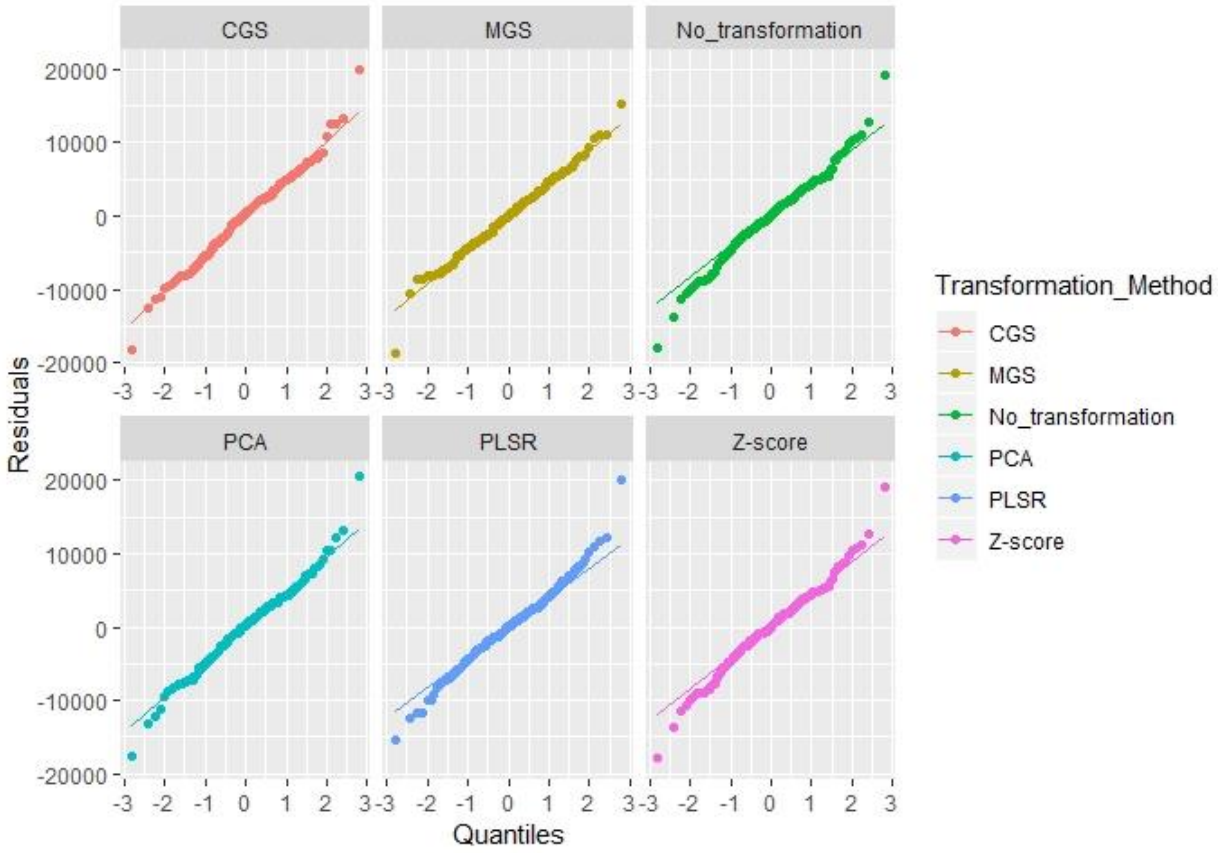

Fig C-4: Residual quartile plots for all transformation method in metropolitan ZCTAs for the full model training set (n = 196) for electricity estimation. These are the results from the selected model as tabulated in Table C-4 of the SI. Note: Electricity use here (originally in Kwh/yr) is log transformed.

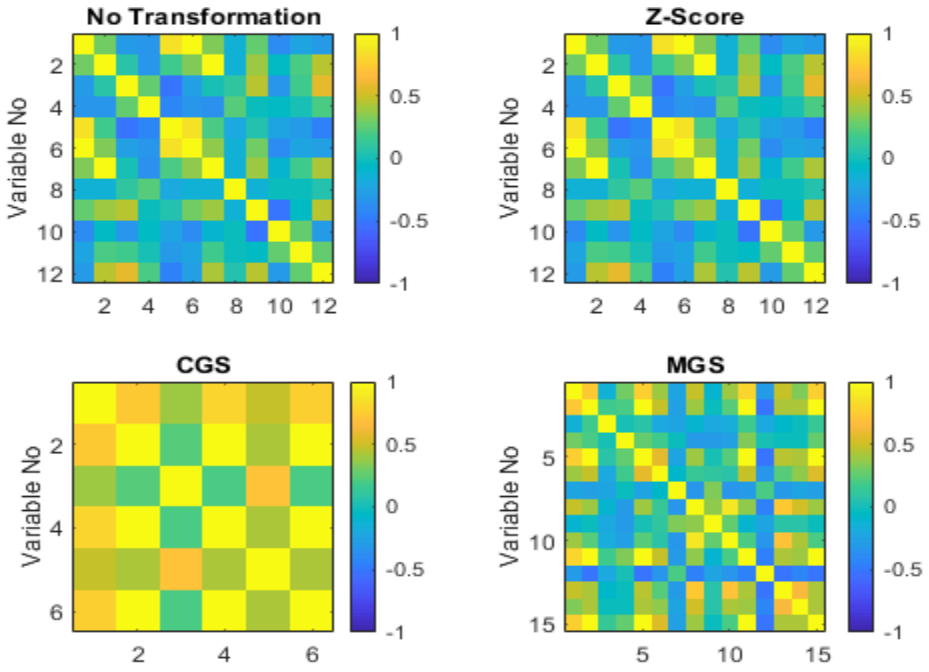

Fig C-5: Correlation matrix plotted as a color map of the selected electricity predictors of each model generated for metropolitan ZCTAs. Plot reflects correlation of variables as untransformed.

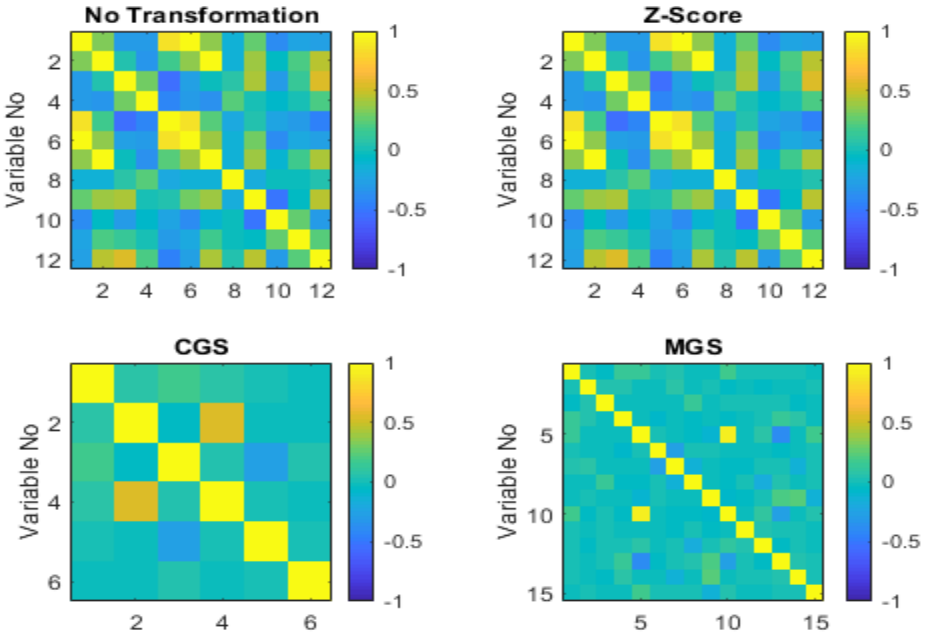

Fig C-6: Correlation matrix plotted as a color map of the selected electricity predictors of each model generated for metropolitan ZCTAs. Plot reflects correlation of variables when transformed according to model.

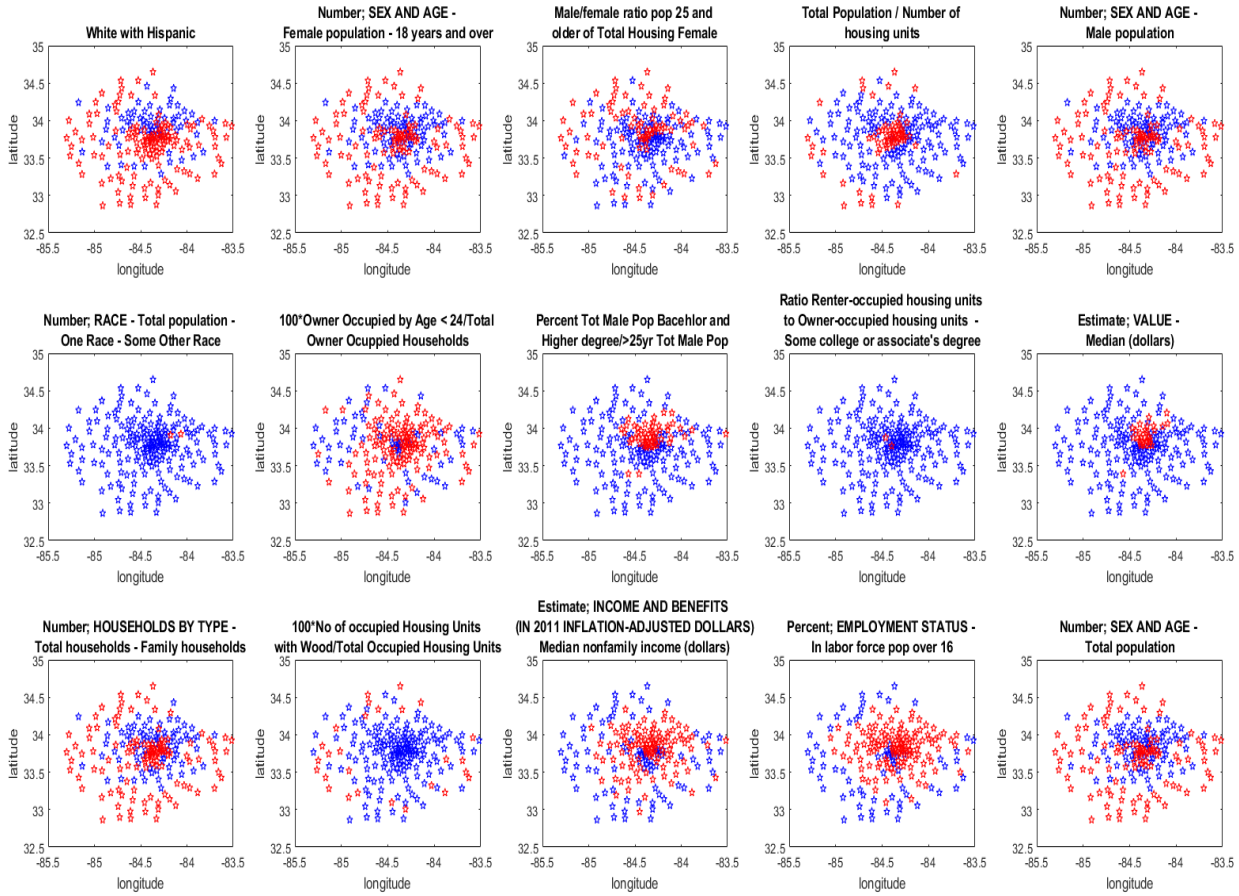

Fig C-7: Clustering of the predictor variables from the MGS model results for electricity model for metropolitan ZCTAs. Predictor variables here are untransformed. This evaluates if the clustering of predictor variables is similar to electricity use clustering.

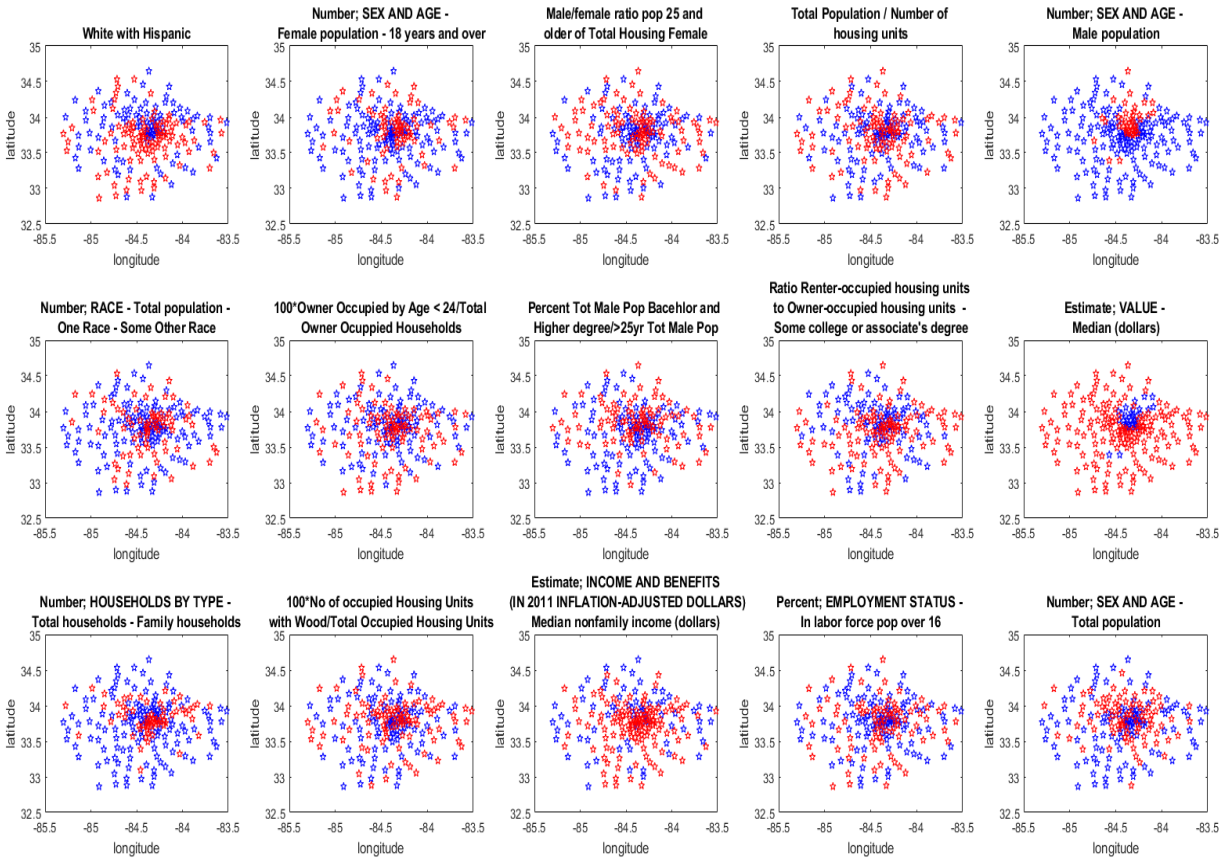

Fig C-8: Clustering of the predictor variables from the MGS model results for electricity model for metropolitan ZCTAs. Predictor variables here are transformed. This evaluates if the clustering of predictor variables is similar to electricity use clustering.

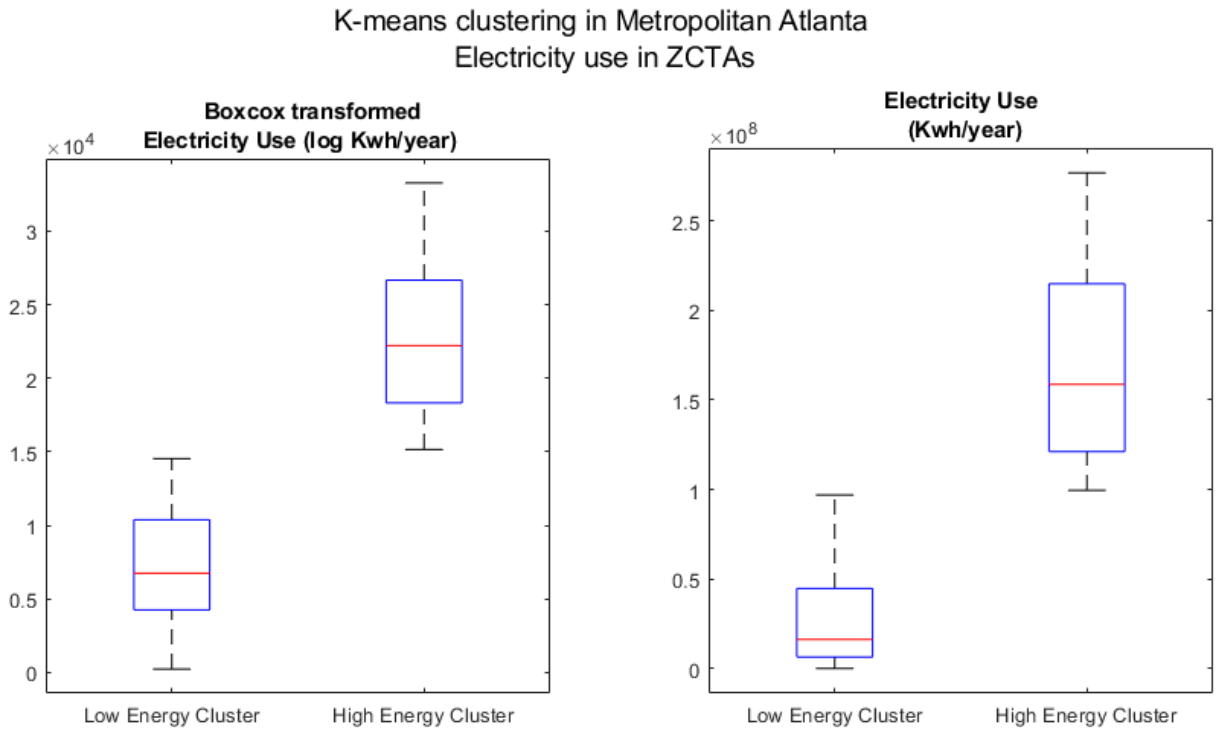

Fig C-9: Electricity boxplots of k-means clustering results of metropolitan ZCTAs.

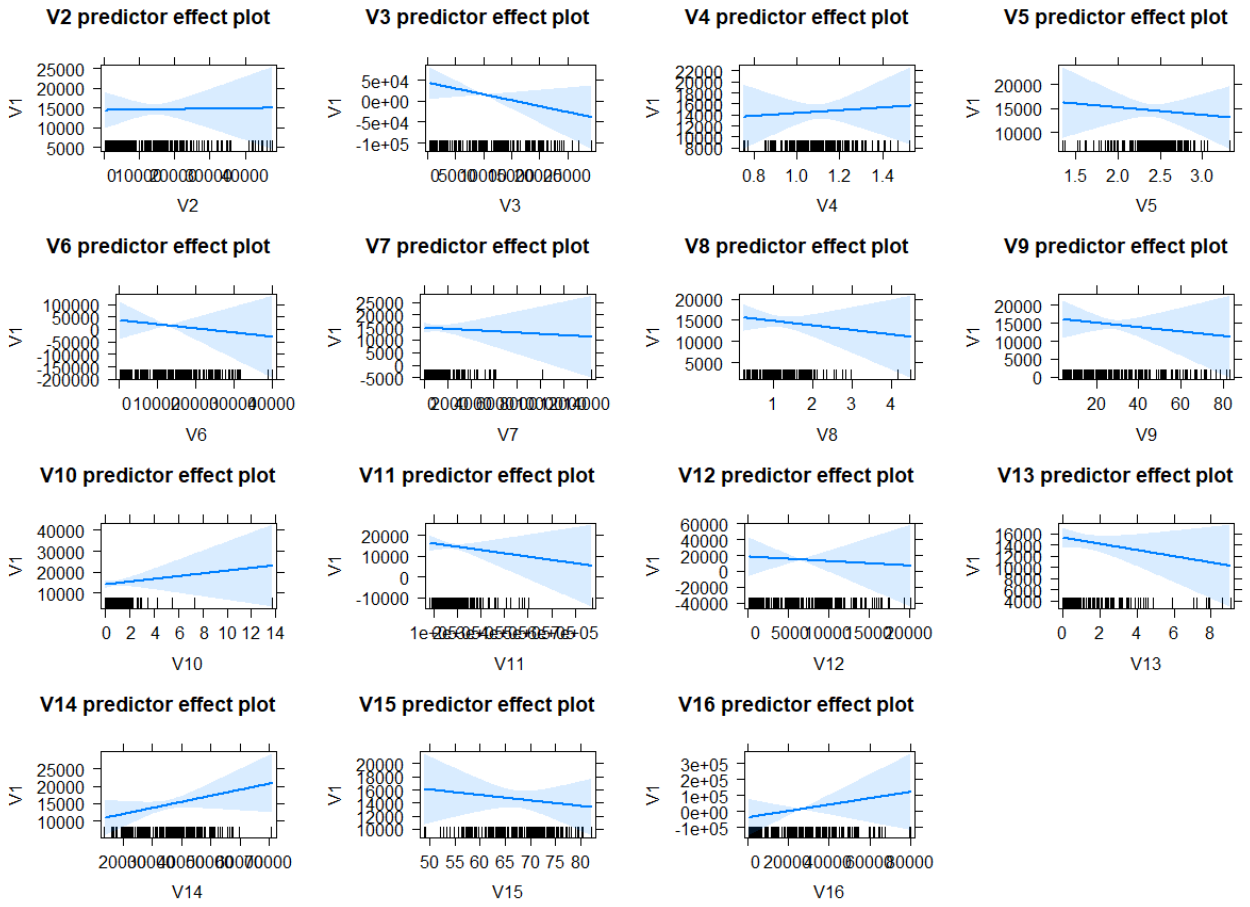

Fig C-10: Interaction effects plot showing how untransformed predictors in final MGS model interact with electricity use. Results are for the metropolitan ZCTAs [175], [176].

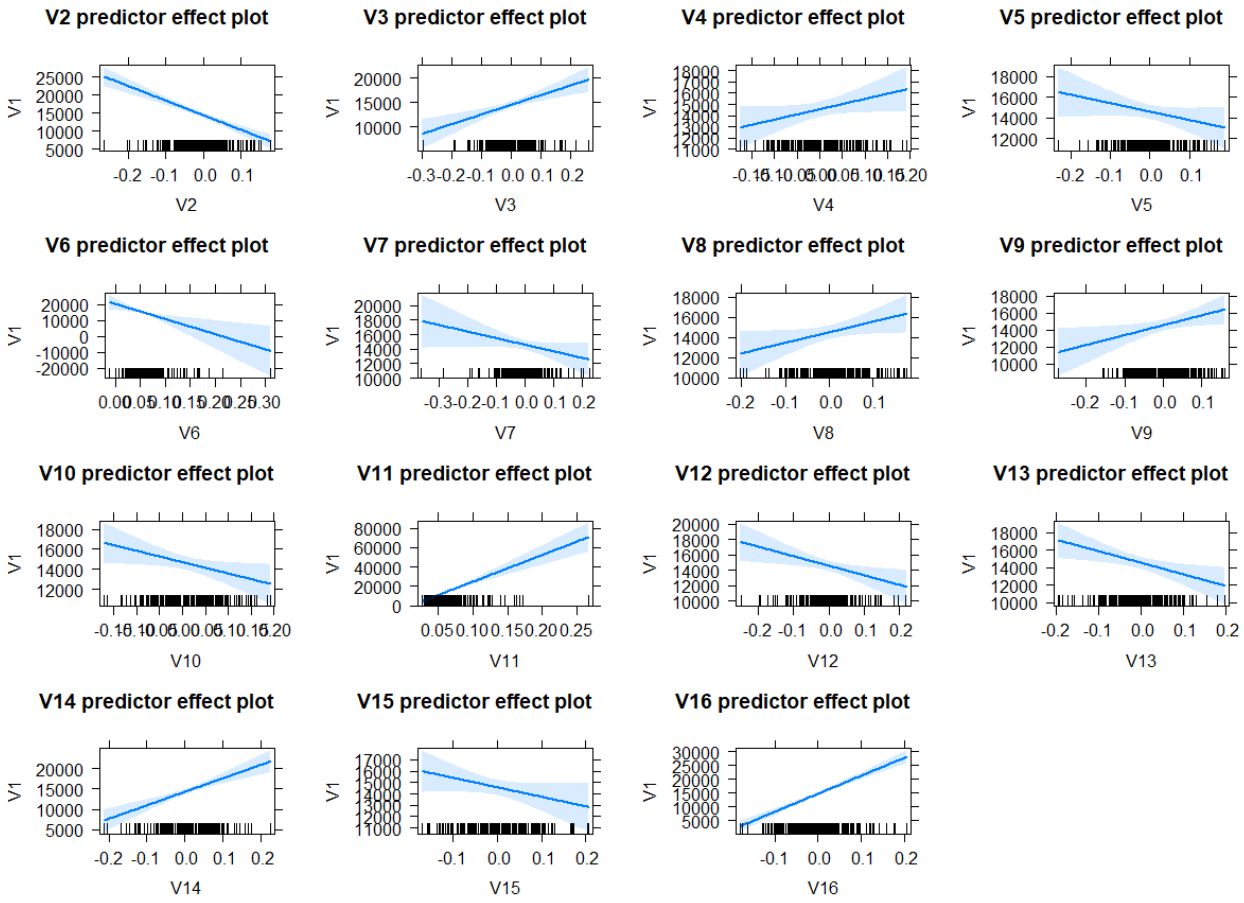

Fig C-11: Interaction effects plot showing how the transformed predictors in final MGS model interact with electricity use. Results are for metropolitan ZCTAs [175], [176].

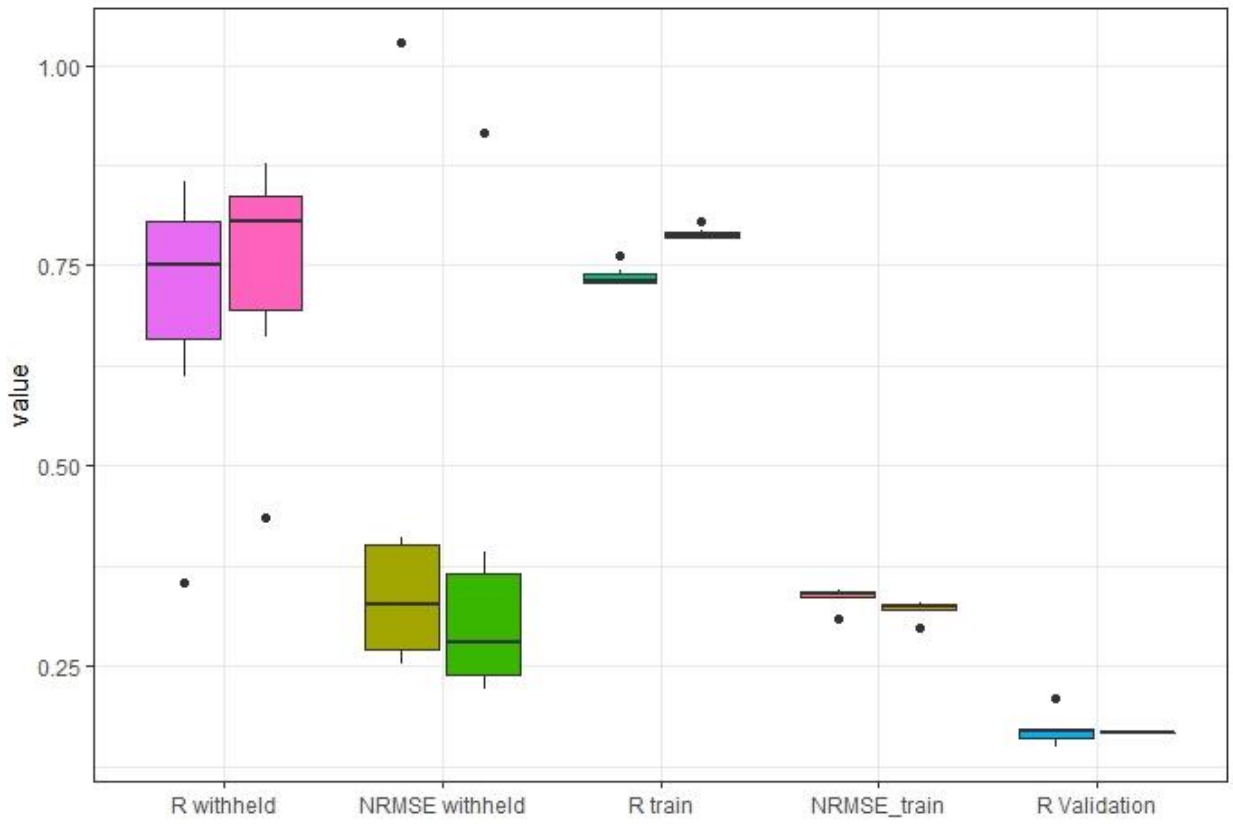

Fig C-12: Effect of Ensemble averaging of the regression coefficients from different sample populations. For each metric, the first is the result of using the regression coefficients for each population sample. The second plot is the result of using the ensemble average to generate the estimates. The results shown here are for electricity estimation, for metropolitan ZCTAs and the MGS method.

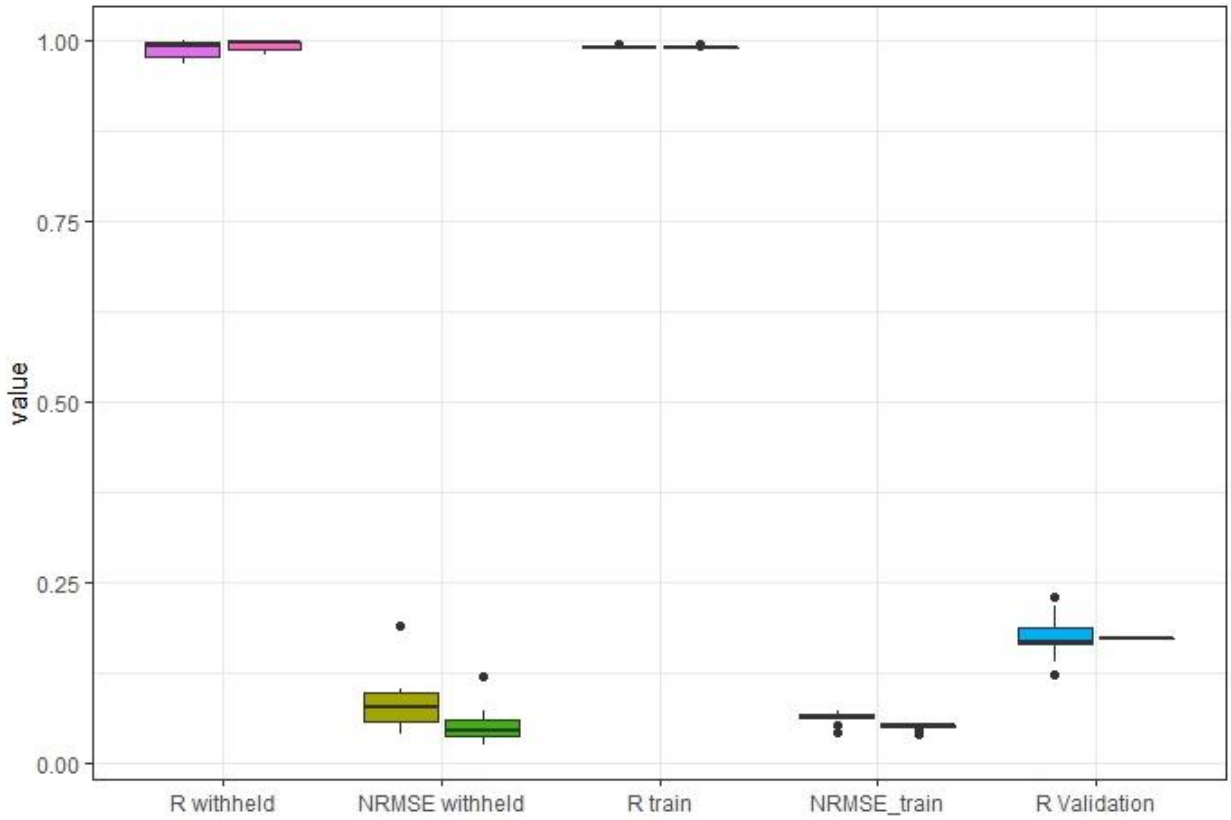

Fig C-13: Effect of Ensemble averaging of the regression coefficients from different sample populations. For each metric, the first is the result of using the regression coefficients for each population sample. The second plot is the result of using the ensemble average to generate the estimates. The results shown here are for natural gas estimation, for metropolitan ZCTAs and the MGS method.

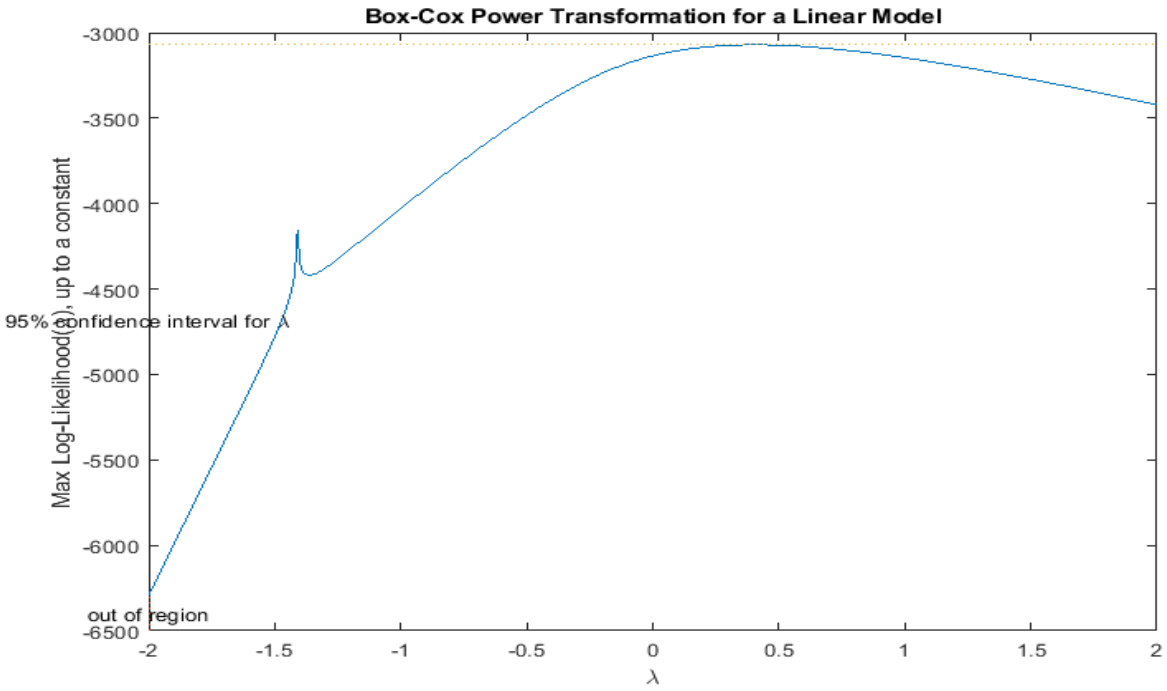

Fig C-14: Recommend transformation for electricity use model development[174].

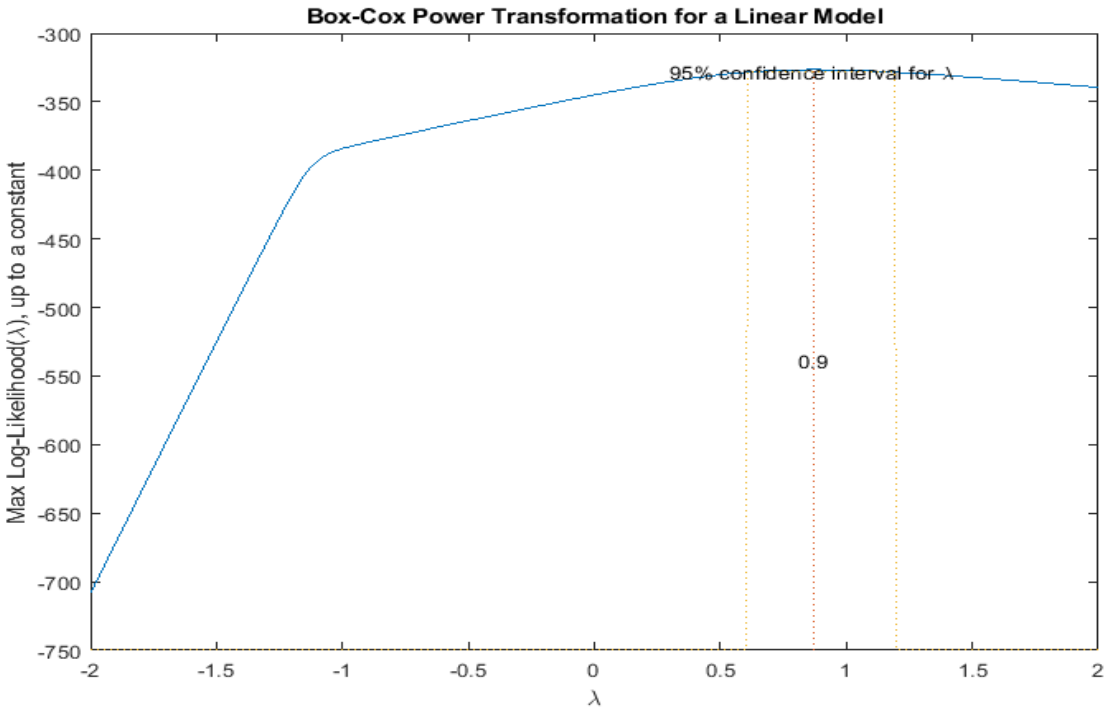

Fig C-15: Recommend transformation for natural gas use model development[174].

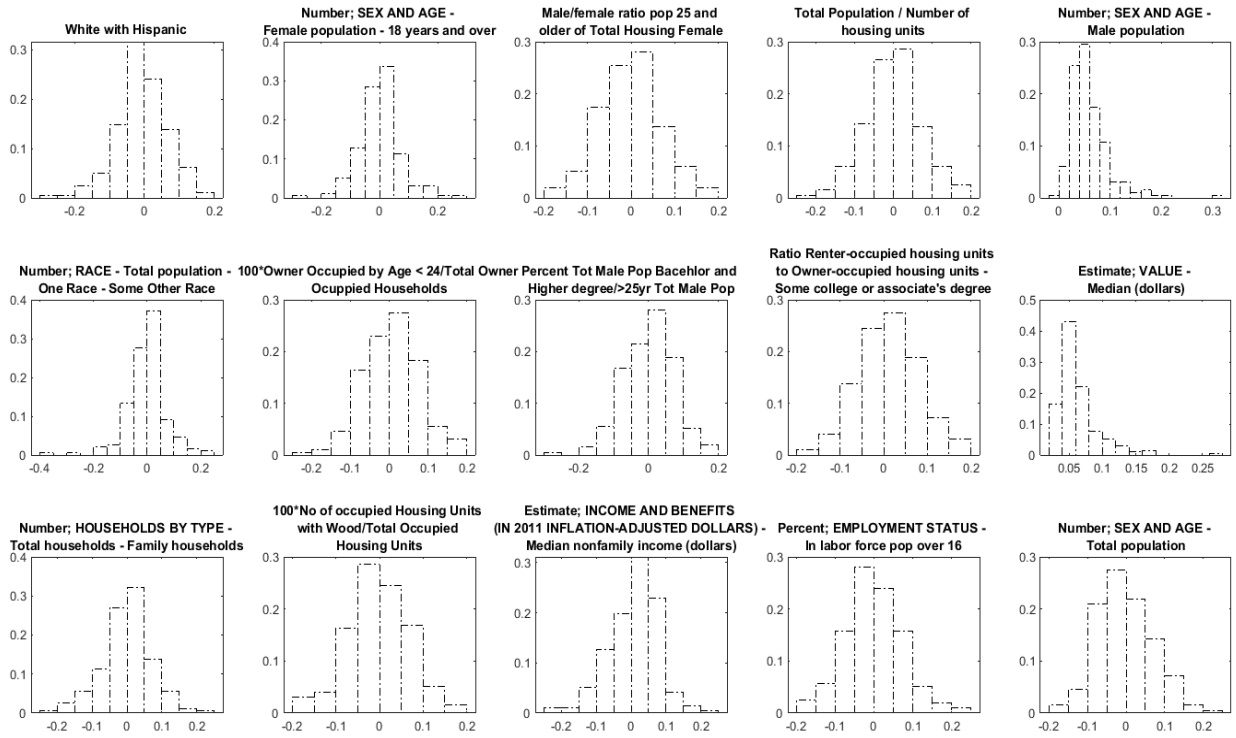

Fig C-16: Clustering of the electricity predictor variables from the MGS model results for electricity model for metropolitan ZCTAs. Plot reflects variables as transformed.

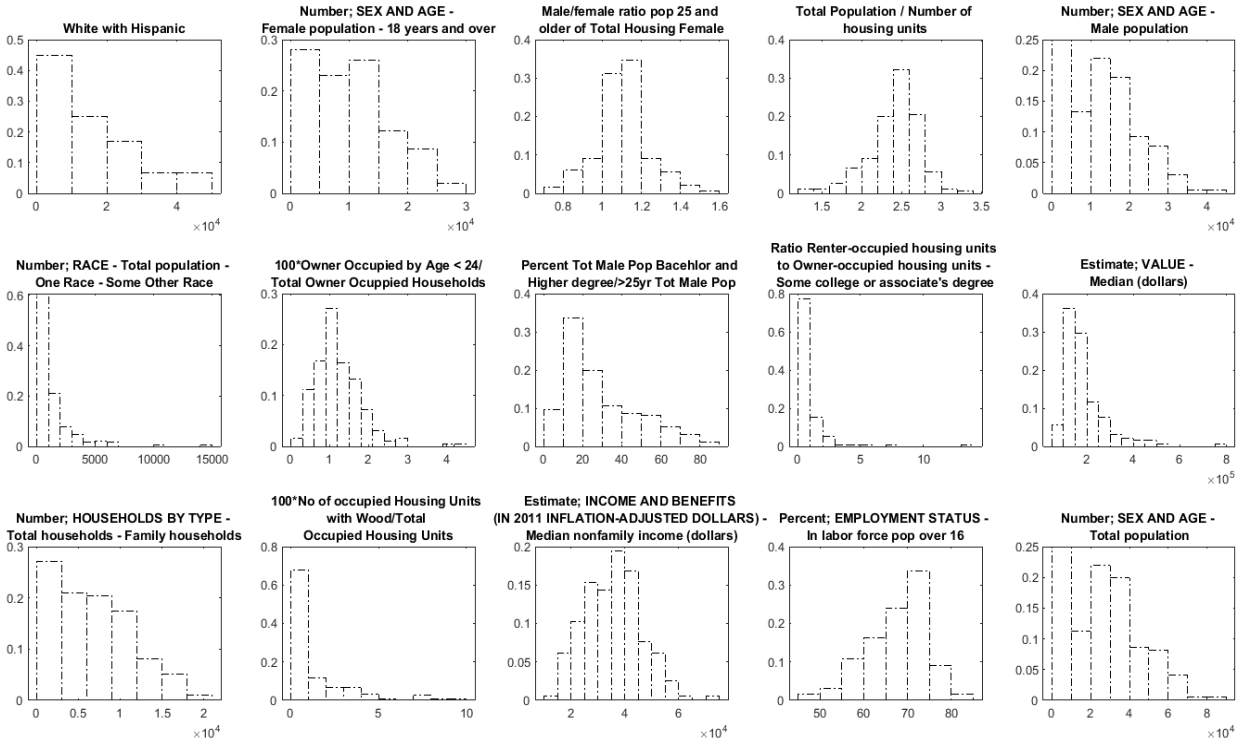

Fig C-17: Clustering of the electricity predictor variables from the MGS model results for electricity model for metropolitan ZCTAs electricity. Plot reflects variables as untransformed.

Results of Metropolitan ZCTA gas estimations

Table C-8: Results from training data set for metropolitan ZCTAs gas use for all different transformation techniques. Results reflect the best performing model from each technique.

METRICS	NO TRANSFORMATION	Z-SCORES	CGS	MGS
FULL TRAIN R^2	0.98	0.98	0.95	0.94
FULL NRMSE	0.08	0.09	0.15	0.17
FULL NMB	0.00	-0.02	-0.02	-0.05
FULL MAX VIF	11	19	13	5
WITHHELD R^2	0.99	1.00	0.95	0.94
WITHHELD NRMSE	0.05	0.04	0.11	0.13
VALIDATION NRMSE	0.17	0.20	0.21	0.28
MODEL SIZE	9	10	9	11

Table C-9: Model variable predictors results as seen in SI table C-8, for model built with CGS transformation. Tabulated here are predictor descriptions, regression coefficients and VIF values. The variable number here can be matched with the variables in SI Table C-1.

VARIABLE NO	VARIABLE NAME	REGRESSION COEFFICIENT	P_VALUES	VIF
23	Number; RACE - Total population - One Race - Black or African American	-1602703	0.03	1
183	Estimate; INCOME AND BENEFITS (IN 2011 INFLATION-ADJUSTED DOLLARS) - Median family income (dollars)	1822286	0.17	1
1	Number; SEX AND AGE - Total population	11132596	0.00	2
9	Number; SEX AND AGE - Male population	-3196000	0.00	3
161	Estimate; VALUE - Median (dollars)	20144155	0.00	13
37	Number; RELATIONSHIP - Total population - In households	2298321	0.01	2
184	Estimate; INCOME AND BENEFITS (IN 2011 INFLATION-ADJUSTED DOLLARS) - Per capita income (dollars)	-2628039	0.00	1
178	Estimate; INCOME AND BENEFITS (IN 2011 INFLATION-ADJUSTED DOLLARS) - Median household income (dollars)	6768871	0.01	8
185	Estimate; INCOME AND BENEFITS (IN 2011 INFLATION-ADJUSTED DOLLARS) - Median nonfamily income (dollars)	-1605688	0.15	4

Table C-10: Model variable predictors results as seen in SI table C-8, for model built with MGS transformation. Tabulated here are predictor descriptions, regression coefficients and VIF values. The variable number here can be matched with the variables in SI Table C-1.

VARIABLE NO	VARIABLE NAME	REGRESSION COEFFICIENT	P_VALUES	VIF
1	Number; SEX AND AGE - Total population	2504289	0.04	2
11	male Population younger than 18	-12113427	0.00	3
17	Female Population younger than 18	16607338	0.00	5
96	100*Owner occupied: - 3-person household/Total Owner Occupied House units	912717	0.74	2
272	100*Number of Housing Units Built 2000 to 2004 or later/Total Housing Units	-2903753	0.00	1
229	Cumulative Percentage of Housing units with zero to 3 bedrooms	1032002	0.55	3
141	Hispanic mortgage free occupied units/Total Hispanic Occupied units	-1438486	0.12	1
177	Percent; INCOME AND BENEFITS (IN 2011 INFLATION-ADJUSTED DOLLARS) - $200,000 or more	3007565	0.01	1
76	100* No of Family Type Households/Total Households	4522850	0.00	3
296	Percent Tot Male Pop Bachelor and Higher degree/>25yr Tot Male Pop	1980080	0.05	2
234	100*No of occupied Housing Units with Fuel oil Kerosene/Total Occupied Housing Units	-1188039	0.22	1

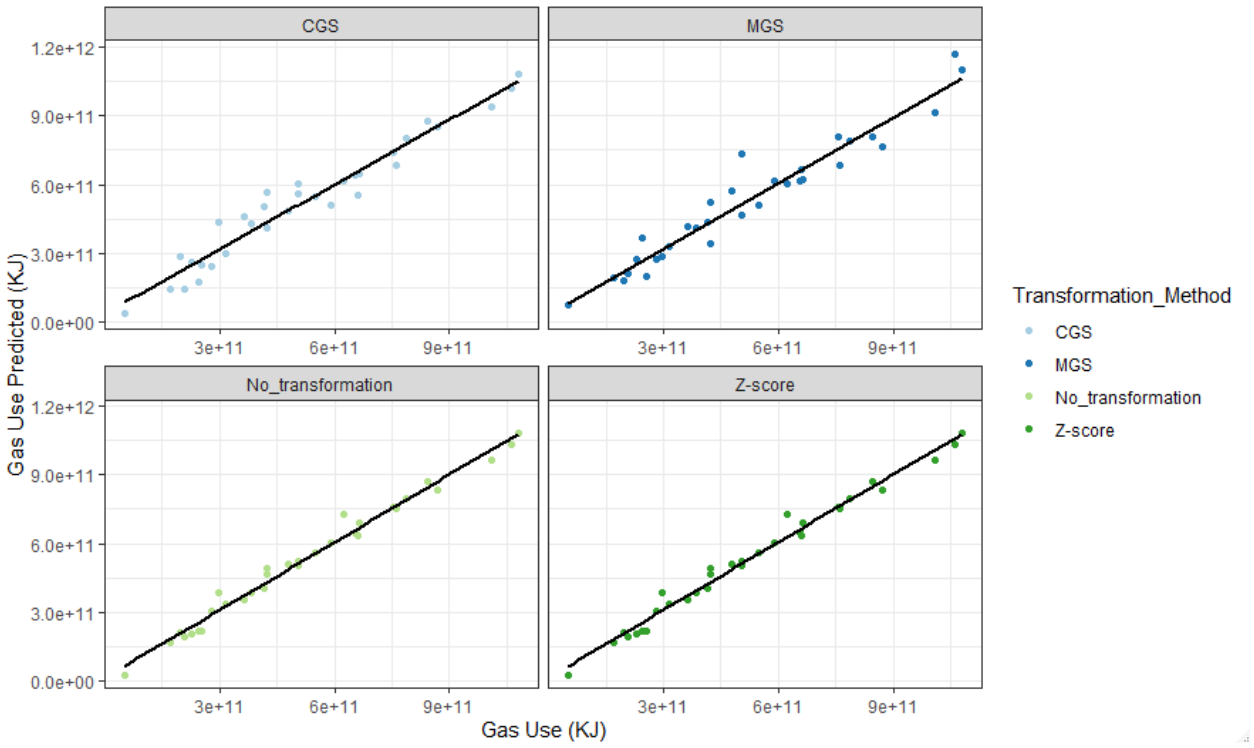

Fig C-18: Results of predicted natural gas use plotted against known natural gas use in the metropolitan ZCTAs for the full model training set (n = 32). These are the results from the selected model as tabulated in Table C-8 of the SI.

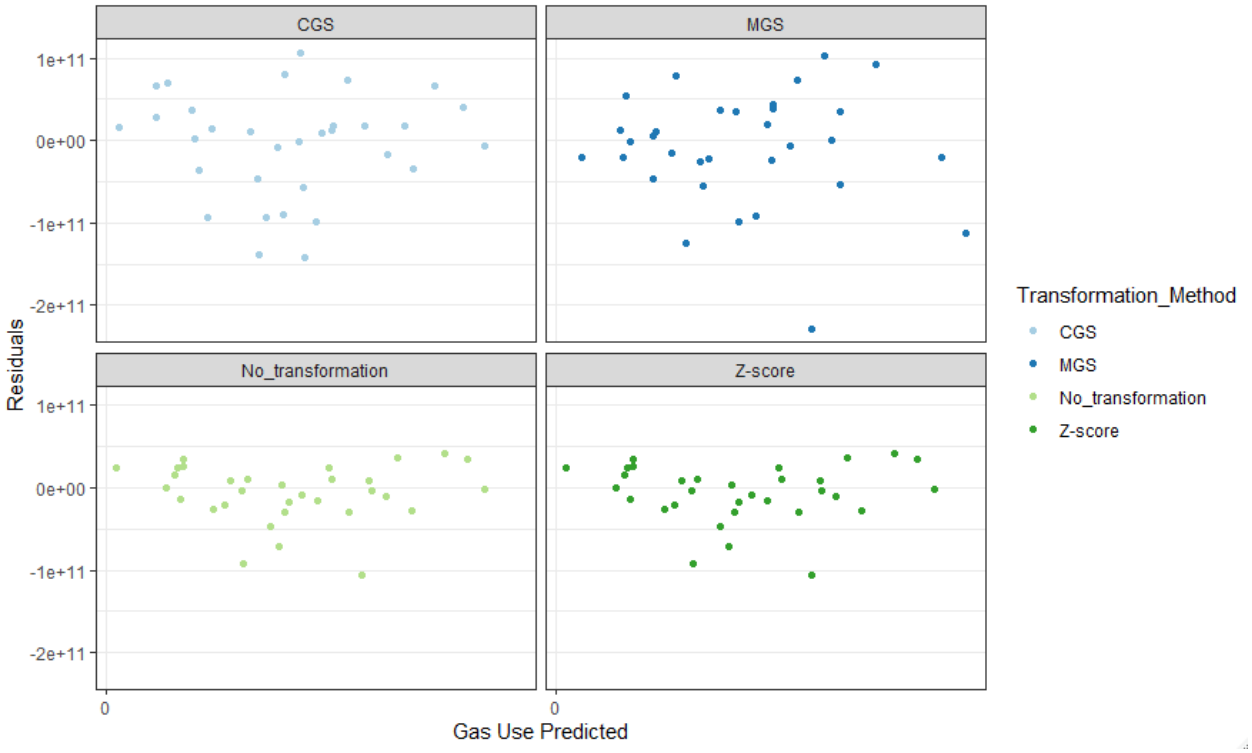

Fig C-19: Model residuals for all transformation methods in metropolitan ZCTAs for the full model training set (n = 32) for natural gas estimation. These are the results from the selected model as tabulated in Table C-8 of the SI.

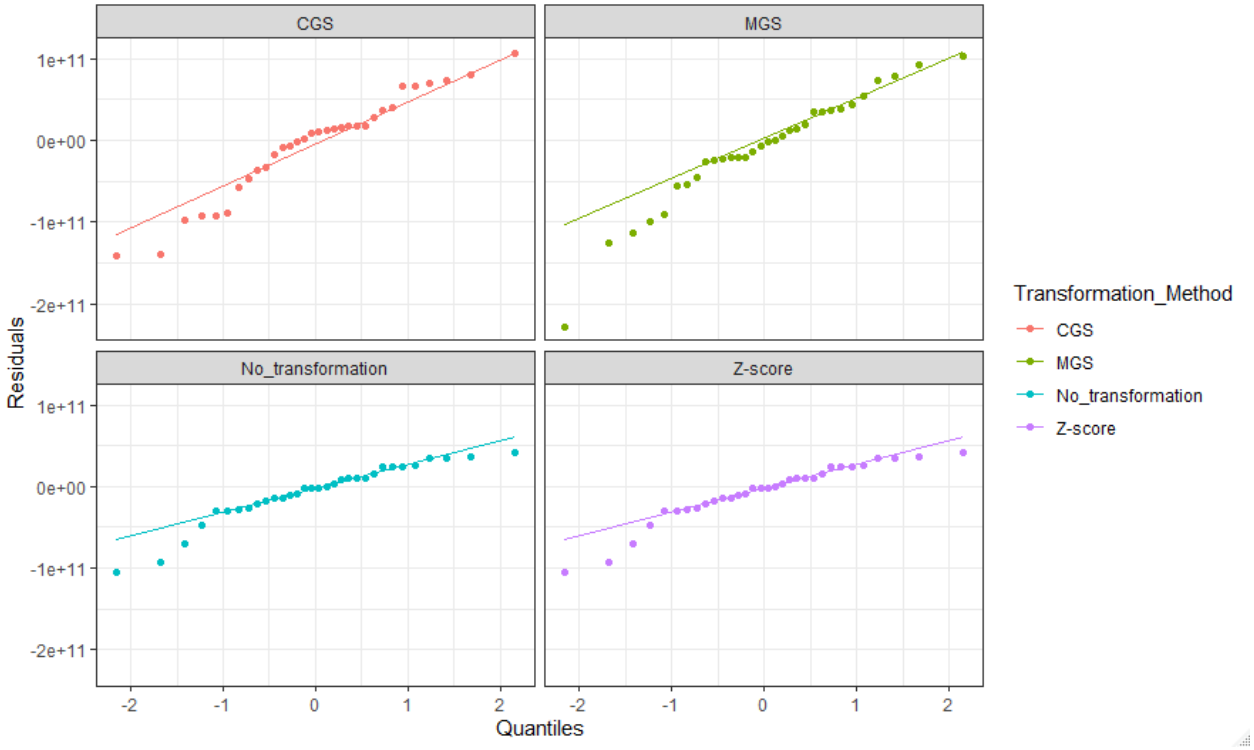

Fig C-20: Residual quartile plots for all transformation methods in metropolitan ZCTAs for the full model training set (n = 32) for natural gas estimation. These are the results from the selected model as tabulated in Table C-8 of the SI.

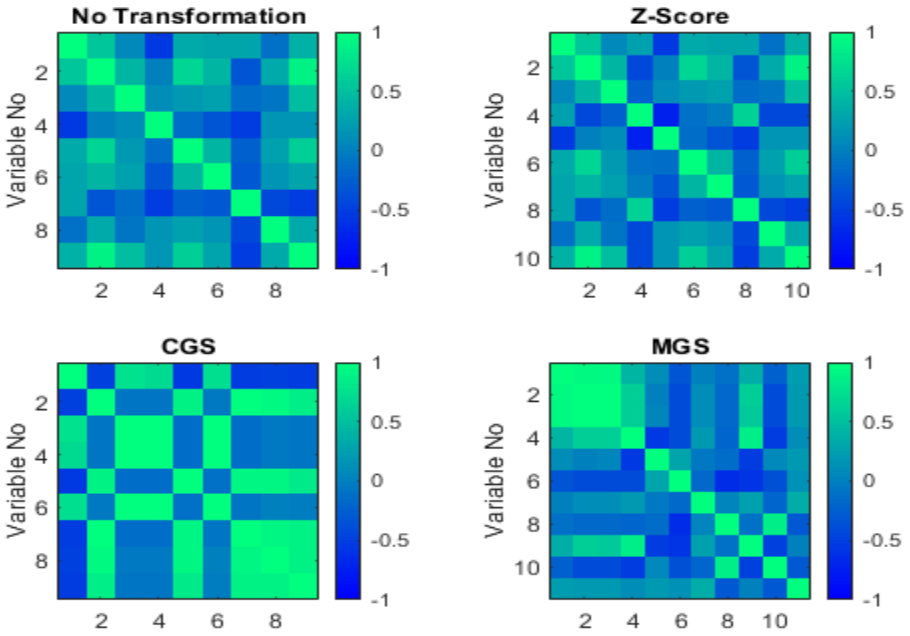

Fig C-21: Correlation matrix plotted as a color map of the selected gas predictors of each model generated for metropolitan ZCTAs. Plot reflects correlation of variables as untransformed.

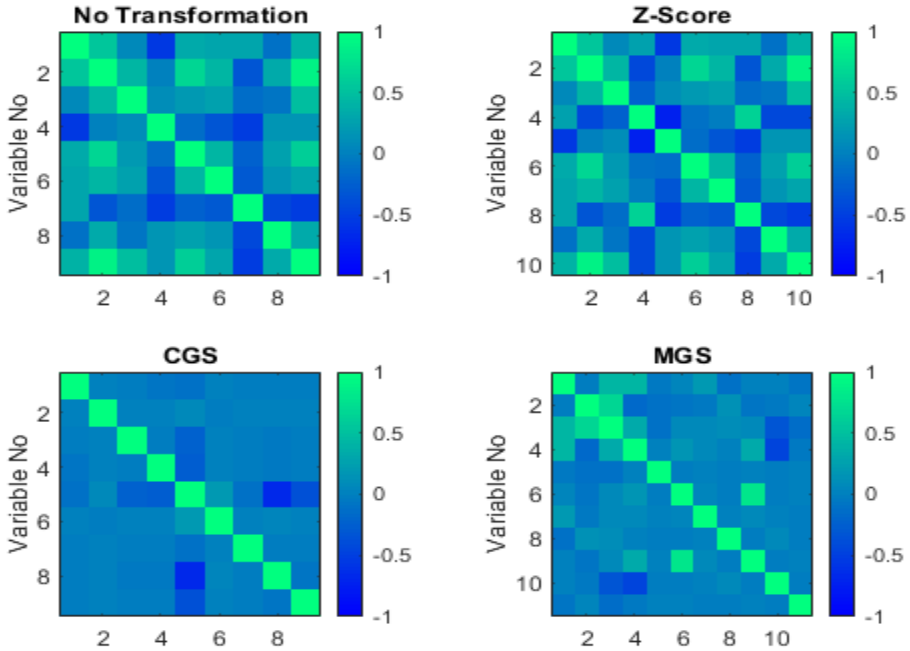

Fig C-22: Correlation matrix plotted as a color map of the selected gas predictors of each model generated for metropolitan ZCTAs natural gas. Plot reflects correlation of variables when transformed according to model.

Figure C-23: Interstate mapping of I-75 and I-285 around metropolitan Atlanta.

Map source: Map and data created using ARCGIS® software by ESRI (ESRI 2015[349]).

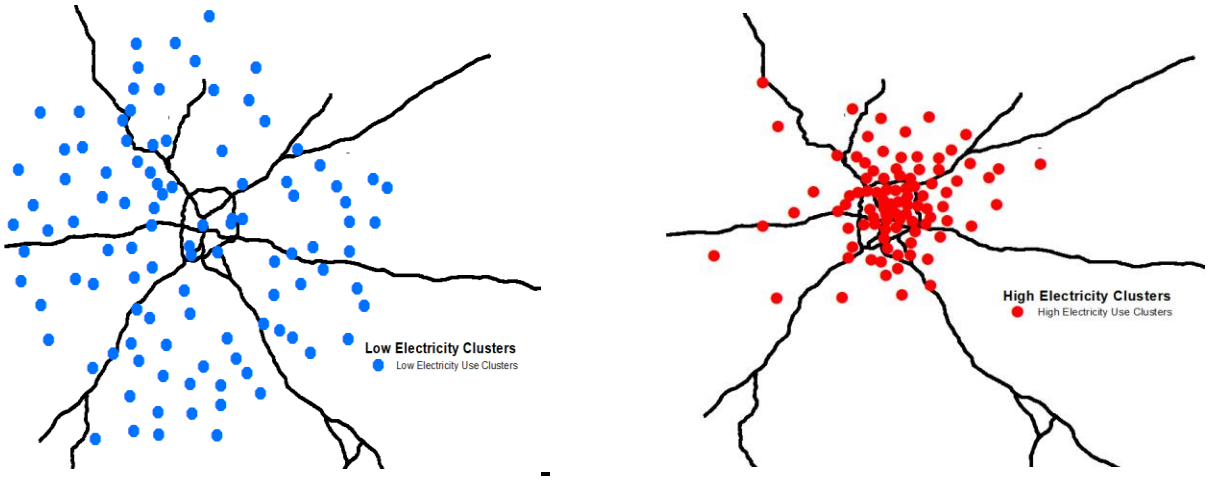

Fig C-24: Log transformed electricity mapping of clusters by k-means for metropolitan ZCTAs. Red indicates high electricity use clusters, while blue indicates low electricity use clusters (See SI Figure 9 for actual cluster averages). The dark lines represent the major interstate highways through Atlanta[182]. (Map source: Map created using ARCGIS® software by ESRI (ESRI 2015) [183].

Results of GA ZCTA electricity estimations

Table C-11: Results after separating the training set (n=196), from the full data set (i.e. GA ZCTAs (n = 606)) for all different transformation techniques for electricity estimation. Results reflect the best performing model from each technique.

METRICS	NO TRANSFORMATION	Z-SCORES	CGS	MGS
FULL TRAIN R^2	0.71	0.71	0.75	0.79
FULL NRMSE	0.40	0.40	0.37	0.34
FULL NMB	-0.92	-0.92	-0.79	-0.55
FULL MAX VIF	1.3	1.3	1.12	1.6
WITHHELD R^2	0.65	0.65	0.75	0.82
WITHHELD NRMSE	0.35	0.35	0.29	0.25
VALIDATION NRMSE	0.30	0.30	0.25	0.24
MODEL SIZE	3	3	6	15

Table C-12: Model variable predictors results as seen in SI table C-11, for model built with MGS transformation. Tabulated here are predictor descriptions, regression coefficients and VIF values. The variable number here can be matched with the variables in SI Table C-1.

VARIABLE NO	VARIABLE NAME	REGRESSION COEFFICIENT	P_VALUES	VIF
209	100*Housing units built later than 1950 with complete plumbing with <1 occupant per room/Total Housing units with complete plumbing	24421	0.01	4
22	White with Hispanic	-55656	0.00	2
229	Cumulative Percentage of Housing units with zero to 3 bedrooms	-20705	0.07	5
201	100*Rented with complete facilities/Total housing units	21365	0.01	3
67	100*Pop in Renter Occupied housing units/Population	-22200	0.03	4
1	Number; SEX AND AGE - Total population	78633	0.00	2
18	Number; SEX AND AGE - Female population - 18 years and over	21629	0.00	2
319	100*Owner-occupied housing units: - High school graduate (including equivalency)/Tot Occupied housing units	-29024	0.00	4
103	100*Renter occupied: - 3-person household/Total Rent Occupied House units	-29906	0.00	4
152	Percent; UNITS IN STRUCTURE - 1-unit, attached of Total Housing Units	22598	0.01	3
27	Number; RACE - Total population - One Race - Native Hawaiian and Other Pacific Islander - Native Hawaiian	17501	0.03	3
161	Estimate; VALUE - Median (dollars)	208670	0.00	2
185	Estimate; INCOME AND BENEFITS (IN 2011 INFLATION-ADJUSTED DOLLARS) - Median nonfamily income (dollars)	43299	0.00	4
17	Female Population younger than 18	-9273	0.32	3
198	100* Total occupied with incomplete facilities/Total housing units	14768	0.19	3

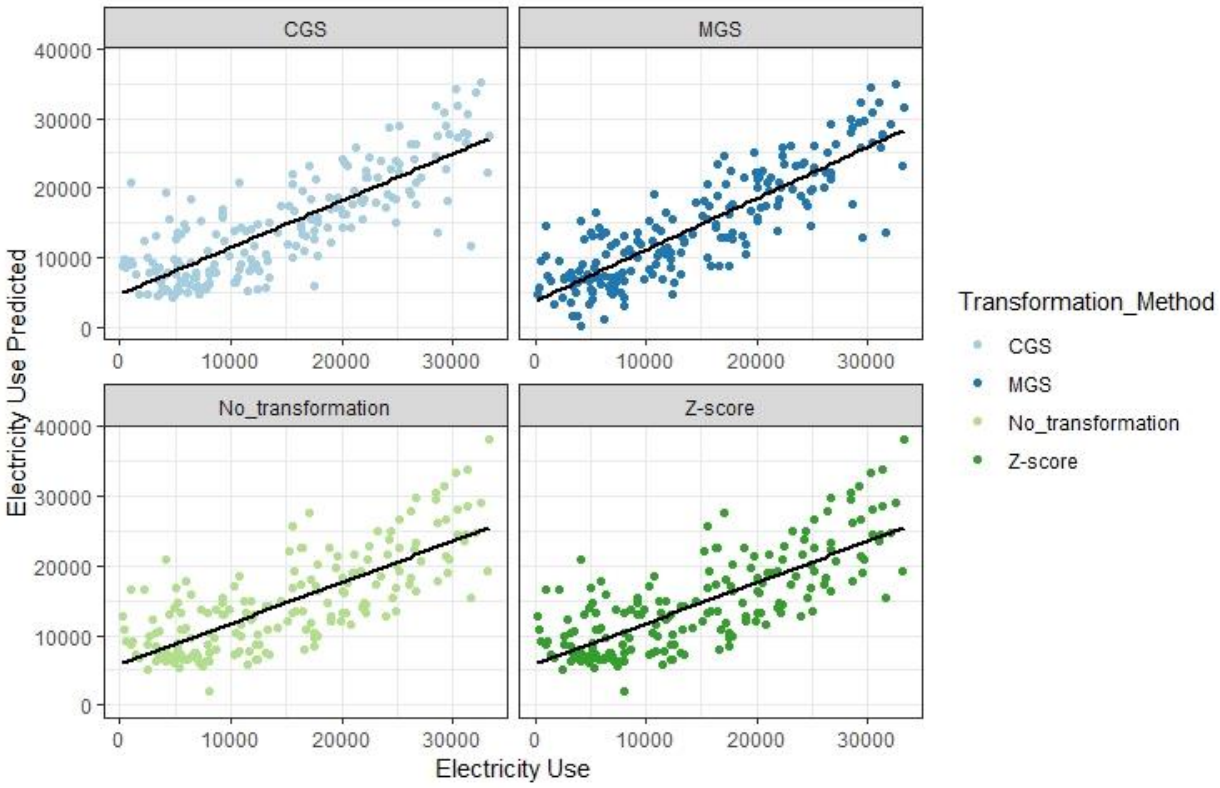

Fig C-25: Results of predicted electricity use plotted against known electricity use for the training set, after separating the training set (n=196), from the full data set (i.e. GA ZCTAs (n = 606)). These are the results from the selected model as tabulated in Table C-11 of the SI. Note: Electricity use here (originally in Kwh/yr) is log transformed.

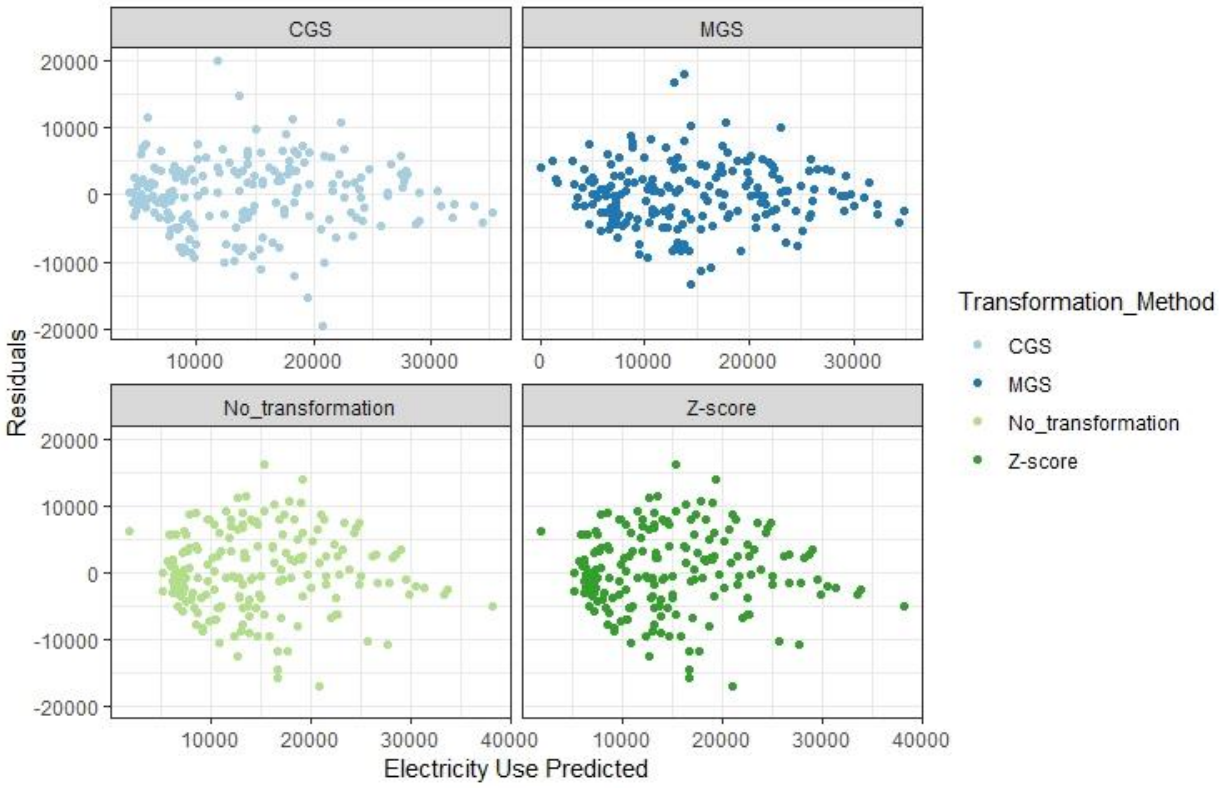

Fig C-26: Model residuals with all transformation methods for the training set, after separating the training set (n=196), from the full data set (i.e. GA ZCTAs (n = 606)). These are the results from the selected model as tabulated in Table C-11 of the SI.

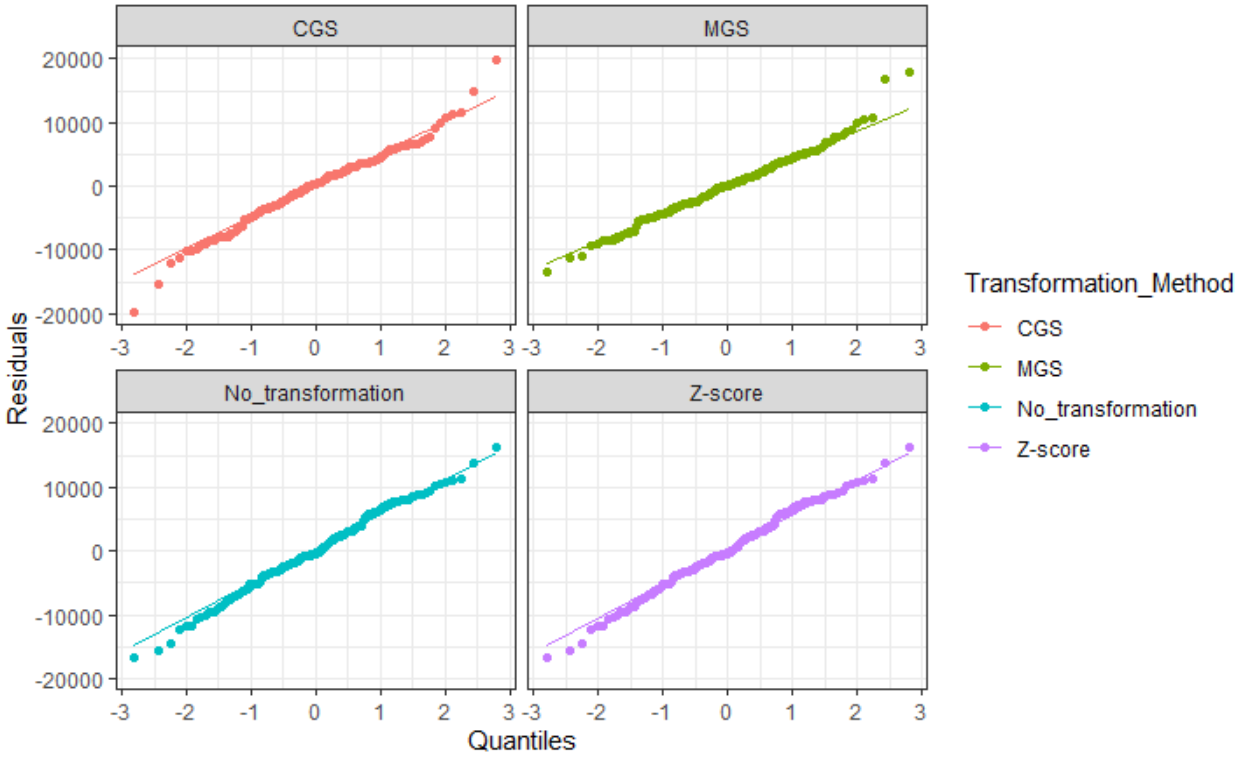

Fig C-27: Residual quartile plots for all transformation methods for the training set, after separating the training set (n=196), from the full data set (i.e. GA ZCTAs (n = 606)). These are the results from the selected model as tabulated in Table C-11 of the SI.

Results of GA ZCTA gas estimations

Table C-13: Results after separating the training set (n=196), from the full data set (i.e. GA ZCTAs (n = 606)) for all different transformation techniques for gas estimation. Results reflect the best performing model from each technique.

METRICS	NO TRANSFORMATION	Z-SCORES	CGS	MGS
FULL TRAIN R^2	0.98	0.98	0.96	0.95
FULL NRMSE	0.09	0.09	0.13	0.15
FULL NMB	0.00	0.00	-0.02	-0.02
FULL MAX VIF	23	23	14	2
WITHHELD R^2	0.99	0.99	0.97	0.93
WITHHELD NRMSE	0.06	0.06	0.11	0.13
VALIDATION NRMSE	0.19	0.19	0.18	0.09
MODEL SIZE	10	10	9	10

Table C-14: Model variable predictors results as seen in SI table C-13, for model built with no transformation. Tabulated here are predictor descriptions, regression coefficients and VIF values. The variable number here can be matched with the variables in SI Table C-1.

VARIABLE NO	VARIABLE NAME	REGRESSION COEFFICIENT	P_VALUES	VIF
177	Percent; INCOME AND BENEFITS (IN 2011 INFLATION-ADJUSTED DOLLARS) - $200,000 or more	-44902	0.09	21
119	Percent Owner occupied: - 5-person household over total occupied units	-48036	0.21	10
7	Older (44+)	577	0.00	5
161	Estimate; VALUE - Median (dollars)	9	0.00	23
61	Number; HOUSING OCCUPANCY - Total housing units - Vacant housing units	208	0.01	3
236	100*No of occupied Housing Units with Wood/Total Occupied Housing Units	-2719997	0.03	2
221	100*No of Housing units with 1 bedroom/Total Housing Units	-23657	0.13	3
42	Number; RELATIONSHIP - Total population - In group quarters - Institutionalized population	-287	0.19	1
286	1980s	-347936	0.96	2
225	100*No of Housing units with >=5 bedroom/Total Housing Units	-10865	0.27	9

Table C-15: Model variable predictors results as seen in SI table C-13, for model built with z-score transformation. Tabulated here are predictor descriptions, regression coefficients and VIF values. The variable number here can be matched with the variables in SI Table C-1.

VARIABLE NO	VARIABLE NAME	REGRESSION COEFFICIENT	P_VALUES	VIF
177	Percent; INCOME AND BENEFITS (IN 2011 INFLATION-ADJUSTED DOLLARS) - $200,000 or more	-154985	0.09	21
119	Percent Owner occupied: - 5-person household over total occupied units	-77832	0.21	10
230	Cumulative Percentage of Housing units with zero to 4 bedrooms	45882	0.27	9
7	Older (44+)	3143926	0.00	5
161	Estimate; VALUE - Median (dollars)	669601	0.00	23
61	Number; HOUSING OCCUPANCY - Total housing units - Vacant housing units	168012	0.01	3
236	100*No of occupied Housing Units with Wood/Total Occupied Housing Units	-6864004	0.03	2
221	100*No of Housing units with 1 bedroom/Total Housing Units	-136333	0.13	3
42	Number; RELATIONSHIP - Total population - In group quarters - Institutionalized population	-140597	0.19	1
286	1980s	-170058	0.96	2

Table C-16: Model variable predictors results as seen in SI table C-13, for model built with CGS transformation. Tabulated here are predictor descriptions, regression coefficients and VIF values. The variable number here can be matched with the variables in SI Table C-1.

VARIABLE NO	VARIABLE NAME	REGRESSION COEFFICIENT	P_VALUES	VIF
264	Cumulative Percentage of Owner-Occupied Housing units with monthly costs =< $899	9316859	0.01	3
1	Number; SEX AND AGE - Total population	31734660	0.00	4
18	Number; SEX AND AGE - Female population - 18 years and over	10003211	0.00	2
270	Estimate; Median monthly housing costs	-1.6E+07	0.03	14
161	Estimate; VALUE - Median (dollars)	34221603	0.00	4
95	100*Owner occupied: - 2-person household/Total Owner-Occupied House Units	-7454718	0.11	4
80	Ratio of young age Non-Family householder to old age Non-Family householder >44	-1.4E+07	0.06	14
49	Number; HOUSEHOLDS BY TYPE - Total households - Family households (families) [7]	2947833	0.15	1
21	Number; RACE - Total population - One Race	13757488	0.00	2

Table C-17: Model variable predictors results as seen in SI table C-13, for model built with MGS transformation. Tabulated here are predictor descriptions, regression coefficients and VIF values. The variable number here can be matched with the variables in SI Table C-1.

VARIABLE NO	VARIABLE NAME	REGRESSION COEFFICIENT	P_VALUES	VIF
1	Number; SEX AND AGE - Total population	21128432	0.00	1
270	Estimate; Median monthly housing costs	-20146603	0.00	1
15	Number; SEX AND AGE - Female population	6778619	0.00	1
349	Population density	-9400355	0.00	2
87	100*Rent Occupied by Age >55/Total Rent Occupied Households	-10325700	0.01	1
245	100*Total Number of Owner-Occupied Households with monthly costs from $400 to $499/Total Owner-Occupied Housing Units	7201781	0.14	2
224	100*No of Housing units with 4 bedroom/Total Housing Units	7998777	0.00	1
266	Cumulative Percentage of Owner-Occupied Housing units with monthly costs =< $1499	11888735	0.00	1
33	Total Hispanic all races	-4529811	0.21	1
91	100*Rent Occupied by Age < 24/Total Households	3452658	0.42	1

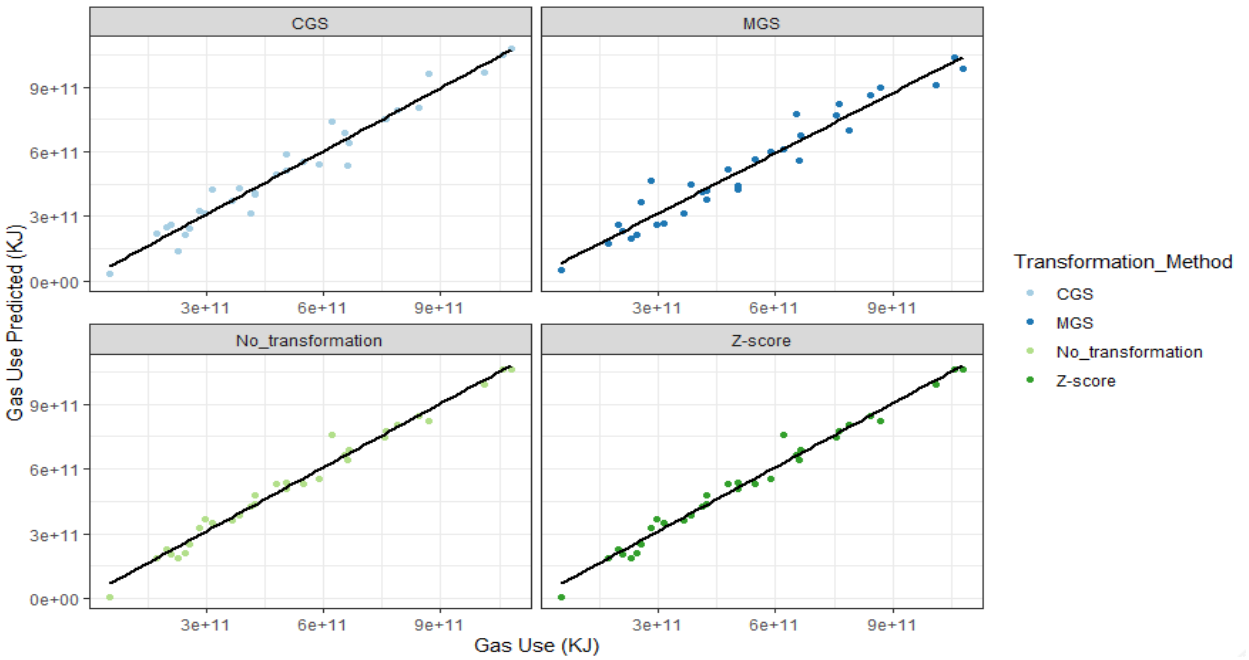

Fig C-28: Results of predicted natural gas use plotted against known natural gas use for the training set, after separating the training set (n=32), from the full data set (i.e. GA ZCTAs (n = 606)). These are the results from the selected model as tabulated in Table C-13 of the SI.

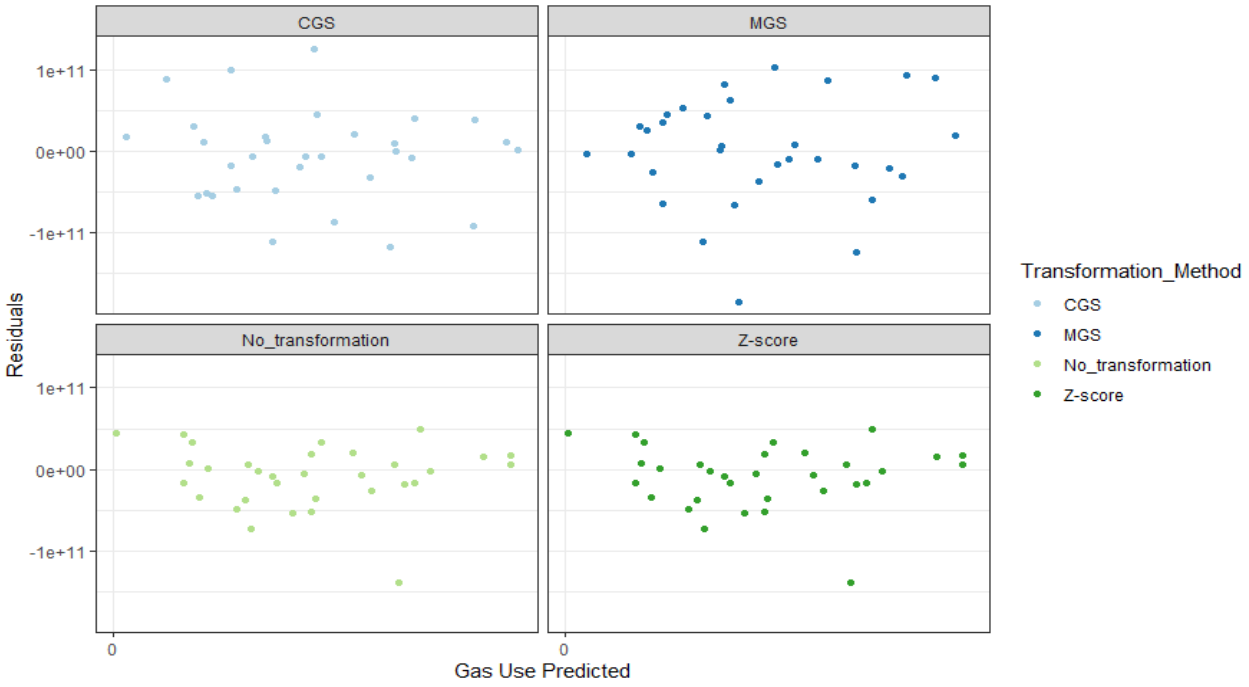

Fig C-29: Model residuals with all transformation for the training set, after separating the training set (n=32), from the full data set (i.e. GA ZCTAs (n = 606)). These are the results from the selected model as tabulated in Table C-13 of the SI.

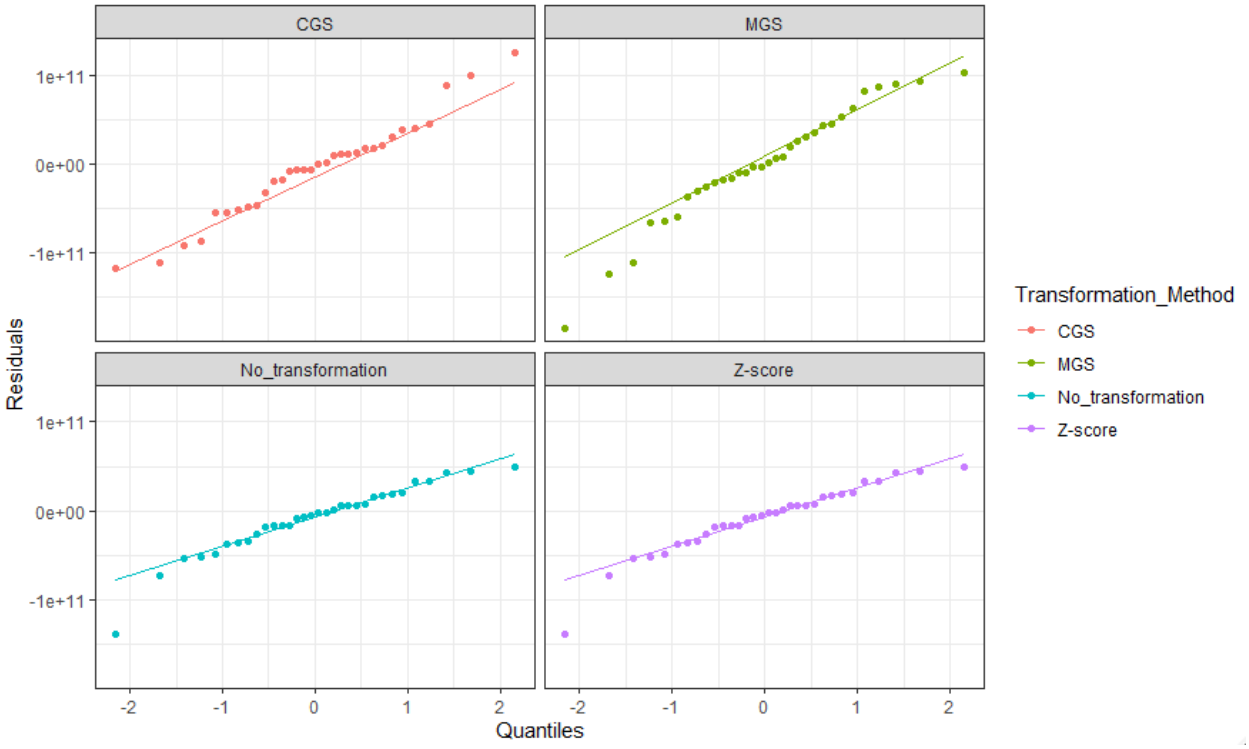

Fig C-30: Residual quartile with all transformation methods for the training set, after separating the training set (n=32), from the full data set (i.e. GA ZCTAs (n = 606)). These are the results from the selected model as tabulated in Table C-13 of the SI.

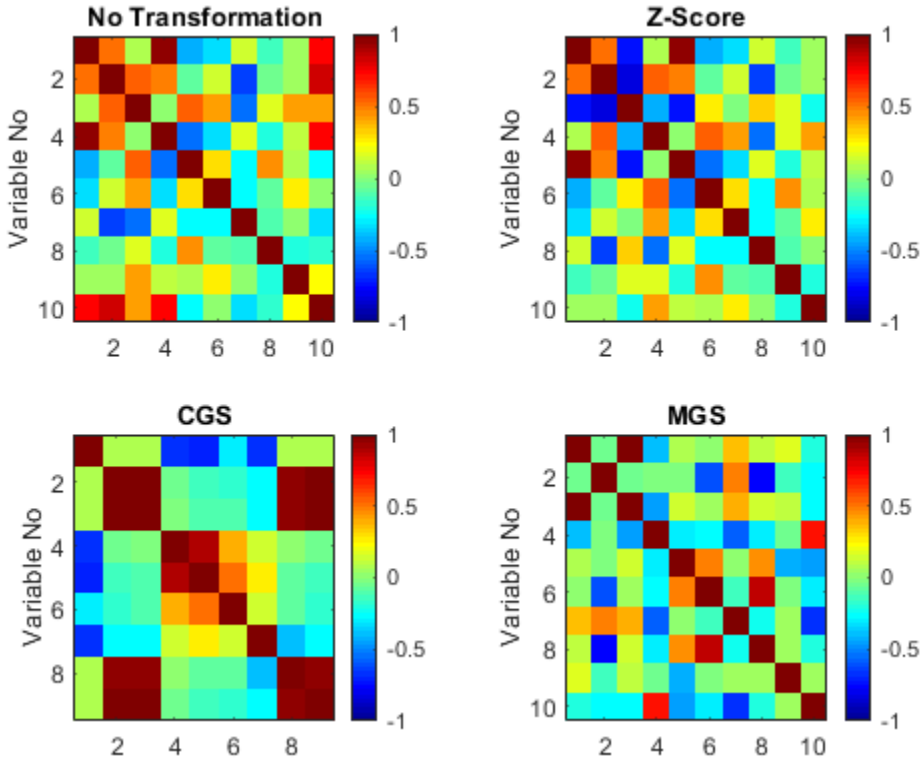

Fig C-31: Correlation matrix plotted as a color map of natural gas predictors of each transformation model generated for the training set, after separating the training set (n=32), from the full data set (i.e. GA ZCTAs (n = 606)). Plot reflects correlation of variables as untransformed.

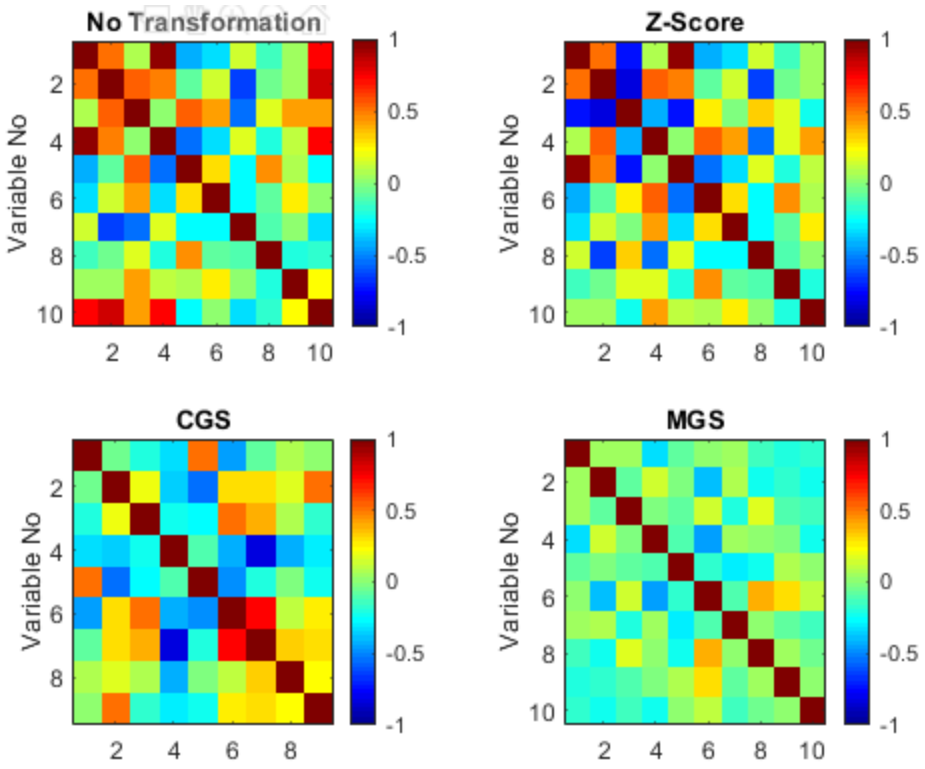

Fig C-32: Correlation matrix plotted as a color map of natural gas predictors of each transformation model generated for the training set, after separating the training set (n=32), from the full data set (i.e. GA ZCTAs (n = 606)). Plot reflects correlation of variables when transformed according to model.

Table C-18: Principle components with significant predictors and electricity use variables

DESCRIPTION	PC1	PC2	PC3	PC4	PC5	PC6	PC7	PC8	PC9	PC10	PC11	PC12
STANDARD OF DEVIATION	1.57	1.26	1.11	1.05	1.03	1.01	1.00	0.93	0.87	0.84	0.43	0.19
PROPORTION OF VARIANCE	0.21	0.13	0.10	0.09	0.09	0.08	0.08	0.07	0.06	0.06	0.02	0.00
CUMULATIVE PROPORTION	0.21	0.34	0.44	0.53	0.62	0.70	0.79	0.86	0.92	0.98	1.00	1.00

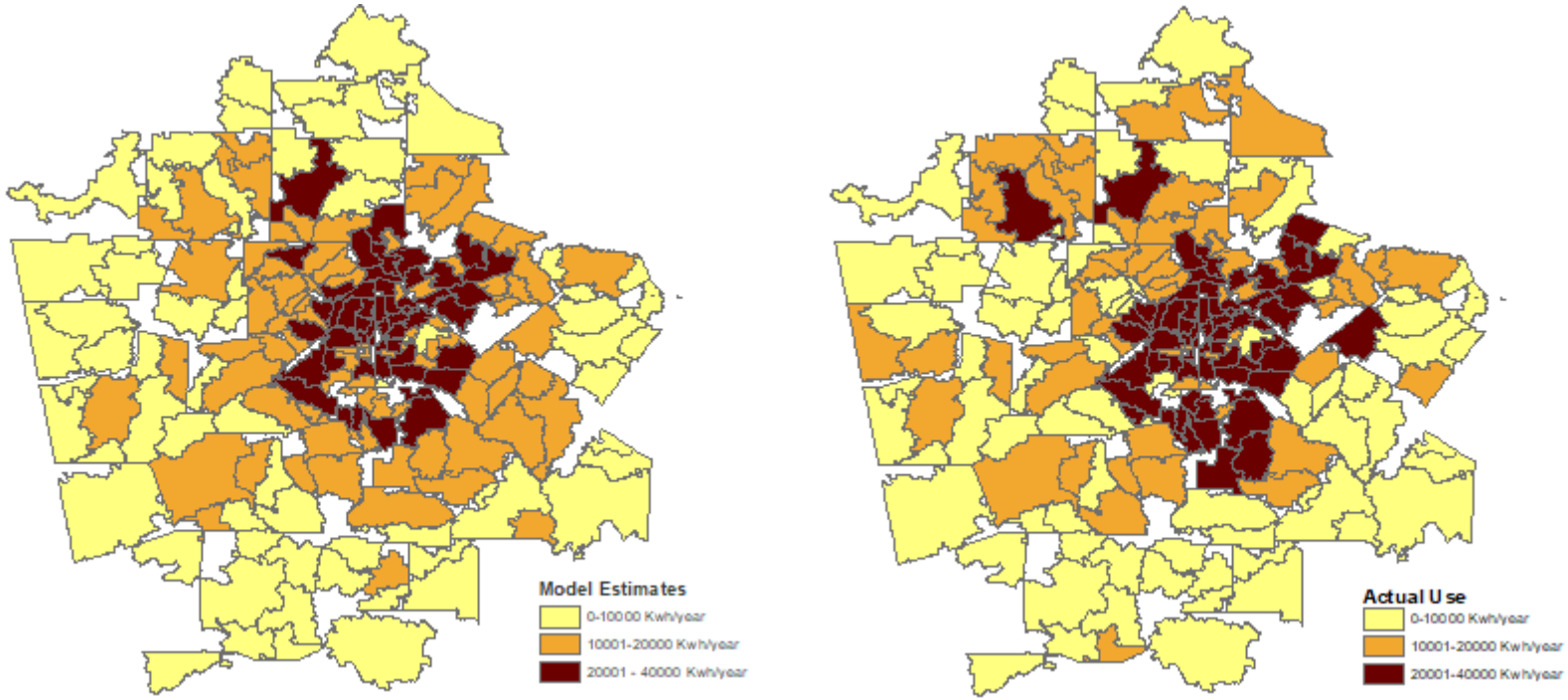

Fig C-33: Electricity mapping for metropolitan ZCTAs. Figure on the left represents estimates generated for 196 ZCTA with the MGS model, while the figure on the right represents actual electricity use from Georgia power for the same ZCTAs. Map source: Map created using ARCGIS® software by ESRI (ESRI 2015) [183], [350].

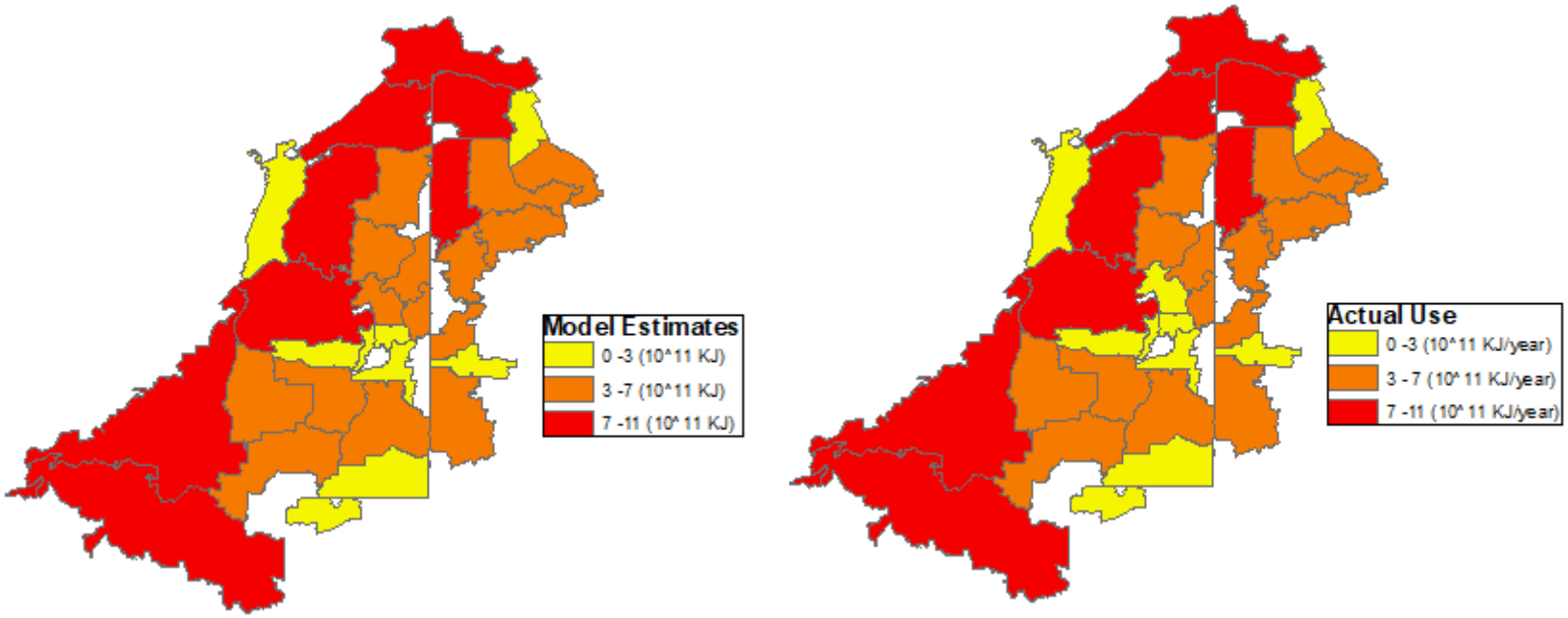

Fig C-34: Natural gas mapping for metropolitan ZCTAs. Figure on the left represents model estimates generated for 32 ZCTA with the CGS model, while the figure on the right represents actual natural gas use from Atlanta Gas Light for the same ZCTAs. Map source: Map created using ARCGIS® software by ESRI (ESRI 2015) [183],[350].

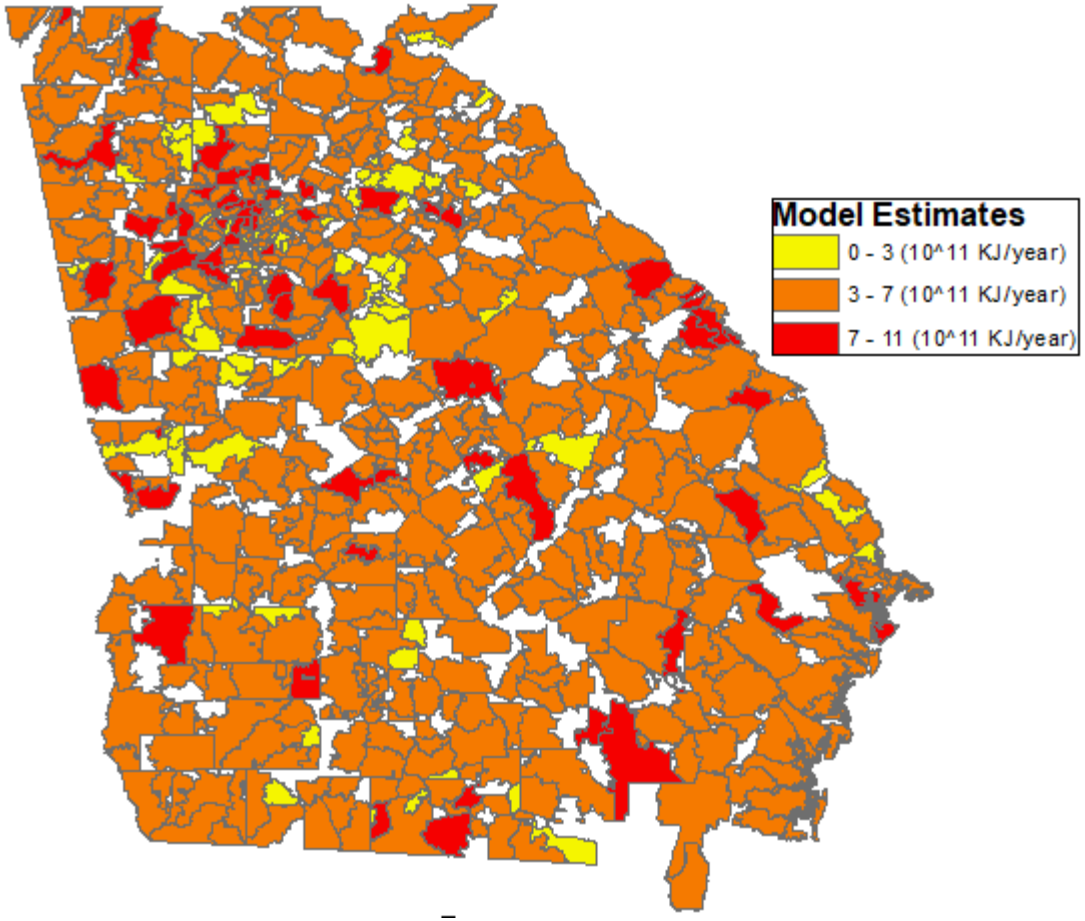

Fig C-35: Natural gas estimate mapping (where values were positive) for Georgia ZCTAs (n = 604) using the MGS model as noted in Table 3-7 from the manuscript. Map source: Map created using ARCGIS® software by ESRI (ESRI 2015) [183],[350].

Fig C-36: Figures show how Electricity use per capita, total population in each metropolitan ZCTA and Occupancy tenancy vary spatially

	Electricity per Capita	Population	Occupancy
Details	a	b	c
Figures 36a-c here represent the spatial distribution of clusters for three variables respectively: 1) Electricity per capita 2) Population by ZCTA 3) Population by Housing units in ZCTA	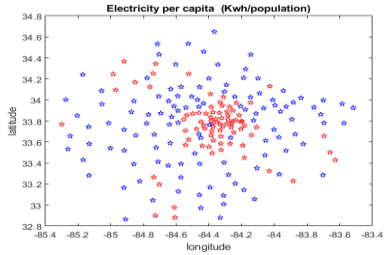	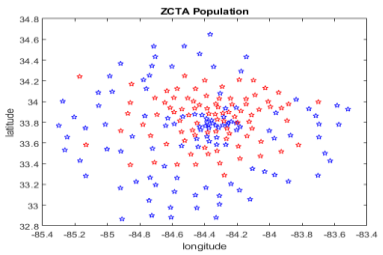	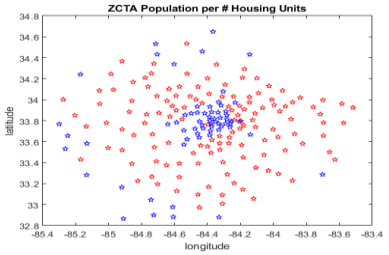
	d	e	f
Figures 36d-f here represent the boxplots for all three variables respectively by cluster: 1) Electricity per capita 2) Population by ZCTA 3) Population in Housing units in ZCTA	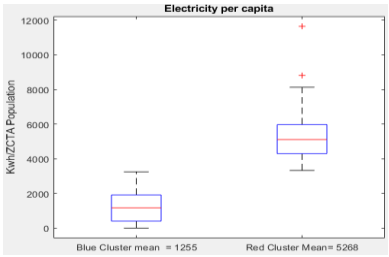	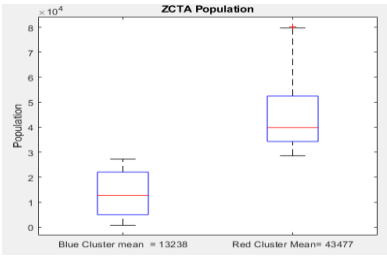	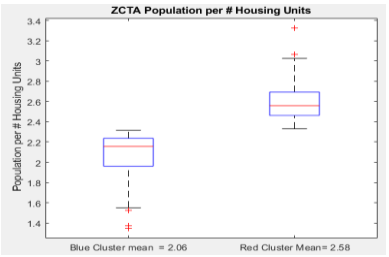
	g	h	i
Figures 36g-i here show the boxplots as follows: 1) Population by Electricity per capita cluster 2) Electricity per capita by ZCTA population cluster. 3) Electricity per capita by Population in Housing units in ZCTA cluster.	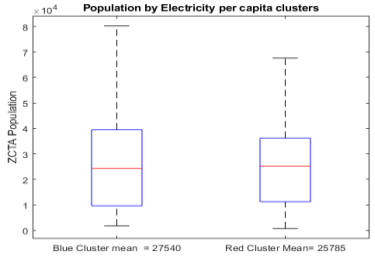	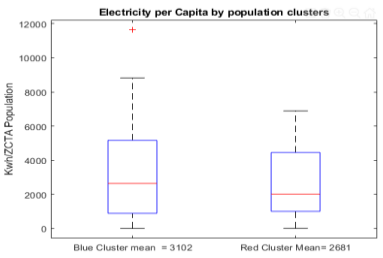	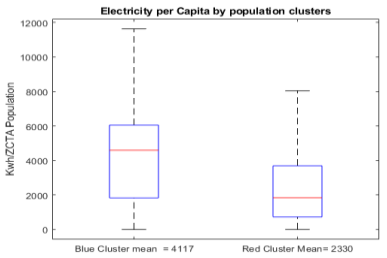

Discussion: We evaluate the spatial correlation between total electricity per capita, total population for each ZCTA and occupancy levels (i.e. ZCTA Population normalized by the number of housing units in each ZCTA). As shown in figures C-36a, b, c, yearly electricity use per capita was similar in clustering pattern to occupancy levels, but not with ZCTA population. The box plot in figure 36g shows that while there are relatively the same number of people in each electricity cluster, those in the inner spatial cluster use more electricity per capita (Figure C-36d). This is also matched by results in figures C-36f and C-36i which also show that lower occupancy units have more electricity use than higher occupancy units.

Orthogonolization

Comparison of Classical Gram Schmidt and the Modified Gram Schmidt

Classical Gram Schmidt Orthogonalization Methods: Classical Gram Schmidt, otherwise referred to as CGS herein, is a sequential method, where each column vector V_k (k = 1:p) in matrix X^{nxp}, is made orthogonal to each of the *k-1* previously orthogonalized column vectors in a series of steps [351], [352]. The formula for orthogonalization of matrix **X** of dimension (**n**x**p**) using CGS is follows in Table 2. However, although commonly used, one disadvantage of the classical Gram Schmidt is that it is highly prone to round off errors which results in a loss of orthogonality and an ill conditioned matrix[173].

Modified Gram Schmidt Orthogonalization Methods: The Modified Gram Schmidt (MGS) orthogonalization method is considered to be numerically more stable than CGS [173], [353]. The main difference between the two methods is that where CGS orthogonalizes the k^{th} vector from the original matrix X, to all previously orthogonalized *k-1* vectors, MGS orthogonalizes each *k+1* vector against only the immediate recently orthogonalized *k* vector. In essence, MGS orthogonalizes normalized *k* vectors from V against un-orthogonalized and un-normalized *k+1* vectors in X. The algorithm for MGS is also shown in Table 19.

Table C-19: CGS and MGS algorithms

MGS	CGS
For matrix: X^{nxp} V = X for k = 1:p-1 $e_k = \frac{v_k}{\| v_k \|}$ for j = k+1:p vj = vj – (vj ek) ek end end $e_p = \frac{v_p}{\| v_p \|}$	For matrix: X^{nxp} V = X $e_1 = \frac{v_1}{\| v_1 \|}$ for k = 2:p for j = k-1:1 vk = vk – (vk ej) ej end $e_k = \frac{v_k}{\| v_k \|}$ end

Orthogonalization order

One critical criteria in these orthogonalization methods here is that the order of orthogonalization matters in these procedures[352]. Different order permutations results in different orthogonal vectors and ultimately can yield different results. While there is no clear method listed in literature, we use the Euclidean norm for each vector of the untransformed predictors as the metric for sorting in a descending order and to orthogonalize in that sequence. The reason for this is that as the initial step in such orthogonalization methods is a projection of one vector onto another, projecting a larger vector against a vector with a smaller Euclidean norm could result in errors. We found that projecting the succeeding vectors against the largest vector in the data set gave the best and most consistent results.

Ensemble Averaging

To illustrate, take the general regression mathematical representation as follows.

$$Y = X\theta^T + \in \quad (1)$$

There are certain assumptions that model 1 has to follow and one of them is that the errors are normally distributed with a zero mean. This assumption holds true especially if the errors are due to random noise caused by measurement errors which are consistent across all observations[134].

$$Y = X\theta^T + \in_{noise} + \in_{model} \quad (2)$$

As shown in model 2, the source of noise error could come sources like random noise in measurements, or sampling variation/error (i.e. $\in_{noise} = \in_{measurement} + \in_{sampling\ variation}$.) Assuming $\in_{model}$ is minimized by choosing the best fit in the regression method and variables from equation C-1, the estimate for Y can be obscured if the noise error is larger than the error coming from the model. In this case, one can assume that $\in_{noise}$ is background noise, which is always consistent and always present. Therefore, if one were to employ ensemble averaging by running multiple simulations to estimate Y, and taking the average, using the data set from the simulations, then in theory the more simulations run, the lower the impact noise error will have on the estimate.

$$\lim_{n\to\infty} \frac{1}{N} \sum_{i=1}^{N} \in_{noise} = 0 \quad (3)$$

As we average out the noise, we will also average the theta estimates from each simulation set as follows $\hat{\theta} = \frac{1}{N} \sum_i^N \theta_i^T$. The $\hat{\theta}$ becomes a better estimate which has minimum contribution from noise. We employ ensemble averaging here to help eliminate noise variability in the final estimate.

Model evaluation procedure

After the random sample for the validation set was removed, about 5% of the remaining observations from the model training were then removed for further withholding and the remaining 95% (reduced training set) kept for variable selection and estimation of model regression coefficients. To conduct ensemble averaging and capture variation in population sampling, this step was repeated several times (total ensembles =10). For each ensemble run, the reduced model training dataset (withheld and validation data set removed) was randomly mixed before being stratified into 10 cross-validation sets for electricity (90% train/10% test split) and 5 cross validation sets for gas use (80% train/20% test split) for input into the variable selection phase. In total, 10 withheld data sets, 100 different training and test cross-validation sets were used for electricity and 10 withheld sets, 50 different training and test cross-validation sets were used for gas use in the ensemble runs.

For each ensemble, the reduced model training data was used as input into a stepwise fit algorithm to select the variables. The stratification with the cross-validation sets helped capture differences in sampling population dynamics and yielded better results overall for the stepwise fit algorithm. Due to the large data set two sequential stepwise fit algorithms (at $\alpha = 0.01$) were set up to generate an intermediate set of predictor variables, and statistical metrics were generated for all test sets for both electricity and gas models. Each ensemble run generated a different set of predictor variables which were all then complied into one array.

At the end of the stepwise fit run, the 10-withheld and un-stratified reduced model training data sets were used to generate statistical metrics with the selected predictors for final variable selection. For final model selection of predictors, two options were considered. The first was to sort out the predictors that gave the best MSE using the withheld or test data sets from the previous step. The second option was to compile all predictors from the stepwise algorithms, and then using the reduced model training set for each ensemble, regress them and select out the predictors that were statistically significant based on a particular significance value from the regression equation. In the end, the second methodology was followed as it gave better results. For electricity final variable selection, five levels of significance were used (0.001, 0.005, 0.01, 0.05, 0.1] while for natural gas, only four levels of significance where chosen (0.05, 0.1, 0.15, 0.2) as a result of the small size of the gas use training data set.

For each significance level, the chosen predictors were used to generate a final regression equation using the reduced model training data set and withheld data set from each simulation and the overall validation data set to develop statistical metrics and diagnostics. The level of significance that yielded the best statistical metrics across all three data sets was chosen as the final model selector. Ensemble averaging of the regression coefficients, generated for all ten ensemble data sets in this step were used as the final regression coefficients for the chosen model.

The best results for each transformation method were compiled and further analyzed in the discussion section. The results of the final model and impact of transformation models in generating the final statistical model are also discussed. To ensure an accurate comparison, we use the same data set and sample set for all simulations and transformation methods.

APPENDIX D. SUPPLEMENTAL MATERIAL FOR CHAPTER 4

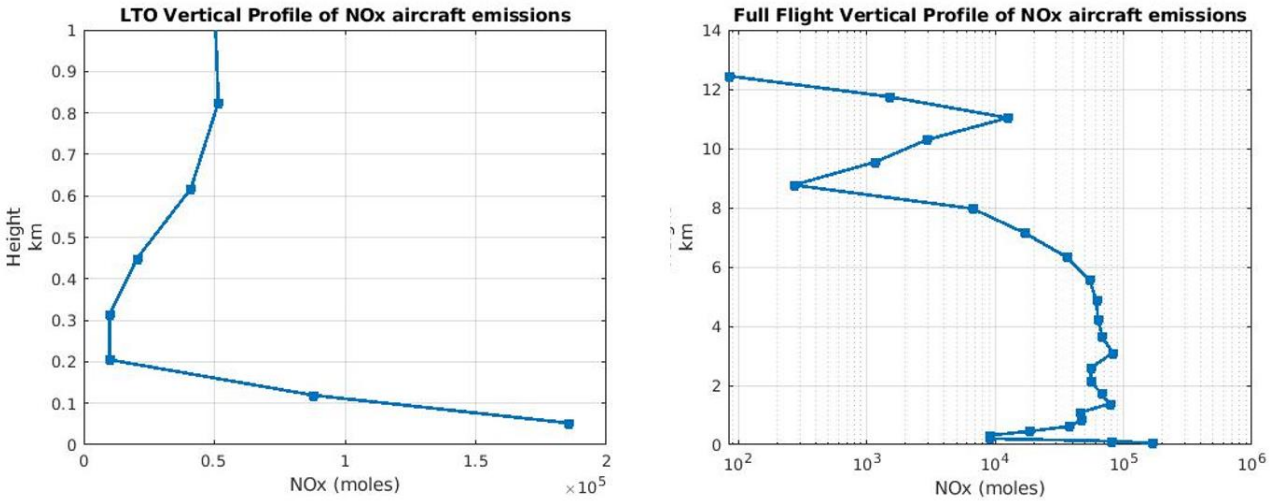

Figure D-1. ATL emission profiles for the 3D inventory. NO_x emissions are totaled for simulation period (August). The plots show the vertical distribution of NO_x emissions below1km and entire vertical height in the model domain.

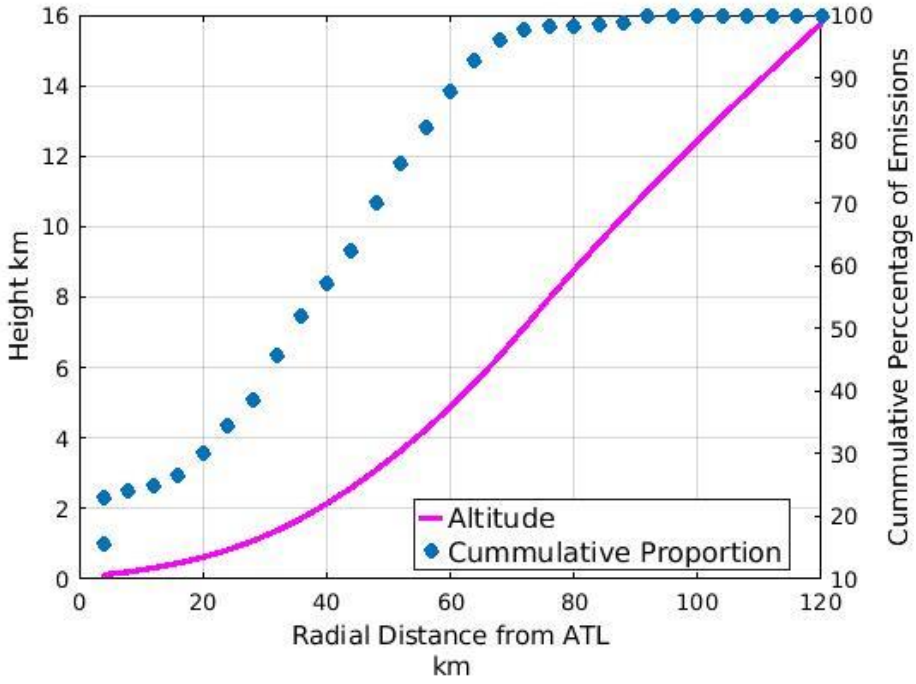

Figure D-2. The cumulative proportion of emissions as allocated both horizontally (distance from airport) and vertically (altitude) is shown.

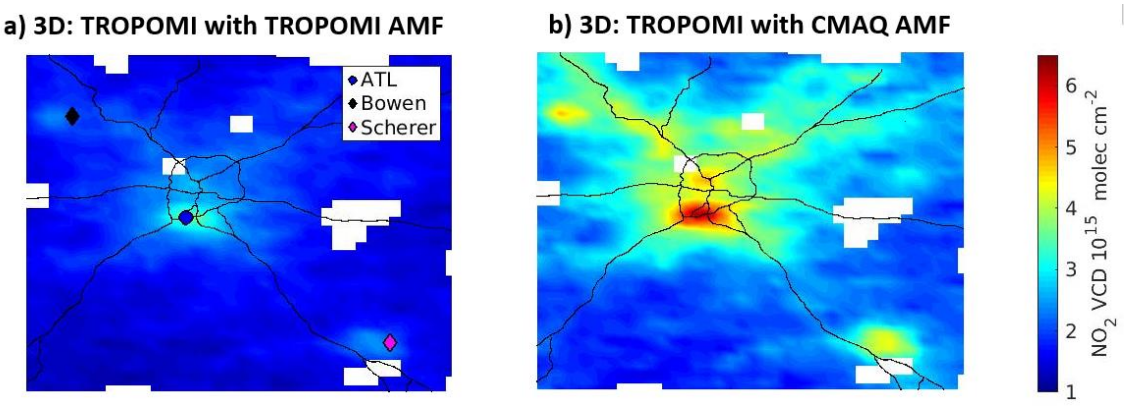

Figure D-3: NO_2 vertical column densities

a) TROPOMI NO_2 default AMF b) TROPOMI NO_2 CMAQ_AMF

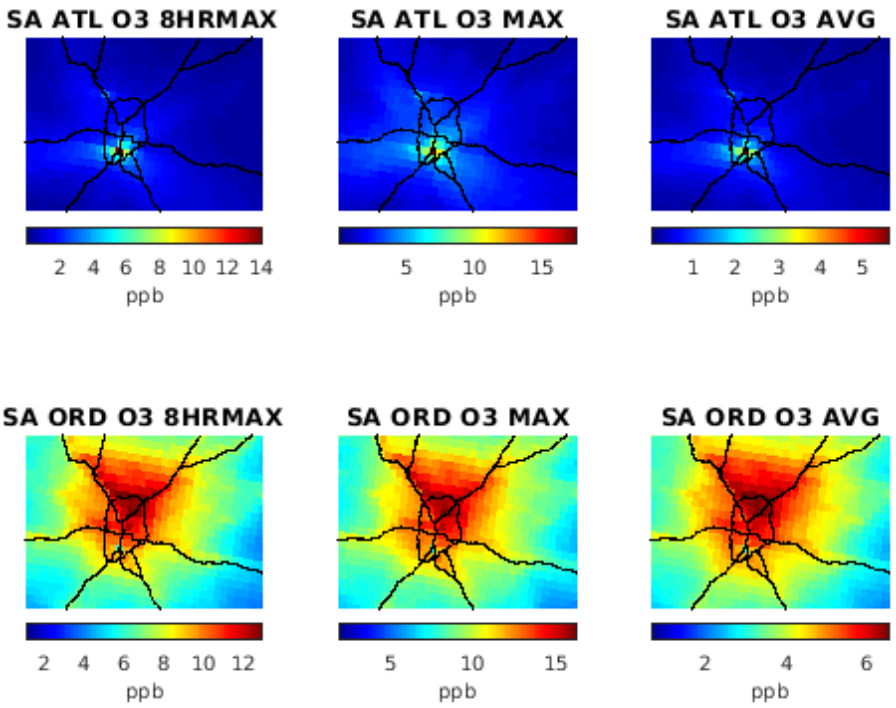

Figure D-4. Results from CMAQ's ISAM source apportionment module[270, 271]. Figures show apportionment contributions of both on road and ATL to ozone for 8hr max, daily max and average ozone for August 2019.

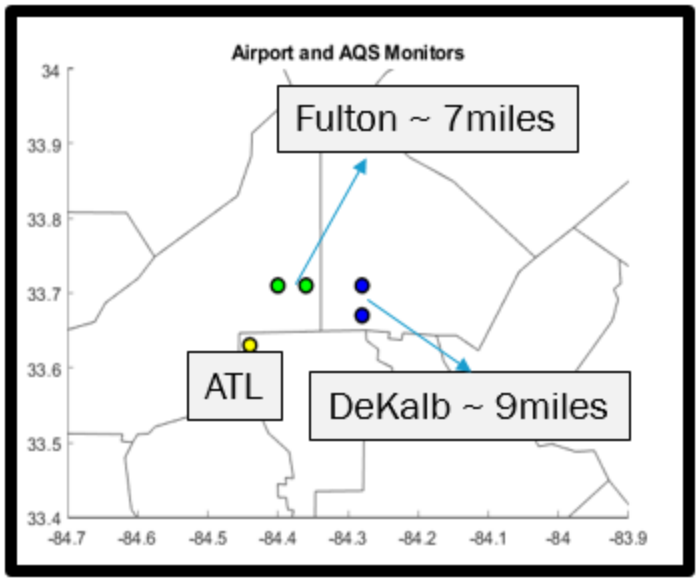

Figure D-5. Location of air quality monitors at Fulton and DeKalb counties and their proximity to the Atlanta Hartsfield Jackson airport (ATL) in the modeling domain.

Equations

Evaluation metrics with CMAQ base cases

$$NMD = 100\% \times \frac{\sum_i^n (3D_i - 2D_i)}{\sum_i^n 2D_i}$$

$$RMSE = \sqrt{\frac{\sum_{i=1}^{N} (3D_i - 2D_i)^2}{N}}$$

Note: $3D_i$ (CMAQ predicted values with 3D inventory), $2D_i$ (CMAQ predicted values with default inventory)

Evaluation metrics with CMAQ and observations

$$NMB = 100\% \times \frac{\sum_i^n (P_i - O_i)}{\sum_i^n O_i}$$

$$RMSE = \sqrt{\frac{\sum_{i=1}^{N} (P_i - O_i)^2}{N}}$$

Note: P_i (CMAQ predicted values), O_i (AQS or TROPOMI)

NMD: Normalized Mean Difference

RMSE: Root Mean Square Error

NMB: Normalized Mean Bias

Table D-1. Speciated emissions from both inventories at a) ATL, and b) model domain for both inventories. Emissions are totalized for the month of August 2019. Totals are in moles. The Normalized Mean Difference (NMD) of the 3D inventory compared to the default is shown as well. ATL emissions for the 3D inventory are biased low when compared to the default, but biased high when tabulated over the entire domain

ATL			
Species	Default (moles)	3D (moles)	NMD
NOx	1.10×10^7	8.24×10^6	-24.9%
SO_2	1.41×10^6	1.02×10^6	-27.5%
CO	6.64×10^7	5.23×10^7	-21.2%
VOC	7.44×10^8	5.31×10^8	-28.7%
All model grids			
Species	Default (moles)	3D (moles)	NMD
NOx	1.25×10^7	3.66×10^7	192.1%
SO_2	1.52×10^6	4.50×10^6	194.9%
CO	7.83×10^7	2.43×10^8	209.8%
VOC	7.85×10^8	2.41×10^9	206.4%

.

Table D-2. Tabulated quantitative metrics of NO_2 vertical column densities for both inventories across the domain. Results were tabulated for the 17 selected simulation days.

Inventory	Data cut off	NMB %	Absolute Difference 10^{15} molecules/ cm^2	Mean CMAQ 10^{15} molecules/ cm^2	Mean TROPOMI 10^{15} molecules/ cm^2	Slope	Pearson Correlation	RMSE 10^{15} molecules / cm^2	No of Data Points
Default	All Data	-46	-1.13	1.4	2.5	0.74	0.79	1.21	2665
	< 4.5	-47	-1.15	1.3	2.5	0.92	0.82	1.45	2644
	>= 4.5	29	1.36	6.1	4.7	0.19	0.48	4.09	21
3D	All Data	-43	-1.04	1.4	2.5	0.76	0.81	1.12	2665
	< 4.5	-44	-1.05	1.4	2.5	0.88	0.82	1.25	2644
	>= 4.5	22	0.93	5.5	4.6	0.17	0.29	2.63	21

Table D-3. Tabulated quantitative metrics of NO_2 vertical column densities for ATL, Bowen and Scherer. Results were tabulated using the represented number of grid points (Fig S1) for the 17 selected simulation days.

Inventory	Sector	NMB %	Absolute Difference 10^{15} molecules/ cm^2	Mean CMAQ 10^{15} molecules/ cm^2	Mean TROPOMI 10^{15} molecules/ cm^2	Slope	Pearson Correlation	RMSE 10^{15} molecules/ cm^2	No of Data Points
Default	**Airport**	1.8	0.08	4.9	4.8	0.13	0.35	1.76	25
3D		-9.9	-0.52	4.3	4.8	0.14	0.25	1.33	25
Default	**Bowen**	-9.8	-0.24	3.8	4.1	0.16	0.83	1.98	9
3D		-6.0	-0.09	3.9	3.99	0.16	0.84	1.97	9
Default	**Scherer**	0.5	0.00	3.64	3.64	0.10	0.29	1.77	9
3D		4.1	0.12	3.71	3.58	0.10	0.29	1.78	9

Temporal, Horizontal and Vertical Distribution of airport emissions

The base inventory consisted of Landing and Take Off (LTO) emissions from the EPAs 2016 National Emission Inventory (NEI)[228]. The development of the 3D inventory included (1) adding cruise emissions using the AEIC inventory[245, 246] and (2) horizontally and vertically allocating total emissions. Each of these modifications are described in further detail below.

Adding cruise emissions and vertical allocation:

1. The AEIC inventory is linearly interpolated to the CMAQ vertical grid. This new emissions profile is called $AEIC_{CMAQ}$.

2. We calculate the ratio between LTO and cruise emissions in $AEIC_{CMAQ}$. The NEI specifies that it accounts for LTO emissions up to 3000 ft., so we use 914 m in the associated calculations.

$$\frac{LTO}{Cruise}_{AEIC_{CMAQ}} = \frac{\sum_{i=0}^{914m} E_{ij}}{\sum_{i=>914m}^{Maximum\ Height} E_{ij}}$$

   Where i = respective height at domain layer, j = species, E = emission rates;

3. The ratio is multiplied by the default inventory (EPA NEI 2016) to obtain NEI cruise emissions, which is then added to the LTO.

$$NEI_{cruise} = \frac{1}{\frac{LTO}{Cruise}_{AEIC_{CMAQ}}} \times NEI_{LTO}$$

$$NEI_{full\ inventory} = NEI_{cruise} + NEI_{LTO}$$

Horizontal allocation of the inventory

We treat the horizontal allocation as follows:

Vertical classification: $AEIC_{CMAQ}$ emissions are separated into two vertical categories, emissions below 914 m and above, which corresponds to the lowest to eight layers, and layers 9 to 32 respectively. Two different horizontal allocation schemes are used for these two categories.

Horizontal allocation: At altitudes below ~1km, for each vertical layer, we calculate the horizontal distance between the airport and a departing plane, using the standard FAA rate of climb rate of 200 feet per nautical mile[249, 250, 354], which is equivalent to 30.5 horizontal meters per vertical meter. The total emissions for that layer are then distributed along a circle above the airport with a radius equal to the horizontal travel distance. The maximum horizontal extent of LTO emissions (emissions below 914 m) are 28 km from the airport center. For the upper layers (> ~ 1km), the vertical distribution of emissions is taken from the AEIC. We apply the same method as above, but we use the vertical profile in the AEIC to allocate the emissions (Figure D-2).

Impact of the NEI temporal aggregation on the spatial allocation methods

Because there was no temporal or operational delineations of the NEI LTO processes, the same treatment had to be applied in the spatial allocation of the 3D emissions inventory, meaning there was no distinguishing between landing, cruising and climb out processes. The temporal profile of airport activity, established with the LTO cycles was applicable as climb, cruise, and landing operations of a full-flight cycle would be coincident with LTO operations. The lack of separation of the processes also meant that to account for both landing and takeoff operations of the aircraft, the ROC rates for both respective vertical regimes were kept constant.

REFERENCES

1. United Nations Climate Change. https://unfccc.int/news/urban-climate-action-is-crucial-to-bend-the-emissions-curve. Access Date 8/17/2021.

2. Barrie, L. A.; Douglas, M. W.; Robert, E. M., Effects of Anthropogenic Emissions on Climate: A Review of Selected Topics. *Ambio* **1976,** *5* (5/6), 209-212.

3. Organization, W. H., 7 million premature deaths annually linked to air pollution. *http://www.who.int/mediacentre/news/releases/2014/air-pollution/en/* **2014**.

4. Disease, G. B. O., Over 7 billion people face unsafe air: State of Global Air 2018. *http://www.healthdata.org/news-release/over-7-billion-people-face-unsafe-air-state-global-air-2018* **2018**.

5. Ramaswami, A.; Weible, C.; Main, D.; Heikkila, T.; Siddiki, S.; Duvall, A.; Pattison, A.; Bernard, M., A Social-Ecological-Infrastructural Systems Framework for Interdisciplinary Study of Sustainable City Systems An Integrative Curriculum Across Seven Major Disciplines. *J Ind Ecol* **2012,** *16* (6), 801-813.

6. Servadio, J. L.; Lawal, A. S.; Davis, T.; Bates, J.; Russell, A. G.; Ramaswami, A.; Convertino, M.; Botchwey, N., Demographic Inequities in Health Outcomes and Air Pollution Exposure in the Atlanta Area and its Relationship to Urban Infrastructure. *J Urban Health* **2019,** *96* (2), 219-234.

7. Corburn, J., Urban Place and Health Equity: Critical Issues and Practices. *Int J Env Res Pub He* **2017,** *14* (2).

8. Nations, U., 68% of the world population projected to live in urban areas by 2050, says UN. *https://www.un.org/development/desa/en/news/population/2018-revision-of-world-urbanization-prospects.html* **2018**.

9. Li, K.; Zhang, P.; Crittenden, J. C.; Guhathakurta, S.; Chen, Y. S.; Fernando, H.; Sawhney, A.; McCartney, P.; Grimm, N.; Kahhat, R.; Joshi, H.; Konjevod, G.; Choi, Y. J.; Fonseca, E.; Allenby, B.; Gerrity, D.; Torrens, P. M., Development of a framework for quantifying the environmental impacts of urban development and construction practices. *Environ Sci Technol* **2007,** *41* (14), 5130-5136.

10. Dockery, D. W.; Pope, C. A.; Xu, X.; Spengler, J. D.; Ware, J. H.; Fay, M. E.; Ferris, B. G.; Speizer, F. E., An Association between Air Pollution and Mortality in Six U.S. Cities. *New England Journal of Medicine* **1993,** *329* (24), 1753-1759.

11. Fang, T.; Guo, H.; Zeng, L.; Verma, V.; Nenes, A.; Weber, R. J., Highly Acidic Ambient Particles, Soluble Metals, and Oxidative Potential: A Link between Sulfate and Aerosol Toxicity. *Environ Sci Technol* **2017,** *51* (5), 2611-2620.

12. Blanchard, C. L.; Tanenbaum, S.; Motallebi, N., Spatial and temporal characterization of PM2.5 mass concentrations in California, 1980-2007. *J Air Waste Manag Assoc* **2011,** *61* (3), 339-51.

13. Weber, R. J.; Guo, H. Y.; Russell, A. G.; Nenes, A., High aerosol acidity despite declining atmospheric sulfate concentrations over the past 15 years. *Nat Geosci* **2016,** *9* (4), 282-+.

14. Administration, U. E. I., Energy consumption by sector. https://www.eia.gov/totalenergy/data/monthly/pdf/sec2.pdf.

15. Hsu, D., Identifying key variables and interactions in statistical models of building energy consumption using regularization. *Energy* **2015,** *83*, 144-155.

16. Asadi, S.; Amiri, S. S.; Mottahedi, M., On the development of multi-linear regression analysis to assess energy consumption in the early stages of building design. *Energ Buildings* **2014,** *85*, 246-255.

17. Hudda, N.; Durant, L. W.; Fruin, S. A.; Durant, J. L., Impacts of Aviation Emissions on Near-Airport Residential Air Quality. *Environ Sci Technol* **2020,** *54* (14), 8580-8588.

18. Hudda, N.; Gould, T.; Hartin, K.; Larson, T. V.; Fruin, S. A., Emissions from an International Airport Increase Particle Number Concentrations 4-fold at 10 km Downwind. *Environ Sci Technol* **2014,** *48* (12), 6628-6635.

19. Agency, E. P., 2016 National Emission Inventory. **2019**.

20. Unal, A.; Hu, Y. T.; Chang, M. E.; Odman, M. T.; Russell, A. G., Airport related emissions and impacts on air quality: Application to the Atlanta International Airport. *Atmos Environ* **2005,** *39* (32), 5787-5798.

21. Masiol, M.; Harrison, R. M., Aircraft engine exhaust emissions and other airport-related contributions to ambient air pollution: A review. *Atmos Environ* **2014,** *95*, 409-455.

22. Woody, M. C.; Arunachalam, S., Secondary organic aerosol produced from aircraft emissions at the Atlanta Airport: An advanced diagnostic investigation using process analysis. *Atmos Environ* **2013,** *79*, 101-109.

23. Arunachalam, S.; Wang, B. Y.; Davis, N.; Baek, B. H.; Levy, J. I., Effect of chemistry-transport model scale and resolution on population exposure to PM2.5 from aircraft emissions during landing and takeoff. *Atmos Environ* **2011,** *45* (19), 3294-3300.

24. Vennam, L. P.; Vizuete, W.; Talgo, K.; Omary, M.; Binkowski, F. S.; Xing, J.; Mathur, R.; Arunachalam, S., Modeled Full-Flight Aircraft Emissions Impacts on Air Quality and Their Sensitivity to Grid Resolution. *J Geophys Res-Atmos* **2017,** *122* (24), 13472-13494.

25. Lee, H.; Olsen, S. C.; Wuebbles, D. J.; Youn, D., Impacts of aircraft emissions on the air quality near the ground. *Atmos Chem Phys* **2013,** *13* (11), 5505-5522.

26. Quarles, N.; Kockelman, K. M., Amercians' plans for acquiring and using electric, shared and self-driving vehicles. *2018 Annual Meeting* **2018,** *6972*, 1-17.

27. Energy Information Administration. https://www.eia.gov/opendata/qb.php?category=1039999&sdid=STEO.MVVMPUS.A.

28. Schnell, J. L.; Naik, V.; Horowitz, L. W.; Paulot, F.; Ginoux, P.; Zhao, M.; Horton, D. E., Air quality impacts from the electrification of light-duty passenger vehicles in the United States. *Atmos Environ* **2019,** *208*, 95-102.

29. Charlson, R. J.; Schwartz, S. E.; Hales, J. M.; Cess, R. D.; Coakley, J. A., Jr.; Hansen, J. E.; Hofmann, D. J., Climate forcing by anthropogenic aerosols. *Science* **1992,** *255* (5043), 423-30.

30. Martin, S. T.; Hung, H. M.; Park, R. J.; Jacob, D. J.; Spurr, R. J. D.; Chance, K. V.; Chin, M., Effects of the physical state of tropospheric ammonium-sulfate-nitrate particles on global aerosol direct radiative forcing. *Atmos Chem Phys* **2004,** *4*, 183-214.

31. Abbatt, J. P.; Benz, S.; Cziczo, D. J.; Kanji, Z.; Lohmann, U.; Mohler, O., Solid ammonium sulfate aerosols as ice nuclei: a pathway for cirrus cloud formation. *Science* **2006,** *313* (5794), 1770-3.

32. Zhang, X. L.; Rao, R. Z.; Huang, Y. B.; Mao, M.; Berg, M. J.; Sun, W. B., Black carbon aerosols in urban central China. *J Quant Spectrosc Ra* **2015,** *150*, 3-11.

33. Valavanidis, A.; Fiotakis, K.; Vlachogianni, T., Airborne particulate matter and human health: toxicological assessment and importance of size and composition of particles for oxidative damage and carcinogenic mechanisms. *J Environ Sci Heal C* **2008,** *26* (4), 339-62.

34. Pope, C. A.; Dockery, D. W., Health effects of fine particulate air pollution: Lines that connect. *J Air Waste Manage* **2006,** *56* (6), 709-742.

35. Utell, M. J.; Frampton, M. W., Acute health effects of ambient air pollution: the ultrafine particle hypothesis. *J Aerosol Med* **2000,** *13* (4), 355-59.

36. Kleinman, M. T.; Phalen, R. F.; Mautz, W. J.; Mannix, R. C.; McClure, T. R.; Crocker, T. T., Health effects of acid aerosols formed by atmospheric mixtures. *Environ Health Persp* **1989,** *79*, 137-45.

37. Utell, M. J., Effects of inhaled acid aerosols on lung mechanics: an analysis of human exposure studies. *Environ Health Persp* **1985,** *63* (Nov), 39-44.

38. Delfino, R. J.; Sioutas, C.; Malik, S., Potential role of ultrafine particles in associations between airborne particle mass and cardiovascular health. *Environmental Health Perspectives* **2005,** *113* (8), 934-946.

39. Thurston, G. D.; Ito, K.; Hayes, C. G.; Bates, D. V.; Lippmann, M., Respiratory hospital admissions and summertime haze air pollution in Toronto, Ontario: consideration of the role of acid aerosols. *Environmental research* **1994,** *65* (2), 271-90.

40. Xu, L.; Guo, H.; Boyd, C. M.; Klein, M.; Bougiatioti, A.; Cerully, K. M.; Hite, J. R.; Isaacman-VanWertz, G.; Kreisberg, N. M.; Knote, C.; Olson, K.; Koss, A.; Goldstein, A. H.; Hering, S. V.; de Gouw, J.; Baumann, K.; Lee, S. H.; Nenes, A.; Weber, R. J.; Ng, N. L., Effects of anthropogenic emissions on aerosol formation from isoprene and monoterpenes in the southeastern United States. *Proc Natl Acad Sci U S A* **2015,** *112* (1), 37-42.

41. Fan, S. M.; Jacob, D. J., Surface Ozone Depletion in Arctic Spring Sustained by Bromine Reactions on Aerosols. *Nature* **1992,** *359* (6395), 522-524.

42. Meskhidze, N.; Chameides, W. L.; Nenes, A.; Chen, G., Iron mobilization in mineral dust: Can anthropogenic SO2 emissions affect ocean productivity? *Geophysical Research Letters* **2003,** *30* (21), 2.1-2.5.

43. Ghio, A. J.; Carraway, M. S.; Madden, M. C., Composition of air pollution particles and oxidative stress in cells, tissues, and living systems. *J Toxicol Env Heal B* **2012,** *15* (1), 1-21.

44. National Academies of Sciences, E., and Medicine, The Future of Atmospheric Chemistry Research: Remembering Yesterday, Understanding Today, Anticipating Tomorrow. Washington, DC: The National Academies Press. **2016**.

45. Ito, T.; Nenes, A.; Johnson, M. S.; Meskhidze, N.; Deutsch, C., Acceleration of oxygen decline in the tropical Pacific over the past decades by aerosol pollutants. *Nat Geosci* **2016,** *9* (6), 443-447.

46. Seinfeld, J. H.; Pandis, S. N., *Atmospheric chemistry and physics : from air pollution to climate change*. John Wiley: New York, 1997; p xxvii, 1326 p.

47. Lipfert, F. W.; Wyzga, R. E., On the Spatial and Temporal Variability of Aerosol Acidity and Sulfate Concentration. *J Air Waste Manage* **1993,** *43* (4), 489-491.

48. Gulsoy, G.; Tayanc, M.; Erturk, F., Chemical analyses of the major ions in the precipitation of Istanbul, Turkey. *Environ Pollut* **1999,** *105* (2), 273-280.

49. Huang, X.; Qiu, R.; Chan, C. K.; Ravi Kant, P., Evidence of high PM2.5 strong acidity in ammonia-rich atmosphere of Guangzhou, China: Transition in pathways of

ambient ammonia to form aerosol ammonium at [NH4+]/[SO42–]=1.5. *Atmos Res* **2011,** *99* (3-4), 488-495.

50. U.S.EPA., Air Pollutant Emission Trends Data. Available at https://www.epa.gov/air-emissions-inventories/air-pollutant-emissions-trends-data. Accessed May 2018.

51. Nopmongcol, U.; Alvarez, Y.; Jung, J.; Grant, J.; Kumar, N.; Yarwood, G., Source contributions to United States ozone and particulate matter over five decades from 1970 to 2020. *Atmos Environ* **2017,** *167*, 116-128.

52. Blanchard, C. L.; Hidy, G. M.; Tanenbaum, S.; Edgerton, E. S.; Hartsell, B. E., The Southeastern Aerosol Research and Characterization (SEARCH) study: Temporal trends in gas and PM concentrations and composition, 1999-2010. *J Air Waste Manage* **2013,** *63* (3), 247-259.

53. Saylor, R.; Myles, L.; Sibble, D.; Caldwell, J.; Xing, J., Recent trends in gas-phase ammonia and PM2.5 ammonium in the Southeast United States. *J Air Waste Manage* **2015,** *65* (3), 347-357.

54. Hidy, G. M.; Blanchard, C. L.; Baumann, K.; Edgerton, E.; Tanenbaum, S.; Shaw, S.; Knipping, E.; Tombach, I.; Jansen, J.; Walters, J., Chemical climatology of the southeastern United States, 1999-2013. *Atmos Chem Phys* **2014,** *14* (21), 11893-11914.

55. Weber, R. J.; Guo, H.; Russell, A. G.; Nenes, A., High aerosol acidity despite declining atmospheric sulfate concentrations over the past 15 years. *Nature Geosci* **2016,** *9* (4), 282-285.

56. Guo, H.; Weber, R. J.; Nenes, A., High levels of ammonia do not raise fine particle pH sufficiently to yield nitrogen oxide-dominated sulfate production. *Sci Rep-Uk* **2017,** *7* (1), 12109.

57. Blanchard, C. L.; Hidy, G. M., Effects of SO2 and NOx emission reductions on PM2.5 mass concentrations in the Southeastern United States. *J Air Waste Manage* **2005,** *55* (3), 265-272.

58. Blanchard, C. L.; Tanenbaum, S.; Hidy, G. M., Effects of sulfur dioxide and oxides of nitrogen emission reductions on fine particulate matter mass concentrations: Regional comparisons. *J Air Waste Manage* **2007,** *57* (11), 1337-1350.

59. Hand, J. L.; Schichtel, B. A.; Malm, W. C.; Pitchford, M. L., Particulate sulfate ion concentration and SO2 emission trends in the United States from the early 1990s through 2010. *Atmos Chem Phys* **2012,** *12* (21), 10353-10365.

60. Pye, H. O. T.; Zuend, A.; Fry, J. L.; Isaacman-VanWertz, G.; Capps, S. L.; Appel, K. W.; Foroutan, H.; Xu, L.; Ng, N. L.; Goldstein, A. H., Coupling of organic and inorganic aerosol systems and the effect on gas-particle partitioning in the southeastern US. *Atmos Chem Phys* **2018,** *18* (1), 357-370.

61. Silvern, R. F.; Jacob, D. J.; Kim, P. S.; Marais, E. A.; Turner, J. R.; Campuzano-Jost, P.; Jimenez, J. L., Inconsistency of ammonium-sulfate aerosol ratios with thermodynamic models in the eastern US: a possible role of organic aerosol. *Atmos Chem Phys* **2017,** *17* (8), 5107-5118.

62. Kim, Y. P.; Seinfeld, J. H.; Saxena, P., Atmospheric Gas Aerosol Equilibrium .1. Thermodynamic Model. *Aerosol Sci Tech* **1993,** *19* (2), 157-181.

63. Wexler, A. S., Second-generation Inorganic Aerosol Model. *Atmos Environ* **1991,** *25A* (12), 2731-2748.

64. Fountoukis, C.; Nenes, A., ISORROPIA II: a computationally efficient thermodynamic equilibrium model for K+-Ca2+-Mg2+-Nh(4)(+)-Na+-SO42--NO3--Cl--H2O aerosols. *Atmos Chem Phys* **2007,** *7* (17), 4639-4659.

65. Edgerton, E. S.; Hartsell, B. E.; Saylor, R. D.; Jansen, J. J.; Hansen, D. A.; Hidy, G. M., The Southeastern Aerosol Research and Characterization Study: Part II. Filter-Based Measurements of Fine and Coarse Particulate Matter Mass and Composition. *J Air Waste Manage* **2005,** *55* (10), 1527-1542.

66. Nenes, A.; Pandis, S. N.; Pilinis, C., ISORROPIA: A new thermodynamic equilibrium model for multiphase multicomponent inorganic aerosols. *Aquat Geochem* **1998,** *4* (1), 123-152.

67. Ansari, A. S.; Pandis, S. N., An analysis of four models predicting the partitioning of semivolatile inorganic aerosol components. *Aerosol Sci Tech* **1999,** *31* (2-3), 129-153.

68. Hennigan, C. J.; Izumi, J.; Sullivan, A. P.; Weber, R. J.; Nenes, A., A critical evaluation of proxy methods used to estimate the acidity of atmospheric particles. *Atmos Chem Phys* **2015,** *15* (5), 2775-2790.

69. Song, S.; Gao, M.; Xu, W.; Shao, J.; Shi, G.; Wang, S.; Wang, Y.; Sun, Y.; McElroy, M. B., Fine Particle pH for Beijing winter haze as inferred from diffrent thermodynamic equilibrium models. *Atmos Chem Phys* **2018,** *18* (10), 7423-7438.

70. Shi, G.; Xu, J.; Peng, X.; Xiao, Z.; Chen, K.; Tian, Y.; Guan, X.; Feng, Y.; Yu, H.; Nenes, A.; Russell, A. G., pH of Aerosols in a Polluted Atmosphere: Source Contributions to Highly Acidic Aerosol. *Environ Sci Technol* **2017,** *51* (8), 4289-4296.

71. Guo, H.; Xu, L.; Bougiatioti, A.; Cerully, K. M.; Capps, S. L.; Hite, J. R.; Carlton, A. G.; Lee, S. H.; Bergin, M. H.; Ng, N. L.; Nenes, A.; Weber, R. J., Fine-particle water and pH in the southeastern United States. *Atmos Chem Phys* **2015,** *15* (9), 5211-5228.

72. Ludwig, J.; Klemm, O., Organic acids in different size classes of atmospheric particulate material. *Tellus B: Chemical and Physical Meteorology* **1988,** *40* (5), 340-347.

73. Nah, T.; Guo, H.; Sullivan, A. P.; Chen, Y.; Tanner, D. J.; Nenes, A.; Russell, A.; Ng, N. L.; Huey, L. G.; Weber, R. J., Characterization of Aerosol Composition, Aerosol Acidity and Organic Acid Partitioning at an Agriculture-Intensive Rural Southeastern U.S. Site (in discussion). *Atmospheric Chemistry and Physics Discussions* **2018**, 1-46.

74. Vasilakos, P.; Russell, A.; Weber, R.; Nenes, A., Understanding nitrate formation in a world with less sulfate (in discussion). *Atmospheric Chemistry and Physics Discussions* **2018**, 1-27.

75. Bian, Y. X.; Zhao, C. S.; Ma, N.; Chen, J.; Xu, W. Y., A study of aerosol liquid water content based on hygroscopicity measurements at high relative humidity in the North China Plain. *Atmos Chem Phys* **2014,** *14* (12), 6417-6426.

76. Dick, W. D.; Saxena, P.; McMurry, P. H., Estimation of water uptake by organic compounds in submicron aerosols measured during the Southeastern Aerosol and Visibility Study. *J Geophys Res-Atmos* **2000,** *105* (D1), 1471-1479.

77. Pye, H. O. T.; Murphy, B. N.; Xu, L.; Ng, N. L.; Carlton, A. G.; Guo, H. Y.; Weber, R.; Vasilakos, P.; Appel, K. W.; Budisulistiorini, S. H.; Surratt, J. D.; Nenes, A.; Hu, W. W.; Jimenez, J. L.; Isaacman-VanWertz, G.; Misztal, P. K.; Goldstein, A. H., On the implications of aerosol liquid water and phase separation for organic aerosol mass. *Atmos Chem Phys* **2017,** *17* (1), 343-369.

78. Guo, H.; Sullivan, A. P.; Campuzano-Jost, P.; Schroder, J. C.; Lopez-Hilfiker, F. D.; Dibb, J. E.; Jimenez, J. L.; Thornton, J. A.; Brown, S. S.; Nenes, A.; Weber, R. J., Fine particle pH and the partitioning of nitric acid during winter in the northeastern United States. *J Geophys Res-Atmos* **2016,** *121* (17), 10355-10376.

79. Seinfeld, J. H.; Pandis, S. N., *Atmospheric chemistry and physics : from air pollution to climate change*. 2nd ed.; Wiley: New York, 2006.

80. Rood, M. J.; Shaw, M. A.; Larson, T. V.; Covert, D. S., Ubiquitous Nature of Ambient Metastable Aerosol. *Nature* **1989,** *337* (6207), 537-539.

81. Liu, Y. C.; Wu, Z. J.; Wang, Y.; Xiao, Y.; Gu, F. T.; Zheng, J.; Tan, T. Y.; Shang, D. J.; Wu, Y. S.; Zeng, L. M.; Hu, M.; Bateman, A. P.; Martin, S. T., Submicrometer Particles Are in the Liquid State during Heavy Haze Episodes in the Urban Atmosphere of Beijing, China. *Environ Sci Tech Let* **2017,** *4* (10), 427-432.

82. Zhang, Q.; Jimenez, J. L.; Worsnop, D. R.; Canagaratna, M., A case study of urban particle acidity and its influence on secondary organic aerosol. *Environ Sci Technol* **2007,** *41* (9), 3213-3219.

83. Sakalys, J.; Meinore, E.; Kvietkus, K., Neutralization of Acidic Sulfates with Ammonia in Volcanic Origin Aerosol Particles. *Lith J Phys* **2016,** *56* (1), 42-48.

84. Losey, D. J.; Ott, E. E.; Freedman, M. A., Effects of High Acidity on Phase Transitions of an Organic Aerosol. *J Phys Chem A* **2018,** *122* (15), 3819-3828.

85. Byun, D.; Schere, K. L., Review of the governing equations, computational algorithms, and other components of the models-3 Community Multiscale Air Quality (CMAQ) modeling system. *Appl Mech Rev* **2006,** *59* (1-6), 51-77.

86. CMAS., Community Modeling and Analysis System. https://www.cmascenter.org/smoke/. **2013**.

87. U.S.EPA., National Emissions Inventory (NEI). https://www.epa.gov/air-emissions-inventories/2011-national-emissions-inventory-nei-documentation. **2011**.

88. Skamarock, W. C.; Klemp., J. B.; Dudhia, J.; Gill, D. O.; Barker, D. M.; Duda, M. G.; Huang, X.-Y.; Wang, W.; Powers., J. G., A Description of the Advanced Research WRF Version 3. NCAR Tech. Note NCAR/TN-475+STR. https://www.mmm.ucar.edu/weather-research-and-forecasting-model. **2008**, 113.

89. Russell, A. G.; Tolbert, P. E.; Henneman, L. R. F.; Abrams, J.; Liu, C.; Klein, M.; Mulholland, J. A.; Sarnat, S.; Hu, Y.; Chang, H.; Odman, T.; Strickland, M.; Shen, H.; Lawal, A., Impacts of Regulations on Air Quality and Emergency Department visits in the Atlanta metropolitan area, 1999-2013. Research Report 195. Boston, MA: The Health Effects Institute. https://www.healtheffects.org/system/files/RussellRR195_0.pdf. **2018**.

90. Henneman, L. R. F.; Liu, C.; Hu, Y. T.; Mulholland, J. A.; Russell, A. G., Air quality modeling for accountability research: Operational, dynamic, and diagnostic evaluation. *Atmos Environ* **2017,** *166*, 551-565.

91. Emery, C.; Liu, Z.; Russell, A. G.; Odman, M. T.; Yarwood, G.; Kumar, N., Recommendations on statistics and benchmarks to assess photochemical model performance. *J Air Waste Manage* **2017,** *67* (5), 582-598.

92. Ding, J.; Zhao, P.; Su, J.; Dong, Q.; Du, X., Aerosol pH and its influencing factors in Beijing (in discussion). *Atmospheric Chemistry and Physics Discussions* **2018**, 1-34.

93. Hettiyadura, A. P. S.; Jayarathne, T.; Baumann, K.; Goldstein, A. H.; de Gouw, J. A.; Koss, A.; Keutsch, F. N.; Skog, K.; Stone, E. A., Qualitative and quantitative analysis of atmospheric organosulfates in Centreville, Alabama. *Atmos Chem Phys* **2017,** *17* (2), 1343-1359.

94. Darer, A. I.; Cole-Filipiak, N. C.; O'Connor, A. E.; Elrod, M. J., Formation and Stability of Atmospherically Relevant Isoprene-Derived Organosulfates and Organonitrates. *Environ Sci Technol* **2011,** *45* (5), 1895-1902.

95. Shi, G. L.; Xu, J.; Peng, X.; Xiao, Z. M.; Chen, K.; Tian, Y. Z.; Guan, X. B.; Feng, Y. C.; Yu, H. F.; Nenes, A.; Russell, A. G., pH of Aerosols in a Polluted Atmosphere: Source Contributions to Highly Acidic Aerosol. *Environ Sci Technol* **2017,** *51* (8), 4289-4296.

96. Rengarajan, R.; Sudheer, A. K.; Sarin, M. M., Aerosol acidity and secondary organic aerosol formation during wintertime over urban environment in western India. *Atmos Environ* **2011,** *45* (11), 1940-1945.

97. Tao, Y.; Ye, X. N.; Jiang, S. Q.; Yang, X.; Chen, J. M.; Xie, Y. Y.; Wang, R. Y., Effects of amines on particle growth observed in new particle formation events. *J Geophys Res-Atmos* **2016,** *121* (1), 324-335.

98. Ivey, C. E.; Holmes, H. A.; Hu, Y. T.; Mulholland, J. A.; Russell, A. G., Development of PM2.5 source impact spatial fields using a hybrid source apportionment air quality model. *Geosci Model Dev* **2015,** *8* (7), 2153-2165.

99. Guo, H. Y.; Liu, J. M.; Froyd, K. D.; Roberts, J. M.; Veres, P. R.; Hayes, P. L.; Jimenez, J. L.; Nenes, A.; Weber, R. J., Fine particle pH and gas-particle phase partitioning of inorganic species in Pasadena, California, during the 2010 CalNex campaign. *Atmos Chem Phys* **2017,** *17* (9), 5703-5719.

100. Guo, H.; Nenes, A.; Weber, R. J., The underappreciated role of nonvolatile cations on aerosol ammonium-sulfate molar ratios (in discussion). *Atmospheric Chemistry and Physics Discussions* **2017**, 1-19.

101. Allen, H. M.; Draper, D. C.; Ayres, B. R.; Ault, A. P.; Bondy, A. L.; Takahama, S.; Modini, R. L.; Baumann, K.; Edgerton, E.; Knote, C.; Laskin, A.; Wang, B.; Fry, J. L., Influence of crustal dust and sea spray supermicron particle concentrations and acidity on inorganic NO3- aerosol during the 2013 Southern Oxidant and Aerosol Study. *Atmos Chem Phys* **2015,** *15* (18), 10669-10685.

102. Paulot, F.; Ginoux, P.; Cooke, W. F.; Donner, L. J.; Fan, S.; Lin, M. Y.; Mao, J.; Naik, V.; Horowitz, L. W., Sensitivity of nitrate aerosols to ammonia emissions and to nitrate chemistry: implications for present and future nitrate optical depth. *Atmos Chem Phys* **2016,** *16* (3), 1459-1477.

103. Motallebi, N., Wintertime PM2.5 and PM10 Source Apportionment at Sacramento, California. *J Air Waste Manage* **1999,** *49* (9), 25-34.

104. Behera, S. N.; Sharma, M.; Aneja, V. P.; Balasubramanian, R., Ammonia in the atmosphere: a review on emission sources, atmospheric chemistry and deposition on terrestrial bodies. *Environ Sci Pollut R* **2013,** *20* (11), 8092-8131.

105. Blanchard, C. L.; Hidy, G. M., Effects of changes in sulfate, ammonia, and nitric acid on particulate nitrate concentrations in the southeastern United States. *J Air Waste Manage* **2003,** *53* (3), 283-290.

106. Shen, J. L.; Chen, D. L.; Bai, M.; Sun, J. L.; Lam, S. K.; Mosier, A.; Liu, X. L.; Li, Y., Spatial variations in soil and plant nitrogen levels caused by ammonia deposition near a cattle feedlot. *Atmos Environ* **2018,** *176*, 120-127.

107. Russell, A. R.; Valin, L. C.; Cohen, R. C., Trends in OMI NO2 observations over the United States: effects of emission control technology and the economic recession. *Atmos Chem Phys* **2012,** *12* (24), 12197-12209.

108. Neuman, J. A.; Parrish, D. D.; Ryerson, T. B.; Brock, C. A.; Wiedinmyer, C.; Frost, G. J.; Holloway, J. S.; Fehsenfeld, F. C., Nitric acid loss rates measured in power plant plumes. *J Geophys Res-Atmos* **2004,** *109* (D23304), 1-13.

109. Guo, H.; Weber, R. J.; Nenes, A., High levels of ammonia do not raise fine particle pH sufficiently to yield nitrogen oxide-dominated sulfate production. *Sci Rep-Uk* **2017,** *7* (1), 12109.

110. Lurmann, F.; Avol, E.; Gilliland, F., Emissions reduction policies and recent trends in Southern California's ambient air quality. *J Air Waste Manage* **2015,** *65* (3), 324-335.

111. He, H.; Vinnikov, K. Y.; Li, C.; Krotkov, N. A.; Jongeward, A. R.; Li, Z. Q.; Stehr, J. W.; Hains, J. C.; Dickerson, R. R., Response of SO2 and particulate air pollution to local and regional emission controls: A case study in Maryland. *Earths Future* **2016,** *4* (4), 94-109.

112. Administration., U. E. I., Energy consumption by sector. https://www.eia.gov/totalenergy/data/monthly/pdf/sec2.pdf.

113. Fikru, M. G.; Gautier, L., The impact of weather variation on energy consumption in residential houses. *Appl Energ* **2015,** *144*, 19-30.

114. Fumo, N.; Biswas, M. A. R., Regression analysis for prediction of residential energy consumption. *Renew Sust Energ Rev* **2015,** *47*, 332-343.

115. Nations, U., World Population Prospects. https://esa.un.org/unpd/wpp/Publications/Files/WPP2017_KeyFindings.pdf. **2017**.

116. Wang, Y.; Lin, H.; Wang, W.; Liu, Y.; Wennersten, R.; Sun, Q., Impacts of climate change on the cooling loads of residential buildings differences between occupants with different age. *Energy Procedia* **2017,** *142*, 2677-2682.

117. (EIA), E. I. A., Annual Energy Outlook 2020 with projections to 2050. https://www.eia.gov/outlooks/aeo/pdf/aeo2020.pdf Accessed August 19th 2020. **2020**.

118. Say, N. P.; Yücel, M., Energy consumption and CO2 emissions in Turkey: Empirical analysis and future projection based on an economic growth. *Energy Policy* **2006,** *34* (18), 3870-3876.

119. Aydin, G., The Modeling of Coal-related CO2 Emissions and Projections into Future Planning. *Energy Sources, Part A: Recovery, Utilization, and Environmental Effects* **2014,** *36* (2), 191-201.

120. Köne, A. Ç.; Büke, T., Forecasting of CO2 emissions from fuel combustion using trend analysis. *Renewable and Sustainable Energy Reviews* **2010,** *14* (9), 2906-2915.

121. Ramaswami, A.; Russell, A. G.; Culligan, P. J.; Sharma, K. R.; Kumar, E., Meta-principles for developing smart, sustainable, and healthy cities. *Science* **2016,** *352* (6288), 940.

122. Nations, U., Make cities and human settlements inclusive, safe, resilient and sustainable. https://unstats.un.org/sdgs/report/2019/goal-11/ Accessed (August 19th 2020).

123. Energy, U. S. D. o., State & Local Energy Data. https://www.eere.energy.gov/sled/#/ Access date (August 19th 2020).

124. Hsu, D., How much information disclosure of building energy performance is necessary? *Energy Policy* **2014,** *64*, 263-272.

125. Swan, L. G.; Ugursal, V. I., Modeling of end-use energy consumption in the residential sector: A review of modeling techniques. *Renew Sust Energ Rev* **2009,** *13* (8), 1819-1835.

126. Tian, W.; Yang, S.; Li, Z. Y.; Wei, S.; Pan, W.; Liu, Y. L., Identifying informative energy data in Bayesian calibration of building energy models. *Energ Buildings* **2016,** *119*, 363-376.

127. Li, X. W.; Wen, J., Review of building energy modeling for control and operation. *Renew Sust Energ Rev* **2014,** *37*, 517-537.

128. Kialashaki, A.; Reisel, J. R., Modeling of the energy demand of the residential sector in the United States using regression models and artificial neural networks. *Appl Energ* **2013,** *108*, 271-280.

129. Djuric, N.; Novakovic, V., Identifying important variables of energy use in low energy office building by using multivariate analysis. *Energ Buildings* **2012,** *45*, 91-98.

130. Motuziene, V.; Vilutiene, T., Modelling the Effect of the Domestic Occupancy Profiles on Predicted Energy Demand of the Energy Efficient House. *Procedia Engineering* **2013,** *57*, 798-807.

131. Marshall, E.; Steinberger, J. K.; Dupont, V.; Foxon, T. J., Combining energy efficiency measure approaches and occupancy patterns in building modelling in the UK residential context. *Energ Buildings* **2016,** *111*, 98-108.

132. (NBI), N. B. I., Sensitivity Analyisis: Comparing the Impact of Design, Operation, and Tenant Behavior on Building Energy Performance. **2011**.

133. Faraway, J. J., *Extending the Linear Model with R (Texts in Statistical Science)*. Chapman \& Hall/CRC: 2005.

134. Faraway, J. J., *Linear Models with R*. CRC Press: 2016.

135. Montgomery, D. C.; Runger, G. C., *Applied statistics and probability for engineers*. 4th ed. ed.; Wiley: Hoboken, NJ, 2007.

136. Jackson, J. E., A User's Guide to Principle Components. John Wiley and Sons. **1991**.

137. Robinson, C.; Dilkina, B.; Hubbs, J.; Zhang, W. W.; Guhathakurta, S.; Brown, M. A.; Pendyala, R. M., Machine learning approaches for estimating commercial building energy consumption. *Appl Energ* **2017,** *208*, 889-904.

138. Aydinalp-Koksal, M.; Ugursal, V. I., Comparison of neural network, conditional demand analysis, and engineering approaches for modeling end-use energy consumption in the residential sector. *Appl Energ* **2008,** *85* (4), 271-296.

139. Pino-Mejias, R.; Perez-Fargallo, A.; Rubio-Bellido, C.; Pulido-Arcas, J. A., Comparison of linear regression and artificial neural networks models to predict heating and cooling energy demand, energy consumption and CO2 emissions. *Energy* **2017,** *118*, 24-36.

140. Wang, D. Q.; Zhang, H.; Liu, R.; Liu, X. L.; Wang, J., Unsupervised feature selection through Gram-Schmidt orthogonalization-A word co-occurrence perspective. *Neurocomputing* **2016,** *173*, 845-854.

141. Lyu, H. Q.; Wan, M. X.; Han, J. Q.; Liu, R. L.; Wang, C., A filter feature selection method based on the Maximal Information Coefficient and Gram-Schmidt Orthogonalization for biomedical data mining. *Comput Biol Med* **2017,** *89*, 264-274.

142. Chamber, M. A., 29-County Metropolitan Statistical Area (MSA).

143. Bureau, C., American Census Survey. https://www.census.gov/programs-surveys/acs.

144. (ACS), A. C. S., Public Use Microdata Sample (PUMS) Documentation. https://www.census.gov/programs-surveys/acs/technical-documentation/pums.html.

145. Zhang, W. W.; Guhathakurta, S.; Pendyala, R.; Garikapati, V.; Ross, C., A Generalizable Method for Estimating Household Energy by Neighborhoods in US Urban Regions. *Enrgy Proced* **2017,** *143*, 859-864.

146. EIA, U. S., Residential Energy Consumption Survery (RECS). https://www.eia.gov/consumption/residential/about.php.

147. Valovcin, S.; Hering, A. S.; Polly, B.; Heaney, M., A statistical approach for post-processing residential building energy simulation output. *Energ Buildings* **2014,** *85*, 165-179.

148. Bureau., U. S. C., Understanding and Using American Community Survey Data. https://www.census.gov/content/dam/Census/library/publications/2018/acs/acs_general_handbook_2018.pdf. **2018.**

149. Bureau, U. S. C., Statistical Quality Standards. https://www.census.gov/content/dam/Census/about/about-the-bureau/policies_and_notices/quality/statistical-quality-standards/Quality_Standards.pdf. **2013**.

150. Bureau, U. S. C., TIGER/Line Shapefiles. https://www.census.gov/cgi-bin/geo/shapefiles/. **2010**.

151. Amiri, S. S.; Mottahedi, M.; Asadi, S., Using multiple regression analysis to develop energy consumption indicators for commercial buildings in the US. *Energ Buildings* **2015,** *109*, 209-216.

152. Witten, I. H.; Frank, E.; Hall, M. A., Data Mining Practical Machine Learning Tools and Techniques Third Edition Preface. *Mor Kauf D* **2011**, Xxi-+.

153. Chen, H.; Huang, Y.; Shen, H. Z.; Chen, Y. L.; Ru, M. Y.; Chen, Y. C.; Lin, N.; Su, S.; Zhuo, S. J.; Zhong, Q. R.; Wang, X. L.; Liu, J. F.; Li, B. G.; Tao, S., Modeling temporal variations in global residential energy consumption and pollutant emissions. *Appl Energ* **2016,** *184*, 820-829.

154. Sedgwick, P., Standardising outcome measures using z scores. *The BMJ*.

155. Jolliffe, I. T.; Cadima, J., Principal component analysis: a review and recent developments. *Philos T R Soc A* **2016,** *374* (2065).

156. Jolliffe, I. T.; Trendafilov, N. T.; Uddin, M., A Modified Principal Component Technique Based on the LASSO. *Journal of Computational and Graphical Statistics* **2003,** *12* (3), 531-547.

157. He, Y.; Monteiro, R. D. C.; Park, H., An algorithm for sparse PCA based on a new sparsity control criterion. In *Proceedings of the 2011 SIAM International Conference on Data Mining*, pp 771-782.

158. Mahmood, N. T.; Allawi, S. T., Modified PCA Based on JK Method for Ranking to Select Features in Statistical DataSets. *International Journal of Computer Science and Information Security* **2016,** *14* (8).

159. Basak, S. C.; Mills, D.; Mumtaz, M. M., A quantitative structure-activity relationship (QSAR) study of dermal absorption using theoretical molecular descriptors. *Sar Qsar Environ Res* **2007,** *18* (1-2), 45-55.

160. Colan, S. D., The Why and How of Z Scores. *J Am Soc Echocardiog* **2013,** *26* (1), 38-40.

161. Bjorck, A., *Numerical Methods for Least Squares Problems*. Society for Industrial and Applied Mathematics: 1996.

162. Householder, A. S., Unitary Triangularization of a Nonsymmetric Matrix. *J Acm* **1958,** *5* (4), 339-342.

163. Gao, X. F.; Malkawi, A., A new methodology for building energy performance benchmarking: An approach based on intelligent clustering algorithm. *Energ Buildings* **2014,** *84*, 607-616.

164. Hsu, D., Comparison of integrated clustering methods for accurate and stable prediction of building energy consumption data. *Appl Energ* **2015,** *160*, 153-163.

165. Vu, D. H.; Muttaqi, K. M.; Agalgaonkar, A. P., A variance inflation factor and backward elimination based robust regression model for forecasting monthly electricity demand using climatic variables. *Appl Energ* **2015,** *140*, 385-394.

166. Perera, D. W. U.; Halstensen, M.; Skeie, N.-O., Prediction of Space Heating Energy Consumption in Cabins Based on Multivariate Regression Modelling. *International Journal of Modeling and Optimization* **2015,** *5* (6).

167. Mocanu, E.; Nguyen, P. H.; Gibescu, M.; Kling, W. L., Deep learning for estimating building energy consumption. *Sustain Energy Grids* **2016,** *6*, 91-99.

168. Yildiz, B.; Bilbao, J. I.; Sproul, A. B., A review and analysis of regression and machine learning models on commercial building electricity load forecasting. *Renew Sust Energ Rev* **2017,** *73*, 1104-1122.

169. Hastie, T.; Tibshirani, R.; Friedman, J., *The Elements of Statistical Learning: Data Mining, Inference, and Prediction, Second Edition*. Springer New York: 2009.

170. *Applied regression analysis and other multivariable methods*. PWS Publishing Co.: 1988; p 718.

171. Salari, M.; Javid, R. J., Modeling household energy expenditure in the United States. *Renew Sust Energ Rev* **2017,** *69*, 822-832.

172. Doymaz, F.; Palazoglu, A.; Romagnoli, J. A., Orthogonal Nonlinear partial least-squares regression. *Ind Eng Chem Res* **2003,** *42* (23), 5836-5849.

173. Chen, S.; Billings, S. A.; Luo, W., Orthogonal Least-Squares Methods and Their Application to Non-Linear System-Identification. *Int J Control* **1989,** *50* (5), 1873-1896.

174. Dror, H., Box-Cox power transformation for Linear Models. https://www.mathworks.com/matlabcentral/fileexchange/10419-box-cox-power-transformation-for-linear-models.

175. Long, J. A., _jtools: Analysis and Presentation of Social Scientific Data_. R package version 2.0.1. https://cran.r-project.org/package=jtools. **2019**.

176. Fox, J.; Weisberg, S., Visualizing Fit and Lack of Fit in Complex Regression Models with Predictor Effect Plots and Partial Residuals. http://doi.org/10.18637/jss.v087.i09. *Journal of Statistical Software* **2018,** *87* (9), 1-27.

177. Finch, B. K.; Beck, A. N., Socio-economic status and z-score standardized height-for-age of US-born children (ages 2-6). *Econ Hum Biol* **2011,** *9* (3), 272-276.

178. Vu, V. Q., ggbiplot: A ggplot2 based biplot. R package version 0.55. http://github.com/vqv/ggbiplot. **2011**.

179. Brounen, D.; Kok, N.; Quigley, J. M., Residential energy use and conservation: Economics and demographics. *European Economic Review* **2012,** *56* (5), 931-945.

180. Ahmed Gassar, A. A.; Yun, G. Y.; Kim, S., Data-driven approach to prediction of residential energy consumption at urban scales in London. *Energy* **2019,** *187*, 115973.

181. Dar-Mousa, R. N.; Makhamreh, Z., Analysis of the pattern of energy consumptions and its impact on urban environmental sustainability in Jordan: Amman City as a case study. *Energy, Sustainability and Society* **2019,** *9* (1), 15.

182. Bureau, U. S. C., TIGER/Line Shapefiles. 2016, nation, U.S., primary Roads National Shapefile. https://catalog.data.gov/dataset/tiger-line-shapefile-2016-nation-u-s-primary-roads-national-shapefile. **2016**.

183. ESRI., ArcGIS® and ArcMap™ are the intellectual property of Esri and are used herein under license. Copyright © Esri. All rights reserved. For more information about Esri® software, please visit www.esri.com.". **2015**.

184. Arifwidodo, S.; Chandrasiri, O., Urban Heat Island and Household Energy Consumption in Bangkok, Thailand. *Energy Procedia* **2015,** *79*, 189-194.

185. Mohajerani, A.; Bakaric, J.; Jeffrey-Bailey, T., The urban heat island effect, its causes, and mitigation, with reference to the thermal properties of asphalt concrete. *J Environ Manage* **2017,** *197*, 522-538.

186. Taha, H., Urban climates and heat islands: Albedo, evapotranspiration, and anthropogenic heat. *Energ Buildings* **1997,** *25* (2), 99-103.

187. Chen, L.; Zhang, M. G.; Zhu, J.; Wang, Y. W.; Skorokhod, A., Modeling Impacts of Urbanization and Urban Heat Island Mitigation on Boundary Layer Meteorology and Air Quality in Beijing Under Different Weather Conditions. *J Geophys Res-Atmos* **2018,** *123* (8), 4323-4344.

188. Akbari, H.; Pomerantz, M.; Taha, H., Cool surfaces and shade trees to reduce energy use and improve air quality in urban areas. *Sol Energy* **2001,** *70* (3), 295-310.

189. Gui, X.; Wang, L.; Yao, R.; Yu, D.; Li, C. a., Investigating the urbanization process and its impact on vegetation change and urban heat island in Wuhan, China. *Environ Sci Pollut R* **2019**.

190. Bates, J. T.; Pennington, A. F.; Zhai, X.; Friberg, M. D.; Metcalf, F.; Darrow, L.; Strickland, M.; Mulholland, J.; Russell, A., Application and evaluation of two model fusion approaches to obtain ambient air pollutant concentrations at a fine spatial resolution (250m) in Atlanta. *Environmental Modelling & Software* **2018,** *109*, 182-190.

191. Group, A. R. C. O. D. a. M., LandPro 2012. Data Source: arcgis.atlantaregional.com **2012**.

192. Gago, E. J.; Roldan, J.; Pacheco-Torres, R.; Ordóñez, J., The city and urban heat islands: A review of strategies to mitigate adverse effects. *Renewable and Sustainable Energy Reviews* **2013,** *25*, 749-758.

193. Kakouei, A.; Vatani, A.; Idris, A. K. B., An estimation of traffic related CO2 emissions from motor vehicles in the capital city of, Iran. *Iranian J Environ Health Sci Eng* **2012,** *9* (1), 13-13.

194. Allen, L. H.; Pan, D. Y.; Boote, K. J.; Pickering, N. B.; Jones, J. W., Carbon dioxide and temperature effects on evapotranspiration and water use efficiency of soybean. *Agron J* **2003,** *95* (4), 1071-1081.

195. Ramirez, J. A.; Finnerty, B., CO2 and temperature effects on evapotranspiration and irrigated agriculture. *J Irrig Drain Eng* **1996,** *122* (3), 155-163.

196. Qiu, G. Y.; Li, H. Y.; Zhang, Q. T.; Chen, W.; Liang, X. J.; Li, X. Z., Effects of Evapotranspiration on Mitigation of Urban Temperature by Vegetation and Urban Agriculture. *J Integr Agr* **2013,** *12* (8), 1307-1315.

197. Qiu, G. Y.; Zou, Z. D.; Li, X. Z.; Li, H. Y.; Guo, Q. P.; Yan, C. H.; Tan, S. L., Experimental studies on the effects of green space and evapotranspiration on urban heat island in a subtropical megacity in China. *Habitat Int* **2017,** *68*, 30-42.

198. Nuruzzaman, M., Urban Heat Island: Causes, Effects and Mitigation Measures -A Review. *International Journal of Environmental Monitoring and Analysis* **2015,** *3*, 67-73.

199. Ghosh, S.; Das, A., Modelling urban cooling island impact of green space and water bodies on surface urban heat island in a continuously developing urban area. *Model Earth Syst Env* **2018,** *4* (2), 501-515.

200. Sun, R. H.; Chen, L. D., How can urban water bodies be designed for climate adaptation? *Landscape Urban Plan* **2012,** *105* (1-2), 27-33.

201. Steeneveld, G. J.; Koopmans, S.; Heusinkveld, B. G.; Theeuwes, N. E., Refreshing the role of open water surfaces on mitigating the maximum urban heat island effect. *Landscape Urban Plan* **2014,** *121*, 92-96.

202. Wong, N. H.; Tan, C.; Nindyani, A.; Jusuf, S.; Tan, E., *Influence of Water Bodies on Outdoor Air Temperature in Hot and Humid Climate*. 2012; p 81-89.

203. Amani-Beni, M.; Zhang, B.; Xie, G. D.; Xu, J., Impact of urban park's tree, grass and waterbody on microclimate in hot summer days: A case study of Olympic Park in Beijing, China. *Urban for Urban Gree* **2018,** *32*, 1-6.

204. Kurn, D. M.; Bretz, S. E.; Huang, B.; Akbari, H. *The potential for reducing urban air temperatures and energy consumption through vegetative cooling*; United States, 1994-05-01, 1994.

205. Declet-Barreto, J.; Knowlton, K.; Jenerette, G. D.; Buyantuev, A., Effects of Urban Vegetation on Mitigating Exposure of Vulnerable Populations to Excessive Heat in Cleveland, Ohio. *Weather Clim Soc* **2016,** *8* (4), 507-524.

206. Doick, K. J.; Peace, A.; Hutchings, T. R., The role of one large greenspace in mitigating London's nocturnal urban heat island. *Science of The Total Environment* **2014,** *493*, 662-671.

207. Ban-Weiss, G. A.; Bala, G.; Cao, L.; Pongratz, J.; Caldeira, K., Climate forcing and response to idealized changes in surface latent and sensible heat. *Environ Res Lett* **2011,** *6* (3), 034032.

208. Taha, H.; Akbari, H.; Rosenfeld, A.; Huang, J., Residential cooling loads and the urban heat island—the effects of albedo. *Building and Environment* **1988,** *23* (4), 271-283.

209. Soto, A. M.; Jentsch, M. F., Comparison of prediction models for determining energy demand in the residential sector of a country. *Energ Buildings* **2016,** *128*, 38-55.

210. Zhang, Z.; Beck, M. W.; Winkler, D. A.; Huang, B.; Sibanda, W.; Goyal, H.; written on behalf of, A. M. E. B.-D. C. T. C. G., Opening the black box of neural networks: methods for interpreting neural network models in clinical applications. *Ann Transl Med* **2018,** *6* (11), 216-216.

211. Catalina, T.; Virgone, J.; Blanco, E., Development and validation of regression models to predict monthly heating demand for residential buildings. *Energ Buildings* **2008,** *40* (10), 1825-1832.

212. Karatasou, S.; Santamouris, M., Socio-economic status and residential energy consumption: A latent variable approach. *Energ Buildings* **2019,** *198*, 100-105.

213. Kim, T.-Y.; Cho, S.-B., Predicting residential energy consumption using CNN-LSTM neural networks. *Energy* **2019,** *182*, 72-81.

214. Kim, M.; Jung, S.; Kang, J.-w., Artificial Neural Network-Based Residential Energy Consumption Prediction Models Considering Residential Building Information and User Features in South Korea. *Sustainability* **2020,** *12* (1).

215. Pecorari, E.; Mantovani, A.; Franceschini, C.; Bassano, D.; Palmeri, L.; Rampazzo, G., Analysis of the effects of meteorology on aircraft exhaust dispersion and deposition using a Lagrangian particle model. *Science of The Total Environment* **2016,** *541*, 839-856.

216. Hu, S.; Fruin, S.; Kozawa, K.; Mara, S.; Winer, A. M.; Paulson, S. E., Aircraft Emission Impacts in a Neighborhood Adjacent to a General Aviation Airport in Southern California. *Environ Sci Technol* **2009,** *43* (21), 8039-8045.

217. Zhu, Y. F.; Fanning, E.; Yu, R. C.; Zhang, Q. F.; Froines, J. R., Aircraft emissions and local air quality impacts from takeoff activities at a large International Airport. *Atmos Environ* **2011,** *45* (36), 6526-6533.

218. Lammers, A.; Janssen, N. A. H.; Boere, A. J. F.; Berger, M.; Longo, C.; Vijverberg, S. J. H.; Neerincx, A. H.; Maitland-van der Zee, A. H.; Cassee, F. R., Effects of short-term exposures to ultrafine particles near an airport in healthy subjects. *Environ Int* **2020,** *141*.

219. Jerrett, M.; Burnett, R. T.; Pope, C. A.; Ito, K.; Thurston, G.; Krewski, D.; Shi, Y. L.; Calle, E.; Thun, M., Long-Term Ozone Exposure and Mortality. *New England Journal of Medicine* **2009,** *360* (11), 1085-1095.

220. Penn, S. L.; Boone, S. T.; Harvey, B. C.; Heiger-Bernays, W.; Tripodis, Y.; Arunachalam, S.; Levy, J. I., Modeling variability in air pollution-related health damages from individual airport emissions. *Environmental research* **2017,** *156*, 791-800.

221. Schwartz, J.; Dockery, D. W.; Neas, L. M., Is Daily Mortality Associated Specifically with Fine Particles? *J Air Waste Manage* **1996,** *46* (10), 927-939.

222. Chen, K.; Schneider, A.; Cyrys, J.; Wolf, K.; Meisinger, C.; Heier, M.; Scheidt, W. v.; Kuch, B.; Pitz, M.; Peters, A.; Breitner, S., Hourly Exposure to Ultrafine Particle Metrics and the Onset of Myocardial Infarction in Augsburg, Germany. **2020,** *128* (1), 017003.

223. Chalupa, D. C.; Morrow, P. E.; Oberdörster, G.; Utell, M. J.; Frampton, M. W., Ultrafine particle deposition in subjects with asthma. **2004,** *112* (8), 879-882.

224. Henneman, L. R. F.; Shen, H.; Hogrefe, C.; Russell, A. G.; Zigler, C. M., Four Decades of United States Mobile Source Pollutants: Spatial–Temporal Trends Assessed by Ground-Based Monitors, Air Quality Models, and Satellites. *Environ Sci Technol* **2021,** *55* (2), 882-892.

225. Environmental Protection Agency. Air Pollutant Emissions Trends Data. https://www.epa.gov/air-emissions-inventories/air-pollutant-emissions-trends-data. Accessed February 7th 2021. .

226. Federal Aviation Administration. Aviation Forecast: FY2020-2040 Full Forecast Document and Tables. https://www.faa.gov/data_research/aviation/. Date Accessed Feb 6th 2021. **2020**.

227. Woody, M. C.; Wong, H. W.; West, J.; Arunachalam, S., Multiscale predictions of aviation-attributable PM2.5 for US airports modeled using CMAQ with plume-in-grid and an aircraft-specific 1-D emission model. *Atmos Environ* **2016,** *147*, 384-394.

228. Environmental Protection Agency . 2016v1 Platform. https://www.epa.gov/air-emissions-modeling/2016v1-platform. Access Date: Aug 9 2021.

229. Yim, S. H. L.; Lee, G. L.; Lee, I. H.; Allroggen, F.; Ashok, A.; Caiazzo, F.; Eastham, S. D.; Malina, R.; Barrett, S. R. H., Global, regional and local health impacts of civil aviation emissions. *Environ Res Lett* **2015,** *10* (3).

230. Quadros, F. D. A.; Snellen, M.; Dedoussi, I. C., Regional sensitivities of air quality and human health impacts to aviation emissions. *Environ Res Lett* **2020,** *15* (10).

231. Byun, D.; Schere, K. L., Review of the Governing Equations, Computational Algorithms, and Other Components of the Models-3 Community Multiscale Air Quality (CMAQ) Modeling System. *Applied Mechanics Reviews* **2006,** *59* (2), 51-77.

232. Skamarock, W. C.; Klemp, J. B.; Dudhia, J.; Gill, D. O.; Liu, Z.; Berner, J.; Wang, W.; Powers, J. G.; Duda, M. G.; Barker, D. M.; Huang, X.-Y., A Description of the Advanced Research WRF Model Version 4 (No. NCAR/TN-556+STR). doi:10.5065/1dfh-6p97. **2019**.

233. Baek, B. H.; Seppanen, C., Sparse Matrix Operator Kernel Emissions (SMOKE) Modeling System (Version SMOKE User's Documentation). http://doi.org/10.5281/zenodo.1421402.

234. US, E. P. A., Hemispheric CMAQ Model Version 5.3beta Output Data – 2016 seasonally averaged 108km for N. Hemisphere. V1 ed.; UNC Dataverse: 2019.

235. Appel, K. W.; Bash, J. O.; Fahey, K. M.; Foley, K. M.; Gilliam, R. C.; Hogrefe, C.; Hutzell, W. T.; Kang, D. W.; Mathur, R.; Murphy, B. N.; Napelenok, S. L.; Nolte, C. G.; Pleim, J. E.; Pouliot, G. A.; Pye, H. O. T.; Ran, L. M.; Roselle, S. J.; Sarwar, G.; Schwede, D. B.; Sidi, F. I.; Spero, T. L.; Wong, D. C., The Community Multiscale Air Quality (CMAQ) model versions 5.3 and 5.3.1: system updates and evaluation. *Geosci Model Dev* **2021,** *14* (5), 2867-2897.

236. Vukovich, J., Eyth, A., Henderson, B., Jang, C., Allen, C., Beidler, J., and Talgo, K., Development of 2016 hemispheric emissions for CMAQ, in: 17th Annual CMAS Conference, 22–24 October 2018, Chapel Hill, North Carolina, USA, available at: https://www.cmascenter.org/conference//2018/slides/1530_vukovich_development_2016_2018.pptx (last access: 1 August 2021), 2018. .

237. US EPA Office of Research and Development. CMAQv5.3.2. doi: 10.5281/zenodo.4081737. **2020**.

238. Saha, S.; Moorthi, S.; Pan, H.-L.; Wu, X.; Wang, J.; Nadiga, S.; Tripp, P.; Kistler, R.; Woollen, J.; Behringer, D.; Liu, H.; Stokes, D.; Grumbine, R.; Gayno, G.; Wang, J.; Hou, Y.-T.; Chuang, H.-Y.; Juang, H.-M. H.; Sela, J.; Iredell, M.; Treadon, R.; Kleist, D.; Van Delst, P.; Keyser, D.; Derber, J.; Ek, M.; Meng, J.; Wei, H.; Yang, R.; Lord, S.; van den Dool, H.; Kumar, A.; Wang, W.; Long, C.; Chelliah, M.; Xue, Y.; Huang, B.; Schemm, J.-K.; Ebisuzaki, W.; Lin, R.; Xie, P.; Chen, M.; Zhou, S.; Higgins, W.; Zou, C.-Z.; Liu, Q.; Chen, Y.; Han, Y.; Cucurull, L.; Reynolds, R. W.; Rutledge, G.; Goldberg, M., NCEP Climate Forecast System Reanalysis (CFSR) 6-hourly Products, January 1979 to December 2010. Research Data Archive at the National Center for Atmospheric Research, Computational and Information Systems Laboratory: Boulder, CO, 2010.

239. NCEP ADP Global Surface Observational Weather Data, October 1999 - continuing. Research Data Archive at the National Center for Atmospheric Research, Computational and Information Systems Laboratory: Boulder, CO, 2004.

240. NCEP North American Regional Reanalysis (NARR). Research Data Archive at the National Center for Atmospheric Research, Computational and Information Systems Laboratory: Boulder, CO, 2005.

241. Otte, T. L.; Pleim, J. E., The Meteorology-Chemistry Interface Processor (MCIP) for the CMAQ modeling system: updates through MCIPv3.4.1. *Geosci. Model Dev.* **2010,** *3* (1), 243-256.

242. National Emissions Inventory Collaborative. 2016v1 Emissions Modeling Platform. Retrieved from http://views.cira.colostate.edu/wiki/wiki/10202. Access date: Aug 2 2021.

243. Kang, D. W.; Pickering, K. E.; Allen, D. J.; Foley, K. M.; Wong, D. C.; Mathur, R.; Roselle, S. J., Simulating lightning NO production in CMAQv5.2: evolution of scientific updates. *Geosci Model Dev* **2019,** *12* (7), 3071-3083.

244. Agency, E. P., SMOKE TOOL FOR MODELS-3 VERSION 4.1 STRUCTURE AND OPERATION DOCUMENTATION. **2011**.

245. Simone, N. W.; Stettler, M. E. J.; Barrett, S. R. H., Rapid estimation of global civil aviation emissions with uncertainty quantification. *Transportation Research Part D: Transport and Environment* **2013,** *25*, 33-41.

246. Stettler, M. E. J.; Eastham, S.; Barrett, S. R. H., Air quality and public health impacts of UK airports. Part I: Emissions. *Atmos Environ* **2011,** *45* (31), 5415-5424.

247. Skamarock, W. C.; Klemp, J. B.; Dudhia, J.; Gill, D. O.; Barker, D. M.; Duda, M. G.; Huang, X.-Y.; Wang, W.; Powers, J. G., A Description of the Advanced Research WRF Version 3. NCAR Tech. Note NCAR/TN-475+STR. **2008**, 113.

248. Commission, A. R., SDEPUB.SDE.Counties_GA.

249. Federal Aviation Administration (FAA). Digital - Terminal Procedures Publication (d-TPP)/Airport Diagrams. **2021**.

250. Federal Aviation Administration (FAA). Aeronautical Lighting and Other Airport Visual Aids. Chapter 5: Section 2. Depature Procedures.

251. Griffin, D.; Zhao, X.; McLinden, C. A.; Boersma, F.; Bourassa, A.; Dammers, E.; Degenstein, D.; Eskes, H.; Fehr, L.; Fioletov, V.; Hayden, K.; Kharol, S. K.; Li, S.-M.; Makar, P.; Martin, R. V.; Mihele, C.; Mittermeier, R. L.; Krotkov, N.; Sneep, M.; Lamsal, L. N.; Linden, M. t.; Geffen, J. v.; Veefkind, P.; Wolde, M., High-Resolution Mapping of Nitrogen Dioxide With TROPOMI: First Results and Validation Over the Canadian Oil Sands. *Geophysical Research Letters* **2019,** *46* (2), 1049-1060.

252. Cooper, M. J.; Martin, R. V.; Henze, D. K.; Jones, D. B. A., Effects of a priori profile shape assumptions on comparisons between satellite NO2 columns and model simulations. *Atmos. Chem. Phys.* **2020,** *20* (12), 7231-7241.

253. Zhu, L.; Jacob, D. J.; Keutsch, F. N.; Mickley, L. J.; Scheffe, R.; Strum, M.; González Abad, G.; Chance, K.; Yang, K.; Rappenglück, B.; Millet, D. B.; Baasandorj, M.; Jaeglé, L.; Shah, V., Formaldehyde (HCHO) As a Hazardous Air Pollutant: Mapping Surface Air Concentrations from Satellite and Inferring Cancer Risks in the United States. *Environ Sci Technol* **2017,** *51* (10), 5650-5657.

254. Sun, K.; Zhu, L.; Cady-Pereira, K.; Chan Miller, C.; Chance, K.; Clarisse, L.; Coheur, P. F.; González Abad, G.; Huang, G.; Liu, X.; Van Damme, M.; Yang, K.; Zondlo, M., A physics-based approach to oversample multi-satellite, multispecies observations to a common grid. *Atmos. Meas. Tech.* **2018,** *11* (12), 6679-6701.

255. Zhang, Y.; Wang, K.; Jena, C., Impact of Projected Emission and Climate Changes on Air Quality in the US: from National to State Level. *Procedia Comput Sci* **2017,** *110*, 167-173.

256. Environmental Protection Agency . List of Designated Reference and Equivalent Methods, December 15, 2020. https://www.epa.gov/sites/production/files/2019-08/documents/designated_reference_and-equivalent_methods.pdf. **2020**.

257. Georgia Department of Natural Resources: Environmental Protection Division. 2016 Ambient Air Monitoring Plan. https://www.epa.gov/sites/production/files/2017-10/documents/gaplan2016.pdf. **2017**.

258. Winer, A. M.; Peters, J. W.; Smith, J. P.; Pitts, J. N., Response of commercial chemiluminescent nitric oxide-nitrogen dioxide analyzers to other nitrogen-containing compounds. *Environ Sci Technol* **1974,** *8* (13), 1118-1121.

259. Dunlea, E. J.; Herndon, S. C.; Nelson, D. D.; Volkamer, R. M.; San Martini, F.; Sheehy, P. M.; Zahniser, M. S.; Shorter, J. H.; Wormhoudt, J. C.; Lamb, B. K.; Allwine,

E. J.; Gaffney, J. S.; Marley, N. A.; Grutter, M.; Marquez, C.; Blanco, S.; Cardenas, B.; Retama, A.; Ramos Villegas, C. R.; Kolb, C. E.; Molina, L. T.; Molina, M. J., Evaluation of nitrogen dioxide chemiluminescence monitors in a polluted urban environment. *Atmos. Chem. Phys.* **2007,** *7* (10), 2691-2704.

260. Harkey, M.; Holloway, T.; Oberman, J.; Scotty, E., An evaluation of CMAQ NO2 using observed chemistry-meteorology correlations. *Journal of Geophysical Research: Atmospheres* **2015,** *120* (22), 11,775-11,797.

261. Ialongo, I.; Virta, H.; Eskes, H.; Hovila, J.; Douros, J., Comparison of TROPOMI/Sentinel-5 Precursor NO2 observations with ground-based measurements in Helsinki. *Atmos. Meas. Tech.* **2020,** *13* (1), 205-218.

262. Kim, H. C.; Kim, S.; Lee, S. H.; Kim, B. U.; Lee, P., Fine-Scale Columnar and Surface NOx Concentrations over South Korea: Comparison of Surface Monitors, TROPOMI, CMAQ and CAPSS Inventory. *Atmosphere-Basel* **2020,** *11* (1).

263. Goldberg, D. L.; Lu, Z.; Streets, D. G.; de Foy, B.; Griffin, D.; McLinden, C. A.; Lamsal, L. N.; Krotkov, N. A.; Eskes, H., Enhanced Capabilities of TROPOMI NO2: Estimating NOX from North American Cities and Power Plants. *Environ Sci Technol* **2019,** *53* (21), 12594-12601.

264. Jhun, I.; Coull, B. A.; Zanobetti, A.; Koutrakis, P., The impact of nitrogen oxides concentration decreases on ozone trends in the USA. *Air Quality, Atmosphere & Health* **2015,** *8* (3), 283-292.

265. Henneman, L. R. F.; Shen, H.; Liu, C.; Hu, Y.; Mulholland, J. A.; Russell, A. G., Responses in Ozone and Its Production Efficiency Attributable to Recent and Future Emissions Changes in the Eastern United States. *Environ Sci Technol* **2017,** *51* (23), 13797-13805.

266. Park, S.-K.; Marmur, A.; Kim, S. B.; Tian, D.; Hu, Y.; McMurry, P. H.; Russell, A. G., Evaluation of Fine Particle Number Concentrations in CMAQ. *Aerosol Sci Tech* **2006,** *40* (11), 985-996.

267. Jiang, W.; Smyth, S.; Giroux, É.; Roth, H.; Yin, D., Differences between CMAQ fine mode particle and PM2.5 concentrations and their impact on model performance evaluation in the lower Fraser valley. *Atmos Environ* **2006,** *40* (26), 4973-4985.

268. Binkowski, F. S.; Roselle, S. J., Models-3 Community Multiscale Air Quality (CMAQ) model aerosol component 1. Model description. **2003,** *108* (D6).

269. Zhang, X.; Karl, M.; Zhang, L.; Wang, J., Influence of Aviation Emission on the Particle Number Concentration near Zurich Airport. *Environ Sci Technol* **2020,** *54* (22), 14161-14171.

270. Kwok, R. H. F.; Napelenok, S. L.; Baker, K. R., Implementation and evaluation of PM2.5 source contribution analysis in a photochemical model. *Atmos Environ* **2013,** *80*, 398-407.

271. Kwok, R. H. F.; Baker, K. R.; Napelenok, S. L.; Tonnesen, G. S., Photochemical grid model implementation and application of VOC, NO_x, and O₃ source apportionment. *Geosci. Model Dev.* **2015,** *8* (1), 99-114.

272. Pan, S.; Roy, A.; Choi, Y.; Eslami, E.; Thomas, S.; Jiang, X. Y.; Gao, H. O., Potential impacts of electric vehicles on air quality and health endpoints in the Greater Houston Area in 2040. *Atmos Environ* **2019,** *207*, 38-51.

273. Monaghan, A. J.; Steinhoff, D. F.; Bruyere, C. L.; Yates, D., NCAR CESM Global Bias-Corrected CMIP5 Output to Support WRF/MPAS Research. Research Data Archive at the National Center for Atmospheric Research, Computational and Information Systems Laboratory: Boulder, CO, 2014.

274. Zhao, X.; Griffin, D.; Fioletov, V.; McLinden, C.; Cede, A.; Tiefengraber, M.; Müller, M.; Bognar, K.; Strong, K.; Boersma, F.; Eskes, H.; Davies, J.; Ogyu, A.; Lee, S. C., Assessment of the quality of TROPOMI high-spatial-resolution NO2 data products in the Greater Toronto Area. *Atmos. Meas. Tech.* **2020,** *13* (4), 2131-2159.

275. Tack, F.; Merlaud, A.; Iordache, M. D.; Pinardi, G.; Dimitropoulou, E.; Eskes, H.; Bomans, B.; Veefkind, P.; Van Roozendael, M., Assessment of the TROPOMI tropospheric NO2 product based on airborne APEX observations. *Atmos. Meas. Tech.* **2021,** *14* (1), 615-646.

276. Patoulias, D.; Fountoukis, C.; Riipinen, I.; Asmi, A.; Kulmala, M.; Pandis, S. N., Simulation of the size-composition distribution of atmospheric nanoparticles over Europe. *Atmos. Chem. Phys.* **2018,** *18* (18), 13639-13654.

277. Patoulias, D.; Fountoukis, C.; Riipinen, I.; Pandis, S. N., The role of organic condensation on ultrafine particle growth during nucleation events. *Atmos. Chem. Phys.* **2015,** *15* (11), 6337-6350.

278. Woody, M. C.; West, J. J.; Jathar, S. H.; Robinson, A. L.; Arunachalam, S., Estimates of non-traditional secondary organic aerosols from aircraft SVOC and IVOC emissions using CMAQ. *Atmos Chem Phys* **2015,** *15* (12), 6929-6942.

279. Koo, B.; Knipping, E.; Yarwood, G., 1.5-Dimensional volatility basis set approach for modeling organic aerosol in CAMx and CMAQ. *Atmos Environ* **2014,** *95*, 158-164.

280. Odum, J. R.; Hoffmann, T.; Bowman, F.; Collins, D.; Flagan, R. C.; Seinfeld, J. H., Gas/particle partitioning and secondary organic aerosol yields. *Environ Sci Technol* **1996,** *30* (8), 2580-2585.

281. Agency, E. P., Latest Version of Motor Vehicle Emission Simulator (MOVES).

282. Energy Information Administration. Use of Energy in the United States Explained. https://www.eia.gov/energyexplained/use-of-energy/. Acess Date: 8/19/2021. *Energy Information Administration*.

283. Karagulian, F.; Belis, C. A.; Dora, C. F. C.; Pruss-Ustun, A. M.; Bonjour, S.; Adair-Rohani, H.; Amann, M., Contributions to cities' ambient particulate matter (PM): A systematic review of local source contributions at global level. *Atmos Environ* **2015,** *120*, 475-483.

284. Lee, S.; Russell, A. G.; Baumann, K., Source apportionment of fine particulate matter in the southeastern united states. *J Air Waste Manage* **2007,** *57* (9), 1123-1135.

285. Malmqvist, E.; Liew, Z.; Källén, K.; Rignell-Hydbom, A.; Rittner, R.; Rylander, L.; Ritz, B., Fetal growth and air pollution - A study on ultrasound and birth measures. *Environmental research* **2017,** *152*, 73-80.

286. Maisonet, M.; Correa, A.; Misra, D.; Jaakkola, J. J., A review of the literature on the effects of ambient air pollution on fetal growth. *Environmental research* **2004,** *95* (1), 106-15.

287. Beckett, W. S., Ozone, air pollution, and respiratory health. *Yale J Biol Med* **1991,** *64* (2), 167-175.

288. Agency., E. P., Regulations to Reduce Mobile Source Pollution (https://www.epa.gov/mobile-source-pollution/regulations-reduce-mobile-source-pollution).

289. Agency., E. P., National Air Quality: Status and Trends of Key Air Pollutants (https://www.epa.gov/air-trends).

290. Song, J.; Webb, A.; Parmenter, B.; Allen, D. T.; McDonald-Buller, E., The impacts of urbanization on emissions and air quality: comparison of four visions of Austin, Texas. *Environ Sci Technol* **2008,** *42* (19), 7294-300.

291. Waldman, S.; Colman, Z., Trump's effort to roll back auto efficiency rules could hinge on debate over safety. *Science* **2018**.

292. York, N., New York Energy Policy. *https://www1.nyc.gov/site/cpp/index.page*.

293. Nopmongcol, U.; Grant, J.; Knipping, E.; Alexander, M.; Schurhoff, R.; Young, D.; Jung, J.; Shah, T.; Yarwood, G., Air Quality Impacts of Electrifying Vehicles and Equipment Across the United States. *Environ Sci Technol* **2017,** *51* (5), 2830-2837.

294. Onat, N. C.; Kucukvar, M.; Tatari, O., Conventional, hybrid, plug-in hybrid or electric vehicles? State-based comparative carbon and energy footprint analysis in the United States. *Appl Energ* **2015,** *150*, 36-49.

295. Nichols, B. G.; Kockelman, K. M.; Reiter, M., Air quality impacts of electric vehicle adoption in Texas. *Transportation Research Part D: Transport and Environment* **2015,** *34*, 208-218.

296. Gardner, G., Our Autonomous Future Will Likely Be an Electric One — Here's Why (https://www.govtech.com/fs/Our-Autonomous-Future-Will-Likely-Be-an-Electric-One-Heres-Why.html) Detroit Free Press. Accessed July 2020. **2016**.

297. Truong, L. T.; De Gruyter, C.; Currie, G.; Delbosc, A., Estimating the trip generation impacts of autonomous vehicles on car travel in Victoria, Australia. *Transportation* **2017,** *44* (6), 1279-1292.

298. Gruel, W.; Stanford, J. M., Assessing the Long-term Effects of Autonomous Vehicles: A Speculative Approach. *Transportation Research Procedia* **2016,** *13*, 18-29.

299. Quarles, N.; Lee, J.; Kockelman, K. M., America's Fleet Evolution in an Automated Future (Under review for presentation and publication in TRB/TRR 2020). *Transportation Research Board* **2020**.

300. Quarles, N. T., Americans' plans for acquiring and using electric, shared, and self-driving vehicles and costs and benefits of electrifying and automating US bus fleets (Master's Thesis, The University of Texas at Austin, Austin, Texas). Retrieved from https://repositories.lib.utexas.edu/handle/2152/64110. **2018**.

301. Diepold, K.; Götzl, K.; Riener, A.; Frison, A. K., *Automated Driving: Acceptance and Chances for Elderly People*. 2017; p 163-167.

302. Skamarock, W. C.; Klemp, J.; Dudhia, J.; Gill, D. O.; Barker, D.; Wang, W.; Powers, J. G., A Description of the Advanced Research WRF Version 3. **2008,** *27*, 3-27.

303. Agency, E. P., 2011 Version 6 Air Emissions Modeling Platforms. **2011**.

304. Shen, H.; Chen, Y.; Li, Y.; Russell, A. G.; Hu, Y.; Henneman, L. R. F.; Odman, M. T.; Shih, J.-S.; Burtraw, D.; Shao, S.; Yu, H.; Qin, M.; Chen, Z.; Lawal, A. S.; Pavur, G. K.; Brown, M. A.; Driscoll, C. T., Relaxing Energy Policies Coupled with Climate Change Will Significantly Undermine Efforts to Attain US Ozone Standards. *One Earth* **2019,** *1* (2), 229-239.

305. Lee, J. a. K., K. M., Energy & Emissions Implications of Self Driving Vehicles. Presented at the 98th Annual Meeting of the Transportation Research Board. *Transportation Research Board.* **2019**.

306. Bureau, U. C., Population projections for the United States from 2015 to 2060 (in millions) *In Statista. Retrieved August 01, 2019, from https://www.statista.com/statistics/183481/united-states-population-projection/* **2014**.

307. Bureau, U. C., Number of households in the U.S. from 1960 to 2018 (in millions). *In Statista. Retrieved August 01, 2019, from https://www.statista.com/statistics/183635/number-of-households-in-the-us/* **2018**.

308. Administration, F. H., State Motor-Vehicle Registrations - 2017. Accesible at https://www.fhwa.dot.gov/policyinformation/statistics/2017/pdf/mv1.pdf. **2017**.

309. Agency, E. P., Motor Vehicle Emission Simulator model version 2014b. **2018**.

310. Guensler, R.; Liu, H.; Xu, Y.; Akanser, A.; Kim, D.; Hunter, M. P.; Rodgers, M. O., Energy Consumption and Emissions Modeling of Individual Vehicles. **2017,** *2627* (1), 93-102.

311. Brown, M. A.; Li, Y., Carbon pricing and energy efficiency: pathways to deep decarbonization of the US electric sector. *Energy Efficiency* **2019,** *12* (2), 463-481.

312. Shen, H., Chen Yilin, Li Yufei, Russell G. Armistead, Hu, Yongtao, Henneman, Lucas R.F, Shih Jhih-Shyang, , Relaxing energy policies on top of climate change will significantly undermine states' efforts to attain U.S. ozone standards **2019**.

313. Administration, E. I., Assumptions to the Annual Energy Outlook 2015. (https://www.eia.gov/outlooks/aeo/assumptions/pdf/0554(2015).pdf). **2015**.

314. Bash, J. O.; Baker, K. R.; Beaver, M. R., Evaluation of improved land use and canopy representation in BEIS v3.61 with biogenic VOC measurements in California. *Geosci Model Dev* **2016,** *9* (6), 2191-2207.

315. Monaghan, A. J.; Steinhoff, D. F.; Bruyere, C. L.; Yates, D., NCAR CESM Global Bias-Corrected CMIP5 Output to Support WRF/MPAS Research. Research Data Archive at the National Center for Atmospheric Research, Computational and Information Systems Laboratory: Boulder, CO, 2014.

316. Simon, H.; Reff, A.; Wells, B.; Xing, J.; Frank, N., Ozone Trends Across the United States over a Period of Decreasing NOx and VOC Emissions. *Environ Sci Technol* **2015,** *49* (1), 186-195.

317. Li, N.; Chen, J. P.; Tsai, I. C.; He, Q.; Chi, S. Y.; Lin, Y. C.; Fu, T. M., Potential impacts of electric vehicles on air quality in Taiwan. *Sci Total Environ* **2016,** *566-567*, 919-928.

318. Li, N.; Chen, J. P.; Tsai, I. C.; He, Q. Y.; Chi, S. Y.; Lin, Y. C.; Fu, T. M., Potential impacts of electric vehicles on air quality in Taiwan. *Science of the Total Environment* **2016,** *566*, 919-928.

319. Brady, J.; O'Mahony, M., Travel to work in Dublin. The potential impacts of electric vehicles on climate change and urban air quality. *Transport Res D-Tr E* **2011,** *16* (2), 188-193.

320. Wang, N.; Lyu, X. P.; Deng, X. J.; Guo, H.; Deng, T.; Li, Y.; Yin, C. Q.; Li, F.; Wang, S. Q., Assessment of regional air quality resulting from emission control in the Pearl River Delta region, southern China. *Sci Total Environ* **2016,** *573*, 1554-1565.

321. Li, Y.; Ha, N.; Li, T., Research on Carbon Emissions of Electric Vehicles throughout the Life Cycle Assessment Taking into Vehicle Weight and Grid Mix Composition. *Energies* **2019,** *12* (19).

322. Dillman, K. J.; Árnadóttir, Á.; Heinonen, J.; Czepkiewicz, M.; Davíðsdóttir, B., Review and Meta-Analysis of EVs: Embodied Emissions and Environmental Breakeven. *Sustainability* **2020,** *12* (22).

323. Senthilkumar, N.; Gilfether, M.; Metcalf, F.; Russell, A. G.; Mulholland, J. A.; Chang, H. H., Application of a Fusion Method for Gas and Particle Air Pollutants between Observational Data and Chemical Transport Model Simulations Over the Contiguous United States for 2005–2014. *Int J Env Res Pub He* **2019,** *16* (18).

324. National Center for Health Statistics. https://www.cdc.gov/nchs/fastats/deaths.htm. Access Date; 8/19/2021.

325. National Center for Atmospheric Research (NCAR). Urban Canopy Model. https://ral.ucar.edu/solutions/products/urban-canopy-model. Access Date: 8/16/2021.

326. Troposheric Emissions: Monitoring of Pollution. http://tempo.si.edu/. Access Date 8/16/2021.

327. Pye, H. O. T.; Luecken, D. J.; Xu, L.; Boyd, C. M.; Ng, N. L.; Baker, K. R.; Ayres, B. R.; Bash, J. O.; Baumann, K.; Carter, W. P. L.; Edgerton, E.; Fry, J. L.; Hutzell, W. T.; Schwede, D. B.; Shepson, P. B., Modeling the Current and Future Roles of Particulate Organic Nitrates in the Southeastern United States. *Environ Sci Technol* **2015,** *49* (24), 14195-14203.

328. Lee, B. H.; Mohr, C.; Lopez-Hilfiker, F. D.; Lutz, A.; Hallquist, M.; Lee, L.; Romer, P.; Cohen, R. C.; Iyer, S.; Kurten, T.; Hu, W.; Day, D. A.; Campuzano-Jost, P.; Jimenez, J. L.; Xu, L.; Ng, N. L.; Guo, H.; Weber, R. J.; Wild, R. J.; Brown, S. S.; Koss, A.; de Gouw, J.; Olson, K.; Goldstein, A. H.; Seco, R.; Kim, S.; McAvey, K.; Shepson, P. B.; Starn, T.; Baumann, K.; Edgerton, E. S.; Liu, J.; Shilling, J. E.; Miller, D. O.; Brune, W.; Schobesberger, S.; D'Ambro, E. L.; Thornton, J. A., Highly functionalized organic nitrates in the southeast United States: Contribution to secondary organic aerosol and reactive nitrogen budgets. *Proc Natl Acad Sci U S A* **2016,** *113* (6), 1516-1521.

329. Vasilakos, P.; Russell, A.; Weber, R.; Nenes, A., Understanding nitrate formation in a world with less sulfate (in press). *Atmos Chem Phys* **2018**, DOI 10.5194/acp-2018-406.

330. Nah2, T.; Guo, H.; Sullivan, A. P.; Chen, Y.; Tanner, D. J.; Nenes, A.; Russell, A.; Ng, N. L.; Huey, L. G.; Weber, R. J., Characterization of Aerosol Composition,

Aerosol Acidity and Organic Acid Partitioning at an Agriculture-Intensive Rural Southeastern U.S. Site (in discussion). *Atmospheric Chemistry and Physics Discussions* **2018**, 1-46.

331. Wang, G. H.; Zhang, F.; Peng, J. F.; Duan, L.; Ji, Y. M.; Marrero-Ortiz, W.; Wang, J. Y.; Li, J.; Wu, C.; Cao, C.; Wang, Y.; Zheng, J.; Secrest, J.; Li, Y.; Wang, Y.; Li, G. H.; Li, N.; Zhang, R. Y., Particle acidity and sulfate production during severe haze events in China cannot be reliably inferred by assuming a mixture of inorganic salts *Atmos Chem Phys* **2018,** *18*, 10123-10132.

332. Marcolli, C.; Luo, B. P.; Peter, T., Mixing of the organic aerosol fractions: Liquids as the thermodynamically stable phases. *Journal of Physical Chemistry A* **2004,** *108* (12), 2216-2224.

333. Rachel F. Silvern, D. J. J., Patrick S. Kim, Eloise A. Marais, Jay R. Turner, Pedro Campuzano-Jost, Jose L. Jimenez, Inconsistency of ammonium–sulfate aerosol ratios with thermodynamic models in the eastern US: a possible role of organic aerosol. *Atmos Chem Phys* **2017,** *17* (8), 5107–5118.

334. Kim, P. S.; Jacob, D. J.; Fisher, J. A.; Travis, K.; Yu, K.; Zhu, L.; Yantosca, R. M.; Sulprizio, M. P.; Jimenez, J. L.; Campuzano-Jost, P.; Froyd, K. D.; Liao, J.; Hair, J. W.; Fenn, M. A.; Butler, C. F.; Wagner, N. L.; Gordon, T. D.; Welti, A.; Wennberg, P. O.; Crounse, J. D.; St Clair, J. M.; Teng, A. P.; Millet, D. B.; Schwarz, J. P.; Markovic, M. Z.; Perring, A. E., Sources, seasonality, and trends of southeast US aerosol: an integrated analysis of surface, aircraft, and satellite observations with the GEOS-Chem chemical transport model. *Atmos Chem Phys* **2015,** *15* (18), 10411-10433.

335. Na, K.; Song, C.; Switzer, C.; Cocker, D. R., Effect of ammonia on secondary organic aerosol formation from alpha-Pinene ozonolysis in dry and humid conditions. *Environ Sci Technol* **2007,** *41* (17), 6096-6102.

336. Liggio, J.; Li, S. M.; Vlasenko, A.; Stroud, C.; Makar, P., Depression of Ammonia Uptake to Sulfuric Acid Aerosols by Competing Uptake of Ambient Organic Gases. *Environ Sci Technol* **2011,** *45* (7), 2790-2796.

337. Kumar, S.; Raman, R. S., Inorganic ions in ambient fine particles over a National Park in central India: Seasonality, dependencies between SO42-, NO3-, and NH4+, and neutralization of aerosol acidity. *Atmos Environ* **2016,** *143*, 152-163.

338. Zhang, Y.; Seigneur, C.; Seinfeld, J. H.; Jacobson, M.; Clegg, S. L.; Binkowski, F. S., A comparative review of inorganic aerosol thermodynamic equilibrium modules: similarities, differences, and their likely causes. *Atmos Environ* **2000,** *34* (1), 117-137.

339. Kim, Y. P.; Seinfeld, J. H.; Saxena, P., Atmospheric Gas-Aerosol Equilibrium II. Analysis of Common Approximations and Activity Coefficient Calculation Methods. *Aerosol Sci Tech* **1993,** *19* (2), 182-198.

340. Nowak, J. B.; Huey, L. G.; Russell, A. G.; Tian, D.; Neuman, J. A.; Orsini, D.; Sjostedt, S. J.; Sullivan, A. P.; Tanner, D. J.; Weber, R. J.; Nenes, A.; Edgerton, E.; Fehsenfeld, F. C., Analysis of urban gas phase ammonia measurements from the 2002 Atlanta Aerosol Nucleation and Real-Time Characterization Experiment (ANARChE). *J Geophys Res-Atmos* **2006,** *111* (D17), 1-14.

341. Dennis, R.; Fox, T.; Fuentes, M.; Gilliland, A.; Hanna, S.; Hogrefe, C.; Irwin, J.; Rao, S. T.; Scheffe, R.; Schere, K.; Steyn, D.; Venkatram, A., A framework for evaluating regional-scale numerical photochemical modeling systems. *Environ Fluid Mech* **2010,** *10* (4), 471-489.

342. Cohan, D. S.; Chen, R., Modeled and observed fine particulate matter reductions from state attainment demonstrations. *J Air Waste Manage* **2014,** *64* (9), 995-1002.

343. Godowitch, J. M.; Pouliot, G. A.; Rao, S. T., Assessing multi-year changes in modeled and observed urban NOX concentrations from a dynamic model evaluation perspective. *Atmos Environ* **2010,** *44* (24), 2894-2901.

344. Marmur, A.; Liu, W.; Wang, Y.; Russell, A. G.; Edgerton, E. S., Evaluation of model simulated atmospheric constituents with observations in the factor projected space: CMAQ simulations of SEARCH measurements. *Atmos Environ* **2009,** *43* (11), 1839-1849.

345. U.S.EPA., Clean Air Status and Trends Network (CASTNET) and the National Atmospheric Deposition Program (NADP). https://www.epa.gov/castnet/. Accessed Nov 2017.

346. R., Original S code by Richard A. Becker, Allan R. Wilks. R version by Ray Brownrigg. Enhancements by Thomas P Minka and Alex Deckmyn. (2017). maps: Draw Geographical Maps. R package version 3.2.0. https://CRAN.R-project.org/package=maps. **2017**.

347. Team., R. C., R: A language and environment for statistical computing. R Foundation for Statistical Computing, Vienna, Austria. URL https://www.R-project.org/. **2016**.

348. USGS, SouthEastern Aerosol Research and Characterization Network (SEARCH) - Sites. https://my.usgs.gov/gcmp/site/list/943855. Accessed Feb 2018.

349. ESRI., World_Street_Map. Credit Sources: Sources: Esri, HERE, Garmin, USGS, Intermap, INCREMENT P, NRCAN, Esri Japan, METI, Esri China (Hong Kong), NOSTRA, © OpenStreetMap contributors, and the GIS User Community. https://www.arcgis.com/home/item.html?id=3b93337983e9436f8db950e38a8629af. **2009**.

350. ESRI, https://services6.arcgis.com/qebPoj1e0VcxT68d/ArcGIS/rest/services/USA_ZipCodes2018/FeatureServer. USA_ZipCodes2018. **2015**.

351. Zill, D. G.; Cullen, M. R., *Advanced engineering mathematics*. 3rd ed.; Jones and Bartlett Publishers: Sudbury, Mass., 2006; p xxxiii, 929, 14, 49, 23 p.

352. Schweinler, H. C.; Wigner, E. P., Orthogonalization Methods. *J Math Phys* **1970,** *11* (5), 1693-+.

353. Björck, Å. J. B. N. M., Solving linear least squares problems by Gram-Schmidt orthogonalization. **1967,** *7* (1), 1-21.

354. Horne, A. T., On Instruments: Launch Rules (Ready for Departure). *AOPA Pilot* **2016**.